

Biofabrication of nanostructures for environmental, agricultural, and biomedical applications

Edited by

Sougata Ghosh, Sirikanjana Thongmee and
Raymond J. Turner

Published in

Frontiers in Chemistry



FRONTIERS EBOOK COPYRIGHT STATEMENT

The copyright in the text of individual articles in this ebook is the property of their respective authors or their respective institutions or funders. The copyright in graphics and images within each article may be subject to copyright of other parties. In both cases this is subject to a license granted to Frontiers.

The compilation of articles constituting this ebook is the property of Frontiers.

Each article within this ebook, and the ebook itself, are published under the most recent version of the Creative Commons CC-BY licence. The version current at the date of publication of this ebook is CC-BY 4.0. If the CC-BY licence is updated, the licence granted by Frontiers is automatically updated to the new version.

When exercising any right under the CC-BY licence, Frontiers must be attributed as the original publisher of the article or ebook, as applicable.

Authors have the responsibility of ensuring that any graphics or other materials which are the property of others may be included in the CC-BY licence, but this should be checked before relying on the CC-BY licence to reproduce those materials. Any copyright notices relating to those materials must be complied with.

Copyright and source acknowledgement notices may not be removed and must be displayed in any copy, derivative work or partial copy which includes the elements in question.

All copyright, and all rights therein, are protected by national and international copyright laws. The above represents a summary only. For further information please read Frontiers' Conditions for Website Use and Copyright Statement, and the applicable CC-BY licence.

ISSN 1664-8714
ISBN 978-2-8325-3621-6
DOI 10.3389/978-2-8325-3621-6

About Frontiers

Frontiers is more than just an open access publisher of scholarly articles: it is a pioneering approach to the world of academia, radically improving the way scholarly research is managed. The grand vision of Frontiers is a world where all people have an equal opportunity to seek, share and generate knowledge. Frontiers provides immediate and permanent online open access to all its publications, but this alone is not enough to realize our grand goals.

Frontiers journal series

The Frontiers journal series is a multi-tier and interdisciplinary set of open-access, online journals, promising a paradigm shift from the current review, selection and dissemination processes in academic publishing. All Frontiers journals are driven by researchers for researchers; therefore, they constitute a service to the scholarly community. At the same time, the *Frontiers journal series* operates on a revolutionary invention, the tiered publishing system, initially addressing specific communities of scholars, and gradually climbing up to broader public understanding, thus serving the interests of the lay society, too.

Dedication to quality

Each Frontiers article is a landmark of the highest quality, thanks to genuinely collaborative interactions between authors and review editors, who include some of the world's best academicians. Research must be certified by peers before entering a stream of knowledge that may eventually reach the public - and shape society; therefore, Frontiers only applies the most rigorous and unbiased reviews. Frontiers revolutionizes research publishing by freely delivering the most outstanding research, evaluated with no bias from both the academic and social point of view. By applying the most advanced information technologies, Frontiers is catapulting scholarly publishing into a new generation.

What are Frontiers Research Topics?

Frontiers Research Topics are very popular trademarks of the *Frontiers journals series*: they are collections of at least ten articles, all centered on a particular subject. With their unique mix of varied contributions from Original Research to Review Articles, Frontiers Research Topics unify the most influential researchers, the latest key findings and historical advances in a hot research area.

Find out more on how to host your own Frontiers Research Topic or contribute to one as an author by contacting the Frontiers editorial office: frontiersin.org/about/contact

Biofabrication of nanostructures for environmental, agricultural, and biomedical applications

Topic editors

Sougata Ghosh — RK University, India

Sirikanjana Thongmee — Kasetsart University, Thailand

Raymond J. Turner — University of Calgary, Canada

Citation

Ghosh, S., Thongmee, S., Turner, R. J., eds. (2023). *Biofabrication of nanostructures for environmental, agricultural, and biomedical applications*. Lausanne: Frontiers Media SA. doi: 10.3389/978-2-8325-3621-6

Table of contents

- 05 **Editorial: Biofabrication of nanostructures for environmental, agricultural, and biomedical applications**
Sougata Ghosh, Raymond J. Turner and Sirikanjana Thongmee
- 08 **Fabrication of Guided Tissue Regeneration Membrane Using Lignin-Mediated ZnO Nanoparticles in Biopolymer Matrix for Antimicrobial Activity**
Bushra Bilal, Rimsha Niazi, Sohail Nadeem, Muhammad Asim Farid, Muhammad Shahid Nazir, Toheed Akhter, Mohsin Javed, Ayesha Mohyuddin, Abdul Rauf, Zulfiqar Ali, Syed Ali Raza Naqvi, Nawshad Muhammad, Eslam B. Elkaeed, Hala A. Ibrahim, Nasser S. Awwad and Sadaf Ul Hassan
- 19 **Use of gold nanoparticle-silibinin conjugates: A novel approach against lung cancer cells**
Rangnath Ravi, Md. Zeyauallah, Shubhrima Ghosh, Mohiuddin Khan Warsi, Renu Baweja, Abdullah M. AlShahrani, Abhijeet Mishra and Razi Ahmad
- 34 **Catalytic dye degradation by novel phytofabricated silver/zinc oxide composites**
Khalida Bloch, Shahansha M. Mohammed, Srikanta Karmakar, Satyajit Shukla, Adersh Asok, Kaushik Banerjee, Reshma Patil-Sawant, Noor Haida Mohd Kaus, Sirikanjana Thongmee and Sougata Ghosh
- 50 **Synergistic and antibiofilm potential of *Curcuma aromatica* derived silver nanoparticles in combination with antibiotics against multidrug-resistant pathogens**
Madhumita S. Tawre, Aishwarya Shiledar, Surekha K. Satpute, Kedar Ahire, Sougata Ghosh and Karishma Pardesi
- 67 **Biogenic metallic nanoparticles as enzyme mimicking agents**
Khanyisile Ngcongco, Suresh Babu Naidu Krishna and Karen Pillay
- 76 **Biogenic silver nanoparticles (AgNPs) from *Tinosporacordifolia* leaves: An effective antibiofilm agent against *Staphylococcus aureus* ATCC 23235**
Sreejita Ghosh, Somdutta Mondol, Dibyajit Lahiri, Moupriya Nag, Tanmay Sarkar, Siddhartha Pati, Soumya Pandit, Abdullah A. Alarfaj, Mohamad Faiz Mohd Amin, Hisham Atan Edinur, Muhammad Rajaei Ahmad Mohd Zain and Rina Rani Ray
- 91 **Phyto-assisted synthesis of zinc oxide nanoparticles for developing antibiofilm surface coatings on central venous catheters**
Akshit Malhotra, Suchitra Rajput Chauhan, Mispaur Rahaman, Ritika Tripathi, Manika Khanuja and Ashwini Chauhan

- 103 **Bacteria assisted green synthesis of copper oxide nanoparticles and their potential applications as antimicrobial agents and plant growth stimulants**
Deepak Singh, Devendra Jain, Deepak Rajpurohit, Gajanand Jat, Himmat Singh Kushwaha, Abhijeet Singh, Santosh Ranjan Mohanty, Mohammad Khalid Al-Sadoon, Wajid Zaman and Sudhir K. Upadhyay
- 113 **Biofabrication of novel silver and zinc oxide nanoparticles from *Fusarium solani* IOR 825 and their potential application in agriculture as biocontrol agents of phytopathogens, and seed germination and seedling growth promoters**
Joanna Trzcińska-Wencel, Magdalena Wypij, Artur P. Terzyk, Mahendra Rai and Patrycja Golińska



OPEN ACCESS

EDITED BY

Rajni Verma,
The University of Melbourne, Australia

REVIEWED BY

Shalini Sharma,
University of Maryland, United States

*CORRESPONDENCE

Sougata Ghosh,
✉ ghoshsibb@gmail.com
Raymond J. Turner,
✉ turnerr@ucalgary.ca
Sirikanjana Thongmee,
✉ fscisjn@ku.ac.th

RECEIVED 26 August 2023

ACCEPTED 14 September 2023

PUBLISHED 20 September 2023

CITATION

Ghosh S, Turner RJ and Thongmee S
(2023), Editorial: Biofabrication of
nanostructures for environmental,
agricultural, and biomedical applications.
Front. Chem. 11:1283676.
doi: 10.3389/fchem.2023.1283676

COPYRIGHT

© 2023 Ghosh, Turner and Thongmee.
This is an open-access article distributed
under the terms of the [Creative
Commons Attribution License \(CC BY\)](#).
The use, distribution or reproduction in
other forums is permitted, provided the
original author(s) and the copyright
owner(s) are credited and that the original
publication in this journal is cited, in
accordance with accepted academic
practice. No use, distribution or
reproduction is permitted which does not
comply with these terms.

Editorial: Biofabrication of nanostructures for environmental, agricultural, and biomedical applications

Sougata Ghosh^{1,2*}, Raymond J. Turner^{3*} and
Sirikanjana Thongmee^{2*}

¹Department of Microbiology, School of Science, RK University, Rajkot, India, ²Department of Physics, Faculty of Science, Kasetsart University, Bangkok, Thailand, ³Department of Biological Sciences, University of Calgary, Calgary, Canada

KEYWORDS

biogenic nanoparticles, metabolites, functionalization, photocatalysis, biocontrol

Editorial on the Research Topic

Biofabrication of nanostructures for environmental, agricultural, and biomedical applications

The Research Topic entitled “Biofabrication of Nanostructures for Environmental, Agricultural, and Biomedical Applications” was dedicated to original research and reviews articles on bio-inspired processes for fabrication of nanomaterials for antimicrobial, antibiofilm, anticancer, tissue engineering, dye degrading and biocontrol applications. Various bacteria, fungi, algae, medicinal plants their metabolites such as lignin, silibinin, curcumin, play active role in the synthesis of the nanoparticles and their stabilization. Challenges exist using biological materials to synthesize nanostructures compared to physical-chemical techniques. This comes from the complexity of the resulting biochemical mixture and limitations within the physical chemical parameters of the synthesis. However, the challenges become advantages as the biomolecules involved in the biogenic synthesis often bestow unique and superior properties. The biogenic nanoparticles tend to be more biocompatible and are thus considered as ideal candidate to design nanomedicine (Patil and Chandrasekaran, 2020). Here in this issue, we see creative examples in using biomaterials to create unique natural materials, and nano structures towards interesting applications.

Bilal et al. developed novel guided tissue regeneration (GTR) membranes from mucilage extracted from the chia seed, Lignin@ZnO, and polyvinyl alcohol (PVA). The ZnONPs were irregular with size lesser than 50 nm. The membrane exhibited randomly interconnected structures, with smooth morphology with Lignin@ZnO. The GTR showed satisfactory swelling and mechanical properties while the degradation started after 24 h. Further, superior antibacterial activity of the GTR was reported against *Staphylococcus aureus* and *Escherichia coli*.

In another study, Ravi et al. developed silibinin conjugated gold nanoparticles (Sb-GNPs) for anticancer applications against lung carcinoma cell line (A549). The hydrodynamic size of GNPs and Sb-GNPs were 107 ± 9 nm and 163 ± 5 nm, respectively while the zeta potentials were -19.6 mV \pm 0.648 and -22.2 mV \pm 0.458 mV,

respectively. The pH responsive release of silibinin was confirmed to be facilitated by an acidic pH up to 200 min. The IC₅₀ value of Sb-GNPs was 4.8 μ M (w.r.t. Sb concentration) while it was 24.8 μ M for the free silibinin.

Bloch et al. reported phytofabrication of zinc oxide particles (ZnOPs) and silver mixed zinc oxide particles (ZnOAg1Ps, ZnOAg10Ps, ZnO10Ag1Ps) using *Plumbago auriculata* leaf extract (PALE) by varying the concentration of the metal precursor salts, i.e., zinc acetate and silver nitrate. It was speculated that the phytochemicals such as polyphenols, flavonoids, reducing sugar, starch, citric acid and plumbagin might have played a significant role in the synthesis and stabilization of the nanoparticles that varied in size from 90 to 400 nm, approximately. The nanocomposite (ZnOAg10Ps) exhibited 95.7% photocatalytic degradation of methylene blue with a rate constant of 0.0463 s⁻¹ that followed a first order kinetics.

Tawre et al. used *Curcuma aromatic* rhizome extract for synthesis of silver nanoparticles (CAAgNPs) with efficient antibacterial, antibiofilm and synergistic effects against multidrug-resistant (MDR) pathogens. The nanoparticles were spherical and monodispersed with size around 13 \pm 5 nm. The minimum inhibitory concentrations (MICs), minimum bactericidal concentrations (MBCs) and minimum biofilm inhibitory concentrations (MBICs) of CAAgNPs against *Pseudomonas aeruginosa*, NCIM 5029 and PAW1, and, *S. aureus*, NCIM 5021 and S8 were in range from 8 to 128 μ g/mL. Pronounced biofilm disruption (50%) and antimicrobial synergy with antibiotics was noted against *P. aeruginosa* PAW1 and *S. aureus* S8.

Yet in another study by Ghosh et al. *T. cordifolia* leaf extract was used for the synthesis of AgNPs with the size ranging from 43.82 \pm 1.023 nm to 91.28 \pm 1.12 nm. Both *Tinospora cordifolia* extract and the AgNPs inhibited the bacteria with the zone of inhibition equivalent to 10–15 mm and 12–18 mm, respectively. The AgNPs inhibited the bacterial biofilm which was speculated to be the result of directly interaction as well as reduction of biofilm associated polysaccharides, lipids, and nucleic acids.

The mini-review by Ngcongco et al. discusses the advances in bacteria, fungi, and plant mediated synthesis metallic nanoparticles with enzymatic activity identical to that of peroxidase, haloperoxidase, oxidase, catalase, hydrolase, and superoxide dismutase. Further, the vital aspects such as toxicity, mechanism and patents in the area of the nanozymes are also covered.

An interesting research by Malhotra et al. reports synthesis of ZnONPs employing an ethanolic extract of *Eupatorium odoratum*. The phytofabricated nanoparticles revealed a hexagonal phase with wurtzite structure with a particle size of ~50 nm that significantly inhibited bacterial pathogens with high killing efficacy (99.99%) at 500 μ g/mL concentration. Further, the commercial central venous catheters (CVCs) coated with the phytofabricated ZnONPs could significantly resist the biofilm formation by *P. aeruginosa*, *E. coli* and *S. aureus*.

Singh et al. employed *Serratia* sp. ZTB29 strain for bacteriogenic fabrication of spherical copper oxide nanoparticles (CuO-NPs) with an average size of 22 nm. It was speculated that the bacterial metabolites with the ester (C=O), carboxyl (C=O), amine (NH),

thiol (S-H), hydroxyl (OH), alkyne (C-H), and aromatic amine (C-N) groups played a key role in the synthesis and stabilization of the CuO-NPs. The nanoparticles could significantly inhibit phytopathogenic bacteria and fungus, such as *Xanthomonas* sp. and *Alternaria* sp., respectively. It is important to note that the treatment with CuO-NPs also improved the growth characteristics of maize plants that support its agricultural applications.

Trzcińska-Wencel et al. reported mycogenic AgNPs and ZnONPs using *Fusarium solani* IOR 825. The AgNPs were spherical with a size of 8.27 nm while the ZnONPs were larger in size (117.79 and 175.12 nm). The nanoparticles inhibited bacterial pathogens, namely, *Agrobacterium tumefaciens* IOR 911, *Pectobacterium carotovorum* PCM 2056, *Pseudomonas syringae* IOR 2188, *Xanthomonas campestris* IOR 512. Also, both AgNPs and ZnONPs inhibited the mycelial growth of *Alternaria alternata*, *Fusarium culmorum*, *Fusarium oxysporum*, *Phoma lingam*, and *Sclerotinia sclerotiorum*. Interestingly, the mycogenic AgNPs exhibited a sterilization effect on maize seeds while ZnONPs promoted the growth of the seedlings with notable improvement in the fresh and dry biomass.

The content of this Research Topic can be summarized as use of biogenic nanomaterials with attractive physicochemical and optoelectronic properties for inhibition of bacteria, fungi, cancer along with environmental and agricultural applications.

Control over the geometry of the nanoparticles can result in the desired optoelectronic and physicochemical properties. Although biogenic nanoparticles are non-toxic and environmentally safe, optimized synthesis methods must be designed. Despite being sustainable and environmentally friendly, biogenic fabrication is often time-consuming because of the cultivation time required to get adequate microbial biomass. Moreover, they are not monodispersed. These challenges can be addressed by rational selection of microorganisms, optimization synthesis parameters such as duration, pH, temperature, concentration of precursors, culture age, and cell density. This may allow scale up for large-scale production of nanoparticles.

Another important aspect is the recovery of the intracellularly synthesized nanoparticles. While it is easier to recover the extracellular nanoparticles by employing either filtration or centrifugation, recovery of the intracellularly produced nanoparticles may involve cell disruption by physical, chemical, and/or biological methods. The cells can be disrupted by ultrasonication, freeze-thaw, SDS, NaOH treatment for release of the nanoparticles from the cell interior. Detailed mechanism for the synthesis can be deciphered by integrated approach using genomics, proteomics and metabolomics. Further, genetically modified microbes can be developed with high nanobiotechnological potential with desired control over shape and size. The functionalization studies will help to understand the surface modification, drug loading efficiency, drug release kinetics, targeted delivery, drug uptake, accumulation, and stability that will help to develop novel nanomedicine. In view of the background, this Research Topic will enable the rational development of bioprocesses for synthesis, recovery, modification and application of tailor made nanostructures using bacteria, fungi, plants and their metabolites.

Author contributions

SG: Conceptualization, Funding acquisition, Validation, Writing–original draft, Writing–review and editing. RT: Conceptualization, Validation, Writing–original draft, Writing–review and editing. ST: Funding acquisition, Validation, Writing–original draft, Writing–review and editing.

Acknowledgments

SG acknowledges Kasetsart University, Bangkok, Thailand for a Post Doctoral Fellowship and funding under the Reinventing University Program (Ref. No. 6501.0207/9219 dated 14 September 2022). SG is also thankful to The Program Management Unit for Human Resources & Institutional Development and Innovation (PMU-B) for funding the proposal entitled “Developing High Performance workforce in Postdoc and Postmaster under Research Topic “Study and Development of Porous Nanofibers, Graphene Oxide Quantum Dot Nanofiber Composite, and Metal Doped Graphene Oxide Quantum Dot Nanofiber Composite for Carbon Dioxide Reduction and

Capture” under the Program of National Postdoctoral and Postgraduate System approved by PMU-B Board Committees (Contract Nos. B13F660065).

Conflict of interest

The authors declare that the research was conducted in the absence of any commercial or financial relationships that could be construed as a potential conflict of interest.

The author declared that they were an editorial board member of Frontiers, at the time of submission. This had no impact on the peer review process and the final decision.

Publisher’s note

All claims expressed in this article are solely those of the authors and do not necessarily represent those of their affiliated organizations, or those of the publisher, the editors and the reviewers. Any product that may be evaluated in this article, or claim that may be made by its manufacturer, is not guaranteed or endorsed by the publisher.

Reference

Patil, S., and Chandrasekaran, R. (2020). Biogenic nanoparticles: a comprehensive perspective in synthesis, characterization, application and its challenges. *J. Genet. Eng. Biotechnol.* 18, 67. doi:10.1186/s43141-020-00081-3



Fabrication of Guided Tissue Regeneration Membrane Using Lignin-Mediated ZnO Nanoparticles in Biopolymer Matrix for Antimicrobial Activity

OPEN ACCESS

Edited by:

Andreas Rosenkranz,
University of Chile, Chile

Reviewed by:

Agnieszka Maria Jastrzebska,
Warsaw University of Technology,
Poland
Yebin Xu,
Huazhong University of Science and
Technology, China

*Correspondence:

Syed Ali Raza Naqvi
draliraza@gcu.edu.pk
Nawshad Muhammad
nawshad.ibms@kmu.edu.pk
Sadaf UI Hassan
sadaf.hassan@umt.edu.pk

Specialty section:

This article was submitted to
Nanoscience,
a section of the journal
Frontiers in Chemistry

Received: 17 December 2021

Accepted: 21 March 2022

Published: 19 April 2022

Citation:

Bilal B, Niazi R, Nadeem S, Farid MA,
Nazir MS, Akhter T, Javed M,
Mohyuddin A, Rauf A, Ali Z, Naqvi SAR,
Muhammad N, Elkaeed EB,
Ibrahim HA, Awwad NS and
Hassan SU (2022) Fabrication of
Guided Tissue Regeneration
Membrane Using Lignin-Mediated
ZnO Nanoparticles in Biopolymer
Matrix for Antimicrobial Activity.
Front. Chem. 10:837858.
doi: 10.3389/fchem.2022.837858

**Bushra Bilal¹, Rimsha Niazi², Sohail Nadeem², Muhammad Asim Farid³,
Muhammad Shahid Nazir¹, Toheed Akhter², Mohsin Javed², Ayesha Mohyuddin²,
Abdul Rauf², Zulfiqar Ali⁴, Syed Ali Raza Naqvi^{5*}, Nawshad Muhammad^{6*},
Eslam B. Elkaeed⁷, Hala A. Ibrahim^{8,9}, Nasser S. Awwad¹⁰ and Sadaf UI Hassan^{1,2*}**

¹Department of Chemistry, COMSATS University Islamabad, Lahore Campus, Lahore, Pakistan, ²Department of Chemistry, School of Sciences, University of Management and Technology, Lahore Campus, Lahore, Pakistan, ³Department of Chemistry, Division of Science and Technology, University of Education, Lahore, Pakistan, ⁴Department of Chemical Engineering, COMSATS University Islamabad, Lahore Campus, Lahore, Pakistan, ⁵Department of Chemistry, Government College University, Faisalabad, Pakistan, ⁶Department of Dental Materials, Institute of Basic Medical Sciences, Khyber Medical University, Peshawar, Pakistan, ⁷Department of Pharmaceutical Sciences, College of Pharmacy, Almaarefa University, Riyadh, Saudi Arabia, ⁸Biology Department, Faculty of Science, King Khalid University, Abha, Saudi Arabia, ⁹Department of Semi Pilot Plant, Nuclear Materials Authority, Cairo, Egypt, ¹⁰Chemistry Department, Faculty of Science, King Khalid University, Abha, Saudi Arabia

Periodontal disease is a common complication, and conventional periodontal surgery can lead to severe bleeding. Different membranes have been used for periodontal treatment with limitations, such as improper biodegradation, poor mechanical property, and no effective hemostatic property. Guided tissue regeneration (GTR) membranes favoring periodontal regeneration were prepared to overcome these shortcomings. The mucilage of the chia seed was extracted and utilized to prepare the guided tissue regeneration (GTR) membrane. Lignin having antibacterial properties was used to synthesize lignin-mediated ZnO nanoparticles (~Lignin@ZnO) followed by characterization with analytical techniques like Fourier-transform infrared spectroscopy (FTIR), UV-visible spectroscopy, and scanning electron microscope (SEM). To fabricate the GTR membrane, extracted mucilage, Lignin@ZnO, and polyvinyl alcohol (PVA) were mixed in different ratios to obtain a thin film. The fabricated GTR membrane was evaluated using a dynamic fatigue analyzer for mechanical properties. Appropriate degradation rates were approved by degradability analysis in water for different intervals of time. The fabricated GTR membrane showed excellent antibacterial properties against *Staphylococcus aureus* (*S. aureus*) and *Escherichia coli* (*E. coli*) bacterial species.

Keywords: ZnO nanoparticles, mucilage, lignin, GTR membrane, antimicrobial activity

INTRODUCTION

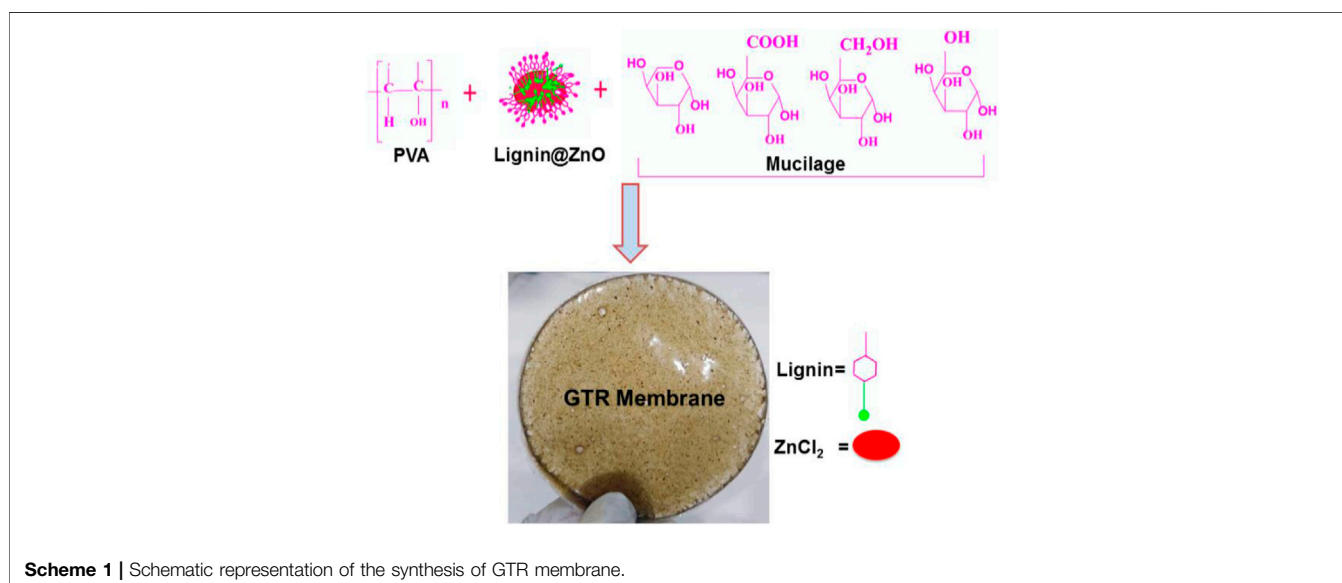
Guided tissue regeneration (GTR) techniques have been effectively used to treat periodontal problems and have supported the possibility of bone regeneration. GTR is a distinctive healing approach for periodontal infections (Caballé-Serrano et al., 2019). This technique uses the membranes as mechanical barriers to produce a gap around the flaws, allowing the formation of a new bone without the struggle for space by the nearby connective tissues. Membranes for GTR treatment must be biocompatible, have the appropriate degradation summary, have good physical and mechanical properties, and have enough continuous power (Shi et al., 2014; He et al., 2017; Khorshidi et al., 2018). GTR membranes should be permeable for cellular adaptation and adequate nutrient approval. Usually, the membranes are distributed into two classes: 1) non-resorbable and 2) bio-resorbable membranes. Non-resorbable membranes like expanded polytetrafluoroethylene (*e*-PTFE) should be detached after implantation through the surgical process.

On the other hand, bio-resorbable membranes involving collagen-based membranes are not essential to be removed since they reduce by period and do not need surgical removal (Caballé-Serrano et al., 2019; Ahmadi et al., 2020; Sadaf Ul et al., 2021). Moreover, non-biodegradable membranes made from titanium and polytetrafluoroethylene (PTFE) seem to be in great danger of postoperative problems as a second surgical process is necessary to recover implantations (Caballé-Serrano et al., 2019). So, biodegradable resources could be highly appropriate for the fabrication of the GTR membrane (Liu et al., 2020). Periodontal infections rise from constant inflammation, started by the accumulation of bacteria inside the dental tissue cells. Periodontitis development will have severe consequences like the fascination of alveolar bone tissues, the parting of epithelial tissues from the tooth, and the disruption of the periodontal ligament cells (PDL). Numerous

biomaterials have been examined for the GTR application (Xue et al., 2014; Liang et al., 2020; Zhang et al., 2020). While choosing an ideal biomaterial for the GTR membranes, the subsequent needs must be measured, such as wound maintenance, space creation and protection, the safety of the fundamental blood clot, and the capability to eliminate undesirable tissues (Mota et al., 2012). Collagen has been one of the most common resources used to fabricate GTR membranes. However, this biomaterial is obtained from animal resources and has a connected danger of infection spread and related moral and ethnic issues, and causes immunogenic responses too.

Chitosan has drawbacks involving poor mechanical strength during its swelling, reducing its usage in various fields. Furthermore, its low mechanical power and the rapid resorption level of this biomaterial are a concern to several clinicians. In addition, by the enzymatic action of macrophages, polymorphonuclear leucocytes, and numerous microbes, fast collagen degradation can generate collagenase, which restricts membrane resistance to collapse. This result permits undesired cells to arrive at the wound place (Sela et al., 2003). Furthermore, the antibacterial action of the chitosan-based membrane is inferior at a neutral pH, restricting its use as an antibacterial (Hezma et al., 2019). Since collagen and chitosan-based membranes have presented such restricted properties, fresh and new resources with good properties are a requisite (Bottino et al., 2011). Natural polymers are sustainable and more biocompatible, and possess a higher biodegradable rate than synthetic polymers.

Moreover, natural polymers can display receptor-binding ligands to the cells. However, low mechanical strength restricts their application. For GTR applications, pure synthetic polymer or natural polymer scaffolds are generally insufficient. Pure synthetic polymers may have poor rigidity, hydrophobic character, or comparatively less bioactivity. On the other hand, the degradation results of the synthetic polymers are occasionally unfavorable for the freshly produced tissue. In contrast, the



natural polymers may reduce so rapidly (biodegradable) to be utilized for the GTR. Therefore, an anticipated method is required that includes the usage of the combinations of synthetic and natural polymers in definite proportions to merge the benefits of both kinds (Abdelaziz et al., 2021).

Current reports show that using ZnO NPs also permits the development of bone growth, increases the osteoblast proliferation process, and prevents both Gram-negative and Gram-positive bacterial growth (Abdulkareem et al., 2015). For several years, Zn has also been utilized in dentistry as the main filler constituent of dental adhesives (Padovani et al., 2015). Lignin is an excellent applicant for the growth of new resources because of the phenolic and aliphatic hydroxyl functional groups in its structure and prevents the development of microbes, including *Staphylococcus aureus* and *Escherichia coli*. The lignin's antimicrobial activity can decrease the danger of bacterial migration on the layer of the material. Mucilage, a natural extract from chia seeds, is unique (Muñoz et al., 2012). Mucilage has an excellent capacity for making films. There is growing attention to natural hydrocolloids for the production of decomposable films due to their non-toxic, low-cost, non-irritating quality, and other benefits (Beigomi et al., 2018). PVA is an extensively used, biocompatible, hydrophilic, water-soluble, and biodegradable synthetic polymer with more excellent mechanical applications appropriate for medical uses, including dental applications, bone regeneration, and wound healing (Zhou et al., 2020). The -OH groups in PVA can be a source of hydrogen bonding and help develop polymer composites (Khodiri et al., 2020).

In this study, we synthesized and introduced the Lignin@ZnO nanoparticles, used extracted mucilage from chia seeds to fabricate the GTR membrane, and used the PVA as a thickener and emulsion stabilizer (**Scheme 1**). Because microbial impurities are also the major reason for periodontal diseases, it is necessary to add materials or agents with antibacterial properties, prepare the infection-responsive GTR membrane, and increase its biological and mechanical strength. For this reason, Lignin@ZnO nanoparticles were added because of their broad-spectrum antibacterial properties.

EXPERIMENTAL

Materials

Zinc chloride (ZnCl_2), sodium hydroxide (NaOH), Luria Bertani (LB) broth, and agar nutrients were obtained from Sigma Aldrich and used as received. PVA was purchased from Deajung. Chia seeds were purchased from the local market in Lahore, Pakistan. Ultra-filtered highly purified deionized water was utilized throughout the experimental procedure.

Extraction of Lignin

Lignin was precipitated and attained by centrifugation and further purified by ethanol and ether. According to the previously reported method, lignin was extracted from bagasse (Joshi et al., 2019). First, 20 g bagasse was soaked in 200 ml HCl (0.1 N) solution for 24 h. Then it was filtered and washed with

distilled water. Then bagasse was placed in 100 ml distilled water containing NaOH (3 mg) and 30% H_2O_2 (3 ml) and was irradiated with microwave in a microwave oven for 400 W for 30 min. This bagasse solution was filtered, and the filtrate was acidified by concentrated sulfuric acid to pH 4.

Synthesis of Lignin@ZnO

The Lignin@ZnO nanoparticles were synthesized by using the probe sonication method. Solution A was prepared by adding 0.05 M zinc chloride (0.47 g) into 70 ml of deionized water. Sodium hydroxide (0.3 g) and lignin (0.6 g) were added to 30 ml of deionized water with continuous stirring until lignin was dissolved entirely (solution B). Afterward, solution B was added dropwise into solution A with further stirring for 15 min. The resulted solution was sonicated for 20 min at 60 amplitudes, using a pulse rate with a gap of 5 s. The synthesized sample was separated by centrifuge at 8000RPM for 10 min and dried in the oven at 80°C for 3 h.

Extraction of Mucilage From Chia Seeds

The chia seeds were cleaned manually to eliminate dust particles. Chia seeds were added to the water with water and seeds in a ratio of 20:1 and continuously stirred at 450 RPM. To remove the mucilage layer from the surface of the seeds, the water-seed mixture was stirred by an overhead mixer using a four-blade propeller at 800 RPM for 2 h (Beigomi et al., 2018). Then mucilage was separated from seeds using cheesecloth (**Supplementary Figure S1**).

Preparation of Membrane

PVA (1.6 g) was dissolved in mucilage (8 ml) with continuous stirring until a homogeneous mixture was formed. Three polymeric solutions were prepared in the PVA/mucilage solution by adding various ratios of Lignin@ZnO (1% (0.08 g), 2.5% (0.2 g), and 5% (0.4 g)). The resultant mixtures were stirred to improve the nanoparticles dispersions. Furthermore, 1% glycerol (0.08 ml) was added to each solution as a filler agent. The resulting solutions were stirred for a further half an hour to ensure that the solutions were completely homogeneous. The prepared solutions were poured into three petri dishes. The petri dishes were placed into the oven at 75°C for 3 h. After 3 h, the petri dishes were taken out of the oven, and three membranes of different compositions were prepared. The prepared membranes were evaluated for the antibacterial and mechanical study (**Supplementary Figures S2, S3**).

Characterization

Chemical analysis (functional group identification) of the reaction mixture was performed using Fourier transform infrared spectroscopy (FTIR, Thermo Scientific Nicolet 6700) over a wavelength range from 400 to 4000 cm^{-1} at a resolution 4 cm^{-1} . The optical properties of the synthesized Lignin@ZnO were characterized using UV-visible spectroscopy. UV spectra of the reaction mixture were recorded at (LAMBDA 25) spectrophotometer in the wavelength range of 200–800 nm, whereas resuspending ZnO NPs monitored the stability of ZnO NPs in distilled

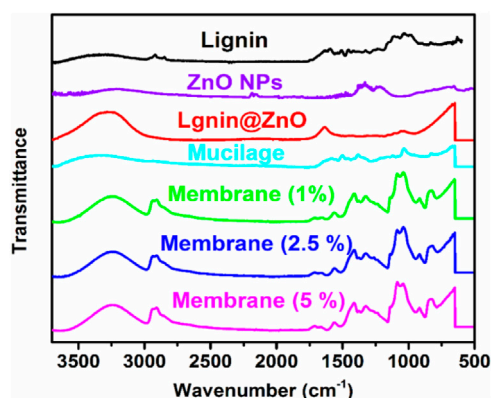


FIGURE 1 | FTIR spectra of lignin, ZnO NPs, Lignin@ZnO, mucilage, 1, 2.5, and 5% Lignin@ZnO-GTR membranes.

water. These aqueous suspensions were sonicated at room temperature (25 min) for the uniform dispersion of ZnO NPs. The surface and cross-sectional morphologies of the fabricated membranes were studied by scanning electron microscopy (SEM, TESCANV LMU). The fabricated novel membranes were observed under an optical microscope (Optika B-600 MET) to evaluate the membrane's morphology and overall fiber structure. The mechanical properties (i.e., tensile strength, Young's modulus, and elongation at break) of all the fabricated membranes were evaluated by using a universal testing machine (electrodynamics fatigue testing machine, Walter + bai AG, Switzerland). Rectangular membranes (30 mm × 5 mm) were tested. The crosshead speed was set at 5 mm/min. The tensile modulus was calculated from the slope of the initial linear part of the curve (Castro et al., 2018). A swelling test determined the swelling index of the membrane. The water content of the GTR membrane was determined by swelling the membrane in pH 7.4 of phosphate-buffered saline (PBS) at room temperature. The dry weight of the membranes was measured to estimate the amount of antibiotic solution that the membrane could absorb. After measuring the dry weight, the membranes were immersed in PBS for different time intervals (30 min, 1, 2, 4, and 24 h) to confirm the perfect swelling.

$$\text{Water intake (\%)} = \frac{W_w - W_i}{W_i} \times 100, \quad (1)$$

where W_i is the initial weight of the sample and W_w is the weight of a sample after dipping in PBS (Lian et al., 2019). The *in vitro* antibacterial activity of the fabricated membrane-synthesized Lignin@ZnO and commercial zinc oxide powder was examined against *Staphylococcus aureus* (*S. aureus*, ATCC 6538 a representative Gram-positive bacteria) and *Escherichia coli* (*E. coli*, ATCC 8739 a representative Gram-negative bacteria) through the detection of the inhibition zone using the disc diffusion method. After that, 0.32 g of nutrient broth was taken in two different flasks with 25 ml of water in each flask,

and it was then autoclaved at 121 °C for 21 min. It was cooled, and in one flask, Gram-positive bacteria were added, and in another flask, Gram-negative bacteria were added. These flasks were kept for 24 h in a shaker. Then in another flask, 200 ml water was taken and 2 g of nutrient broth and 4 g agar were added to it. It was heated and stirred until the water boiled. Then this mixture was poured into a petri dish and was cooled, and the flask placed in the incubator was taken out from the incubator after 24 h of incubation. Bacterial culture was carried out using the incubated bacteria, and nutrient agar plates were swabbed with bacterial strain broth to form a lawn growth of *E. coli* and *S. aureus*. Small pieces of the prepared membrane were placed on the petri plates. The plate was then placed in an incubator at 37 °C for 24 h (Lian et al., 2019).

Amoxicillin and tetracycline disks were used as standard antibiotic discs. Tetracyclines are a collection of broad-spectrum antibiotics that can prevent protein synthesis by binding to the ribosomal subunit in the mRNA translation complex (Qiu et al., 2020). Amoxicillin is used to treat a large diversity of bacterial contaminations. This medication is a penicillin-type antibiotic. It works by preventing bacterial growth. This antibiotic treats only bacterial infections. Amoxicillin is used in dentistry to treat dental alveolar abscesses, endodontic infections, and advanced forms of periodontal diseases. So, elements that promote an increase in amoxicillin resistance in the oral microbiota are of concern to both medical and dental practitioners (Zhao et al., 2021). After 24 h, plates were taken out from the incubator, and the diameter of the zone of inhibitions around the antibiotic disc was measured in millimeters. The experiments were performed in triplicate. Results showed that both synthesized Lignin@ZnO and fabricated novel membranes presented prominent bactericidal activity against both bacterial strains.

Morphology Investigation of Bacteria

The cultures of bacteria were centrifuged for 2 min at 6,000 rpm, washed three times with phosphate-buffered saline (PBS, 7.4), and mixed with 2.5% glutaraldehyde solution for 4 h. The cells were dehydrated with consecutive treatment of 30, 50, 70, 80, 90, and 100% ethanol for 15 min, respectively. The dehydrated cells were coated with gold by sputtering under vacuum and imaged using a FE-SEM. Using the FE-SEM, the morphological changes of bacterial cells were observed after treating the samples for 24 h.

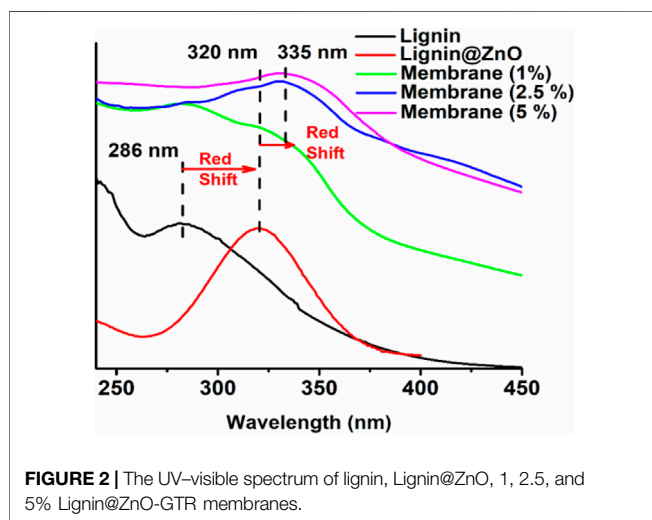
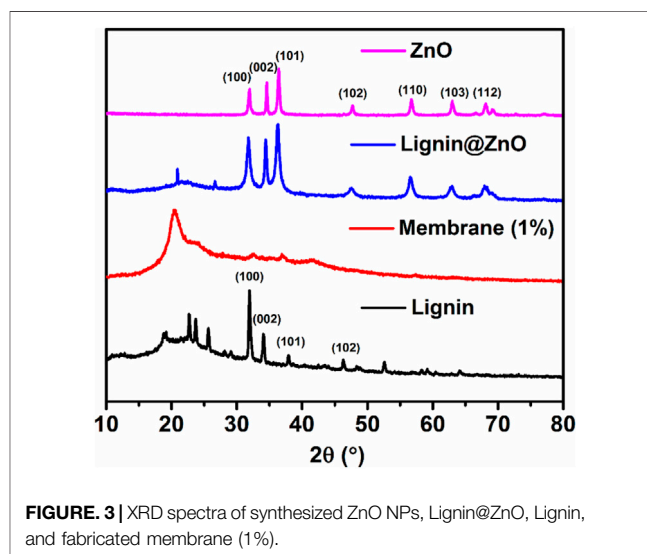
RESULTS AND DISCUSSION

FTIR Analysis

FTIR spectra was used to identify the presence of different functional groups in the tested samples. FTIR spectra of ZnO, mucilage, Lignin@ZnO, and 1, 2.5, and 5% Lignin@ZnO-GTR membranes is shown in **Figure 1** while all the frequencies exhibited by the different functional groups are compiled in **Table 1**. The pure ZnO spectrum peaks at 530 cm⁻¹, which shows the ν -Zn-O stretching frequency (Jose et al., 2020). Mucilage shows various peaks at 3,340 cm⁻¹, 1,045 cm⁻¹, 1,607 cm⁻¹, and 1,508 cm⁻¹ for ν -OH (broad), ν -C-O-C of

TABLE 1 | FTIR data of ZnO, Lignin@ZnO, mucilage, 1, 2.5, and 5% Lignin@ZnO-GTR membranes.

ZnO	Lignin	Lignin@ZnO	Mucilage	Membranes			Assignments
				1%	2.5%	5%	
-	-	3,270	3,344	3,251	3,239	3,245	ν (OH stretching) from carbohydrate and lignin
-	-	-	-	2,928	2,923	2,923	ν (C-H aromatic) from phenolic lignin
-	-	-	-	1,707	1,707	1,719	ν (C=O stretching) from carbohydrate
-	-	1,639	1,601	1,564	1,551	1,558	ν (C-H aliphatic stretching) from mucilage
-	1,457	1,639	-	1,558	1,570	1,558	ν (C=C aromatic stretching) from lignin
-	-	-	1,508	1,409	1,415	1,421	ν (-COO carboxyl group) from mucilage and uronic acid
-	1,515	-	-	1,409	1,415	1,415	ν (-CH ₃ stretching) from lignin phenolic compounds
-	-	1,130	1,124	1,130	1,130	1,136	ν (C-O bending) from pyranose
-	-	1,043	1,037	1,043	1,037	1,031	ν (C-O-C) stretch and ν (C-O-H) bending
-	-	-	1,037	1,056	1,043	1,074	ν (C-O-C stretching) from glycosidic linkage
500–600	-	525	-	528	527	529	Stretching of ZnO NPs

**FIGURE 2** | The UV-visible spectrum of lignin, Lignin@ZnO, 1, 2.5, and 5% Lignin@ZnO-GTR membranes.**FIGURE 3** | XRD spectra of synthesized ZnO NPs, Lignin@ZnO, Lignin, and fabricated membrane (1%).

glycosidic linkage imide-1 in chia seeds mucilage, and ν -COO for uronic acids, respectively (Darwish et al., 2018). Spectrum for Lignin@ZnO shows peaks at 3,270 cm^{-1} (broad, ν -OH stretching), 1,037 cm^{-1} (ν -C-O-C stretching) for phenol units, and 1,639 cm^{-1} (ν -C-H stretching aliphatic) (Jose et al., 2020). The peaks at 1,080 cm^{-1} and 1,180 cm^{-1} are characterized as C-O-C stretching. The FTIR spectrum for Lignin@ZnO exhibits almost all peaks of pure lignin, which indicates that mediation of ZnO into lignin is successfully done. Different membranes are formed by adding mucilage and different loading ratios of Lignin@ZnO, which shows other peaks corresponding to mucilage and lignin. The FTIR spectrum of membranes shows a peak at 3,251 cm^{-1} (ν -OH stretching), but the peak value is lower than the lignin and mucilage -OH peak, which confirms the presence of hydrogen bonding between different components in the membrane (Pulit-Prociak et al., 2020).

A fragile band around 1,500 cm^{-1} is the characteristic band of the lignin (Cámara et al., 2020). A peak around 1,457 cm^{-1} is a deformation of lignin CH₂, and CH₃ is stated to be stretching the C=O and C=C lignin aromatic rings (Lun et al., 2017). Membranes also show stretching frequency at 2,928 cm^{-1} for aromatic ν -C-H bonds, indicating the presence of phenolic units

from lignin. A peak at 1,037 cm^{-1} showed the C-O-C glycosidic linkage from mucilage polysaccharides. In membranes, band at 1,419 cm^{-1} indicates the CH₂ bending, the peak at 1,165 cm^{-1} shows the stretching of C-O, the band at 1,080 cm^{-1} to 1,090 cm^{-1} represents the bending of the OH group, and the peak at 843 cm^{-1} carbon-carbon stretching. Furthermore, the peak at 1,409 cm^{-1} (for ν -COO carboxylic group) from uronic acids of polysaccharide of mucilage, 1,558 cm^{-1} (for ν -C=C stretch) from phenolic units, 1,564 cm^{-1} (aliphatic ν -C-H stretching) from lignin and mucilage, and 500–600 cm^{-1} from ZnO further confirm the formation of the GTR membrane (Figure 1 and Table 1).

UV-Visible Analysis

The UV-visible spectra of lignin, Lignin@ZnO, 1, 2.5, and 5% membranes are shown in Figure 2. The peak at 286 nm is attributed to extended conjugation with different substituents on the cyclic benzene ring of lignin (Joshi et al., 2019). The peak at 320 nm is associated with lignin-mediated ZnO nanoparticles (Lignin@ZnO). The absorption peak shift toward the higher wavelength (redshift) is observed twice during this whole

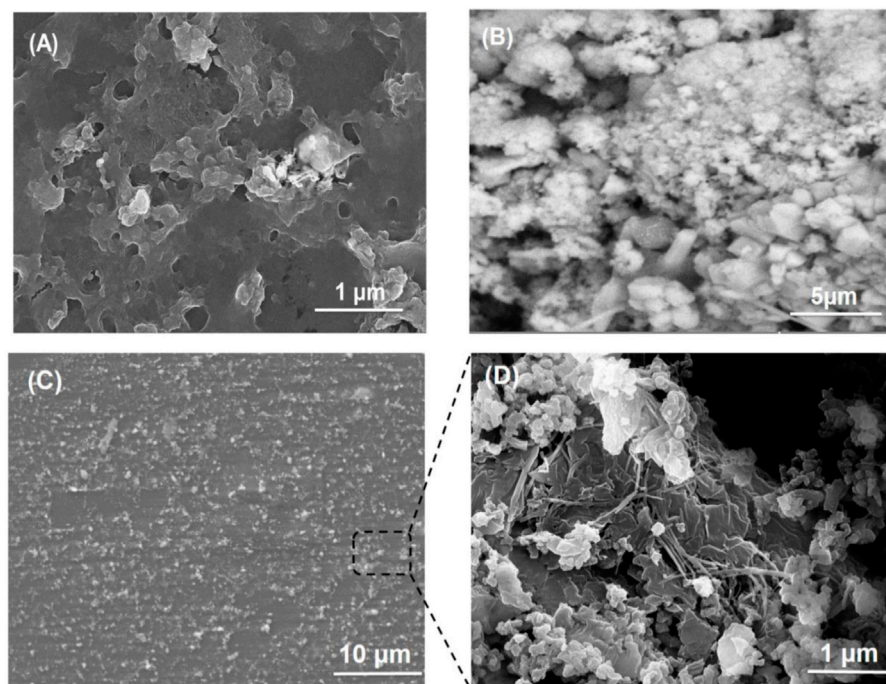


FIGURE 4 | SEM images of (A) PVA/mucilage, (B) Lignin@ZnO, and (C) Lignin@ZnO-GTR membrane, and (D) zoom image of the cross section from (C).

procedure: first, during the complex formation of Lignin@ZnO and second, when the GTR membrane was formed by adding the mucilage and PVA into the Lignin@ZnO with different loading ratios such as 1%, 2.5%, and 5% (wt./wt.). The peak intensities are increased as we increase the loading ratios of Lignin@ZnO. The broad peaks are observed at ~ 335 nm for differently loaded membranes (1%, 2.5%, and 5%). This redshift phenomenon confirmed the Lignin@ZnO and GTR membrane formation in the first and second steps, respectively (Patra et al., 2014; Joshi et al., 2019; Jose et al., 2020).

XRD Results

The crystalline structure, crystal orientation, phase purity, and the crystallite size of the synthesized ZnO NPs, Lignin@ZnO, pure lignin, and fabricated GTR membrane were characterized by XRD analysis. XRD diffractogram of ZnO NPs and Lignin@ZnO displayed characteristic peaks at 31.87° , 34.54° , 36.46° , 47.67° , 56.85° , 62.84° , and 68.19° , which can be attributed to 100, 002, 101, 102, 110, 103, and 112 reflection planes of a hexagonal wurtzite structure of ZnO NPs (Figure 3).

Similarly, a diffractogram of lignin displays the diffraction peaks at 31.87° , 34.16° , 37.99° , 46.27° , and 52.51° , which also agree with 100, 002, 101, 102, 110, 103, and 112 reflection planes. Previously, many studies have reported the hexagonal wurtzite structure of ZnO NPs. The vigorous intensity and narrow width of diffraction peaks of both types of synthesized ZnO NPs revealed that the resulting nanoparticles were highly crystalline (Abbasi et al., 2017). Lignin@ZnO showed an intense peak, which belonged to the (100) plane; it was higher than that observed for the (100) plane. As no characteristic peak for impurity originated,

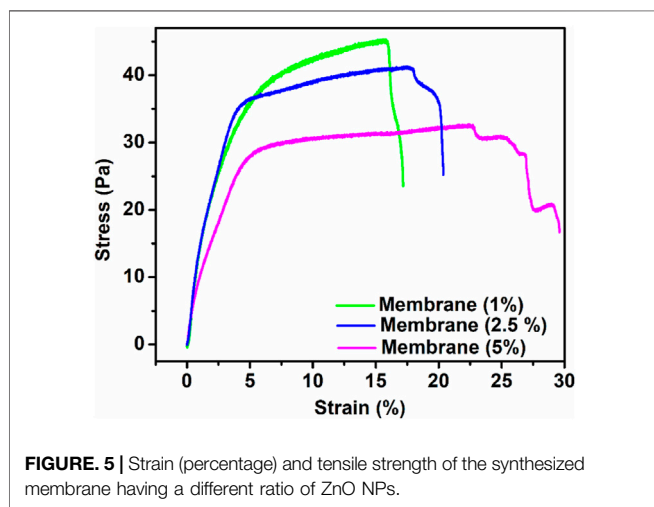
the synthesized ZnO nanoparticles can be considered to have excellent crystalline nature. The main change was detected in the peak widths with the similarity in the unit cell parameters of both forms of synthesized ZnO nanoparticles with lignin and without lignin. The broadening of peaks in XRD was a consequence of a decrease in crystallite size. In the XRD pattern of the GTR membrane, the diffraction peak situated at 20.51° is allocated to a semicrystalline structure of the GTR membrane (Joshi et al., 2019).

SEM Study

SEM images of PVA/mucilage, Lignin@ZnO, and Lignin@ZnO-GTR membrane (containing 1% @Lignin@ZnO) are shown in Figure 4. Figure 4A shows an SEM micrograph of chia seed mucilage with PVA. When PVA is added with chia seed mucilage, then there will be smooth morphology like a polymer structure inside (Dehghani et al., 2020); on the upper surface, agglomeration is shown due to evaporation of water from the surface that would lead toward the partial insolubility of mucilage and its accumulation (Salazar Vega et al., 2020). In this study, attained ZnO NPs seemed irregular in shape, and the size of the particles is in the nano range, mostly less than 50 nm. However, the particles are agglomerated, as shown in Figure 4B. The obtained results clearly illustrate that the Lignin@ZnO was well prepared without impurities. But in the membrane, Lignin@ZnO particles dispersed throughout the membrane because of biopolymer addition and cavities provided by those polymers. EDX studies of ZnO NPs and membranes are shown in Supplementary Figures S4, S5.

TABLE 2 | E modulus, strain (percentage), and tensile strength of the synthesized 1, 2.5, and 5% Lignin@ZnO-GTR membranes.

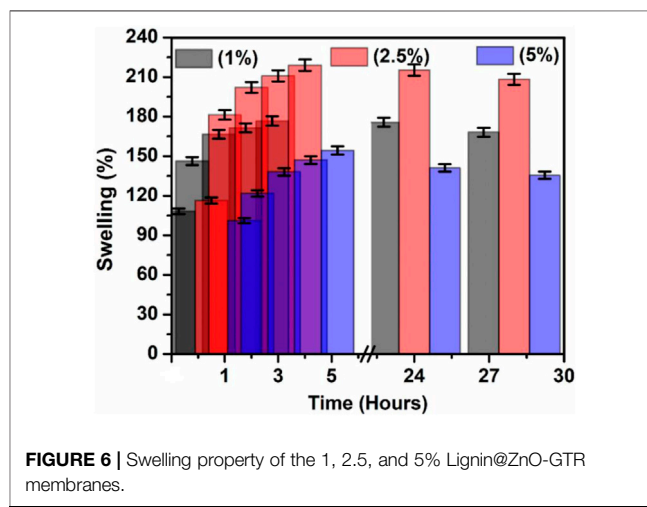
Sample	E-modulus (GPa)	Tensile strength (Pa)	Strain percentage (%)
Lignin@ZnO-GTR membranes (1%)	0.12	22.66	66.43
Lignin@ZnO-GTR membranes (2.5%)	0.07	18.73	71.42
Lignin@ZnO-GTR membranes (5%)	0.19	14.36	91.59



Morphological Analysis

Figure 4 shows the microscopic evaluation of the membranes in which randomly interconnected structures, smooth morphology, and distributions of Lignin@ZnO are observed. As stated previously, morphological examinations of membranes revealed that Lignin@ZnO percentage increased, and fibers became rougher in membranes (Münchow et al., 2015). The water drop could not penetrate wild and smooth fibers. The observed difference could be a consequence of the change in the surface properties of membranes like roughness (Türkkan et al., 2017). However, it could be found that the morphology of fibers, including diameter, porosity, and surface structure, was influenced by many processing parameters such as viscosity of suspension determined by polymer concentration and additives (Ahmadi et al., 2020).

When biopolymers (PVA/mucilage) solutions are mixed with Lignin@ZnO, they exhibit the electrostatic force of interactions (i.e., hydrogen bonding) between PVA, mucilage, and Lignin@ZnO. During the hydrogen bonding formation, the interaction of polymers with each other would not be fine but random-like structure because of the extraction procedure. When the extraction is applied, it causes disturbance in the orientation of the polymer matrix. Figure 4 membrane image shows some cracks presumably caused by air bubbles incorporated during membranes formation (Figure 4B). Moreover, some particles with thread forms (increased as Lignin@ZnO concentration increased) were observed, which can be attributed to the mucilage structure (Beigomi et al., 2018).



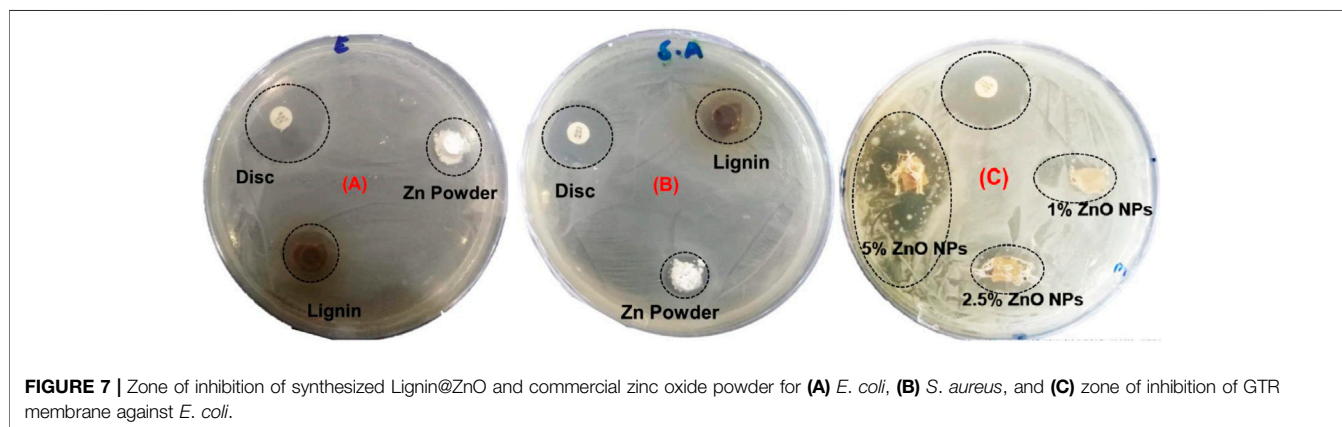
Mechanical Properties

First, prepared membranes were cut into 5-mm-width and 35-mm-long strips. The load–deformation curves at a speed of 5 mm/min were recorded (He et al., 2019) to obtain the stress–strain curves of the membranes. The mechanical performance (e.g., tensile strength, Young's modulus, and strain) of the synthesized membranes is presented in Table 2. According to previous results, the mechanical properties of the polymer matrix composites filled with nanoparticles could be influenced by fixed or variable parameters such as the chemical composition of matrix and filler and interaction between them, membrane architecture, morphology, size, and dispersion nanoparticles. Among the aforementioned parameters, distribution of Lignin@ZnO, fiber diameter, and interaction between Lignin@ZnO and polymer chains play essential roles in the final mechanical properties of the membrane (Ahmadi et al., 2020). The addition of the Lignin@ZnO decreased the mechanical characteristics; however, strain increased, which was improved with an increased percentage of Lignin@ZnO, as shown in Figure 5 (Münchow et al., 2015).

The tensile strength of the membrane having Lignin@ZnO (5 wt%) was lower than the other membrane having 2.5 and 1 Lignin@ZnO wt%. It may be attributed to the fact that during solution casting, the Lignin@ZnO particles dispersed in the polymer matrix decreased the physical cross-link strength between the polymer blend chains and Lignin@ZnO due to aggregation nano-filler in a polymer matrix; as a result, fractures quickly developed. The increase in toughness value with an increase in the content of Lignin@ZnO has been

TABLE 3 | Membrane swelling degrees of various types of fabricated membranes.

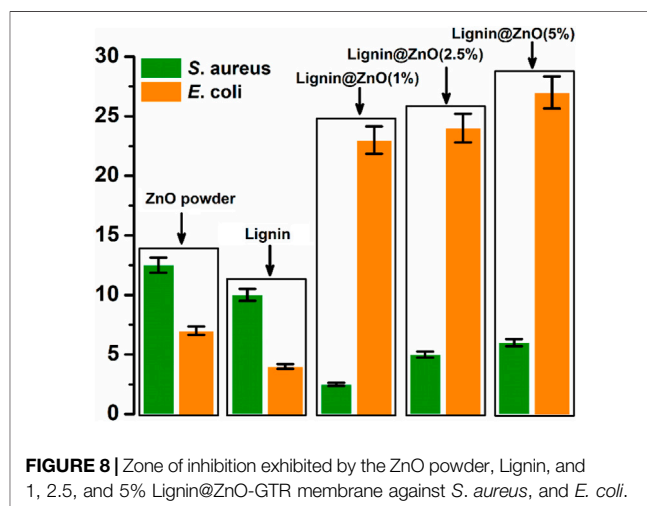
Time	Swelling ratio of Lignin@ZnO-GTR membrane (1 %)	Swelling ratio of Lignin@ZnO-GTR membrane (2.5 %)	Swelling ratio of Lignin@ZnO-GTR membrane (5 %)
30 min	108.2	116.4	101.1
Hour	146.3	181.3	121.8
2 h	166.6	202.1	138.1
3 h	171.4	210.9	147.1
4 h	176.6	219.0	154.3
24 h	175.7	215.3	141.1
28 h	168.1	208.3	135.5



ascribed to the rise in the polymeric matrix local density. This result reveals that the dispersion of the Lignin@ZnO in composites plays a significant role in determining the elasticity modulus, tensile strength, and toughness (Hezma et al., 2019). Enhancing the ratio of the Lignin@ZnO causes the disposition of the accumulations. The occurrence of these bunches reduced the actual weight move from the polymer medium to the filler by decreasing the surface capacity in association with NPs and causing the stress ratio, causing the lower stress transmission at the boundary and eventually the mechanical characteristics (Figure 5; Table 2) (Makaremi et al., 2016).

Swelling Properties

The detection of water absorption properties is essential in studies on barrier membranes. Higher water absorption performance results in better nutritional uptake ability and exudate absorption by a GTR membrane, which will promote cell growth and the absorption of inflammatory exudates by the GTR membrane. Different types of cross-linked hydrogel swelling studies have been conducted using this procedure (Türkkan et al., 2017). Then there is a slight decrease in swelling capacity for all samples until equilibrium after 24 h was reached (Kowalski et al., 2019). The degree of swelling also decreases with the increasing concentration of Lignin@ZnO (He et al., 2017). Based on the literature, the appropriate penetration, uniform distribution, and effective size of zinc oxide nanoparticles may decrease the hygroscopicity (Soltani et al.,



2013). The swelling data show that the membrane having 1% Lignin@ZnO has the highest swelling ratio and that of the 5% Lignin@ZnO membrane was the smallest, as shown in Figure 6. Analyzing the water absorption results, the maximum amount of water absorption after 30 min can be observed. The result indicates that an increased concentration of Lignin@ZnO reduced the actual water absorption performance of the GTR membrane. The swelling degree of each of the membranes is presented in Table 3.

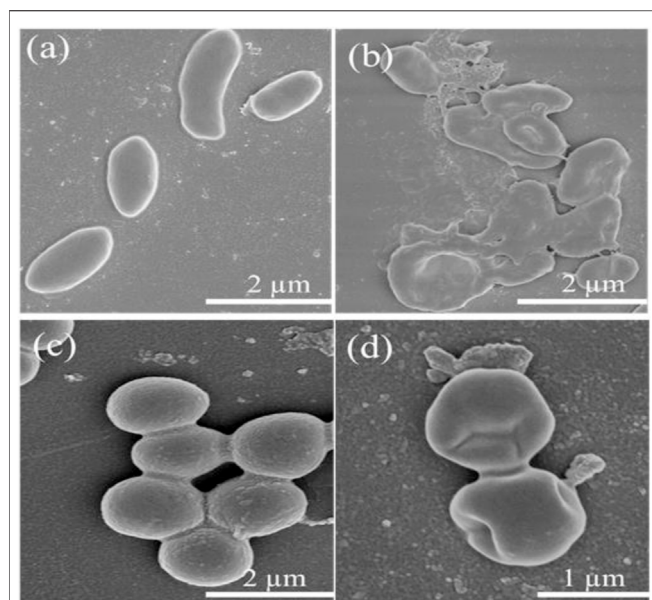


FIGURE 9 | FESEM images of (A–B) *E. coli* and (C–D) *S. aureus* treated with different time: (A,C) 0 h and (B,D) 24 h.

Antibacterial Activity

Among all metal nanoparticles, ZnO NPs are biocompatible and show non-toxicity with human cells. These features of ZnO NPs make them potent against many microorganisms (Abbasi et al., 2017). The agar disk diffusion process was utilized to detect the antibacterial activity, as shown in **Figure 7**. This study evaluated the antibacterial efficacy of synthesized ZnO NPs, commercial zinc oxide powder (ZnO), and fabricated GTR membranes toward two bacterial strains *Escherichia coli* and the *Staphylococcus aureus*. Sterilization of membranes, by irradiation, has been examined and analyzed. All the samples were sterilized using UV light, which successfully inactivates microorganisms. The optical images showed that synthesized Lignin@ZnO and fabricated membranes showed strong antibacterial results compared to commercial zinc oxide powder and lignin alone, as shown in **Figure 7A–C**.

The comparative results are also shown in **Figure 7**. The antibacterial action in the membrane and ZnO NPs is due to the production of reactive oxygen species (ROS) and metal ions (Zn^{2+}) (Aadil et al., 2019). These bind to the membrane of the bacteria and hinder the protein transport channels that disturb the transport of materials within the membrane. These can also attach to the DNA and different enzymes alter the shape and structure of the enzymes and DNA and disturb their functioning (Aadil et al., 2019). The bactericidal property of zinc oxide nanoparticles may be recognized for their capability to interrelate with the cell membrane of numerous bacterial classes. Zinc powerfully combines with proteins and lipids, altering the osmotic equilibrium and enhancing the membrane permeability (Abdulkareem et al., 2015). Furthermore, ZnO NPs enhance the oxidative pressure inside the bacteria cell due to their capability to produce Zn^{2+} ions and the reactive oxygen species

(ROs) inside the microbial cells, which can also prevent the development of the planktonic bacterial species (Padovani et al., 2015). ZnO NPs have selected poisonousness to bacterial species and have antibacterial properties against spores (microorganisms) that are temperature-resistant and pressure-resistant (Murfadunnisa et al., 2019). Some studies display a negative association between the size of the nanoparticles and cytotoxicity. However, there is no such relation in the literature about this activity for the zinc oxide NPs (Garcia et al., 2018). ZnO NPs are also biocompatible and biologically safe with distinctive structural, thermal, and electrical applications, changing particle morphology, size, orientation, and shape (Abbasi et al., 2017).

The zone of inhibition around the membrane displays the limit of progress of the bacteria around the membrane locality. This procedure shows that the membrane and Lignin@ZnO NPs can prevent the gain of the microbes, so in the periodontal tissue, it can inhibit the colonization of the bacteria. The zone of inhibition is explained via the graph in **Figure 8**. The antibacterial property of Lignin@ZnO and membranes is greater than that of commercial ZnO powder. Lignin@ZnO showed greater efficacy for *S. aureus* than for *E. coli*. All membranes (1, 2.5, 5%) showed excellent antibacterial properties against *E. coli* compared to *S. aureus*. The inhibition zone test demonstrates that Lignin@ZnO-GTR has a better antimicrobial ability than free ZnO.

Furthermore, the morphological changes of Lignin@ZnO-GTR toward the bacteria (*E. coli* and *S. aureus*) were observed using the field emission scanning electron microscope (FE-SEM). Intact *E. coli* and *S. aureus* in **Figures 9A,C** have distinct outer membranes, indicating that high-vacuum and high-energy electron beams do not affect bacteria cell structure. However, after co-incubation with Lignin@ZnO-GTR for 24 h, the cellular cohesion was weakened with heavy damage to the outer membranes (**Figures 9B,D**), and death of bacteria may occur due to cytoplasm outflow. In general, the cell of *E. coli* is less thick than *S. aureus*, and more damage to *E. coli* was observed (Abdul et al., 2019; Rauf et al., 2019; Liu et al., 2021).

CONCLUSION

The present study fabricated the guided tissue regeneration membrane (GTR) using Lignin@ZnO and extracted mucilage from chia seeds. In periodontal regeneration, GTR membranes are seen as an attractive strategy. The addition of Lignin@ZnO nanoparticles to the membrane enhanced the antibacterial properties and strength of the membrane. The chemical structures and properties of the materials were characterized using UV–visible spectroscopy, FTIR, and SEM after every reaction process. Moreover, the FTIR results presented satisfactory relations between ZnO nanoparticles, polymer, and mucilage. The SEM images showed that the ZnO NPs have agglomeration and a diameter of less than 50 nm. The study of swelling and mechanical properties of fabricated membranes presented satisfactory results; degradation of the fabricated

membrane was started after 24 h. The zone of inhibition against bacterial species for the zinc oxide nanoparticles and membrane was measured more than that for commercial zinc oxide powder. The antibacterial properties of Lignin@ZnO-based GTR membranes resulted in a reduction of *S. aureus* and *E. coli* viability. The membrane exhibited successful results, which proved the potential of the membrane to be used in periodontal regeneration. MTT biocompatibility and hemocompatibility assay can be performed to further evaluate the GTR membrane *in vivo* in a mouse model.

DATA AVAILABILITY STATEMENT

The original contributions presented in the study are included in the article/**Supplementary Material**, further inquiries can be directed to the corresponding authors.

AUTHOR CONTRIBUTIONS

SARN, NM, and SH conceived and designed the experimental project. BB and RN performed the experiments. MF, MN, ZA,

and RA performed FTIR, UV-visible, and antibacterial studies. SARN, SH, SoN, TA, MJ, and AM wrote, edited, and revised the manuscript. EE, HI, and NA performed FE-SEM and XRD characterization. All authors have read and approved the final manuscript.

ACKNOWLEDGMENTS

The authors thank CUI, Lahore campus, and UMT Pakistan, for their financial support. The authors extend their appreciation to the Deanship of Scientific Research at King Khalid University for supporting this work through research groups program (grant number R.G.P.2/107/42). The authors extend their appreciation to Research center at Almaarefa University for funding this work as well.

SUPPLEMENTARY MATERIAL

The Supplementary Material for this article can be found online at: <https://www.frontiersin.org/articles/10.3389/fchem.2022.837858/full#supplementary-material>

REFERENCES

- Aadil, K. R., Pandey, N., Mussatto, S. I., and Jha, H. (2019). Green Synthesis of Silver Nanoparticles Using acacia Lignin, Their Cytotoxicity, Catalytic, Metal Ion Sensing Capability and Antibacterial Activity. *J. Environ. Chem. Eng.* 7, 103296. doi:10.1016/j.jece.2019.103296
- Abbasi, B. H., Anjum, S., and Hano, C. (2017). Differential Effects of *In Vitro* Cultures of *Linum usitatissimum* L. (Flax) on Biosynthesis, Stability, Antibacterial and Antileishmanial Activities of Zinc Oxide Nanoparticles: a Mechanistic Approach. *RSC Adv.* 7, 15931–15943. doi:10.1039/c7ra02070h
- Abdelaziz, D., Hefnawy, A., Al-Wakeel, E., El-Fallal, A., and El-Sherbiny, I. M. (2021). New Biodegradable Nanoparticles-In-Nanofibers Based Membranes for Guided Periodontal Tissue and Bone Regeneration with Enhanced Antibacterial Activity. *J. Adv. Res.* 28, 51–62. doi:10.1016/j.jare.2020.06.014
- Abdul, R., Junwei, Y., Siqi, Z., Ye, Q., Guangyao, W., Ying, C., et al. (2019). Copper(ii)-based Coordination Polymer Nanofibers as a Highly Effective Antibacterial Material with a Synergistic Mechanism. *Dalton Trans.* 48, 17810–17817. doi:10.1039/C9DT03649K
- Abdulkareem, E. H., Memarzadeh, K., Allaker, R. P., Huang, J., Pratten, J., and Spratt, D. (2015). Anti-biofilm Activity of Zinc Oxide and Hydroxyapatite Nanoparticles as Dental Implant Coating Materials. *J. Dentistry* 43, 1462–1469. doi:10.1016/j.jdent.2015.10.010
- Ahmadi, T., Monshi, A., Mortazavi, V., Fathi, M. H., Sharifi, S., Kharaziha, M., et al. (2020). Fabrication and Characterization of Polycaprolactone Fumarate/gelatin-Based Nanocomposite Incorporated with Silicon and Magnesium Co-doped Fluorapatite Nanoparticles Using Electrospinning Method. *Mater. Sci. Eng. C.* 106, 110172. doi:10.1016/j.msec.2019.110172
- Beigomi, M., Mohsenzadeh, M., and Salari, A. (2018). Characterization of a Novel Biodegradable Edible Film Obtained from *Dracocephalum Moldavica* Seed Mucilage. *Int. J. Biol. Macromol.* 108, 874–883. doi:10.1016/j.ijbiomac.2017.10.184
- Bottino, M. C., Thomas, V., and Janowski, G. M. (2011). A Novel Spatially Designed and Functionally Graded Electrospun Membrane for Periodontal Regeneration. *Acta Biomater.* 7, 216–224. doi:10.1016/j.actbio.2010.08.019
- Caballé-Serrano, J., Abdeslam-Mohamed, Y., Munar-Frau, A., Fujioka-Kobayashi, M., Hernández-Alfaro, F., and Miron, R. (2019). Adsorption and Release Kinetics of Growth Factors on Barrier Membranes for Guided Tissue/bone Regeneration: A Systematic Review. *Arch. Oral Biol.* 100, 57–68. doi:10.1016/j.archoralbio.2019.02.006
- Câmara, A. K. F. I., Okuro, P. K., Cunha, R. L. d., Herrero, A. M., Ruiz-Capillas, C., and Pollonio, M. A. R. (2020). Chia (*Salvia Hispanica* L.) Mucilage as a New Fat Substitute in Emulsified Meat Products: Technological, Physicochemical, and Rheological Characterization. *LWT* 125, 109193. doi:10.1016/j.lwt.2020.109193
- Castro, A. G. B., Diba, M., Kersten, M., Jansen, J. A., van den Beucken, J. J. P., and Yang, F. (2018). Development of a PCL-Silica Nanoparticles Composite Membrane for Guided Bone Regeneration. *Mater. Sci. Eng. C.* 85, 154–161. doi:10.1016/j.msec.2017.12.023
- Darwish, A. M. G., Khalifa, R. E., and El Sohaimy, S. A. (2018). Functional Properties of Chia Seed Mucilage Supplemented in Low Fat Yoghurt. *Alexandria Sci. Exchange J.* 39, 450–459. doi:10.21608/asejaigjsae.2018.13882
- Dehghani, S., Noshad, M., Rastegarzadeh, S., Hojjati, M., and Fazlara, A. (2020). Electrospun Chia Seed Mucilage/PVA Encapsulated with green Cardamomum Essential Oils: Antioxidant and Antibacterial Property. *Int. J. Biol. Macromol.* 161, 1–9. doi:10.1016/j.ijbiomac.2020.06.023
- Garcia, I. M., Leitune, V. C. B., Visioli, F., Samuel, S. M. W., and Collares, F. M. (2018). Influence of Zinc Oxide Quantum Dots in the Antibacterial Activity and Cytotoxicity of an Experimental Adhesive Resin. *J. Dentistry* 73, 57–60. doi:10.1016/j.jdent.2018.04.003
- He, M., Jiang, H., Wang, R., Xie, Y., and Zhao, C. (2017). Fabrication of Metronidazole Loaded Poly (ε-Caprolactone)/zein Core/shell Nanofiber Membranes via Coaxial Electrospinning for Guided Tissue Regeneration. *J. Colloid Interf. Sci.* 490, 270–278. doi:10.1016/j.jcis.2016.11.062
- He, P., Li, Y., Huang, Z., Guo, Z.-Z., Luo, B., Zhou, C.-R., et al. (2019). A Multifunctional Coaxial Fiber Membrane Loaded with Dual Drugs for Guided Tissue Regeneration. *J. Biomater. Appl.* 34, 1041–1051. doi:10.1177/0885328219894001
- Hezma, A. M., Rajeh, A., and Mannaa, M. A. (2019). An Insight into the Effect of Zinc Oxide Nanoparticles on the Structural, thermal, Mechanical Properties and Antimicrobial Activity of Cs/PVA Composite. *Colloids Surf. A: Physicochem. Eng. Aspects* 581, 123821. doi:10.1016/j.colsurfa.2019.123821
- Jose, L. M., Kuriakose, S., and Thomas, S. (2020). Fabrication, Characterization and *In Vitro* Antifungal Property Evaluation of Biocompatible Lignin-Stabilized Zinc Oxide Nanoparticles against Selected Pathogenic Fungal Strains. *BioNanoSci.* 10, 583–596. doi:10.1007/s12668-020-00748-8

- Joshi, K. M., Shinde, D. R., Nikam, L. K., Panmand, R., Sethi, Y. A., Kale, B. B., et al. (2019). Fragmented Lignin-Assisted Synthesis of a Hierarchical ZnO Nanostructure for Ammonia Gas Sensing. *RSC Adv.* 9, 2484–2492. doi:10.1039/c8ra05874a
- Khodiri, A. A., Al-Ashry, M. Y., and El-Shamy, A. G. (2020). Novel Hybrid Nanocomposites Based on Polyvinyl Alcohol/graphene/magnetite Nanoparticles for High Electromagnetic Shielding Performance. *J. Alloys Compd.* 847, 156430. doi:10.1016/j.jallcom.2020.156430
- Khorshidi, H., Haddadi, P., Raoofi, S., Badiee, P., and Dehghani Nazhvani, A. (2018). Does Adding Silver Nanoparticles to Leukocyte- and Platelet-Rich Fibrin Improve its Properties? *Biomed. Res. Int.* 2018, 8515829. doi:10.1155/2018/8515829
- Kowalski, G., Kijowska, K., Witczak, M., Kuterasiński, Ł., and Łukasiewicz, M. (2019). Synthesis and Effect of Structure on Swelling Properties of Hydrogels Based on High Methylated Pectin and Acrylic Polymers. *Polymers (Basel)* 11, 114. doi:10.3390/polym11010114
- Lian, M., Sun, B., Qiao, Z., Zhao, K., Zhou, X., Zhang, Q., et al. (2019). Bi-layered Electrospun Nanofibrous Membrane with Osteogenic and Antibacterial Properties for Guided Bone Regeneration. *Colloids Surf. B: Biointerfaces* 176, 219–229. doi:10.1016/j.colsurfb.2018.12.071
- Liang, Y., Luan, X., and Liu, X. (2020). Recent Advances in Periodontal Regeneration: A Biomaterial Perspective. *Bioactive Mater.* 5, 297–308. doi:10.1016/j.bioactmat.2020.02.012
- Liu, X., He, X., Jin, D., Wu, S., Wang, H., Yin, M., et al. (2020). A Biodegradable Multifunctional Nanofibrous Membrane for Periodontal Tissue Regeneration. *Acta Biomater.* 108, 207–222. doi:10.1016/j.actbio.2020.03.044
- Liu, Z., Ye, J., Rauf, A., Zhang, S., Wang, G., Shi, S., et al. (2021). A Flexible Fibrous Membrane Based on Copper(ii) Metal-Organic Framework/poly(lactic Acid) Composites with superior Antibacterial Performance. *Biomater. Sci.* 9 (10), 3851–3859. doi:10.1039/d1bm00164g
- Lun, L. W., Gunny, A. A. N., Kasim, F. H., and Arbain, D. (2017). Fourier Transform Infrared Spectroscopy (FTIR) Analysis of Paddy Straw Pulp Treated Using Deep Eutectic Solvent. *AIP Conf. Proc.* 1835, 020049. doi:10.1063/1.4981871
- Makaremi, M., Lim, C. X., Pasbakhsh, P., Lee, S. M., Goh, K. L., Chang, H., et al. (2016). Electrospun Functionalized Polyacrylonitrile-Chitosan Bi-layer Membranes for Water Filtration Applications. *RSC Adv.* 6, 53882–53893. doi:10.1039/c6ra05942b
- Mota, J., Yu, N., Caridade, S. G., Luz, G. M., Gomes, M. E., Reis, R. L., et al. (2012). Chitosan/bioactive Glass Nanoparticle Composite Membranes for Periodontal Regeneration. *Acta Biomater.* 8, 4173–4180. doi:10.1016/j.actbio.2012.06.040
- Münchow, E. A., Albuquerque, M. T. P., Zero, B., Kamocki, K., Piva, E., Gregory, R. L., et al. (2015). Development and Characterization of Novel ZnO-Loaded Electrospun Membranes for Periodontal Regeneration. *Dental Mater.* 31, 1038–1051. doi:10.1016/j.dental.2015.06.004
- Muñoz, L. A., Aguilera, J. M., Rodríguez-Turiénzo, L., Cobos, A., and Diaz, O. (2012). Characterization and Microstructure of Films Made from Mucilage of *Salvia Hispanica* and Whey Protein Concentrate. *J. Food Eng.* 111, 511–518. doi:10.1016/j.jfoodeng.2012.02.031
- Murfadunnisa, S., Vasantha-Srinivasan, P., Ganesan, R., Senthil-Nathan, S., Kim, T.-J., Ponsankar, A., et al. (2019). Larvicidal and Enzyme Inhibition of Essential Oil from *Spharanthus Amaranthoides* (Burm.) against Lepidopteran Pest *Spodoptera Litura* (Fab.) and Their Impact on Non-target Earthworms. *Biocatal. Agric. Biotechnol.* 21, 101324. doi:10.1016/j.bcab.2019.101324
- Padovani, G. C., Feitosa, V. P., Sauro, S., Tay, F. R., Durán, G., Paula, A. J., et al. (2015). Advances in Dental Materials through Nanotechnology: Facts, Perspectives and Toxicological Aspects. *Trends Biotechnol.* 33, 621–636. doi:10.1016/j.tibtech.2015.09.005
- Patra, P., Mitra, S., Debnath, N., Pramanik, P., and Goswami, A. (2014). Ciprofloxacin Conjugated Zinc Oxide Nanoparticle: A Camouflage towards Multidrug Resistant Bacteria. *Bull. Mater. Sci.* 37, 199–206. doi:10.1007/s12034-014-0637-6
- Pulit-Prociak, J., Staroń, A., Staroń, P., Chmielowiec-Korzeniowska, A., Drabik, A., Tymczyna, L., et al. (2020). Preparation and of PVA-Based Compositions with Embedded Silver, Copper and Zinc Oxide Nanoparticles and Assessment of Their Antibacterial Properties. *J. Nanobiotechnol.* 18, 148. doi:10.1186/s12951-020-00702-6
- Qiu, W., Zhou, Y., Li, Z., Huang, T., Xiao, Y., Cheng, L., et al. (2020). Application of Antibiotics/Antimicrobial Agents on Dental Caries. *Biomed. Res. Int.* 2020, 5658212. doi:10.1155/2020/5658212
- Rauf, A., Ye, J., Zhang, S., Shi, L., Akram, M. A., and Ning, G. (2019). Synthesis, Structure and Antibacterial Activity of a Copper(II) Coordination Polymer Based on Thiophene-2,5-Dicarboxylate Ligand. *Polyhedron* 166, 130–136. doi:10.1016/j.poly.2019.03.039
- Sadaf Ul, H., Bushra, B., Muhammad Shahid, N., Syed Ali Raza, N., Zufiqar, A., Sohail, N., et al. (2021). Recent Progress in Materials Development and Biological Properties of GTR Membranes for Periodontal Regeneration. *Chem. Biol. Drug Des.* 98, 1007–1024. doi:10.1111/cbdd.13959
- Salazar Vega, I. M., Quintana Owen, P., and Segura Campos, M. R. (2020). Physicochemical, thermal, Mechanical, Optical, and Barrier Characterization of *Chia* (*Salvia Hispanica* L.) Mucilage-protein Concentrate Biodegradable Films. *J. Food Sci.* 85, 892–902. doi:10.1111/1750-3841.14962
- Sela, M. N., Kohavi, D., Krausz, E., Steinberg, D., and Rosen, G. (2003). Enzymatic Degradation of Collagen-Guided Tissue Regeneration Membranes by Periodontal Bacteria. *Clin. Oral Implants Res.* 14, 263–268. doi:10.1034/j.1600-0501.2003.140302.x
- Shi, R., Xue, J., He, M., Chen, D., Zhang, L., and Tian, W. (2014). Structure, Physical Properties, Biocompatibility and *In Vitro/vivo* Degradation Behavior of Anti-infective Polycaprolactone-Based Electrospun Membranes for Guided Tissue/bone Regeneration. *Polym. Degrad. Stab.* 109, 293–306. doi:10.1016/j.polydegradstab.2014.07.017
- Soltani, M., Najafi, A., Yousefian, S., Naji, H. R., and Bakar, E. S. (2013). Water Repellent Effect and Dimension Stability of Beech wood Impregnated with Nano-Zinc Oxide. *Biores* 8, 6280–6287. doi:10.15376/biores.8.4.6280-6287
- Türkkan, S., Pazarçeviren, A. E., Keskin, D., Machin, N. E., Duygulu, Ö., and Tezcaner, A. (2017). Nanosized CaP-Silk Fibroin-PCL-PEG-PCL/PCL Based Bilayer Membranes for Guided Bone Regeneration. *Mater. Sci. Eng. C* 80, 484–493. doi:10.1016/j.msec.2017.06.016
- Xue, J., He, M., Niu, Y., Liu, H., Crawford, A., Coates, P., et al. (2014). Preparation and *In Vivo* Efficient Anti-infection Property of GTR/GBR Implant Made by Metronidazole Loaded Electrospun Polycaprolactone Nanofiber Membrane. *Int. J. Pharmaceutics* 475, 566–577. doi:10.1016/j.ijpharm.2014.09.026
- Zhang, L., Dong, Y., Zhang, N., Shi, J., Zhang, X., Qi, C., et al. (2020). Potentials of sandwich-like Chitosan/polycaprolactone/gelatin Scaffolds for Guided Tissue Regeneration Membrane. *Mater. Sci. Eng. C* 109, 110618. doi:10.1016/j.msec.2019.110618
- Zhao, H., Hu, J., and Zhao, L. (2021). The Effect of Drug Dose and Duration of Adjuvant Amoxicillin-Plus-Metronidazole to Full-Mouth Scaling and Root Planing in Periodontitis: a Systematic Review and Meta-Analysis. *Clin. Oral Invest.* 25, 5671–5685. doi:10.1007/s00784-021-03869-w
- Zhou, T., Zheng, K., Sui, B., Boccaccini, A. R., and Sun, J. (2020). *In Vitro* evaluation of Poly (Vinyl Alcohol)/collagen Blended Hydrogels for Regulating Human Periodontal Ligament Fibroblasts and Gingival Fibroblasts. *Int. J. Biol. Macromol.* 163, 1938–1946. doi:10.1016/j.ijbiomac.2020.09.033

Conflict of Interest: The authors declare that the research was conducted in the absence of any commercial or financial relationships that could be construed as a potential conflict of interest.

Publisher's Note: All claims expressed in this article are solely those of the authors and do not necessarily represent those of their affiliated organizations, or those of the publisher, the editors, and the reviewers. Any product that may be evaluated in this article, or claim that may be made by its manufacturer, is not guaranteed or endorsed by the publisher.

Copyright © 2022 Bilal, Niazi, Nadeem, Farid, Nazir, Akhter, Javed, Mohyuddin, Rauf, Ali, Naqvi, Muhammad, Elkaed, Ibrahim, Awwad and Hassan. This is an open-access article distributed under the terms of the Creative Commons Attribution License (CC BY). The use, distribution or reproduction in other forums is permitted, provided the original author(s) and the copyright owner(s) are credited and that the original publication in this journal is cited, in accordance with accepted academic practice. No use, distribution or reproduction is permitted which does not comply with these terms.



OPEN ACCESS

EDITED BY

Sirikanjana Thongmee,
Kasetsart University, Thailand

REVIEWED BY

Sherif Ashraf Fahmy,
American University in Cairo, Egypt
Vijay Sagar Madamsetty,
Seqirus.com, United States

*CORRESPONDENCE

Abhijeet Mishra,
abhijeetjmi@gmail.com
Razi Ahmad,
razi.jmi@gmail.com

SPECIALTY SECTION

This article was submitted to
Nanoscience,
a section of the journal
Frontiers in Chemistry

RECEIVED 13 August 2022

ACCEPTED 23 September 2022

PUBLISHED 13 October 2022

CITATION

Ravi R, Zeyaulah M, Ghosh S,
Khan Warsi M, Baweja R, AlShahrani AM,
Mishra A and Ahmad R (2022), Use of
gold nanoparticle-silibinin conjugates:
A novel approach against lung
cancer cells.
Front. Chem. 10:1018759.
doi: 10.3389/fchem.2022.1018759

COPYRIGHT

© 2022 Ravi, Zeyaulah, Ghosh, Khan Warsi, Baweja, AlShahrani, Mishra and Ahmad. This is an open-access article distributed under the terms of the [Creative Commons Attribution License \(CC BY\)](#). The use, distribution or reproduction in other forums is permitted, provided the original author(s) and the copyright owner(s) are credited and that the original publication in this journal is cited, in accordance with accepted academic practice. No use, distribution or reproduction is permitted which does not comply with these terms.

Use of gold nanoparticle-silibinin conjugates: A novel approach against lung cancer cells

Rangnath Ravi¹, Md. Zeyaulah², Shubhrima Ghosh³,
Mohiuddin Khan Warsi⁴, Renu Baweja⁵,
Abdullah M. AlShahrani², Abhijeet Mishra^{5*} and Razi Ahmad^{6,7*}

¹Department of Chemistry, Shivaji College, University of Delhi, New Delhi, India, ²Department of Basic Medical Science, College of Applied Medical Sciences, King Khalid University (KKU), Khamsi Mushayt Campus, Abha, Saudi Arabia, ³Trinity Translational Medicine Institute, Trinity College Dublin, Dublin, Ireland, ⁴Department of Biochemistry, College of Science, University of Jeddah, Jeddah, Saudi Arabia, ⁵Department of Biochemistry, Shivaji College, University of Delhi, New Delhi, India, ⁶Department of Chemistry, Indian Institute of Technology Delhi, New Delhi, India, ⁷Quality and Research Department, Anantaa GSK Innovations Pvt Ltd., DLF Industrial Area, Faridabad, India

Lung cancer presents one of the most challenging carcinomas with meager 5-year survival rates (less than 20%), high metastasis and high recurrence due to chemo- and radio- resistance. An alternative or complementation to existing prognosis modalities is the use of phytochemicals such as silibinin, which targets essential cytokines, angiogenic factors and transcription factors for a profound anti-tumor effect. However, the problems of low solubility in an aqueous physiological environment, poor penetration, high metabolism and rapid systemic clearance limit the therapeutic use of silibinin. Conjugation of gold nanoparticles (GNPs) with silibinin may overcome the above challenges along with distinct advantages of biocompatibility, optical properties for monitoring and causation of cytotoxicity in cancer cells. The current study thus aims to develop silibinin conjugated gold nanoparticles (Sb-GNPs) with pH responsive release in the cancer microenvironment, optimizing several parameters for its higher activity and further evaluate the nanoplatform for their efficacy in inducing cell death *in vitro* against A549 lung cancer cells. GNPs was synthesized using trisodium citrate dihydrate as the reducing agent and further used for the conjugation of silibinin. The synthesized GNPs were found to be monodispersed and spherical in shape. The silibinin was successfully conjugated with gold nanoparticles and long-term stability of GNPs and Sb-GNPs nanoconjugates in suspension phase was confirmed by FTIR and DLS. Anticancer properties of Sb-GNPs were confirmed by different assay using MTT, Trypan blue dye exclusion assay and cell cycle analysis assay. After conjugation of silibinin with GNPs, the efficacy of silibinin increased 4–5 times in killing the cancer cells. This is the first report on using silibinin gold nanoconjugate system for lung cancer therapy with promising future applications.

KEYWORDS

gold nanoparticles, silibinin, lung cancer, phytochemicals, cancer therapy

Introduction

Despite breakthroughs in cancer understanding, treatment techniques, and novel treatments, cancer patient survival rates have slightly improved. Chemotherapy, immunotherapy, and radiotherapy alone are ineffective cancer treatments. New cancer survival and mortality control techniques are needed (Da Silva et al., 2016; Dai et al., 2017; Pucci et al., 2019; Mahdinloo et al., 2020; Bagherifar et al., 2021). As an alternative or complementary to traditional chemo or radiotherapy, naturally occurring phytochemicals (such as flavonoids, isoflavones, and lignans) with antioxidant or hormone-like actions are being explored for cancer (Ghosh et al., 2021a; Ahmad et al., 2021; Aboushanab et al., 2022; Lim & Park, 2022). These cancer-suppressing phytochemicals act mainly by affecting the signaling molecules that have either been abnormally activated or silenced. These signaling molecules, which are usually kinases, are responsible for activating genes that regulate cell growth, differentiation, and apoptosis (Melim et al., 2022). In order to minimize the chemotherapeutic induced drug toxicities and associated drug resistance in lung cancers, the use of nutraceuticals such as silibinin has taken precedence in recent times. Silibinin is a flavanolignan obtained from the silymarin extract of *Silybum marianum* (milk thistle) plant often explored historically for liver disorders as well as cancers (Abenavoli et al., 2018; Verdura et al., 2021). In some *in-vivo* studies, silibinin has been reported to inhibit angiogenesis, cell proliferation, drug resistance and metastasis in lung cancer models (Mateen et al., 2013). The anti-cancer activity of silibinin is attributed to the suppression of the angiogenic factor VEGF (Vascular Angiogenic Growth Factor) and targeting of multiple cytokines such as IL-1 β , TNF- α and IFN γ (Singh et al., 2006; Tyagi et al., 2009). Moreover, transcription factor STAT3 is known to be the intrinsic target of silibinin in primary lung cancers. When activated by the phytochemical, silibinin lowers the levels of VEGF regulators such as cyclooxygenase-2 (COX2) and inducible nitric oxide synthase (iNOS) (Singh et al., 2006; Verdura et al., 2021). Additionally, silibinin is also reported to increase drug sensitivity in drug-resistant lung cancers with acquired mutations in ALK-TKI and EGFR receptors (Singh et al., 2006).

The delivery of any therapeutic molecule comes with a series of challenges. Rapid renal clearance, difficulty in crossing the cell membrane to the cytosol, relatively larger sizes, poor stability, reduced systemic delivery and uneven release profiles are major challenges of using phytochemical molecules without any transfection agents. In terms of pharmacokinetics, only 23%–47% of orally administered silibinin is absorbed from the gastrointestinal tract and is metabolized by cytochrome class of enzymes (Jančová et al., 2007; Ahmad et al., 2021). Conjugation of phytochemical molecules with nanoparticles helps in overcoming the above challenges along with distinct advantages such as

desired penetration, controlled release, optimal distribution and specificity (Ghosh et al., 2021b; Srivastava et al., 2021; Melim et al., 2022; Nikdouz et al., 2022). Several nanoplatforms such as those based on glycyrrhizic acid, PVP PEG, PLGA, chitosan, carbon nanotubes, lipid, and magnetic nanoparticles have been explored for conjugation with silibinin (Takke & Shende, 2019). The state-of-the-art has fewer reports on silibinin conjugated metal nanoparticles which could be a nascent, promising area of research with advantageous properties. In this respect, gold (Au) nanoparticles find several medicinal uses because of their inherent biocompatibility (being a non-reactive element), optical properties (for easy detection) and advantageous surface functionalization. Additionally, Au nanoparticles are reported to possess antibacterial and anticancer properties caused by oxidative stress as well as cell DNA damage (Aljarba et al., 2022).

Lung cancer, also known as bronchogenic carcinoma, is a condition characterized by uncontrolled cell development in the lungs. It is the leading cause of cancer-related deaths. Usually, primary lung cancers are carcinomas and develop within the wall or epithelial cells of the bronchial tree (Lemjabbar-Alaoui et al., 2015). Cancers can also arise from the lung's pleura, mesothelioma, or sometimes from supporting tissues such as blood vessels (Rao & Wei, 2022). Lung cancer is one of the most dangerous and difficult to treat malignancies because it tends to spread early in its course. While lung cancer can spread to any organ in the body, it most commonly spreads to the adrenal glands, liver, brain, and bone (Wang et al., 2022). Various other types of tumours can also metastasize to the lungs. The survival rate in the case of lung cancer is relatively low, although if detected at an early stage, the 5-year survival rate increases to 5–10% through chemotherapy (Pirker & Zhou, 2022). Lung cancer is classified as NSCLC (non-small cell lung carcinoma) or SCLC (small cell lung carcinoma). NSCLC is more common than SCLC but responds less well to chemotherapy. There are three main subtypes of NSCLC, namely squamous cell lung carcinoma, adenocarcinoma and large cell carcinoma or undifferentiated carcinoma. Small cell lung carcinoma (SCLC) is strongly related to smoking. It often originates in the primary and secondary bronchi and proliferates to form large tumors that spread to other parts (Lemjabbar-Alaoui et al., 2015; Pirker & Zhou, 2022). Initial response to chemotherapy is good, but metastasis is high and results in a worse prognosis. Other lung cancers include pleuropulmonary blastoma, carcinoid tumor and metastatic tumors. Mutations that cause the uncontrolled growth of cancer cells are either inherited or acquired. Often, between exposure to a carcinogen and the appearance of cancer, a latency period of years or decades might exist. Mutations in the *K-ras* proto-oncogene are responsible for 10–30% of lung adenocarcinomas (Aviel-Ronen et al., 2006; Herbst et al., 2008; Ghimessy et al., 2020; Tian et al., 2022).

The anticancer activity of silibinin gold nanoconjugate is an unexplored but promising area of research. Conjugates of silibinin and Au nanoparticles are expected to result in a two-way action against persistent tumours. NPs can co-load multiple components for simultaneous administration, shield payloads from degradation and premature release, and passively or actively target tumours through increased permeability and retention or surface modification with ligands (Duan et al., 2019). In the current study, we reported the conjugation of gold nanoparticles with silibinin with pH-responsive release, optimizing several parameters for its increased activity and have further explored their efficacy in inducing cell-death *in-vitro* against A549 lung cancer cells. Collectively, we proposed that such a nanoparticle-mediated system provides a natural product-based anticancer therapeutic platform with promising biomedical applications.

Material and methods

Tetrachloroauric (III) acid ($\text{HAuCl}_4 \cdot 3\text{H}_2\text{O}$), trisodium citrate dihydrate ($\text{C}_6\text{H}_5\text{Na}_3\text{O}_7 \cdot 2\text{H}_2\text{O}$) were procured from SRL, Mumbai, India. Silibinin, DMSO, RPMI (Roswell Park Memorial Institute medium), fetal bovine serum, 1X trypsin-EDTA solution, MTT powder, were purchased from Sigma Aldrich Chemicals Pvt. Ltd. Human lung adenocarcinoma cell line A549 was obtained from National Centre for Cell Science, Pune (India).

Preparation of stock solutions of gold salt, trisodium citrate dihydrate and silibinin

Tetrachloroauric acid (1 gm) was dissolved in 50 ml of autoclaved MilliQ water to yield a final concentration of 50.78 mM stock solution of tetrachloroauric acid. Trisodium citrate dihydrate (2.94 gm) was dissolved in 200 ml of autoclaved MilliQ water to yield a final concentration of 50 mM stock solution. The silibinin powder (4.824 mg) was dissolved in 10 ml ethanol (100%) to yield a final concentration of 1 mM stock solution.

Synthesis of gold nanoparticles

Gold nanoparticles were synthesized by the standard defined method of Turkevich and Frens with slight modifications, where citrate is used as a reducing agent at 100°C (Wuithschick et al., 2015). For the synthesis of gold nanoparticles, the reduction of tetrachloroauric acid solution was carried out by mixing of tetrachloroauric acid (0.5 mM) and trisodium citrate (2.5 mM) and by heating the reaction solution with continuous stirring. Several reaction parameters, including tetrachloroauric acid concentration,

trisodium citrate concentration, temperature, and stirring speed were optimised to achieve controlled shape and size of GNPs. Synthesis of GNPs was monitored by using UV-Visible spectroscopy.

Optimization of concentration of tetrachloroauric acid for GNPs synthesis

Keeping all the other reaction parameters constant, different concentration of tetrachloroauric acid ranging from 0.1 mM to 1.00 mM was taken for the synthesis of GNPs. The reaction was carried out by mixing the tetrachloride with trisodium citrate to provide reducing environment followed by its incubation at 100°C for 30 min to obtain the GNPs. UV-Visible spectra of synthesized GNPs colloidal solution was taken in the range of 200 nm – 900 nm.

Optimization of concentration of trisodium citrate dihydrate for GNPs synthesis

A range of concentrations of trisodium citrate dihydrate were taken for the optimizing the concentration for the synthesis of GNPs, while keeping all the other reaction parameters constant. The concentrations of trisodium citrate dihydrate ranges from 1.5 mM to 20 mM. A fixed optimized concentration of tetrachloroauric acid was mixed with these different concentrations of trisodium citrate dihydrate for the synthesis of Gold NPs at 100°C for 30 min. UV-Visible spectra of Gold NPs colloidal solution was taken to determine the required optimum concentration of trisodium citrate dihydrate for nanoparticles synthesis.

Optimization of temperature for the GNPs synthesis

Keeping other reaction parameters constant, the synthesis of GNPs were carried out at different temperatures (30°C, 45°C, 60°C, 90°C, 105°C and 120°C). A fixed optimized concentration of tetrachloroauric acid and trisodium citrate dihydrate was mixed, and the reaction was done at these different temperatures for 30 min to synthesized GNPs. UV-Visible spectra of synthesized GNPs colloidal solution was taken to determine the optimum temperature.

Optimization of reaction time for the GNPs synthesis

A range of different time periods were taken for the GNPs synthesis while keeping all the others parameters constant including 1 min, 5 min, 10 min, 20 min, 30 min, 40 min, 50 min, and 60 min respectively. A fixed optimized concentration of tetrachloroauric

acid and trisodium citrate dihydrate was mixed, and the reaction was done for the above mentioned time periods at the optimized temperature for the Gold NPs synthesis. UV-Visible spectra of Gold NPs colloidal solution was taken to determine the optimum time of incubation required for the synthesis of GNPs.

Optimization of stirring speed for the GNPs synthesis

In an attempt to optimize the stirring speed of incubation, the synthesis of GNPs were carried out at 300 rpm, 400 rpm, 500 rpm, 600 rpm, and 700 rpm respectively keeping other parameters constant. After 30 min of incubation, UV-Visible spectra of GNPs colloidal solution were taken to determine the optimum time period required for its synthesis.

Purification of GNPs

GNPs were purified by centrifuging a prepared sample of colloidal solution for 30 min at 10,000 rpm followed by washing the pellet 2–3 times with double distilled water. The colloidal GNPs solution was centrifuged until a pellet containing clear solution was obtained. The pellet was further dried at 37°C. The pellet was then scraped with a spatula and grounded with a mortar and pestle to produce a fine powder of GNPs for further experiment.

Conjugation of silibinin with GNPs using physical adsorption process to form silibinin-gold nanoparticles (Sb-GNPs) nanoconjugates

The stock solution of Gold NPs (1 mg/ml) was prepared from the purified powder in double distilled water. This solution was sonicated for an hour at room temperature to obtain the uniform and homogeneous colloidal solution of nanoparticles. Freshly prepared silibinin solution (concentration ranges from 5 μ M to 100 μ M) was then added to GNPs solution and mixed by continuous stirring at 500 rpm for 1 h at 4°C. This process ensured the conjugation of silibinin over the surface of gold nanoparticles. Excess silibinin was removed by centrifuging the sample at 10,000 rpm for 10 min and discarding the supernatant. The pellet of Sb-GNPs nanoconjugates was washed 2–3 times with double distilled water and used for further experiment.

The optimization of silibinin concentration was done by making a saturation curve of silibinin. For this optimization, a range of concentrations of silibinin were taken to be conjugated with GNPs. The different concentrations were 5 μ M, 10 μ M, 15 μ M, 25 μ M, 50 μ M, 75 μ M, and 100 μ M, respectively. During these conjugation reactions, the concentration of GNPs as well as other important reaction parameters were kept constant. Further, a

saturation curve of silibinin conjugated with gold nanoparticles at different concentrations of silibinin was plotted by taking the absorbance at 288 nm and 528 nm respectively. The amount of unconjugated silibinin in the supernatant of nanoconjugates and the percentage of silibinin binding in nanoconjugates was calculated using the standard curve.

Characterization

Absorption spectra of the GNPs and nanoconjugates were measured by UV-Visible spectroscopy. The size, shape and morphology of GNPs and nanoconjugates were examined using transmission electron microscopy (TEM), JEOL 2100F microscope operated at 100 kV. Energy-dispersive X-ray analysis was also done using this instrument. Samples for TEM and EDAX were prepared by drop coating purified GNPs onto carbon-coated copper TEM grids. DLS measurements were used to determine the Zeta potential and polydispersity index of the GNPs and nanoconjugates were carried out using the spectroscatterer RiNA, GmbH class3B. The 1 mg powder was dispersed in distilled H₂O to produce a suitable scattering intensity and values were obtained at an angle of 90° in 10 mm diameter cells at 20°C for 10 cycles. Fourier transforms infrared (FTIR) spectroscopy was used to determine the functional groups present in silibinin and nanoconjugates respectively. FTIR spectra of the purified GNPs and nanoconjugates were recorded between 4,000 cm^{-1} and 400 cm^{-1} with a resolution of 4 cm^{-1} .

Release study of silibinin with different pH values

Centrifugation of 200 ml of the nanoconjugates solution at 10,000 rpm for 30 min at 4°C resulted in the collection of red pellet at the bottom of centrifuge tube. The collected pellet was distributed into several fractions. The 100 μ l of each fraction was diluted with 900 μ l of phosphate buffer solution (PBS), which had pH values of 7.4 (physiological) and 5 (acidic, mimicking tumour microenvironment), respectively. The diluted fraction was incubated at 0 min to 6 h, then centrifuged at 10,000 for 10 min at 4°C and collect the supernatants of respective solutions. Further, the absorbance of each supernatant was measured at 288 nm using a UV-Visible spectrophotometer. Further, obtained results were plotted against the percentage release and corresponding time points.

In vitro evaluation of anticancer efficacy of Sb-GNPs nanoconjugates

A549 cells were grown as adherent monolayer in RPMI 1640 containing 10% FBS and 1% antibiotic (pen-strep) at

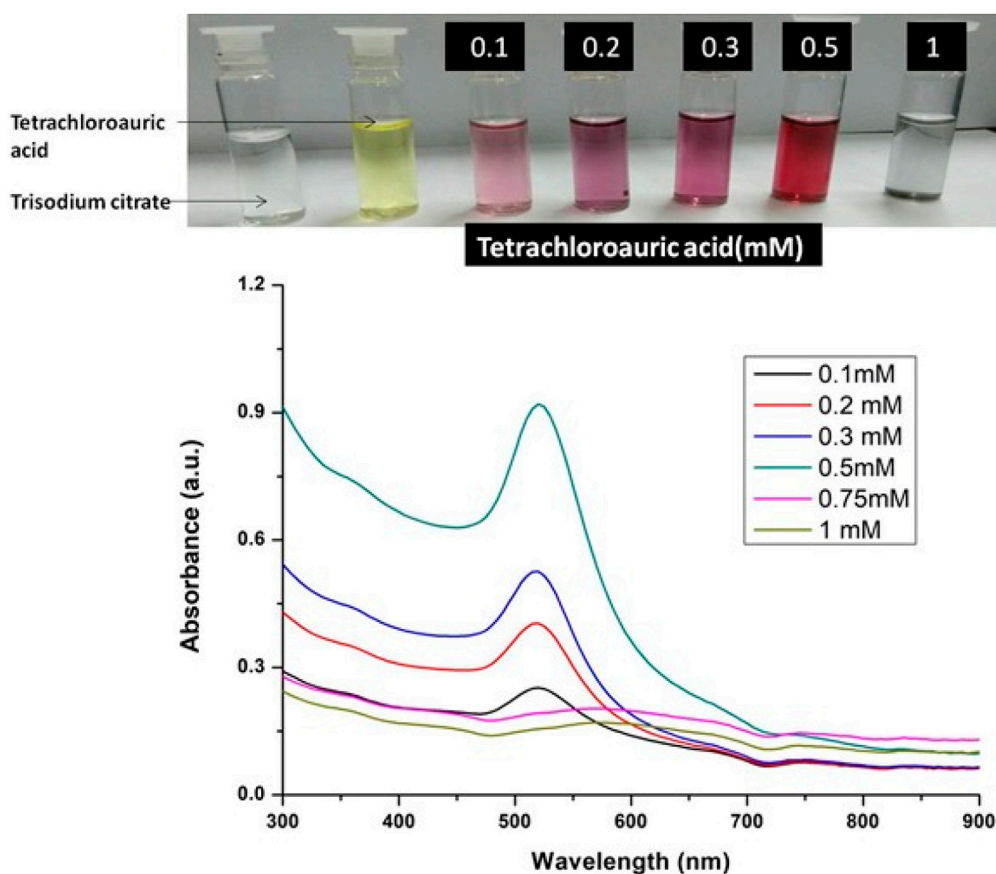


FIGURE 1

UV-Vis Spectra of Gold nanoparticles solutions synthesised by varying concentrations of tetrachloroauric acid. The experiments were done in triplicate and results within each pair differed by < 3 .

37°C, and 95% humidified incubator with 5% CO₂. Sterile conditions were maintained all the times. Exponentially growing cells (sub confluent cells) were used in the entire set of experiments. For treatment with the drug, 10⁵ cells were seeded in a 60 mm culture dish and incubated at 37°C for 48 h. After 24 h of seeding the cells, the consumed medium was removed from the plates. The cells were treated with different concentrations of the drug suspended in the medium and control was treated with the medium without the drug. Each set of treatments was done in triplicates to minimize experimental error. The medium containing different concentrations of the drug was added to each set of plates and the plates were incubated at 37°C.

MTT assay

Cells were treated with different concentration of drug. After treatment (24 h and 48 h respectively), media was removed and 100 μ l of MTT at the concentration of 5 mg/ml in 1X PBS was added to each well. The 96 well plate was

incubated at 37°C in 5% CO₂ incubator for 4 h. The MTT solution was removed and 100 μ l of DMSO was added per well. The wells of the plate were read on an ELISA plate reader at 570 nm wavelength after 10 min of incubation in the dark. The data were recorded using the software package SoftPro Max. The cell viability was represented as percent cell viability (Bahuguna et al., 2017).

Cell death/viability assay by trypan blue dye exclusion

After desired treatments, the cells in the supernatants were collected from each plate and transferred to the corresponding 15 ml tubes. The attached cells were removed after trypsinization (1 ml of trypsin/plate). Once the cells were completely detached, 2 ml of chilled 1x PBS was added to each plate. Cells were flushed out of the plate completely and were transferred to corresponding falcon tubes. The cell suspension was spun at 1,500 rpm for 5 min. The supernatant was discarded slowly. The

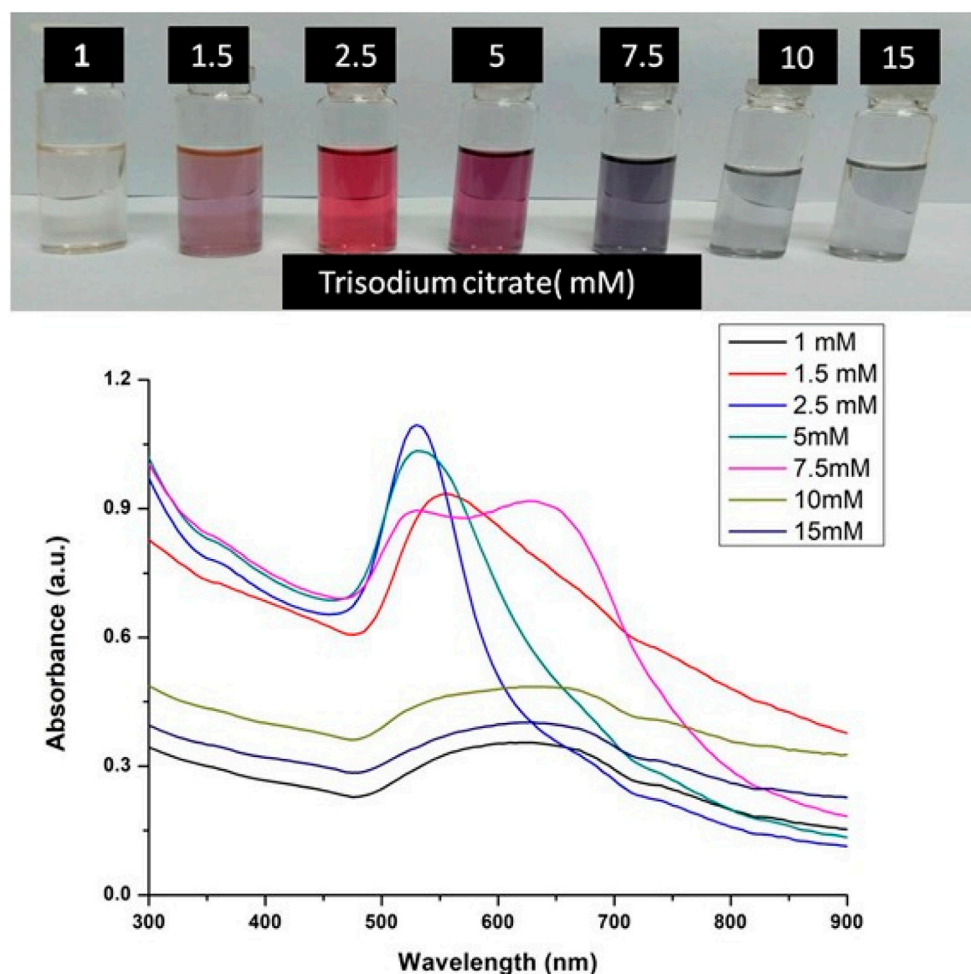


FIGURE 2

UV-Vis Spectra of Gold nanoparticles solutions synthesised by varying concentrations of trisodium citrate dihydrate. The experiments were done in triplicate and results within each pair differed by < 3.

pellet was washed with 1x PBS and the pellet was resuspended in 1 ml fresh 1x PBS. For viability assay, 100 μ l of the homogeneous cell suspension was transferred to a microcentrifuge tube. To this suspension, 10 μ l of 0.4% trypan blue dye was added. The suspension was mixed well and left for 5–10 min at room temperature. 10 μ l of stained cell suspension was pipetted out of the tube and loaded on each chamber of haemocytometer. The procedure was repeated for each set of samples. The percentage of viable cells was calculated by dividing the number of viable cells by a total number of cells multiplied by 100.

Biocompatibility of silibinin, GNPs and silibinin conjugated GNPs

Biocompatibility study of any drug is very important before its use as a therapeutic. Therefore, in the present study, the

biocompatibility of silibinin, GNPs and silibinin conjugated GNPs (Sb-GNPs) against normal human (HEK293T) cell were investigated with the help of MTT assay.

Hemolysis assay

The hemolytic activity of GNPs, silibinin, and Sb-GNPs were determined as described in our earlier publication (Mishra et al., 2013b). Fresh RBCs were collected from healthy human and washed (1500 RPM; 10 min) three times in PBS buffer (150 mM NaCl, pH 7.4) and re-suspended in PBS at 2% hematocrit. Aliquots of 100 μ l suspension were added to wells of 96-well plate containing different concentrations of GNPs, silibinin and Sb-GNPs respectively. PBS alone taken for obtaining baseline values and Triton X-100 (0.4%) in PBS to get 100% hemolysis. After incubation at 37°C for 3 h, the samples were centrifuged

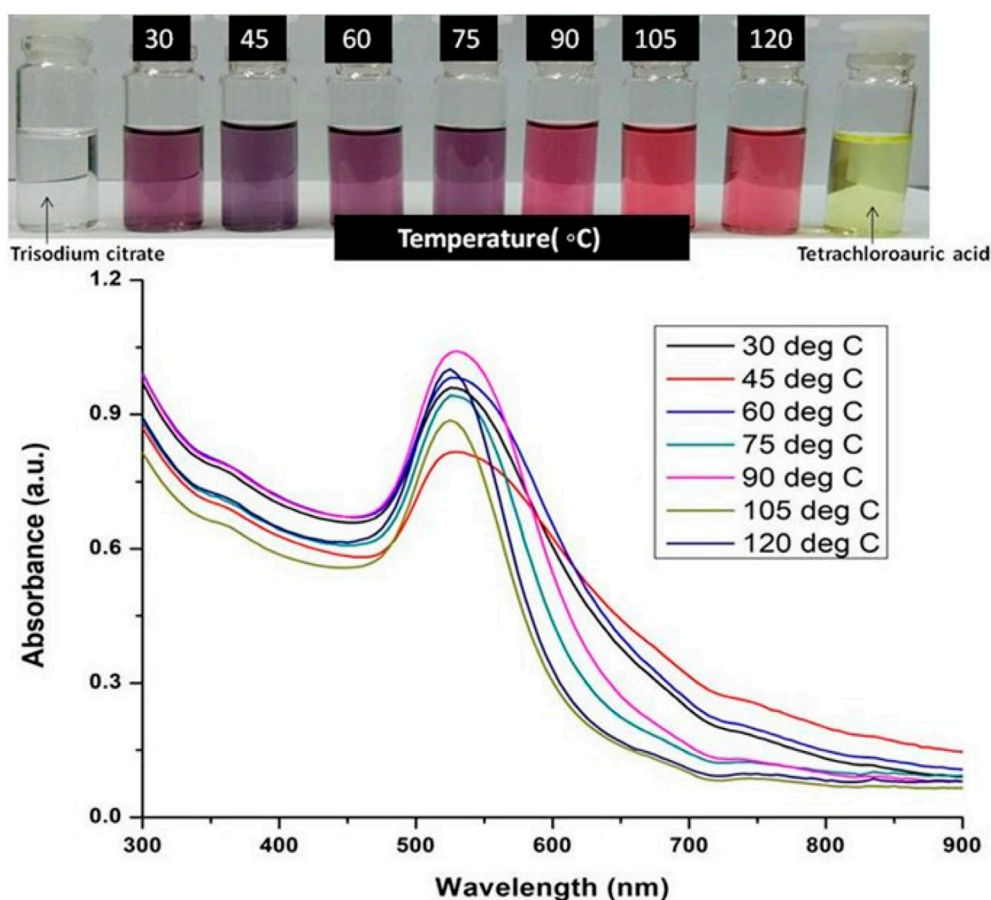


FIGURE 3

UV-Vis Spectra of Gold nanoparticles solutions synthesised by varying temperature. The experiments were done in triplicate and results within each pair differed by < 3.

and supernatant was used to determine the hemolytic activity measured in terms of hemoglobin release as monitored by absorbance at 415 nm (Molecular Devices, Sunnyvale, CA, United States). Triton X-100 treated control samples were diluted 10-fold before measuring absorbance. Further, Base line value was subtracted from each data point. Percent hemolysis expressed with reference to 100% hemolysis value (positive control; Triton X-100 treated RBCs).

Cell cycle analysis

20,000 cells of lung cancer (A549) were attached in 6 well plates and treated with silibinin conjugated gold nanoparticles. After the termination of experiment, all cells were obtained using trypsinization process and centrifuged at 1,200 rpm followed by their processing and FACS study as per earlier reported method (Singh et al., 2021). The cell suspension was ready using the silibinin conjugated gold nanoparticles treated plates, and

centrifuged at 1,500 rpm for 5 min. Further, supernatant of centrifuged sample was discarded, and the pellet was again suspended in 500 μ l of mixture of saponin and PI solutions [saponin (0.3%), PI (25 mg/ml), EDTA (0.1 mM), and RNase A (10 mg/ml)]. The process was carried out in dark condition. The data were obtained and processed with the help of Cell Quest software in a FACS Calibur (Becton Dickinson, United States) system for 10,000 events per sample and analyzed after proper gating, to get the cell percentage in each stage of the cell cycle.

Statistical analysis

All experiments were conducted three times. Their mean \pm SD data were observed for statistical significance, values based on one-way ANOVA software along with Dunnett's post hoc test (Singh et al., 2021). The statistical mean average values are found $p^* < 0.05$, $p^{**} < 0.01$, and $p^{***} < 0.001$, matching those of reported value.

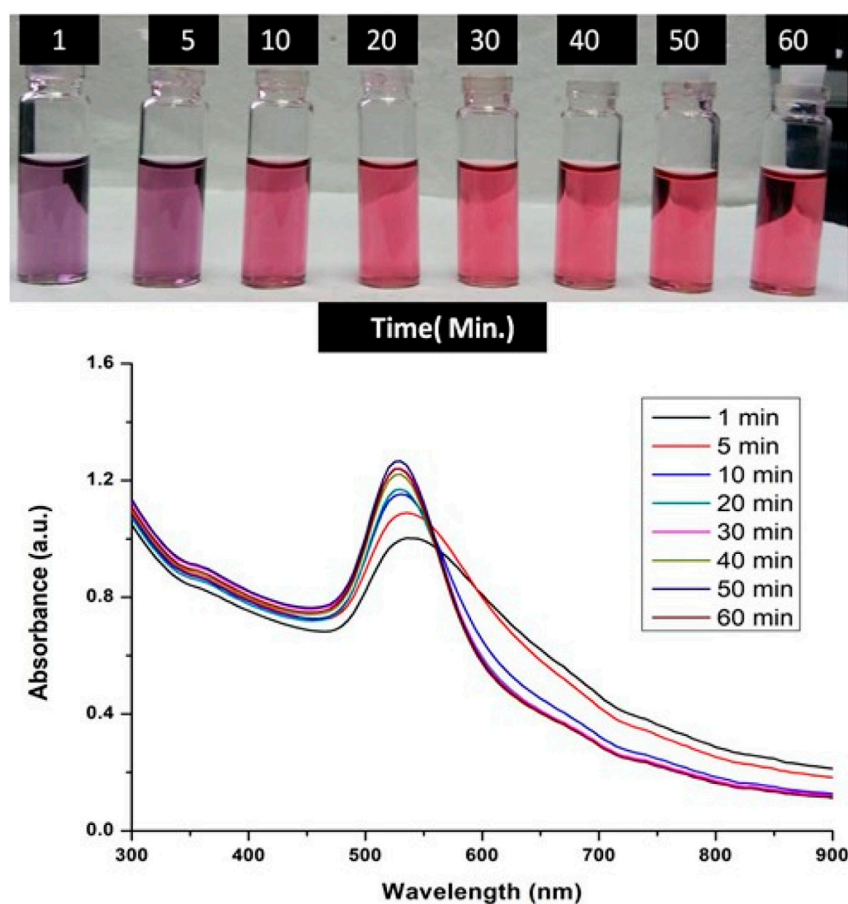


FIGURE 4

UV-Vis Spectra of Gold nanoparticles solutions synthesised by varying time points of synthesis reaction. The experiments were done in triplicate and results within each pair differed by < 3.

Results and discussion

The formation of gold nanoparticles (AuNPs) using trisodium citrate as the reducing agent was observed under visible light due to a change in the color of the solution. The

reaction mixture turned brownish-black after 2–3 min of the reaction and then ruby-red due to excitation of surface plasmon vibrations in gold nanoparticles. The appearance of brownish-black colour initially validated the occurrence of a redox reaction whereby Au^{3+} ions are reduced to Au^0 by

TABLE 1 Table showing the % of conjugated Silibinin to GNPs and % of unbound free Silibinin during conjugation reaction when varying concentrations of silibinin taken for the reaction. The experiments were done in triplicate and results within each pair differed by < 3.

Concentration of silibinin (μM)	Silibinin-GNPs conjugated (%)	Unbound free silibinin (%)
5	54.67	45.33
10	71.77	28.23
15	71.3	28.7
25	75.88	24.12
50	80.6	19.4
75	80.4	19.6
100	77	23.00

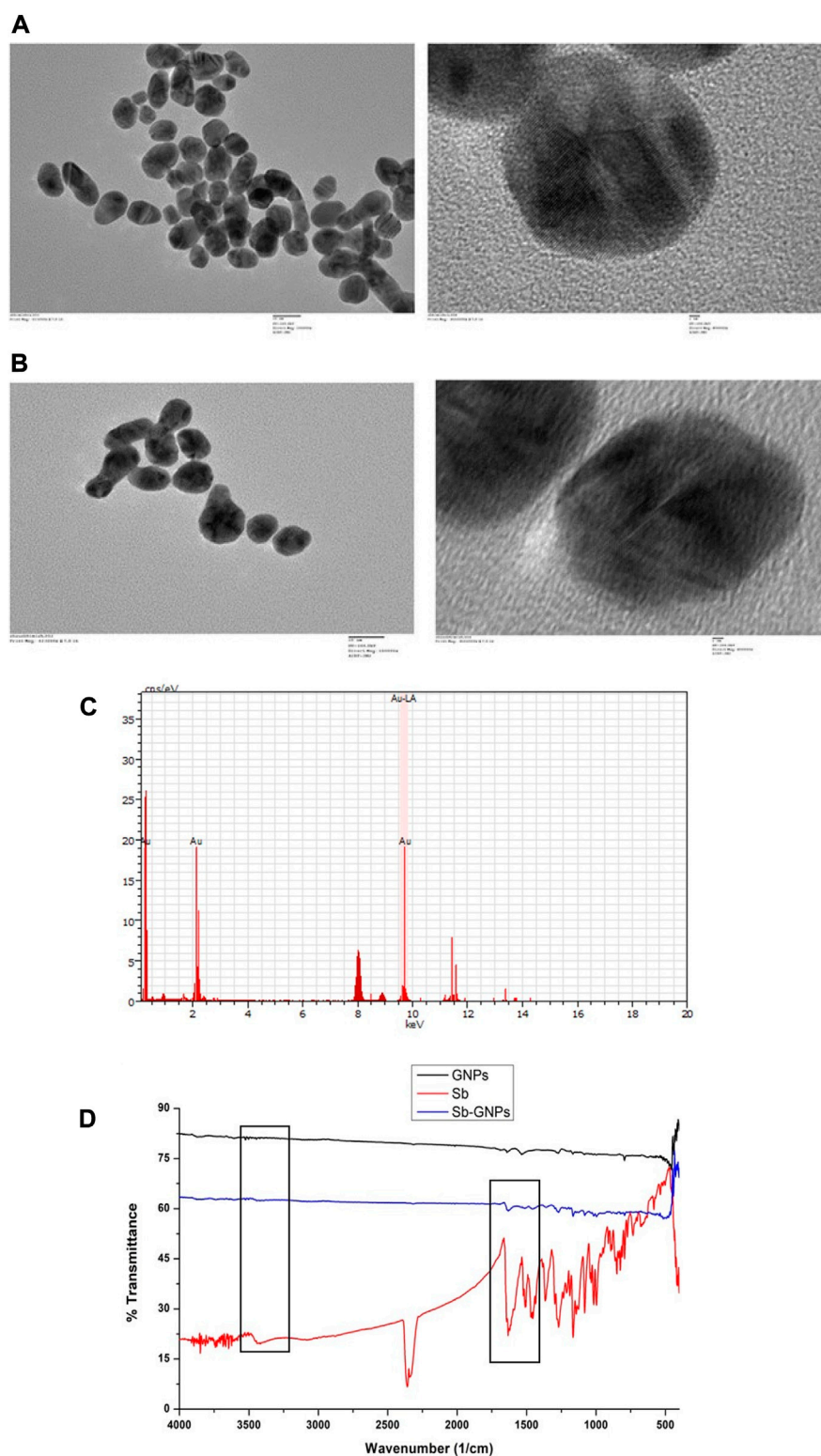
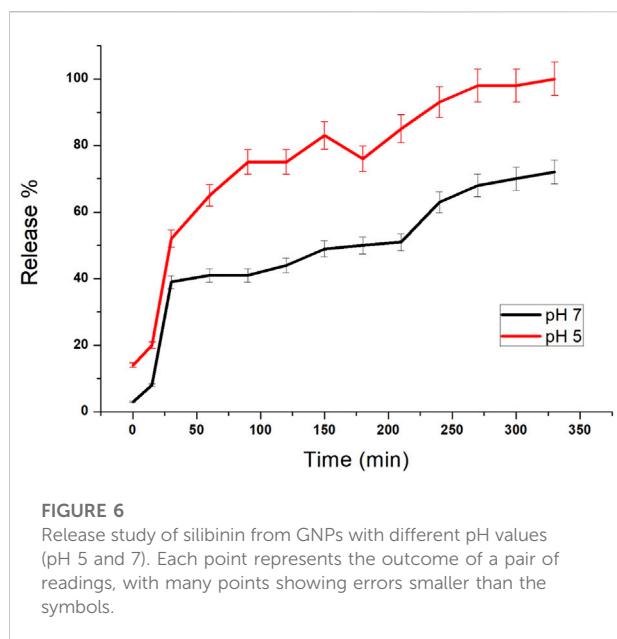


FIGURE 5

(A) Transmission electron microscopy (TEM) images of free, purified gold nanoparticles; (B) Transmission electron microscopy (TEM) images of Silibinin conjugated gold nanoparticles; (C) Energy dispersive X-ray analysis (EDAX) of gold nanoparticles and Silibinin conjugated gold nanoparticles; (D) Fourier transformed infrared spectroscopy (FTIR) spectra of free, purified gold nanoparticles, free Silibinin and Silibinin conjugated gold nanoparticles.



localized surface plasmon resonance (LSPR) which is the collective oscillation of electrons in the conduction band of gold nanoparticles in resonance with a specific wavelength of incident light. LSPR of gold nanoparticles resulted a strong absorbance band which can be measured spectroscopically (Figure 1). The LSPR spectrum is dependent both on the size and shape of gold nanoparticles. The peak absorbance wavelength increases with particle diameter and for unevenly shaped particles such as gold nanourchins, the absorbance spectrum shifts significantly into the far-red region of the spectrum when compared to a spherical particle of the same diameter. The absorbance of the sample correlates linearly to the concentration of nanoparticles in the solution. The synthesis of gold nanoparticles at a varying concentration of trisodium citrate dihydrate is shown in Figure 2. This spectrum shows that when the concentration of trisodium citrate dihydrate is 2.5 mM, the sharpest and narrowest peak appears, indicating that nanoparticles of nearly uniform shape and size are synthesized at this concentration. As a result, the optimal concentration of trisodium citrate dihydrate was observed to be 2.5 mM. The synthesis of gold nanoparticles at various temperatures is depicted in

trisodium citrate (reducing agent). Gold nanoparticles exhibit a distinct optical feature commonly referred to as

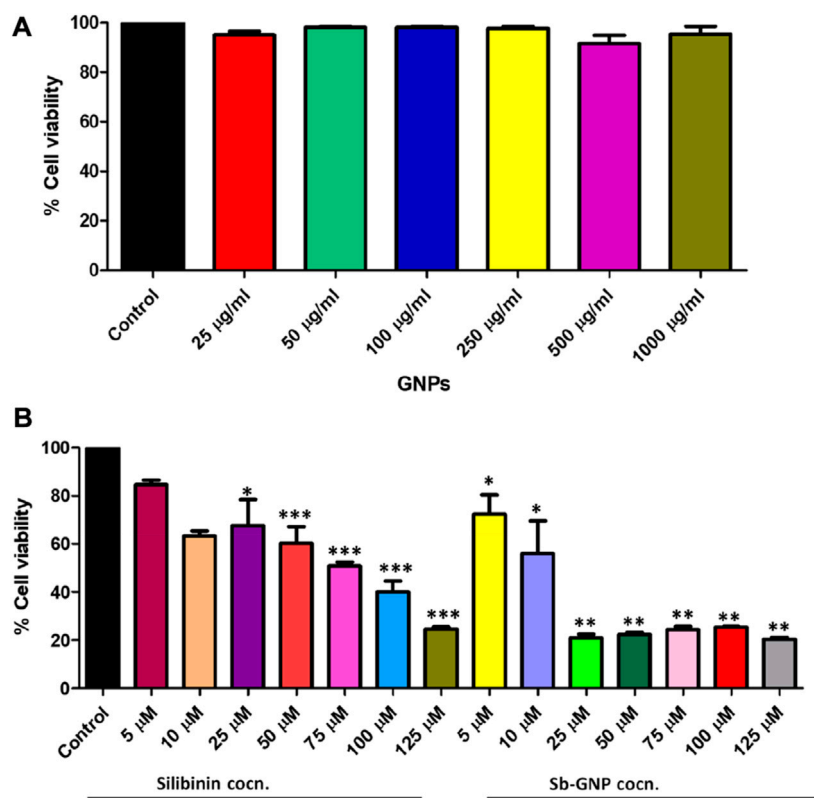


FIGURE 7

(A) *In vitro* anticancer efficacy of free GNPs; (B) *In vitro* anticancer efficacy of free Silibinin and Sb-GNPs.

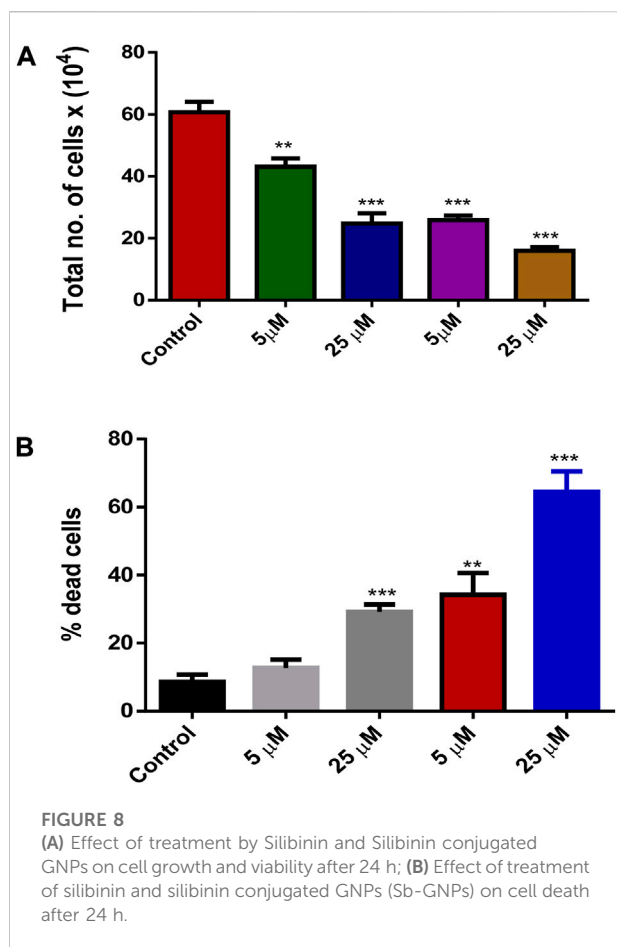


Figure 3. This spectrum shows that when gold nanoparticles are synthesized at 90°C, the sharpest and narrowest peak appears, indicating that nanoparticles of nearly uniform shape and size are synthesized at this temperature. As a result, the synthesis reaction's optimal temperature was determined to be 90°C. **Figure 4** depicts the synthesis of gold nanoparticles over time. When comparing the spectra of solutions before and after 30 min, the spectra at 30 min and beyond 30 min displayed a strong and narrow peak. This suggested that the optimum time to make gold nanoparticles was 30 min.

Humans have traditionally used silibinin for various applications, and acute and chronic levels of silibinin administration in animals and humans have shown no harm (Dheeraj et al., 2018). In several pre-clinical cancer models, such as skin, prostate, colorectal, and lung cancer, it has shown significant efficacy in reducing or delaying both tumor initiation and promotion associated events. Because of its widespread use as a popular dietary supplement, biological-tolerance, and low toxicity, silibinin intake has been shown to be beneficial for preventing several disorders. In the given study, we have sought to conjugate silibinin to gold

nanoparticles to enhance its efficacy against lung cancer. For this, different concentrations of silibinin were taken for conjugation to gold nanoparticles and maximum binding was observed at 50 μ M of silibinin as shown in Table 1. At 50 μ M, 80.6% of initial silibinin taken for the conjugation reaction binds to the gold nanoparticles, while only 19.4% remained unconjugated in the reaction mixture. Similar trends in immobilization efficiency with increasing enzyme load have been reported by other researchers (Mishra et al., 2013a; Ahmad et al., 2014b). Based on this observation, for further use in bulk conjugation reactions, 50 μ M concentration of silibinin was chosen as the optimum concentration for further experiments.

The optical and physical properties of gold nanoparticles were determined by their size (diameter), shape, surface structure, and aggregation state. For functionalizing or conjugating the surface of gold nanoparticles with a biological compound, it is necessary to characterize them to assess the effect of surface functionalization on naked gold nanoparticles. For this, a variety of techniques must be used to characterize both bare and surface-functionalized gold nanoparticles. We have performed TEM to analyse the size, shape and morphology of the GNPs and Silibinin conjugated GNPs. The TEM images of free GNPs and silibinin conjugated GNPs showed nearly monodispersed and spherical shape (Figures 5A,B). Energy-dispersive X-ray spectroscopy (EDAX) is an analytical technique intended for the chemical or elemental analysis of gold nanoparticles. EDAX analysis was performed using TEM. EDAX analysis of silibinin conjugated GNPs showed the presence of gold atom (Figure 5C). The DLS studies were carried out to determine the hydrodynamic radius which reveals that the average diameter was found to be 107 ± 9 nm for GNPs and 163 ± 5 nm for silibinin GNPs nanoconjugates. The increase in size indicates that the silibinin was successfully conjugates with GNPs. The particle size distribution was determined by calculating Polydispersity index (PDI). PDI was found to be 0.3 (GNPs) and 0.5 (Sb-GNPs conjugates). Further, zeta potentials were determined to check the stability of colloidal suspensions and found to be -19.6 mV \pm 0.648 (GNPs) and -22.2 mV \pm 0.458 mV (Sb-GNPs nanoconjugates), which indicate a long-term stability of gold and Sb-GNPs nanoconjugates in suspension phase. FTIR spectra has indicated sharp peak to understand the possible mechanism of association of silibinin on GNPs (Figure 5D). The IR peak at $1,670$ cm⁻¹ appeared for stretching vibration of C=O (observed for silibinin) shifting to lower wavenumber in the case of silibinin conjugated gold nanoparticles with reduced intensity thereby indicated the possible interaction of silibinin by its C=O functional group during conjugation to gold nanoparticles. Also, at around $3,400$ cm⁻¹, peak which showed absorption by -OH functional

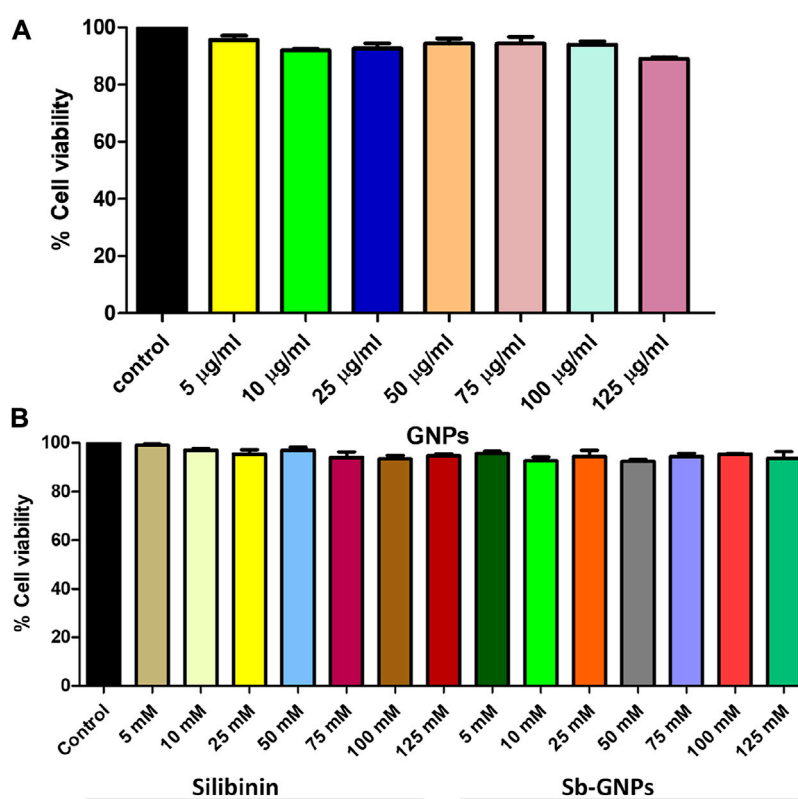


FIGURE 9
Effect of (A) Free GNPs; (B) Silibinin and Sb-GNPs against normal cell viability (HEK293T).

group of silibinin was observed with reduced intensity in case of silibinin conjugated gold nanoparticles, which indicates the interaction of $-\text{OH}$ group of silibinin during conjugation with gold nanoparticles (Ahmad et al., 2015; Sadaf et al., 2020).

The release of silibinin in pH 7 (physiological pH) and pH 5 (acidic pH mimicking tumour microenvironment) was monitored by UV-Vis spectroscopy. The result showed that the release of silibinin in acidic pH increased with time from up to 25–200 min and got saturated at 300 min. However, in physiologic pH (pH - 7) lower release of silibinin was observed as compared to release in acidic pH (pH \sim 5). It is well established that the physiological pH is around 7.4 while that of the tumor microenvironment is in the acidic range. Our results showed that silibinin conjugated gold nanoparticles enhanced the delivery of silibinin to cancer cells (Figure 6). Free gold nanoparticles did not show significant cytotoxicity toward cancer cell lines (Figure 7A). Cell viability of free silibinin and silibinin conjugated gold nanoparticles were tested on lung carcinoma cell line (A549) by performing the MTT assay, and it was found that both have decreased the cell viability. Silibinin conjugated gold

nanoparticles showed IC_{50} value at $4.8 \mu\text{M}$ (w.r.t. Sb concentration) while the IC_{50} value in the case of free silibinin is $24.8 \mu\text{M}$. Free gold nanoparticles did not show significant cytotoxicity toward cancer cell lines (Figure 7B). IC_{50} value for the formulation was calculated using freely available COMPUSYN software. Trypan blue dye exclusion assay was performed to assess the percentage cell viability after the treatment with silibinin and Sb-GNPs. It was observed that the cell viability decreased more when treated with Sb-GNPs than treatment with free silibinin. The $5 \mu\text{M}$ dose of conjugated silibinin showed the same decreased in cell viability (approx. 35–40%) as compared to the $25 \mu\text{M}$ of free silibinin. The results indicate that the low concentration of Sb-GNPs nonconjugates have achieved the same effect as compared to high concentration of free silibinin. The similar effects can be observed in terms of cell death of the cancer cells. This observation clearly showed that on conjugation with gold nanoparticles, the efficacy of silibinin increased 4–5 times in inhibiting and killing the cancer cells (Figures 8A,B). Further, data of biocompatibility of GNPs, silibinin, Sb-GNPs on normal

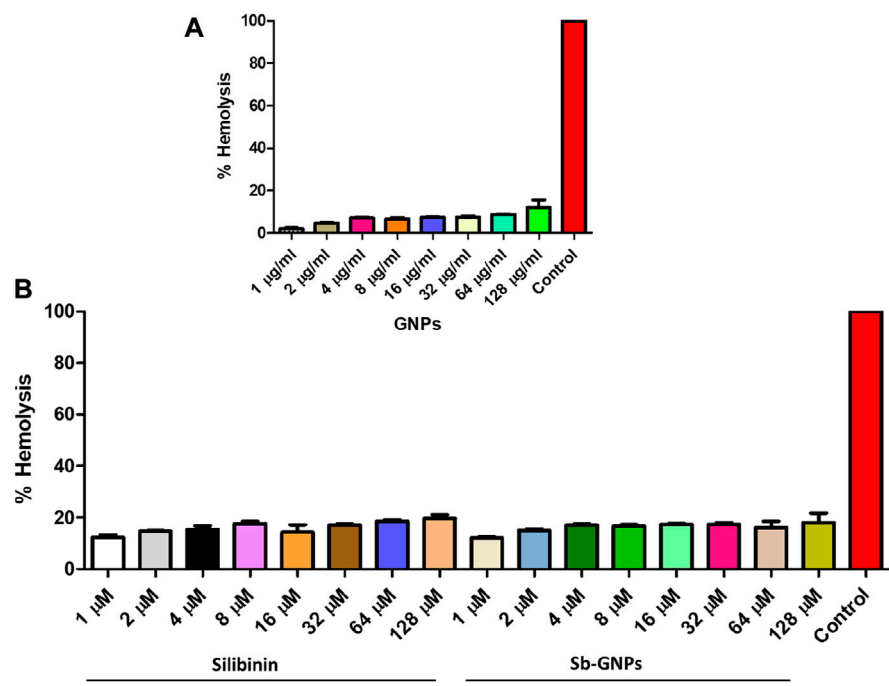


FIGURE 10
(A) Percentage hemolysis of human RBCs caused by GNPs; (B) Percentage hemolysis of human RBCs caused by Silibinin and Sb-GNPs. Triton-X-100 (0.4%) was used as positive control.

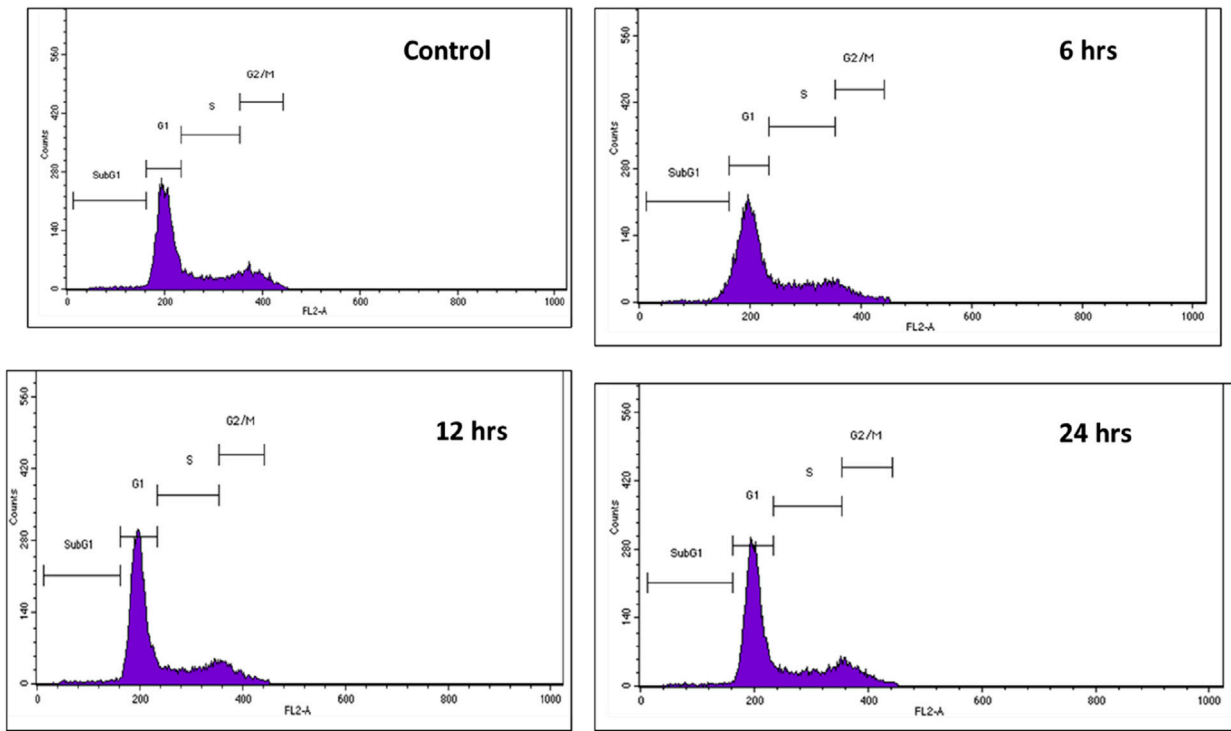


FIGURE 11
Effect of Silibinin and Sb-GNPs on cell cycle arrest in lung cancer cells.

cell (HEK293) clearly indicate that these compounds are non-toxic in nature. (Figures 9A,B). The investigation of hemolytic activity is important to determine the biocompatibility of GNPs, silibinin and Sb-GNPs with RBCs. Therefore, the hemolytic activity of GNPs at different concentrations (1–128 µg/ml) and for silibinin and Sb-GNPs (1–128 µM) was determined against freshly human RBCs. Figure 10 showed the percentage of hemolysis, which depicts that the hemolysis caused by the GNPs, silibinin and Sb-GNPs is very less as compared with positive control (Triton X100). Thus, the result of the present study indicating the safety of these nanoconjugates (Sb-GNPs) at low concentrations provides support for further investigations. Similar studies were done by others (Mishra et al., 2013b; Ahmad et al., 2014a). The effect of Sb-GNPs on cell cycle progression of A549 (lung cancer cells) were studied with IC₅₀ concentrations obtained by MTT assay. It was found that the IC₅₀ dose treatment of Sb-GNPs arrest the growth of cancer cells in G1 phase (Figure 11). Several studies have explored the preparation of silibinin conjugated inhalable nanoparticles as well as Silibinin-loaded PLGA/PEG NPs but that of gold-conjugated ones are few in comparison (Mogheri et al., 2021; Raval et al., 2021). Thus, the above study provides a promising route to develop formulations using silibinin conjugated metal nanoparticles with novel anticancer applications.

Conclusion

In the present study, Silibinin conjugated GNPs was synthesized and further investigated their cytotoxic effect on lung cancer cells. Silibinin is of considerable importance which could help prevent normal tissue cytotoxicity in lung cancer patients. Beyond its hepatoprotective effects, the pharmacological activity of silymarin is being revisited due to growing evidence that suggests potential anti-cancer activity. Various evidence indicates that silibinin is a possible drug candidate for tumor growth inhibition and further its efficacy can be enhanced by using nanoparticles (Liu et al., 2020). GNPs was synthesized using trisodium citrate dihydrate as the reducing agent and further it was used as a matrix for the conjugation of silibinin. The techniques TEM, EDAX, DLS and FTIR were performed to characterize the optical and physical properties of gold nanoparticles and its conjugates. The results indicate that the silibinin was successfully conjugated with monodispersed and spherical shape gold nanoparticles.

After characterization, the anticancer efficacy of silibinin and silibinin conjugated gold nanoparticles was evaluated by *in vitro* assays such as MTT assay and Trypan blue dye

exclusion assay. It was found that the enhanced cytotoxic and growth inhibitory effects of Gold-Silibinin nanoconjugates as compared to silibinin alone. This opens up the possibility of developing anti-cancer compositions based on silibinin linked nanoparticles.

Data availability statement

The original contributions presented in the study are included in the article/supplementary material, further inquiries can be directed to the corresponding authors.

Author contributions

RR, MZ, SG, MKW, RB, AMA, AM and RA have conceptualized, prepared and critically reviewed the manuscript. All authors contributed to the article and approved the submitted version.

Acknowledgments

The authors extend their appreciation to the Deanship of Scientific Research at King Khalid University, KSA, for funding this work through a research group program under grant number RGP. 2/181/43. Prof. RP Singh, SLS, Jawaharlal Nehru University is greatly acknowledged for helping in cancer cell line study.

Conflict of interest

RA was employed by the company Anantaa GSK Innovations Pvt. Ltd.

The remaining authors declare that the research was conducted in the absence of any commercial or financial relationships that could be construed as a potential conflict of interest.

Publisher's note

All claims expressed in this article are solely those of the authors and do not necessarily represent those of their affiliated organizations, or those of the publisher, the editors and the reviewers. Any product that may be evaluated in this article, or claim that may be made by its manufacturer, is not guaranteed or endorsed by the publisher.

References

- Abenavoli, L., Izzo, A. A., Milić, N., Cicala, C., Santini, A., and Capasso, R. (2018). Milk thistle (*Silybum marianum*): A concise overview on its chemistry, pharmacological, and nutraceutical uses in liver diseases. *Phytotherapy Res.* 32 (11), 2202–2213. doi:10.1002/ptr.6171
- Aboushanab, S. A., Shevyrin, V. A., Slesarev, G. P., Melekhin, V. V., Shcheglova, A. V., Makeev, O. G., et al. (2022). Antioxidant and cytotoxic activities of kudzu roots and soy molasses against pediatric tumors and phytochemical analysis of isoflavones using HPLC-DAD-ESI-HRMS. *Plants* 11 (6), 741. doi:10.3390/plants11060741
- Ahmad, R., Khatoon, N., and Sardar, M. (2014a). Antibacterial effect of green synthesized TiO₂ nanoparticles. *Adv. Sci. Lett.* 20 (7-9), 1616–1620. doi:10.1166/asl.2014.5563
- Ahmad, R., Mishra, A., and Sardar, M. (2014b). Simultaneous immobilization and refolding of heat treated enzymes on TiO₂ nanoparticles. *Adv. Sci. Eng. Med.* 6 (12), 1264–1268. doi:10.1166/ase.2014.1644
- Ahmad, R., Mohsin, M., Ahmad, T., and Sardar, M. (2015). Alpha amylase assisted synthesis of TiO₂ nanoparticles: Structural characterization and application as antibacterial agents. *J. Hazard. Mater.* 283, 171–177. doi:10.1016/j.jhazmat.2014.08.073
- Ahmad, R., Srivastava, S., Ghosh, S., and Khare, S. K. (2021). Phytochemical delivery through nanocarriers: A review. *Colloids Surfaces B Biointerfaces* 197, 111389. doi:10.1016/j.colsurfb.2020.111389
- Aljarba, N. H., Imtiaz, S., Anwar, N., Alanazi, I. S., and Alkahtani, S. (2022). *Anticancer and microbial activities of gold nanoparticles: A mechanistic review*. Journal of King Saud University-Science 34, 101907. doi:10.1016/j.jksus.2022.101907
- Aviel-Ronen, S., Blackhall, F. H., Shepherd, F. A., and Tsao, M.-S. (2006). K-Ras mutations in non-small-cell lung carcinoma: A review. *Clin. lung cancer* 8 (1), 30–38. doi:10.3816/clc.2006.n.030
- Bagherifar, R., Kiaie, S. H., Hatami, Z., Ahmadi, A., Sadeghnejad, A., Baradaran, B., et al. (2021). Nanoparticle-mediated synergistic chemimmunotherapy for tailoring cancer therapy: Recent advances and perspectives. *J. Nanobiotechnology* 19 (1), 110–118. doi:10.1186/s12951-021-00861-0
- Bahuguna, A., Khan, I., Bajpai, V. K., and Kang, S. C. (2017). MTT assay to evaluate the cytotoxic potential of a drug. *Bangladesh J. Pharmacol.* 12 (2), 115–118. doi:10.3329/bjp.v12i2.30892
- Da Silva, C. G., Rueda, F., Löwik, C. W., Ossendorp, F., and Cruz, L. J. (2016). Combinatorial prospects of nano-targeted chemoimmunotherapy. *Biomaterials* 83, 308–320. doi:10.1016/j.biomaterials.2016.01.006
- Dai, W., Wang, X., Song, G., Liu, T., He, B., Zhang, H., et al. (2017). Combination antitumor therapy with targeted dual-nanomedicines. *Adv. Drug Deliv. Rev.* 115, 23–45. doi:10.1016/j.addr.2017.03.001
- Dheeraj, A., Tailor, D., Singh, S. P., and Singh, R. P. (2018). *Anticancer attributes of silibinin: Chemo- and radiosensitization of cancer. in: Role of nutraceuticals in cancer chemosensitization*. Elsevier, 199–220.
- Duan, X., Chan, C., and Lin, W. (2019). Nanoparticle-mediated immunogenic cell death enables and potentiates cancer immunotherapy. *Angew. Chem. Int. Ed.* 58 (3), 670–680. doi:10.1002/anie.201804882
- Ghimessy, A., Radecky, P., Laszlo, V., Hegedus, B., Renyi-Vamos, F., Fillinger, J., et al. (2020). Current therapy of KRAS-mutant lung cancer. *Cancer Metastasis Rev.* 39 (4), 1159–1177. doi:10.1007/s10555-020-09903-9
- Ghosh, S., Ahmad, R., Banerjee, K., AlAjmi, M. F., and Rahman, S. (2021a). Mechanistic aspects of microbe-mediated nanoparticle synthesis. *Front. Microbiol.* 12, 638068. doi:10.3389/fmicb.2021.638068
- Ghosh, S., Ahmad, R., Zeyaulah, M., and Khare, S. K. (2021b). Microbial nanofactories: Synthesis and biomedical applications. *Front. Chem.* 9, 626834. doi:10.3389/fchem.2021.626834
- Herbst, R. S., Heymach, J. V., and Lippman, S. (2008). Lung cancer. *N. Engl. J. Med. Overseas. Ed.* 359 (13), 1367–1380. doi:10.1056/nejmra0802714
- Jančová, P., Anzenbacherova, E., Papoušková, B., Lemr, K., Lužná, P., Veinlichová, A., et al. (2007). Silibinin is metabolized by cytochrome P450 2C8 *in vitro*. *Drug Metab. Dispos.* 35 (11), 2035–2039. doi:10.1124/dmd.107.016410
- Lemjabbar-Alaoui, H., Hassan, O. U. I., Yang, Y.-W., and Buchanan, P. (2015). Lung cancer: Biology and treatment options. *Biochimica Biophysica Acta - Rev. Cancer* 1856 (2), 189–210. doi:10.1016/j.bbcan.2015.08.002
- Lim, H. M., and Park, S.-H. (2022). Regulation of reactive oxygen species by phytochemicals for the management of cancer and diabetes. *Crit. Rev. Food Sci. Nutr.* 1–26. doi:10.1080/10408398.2022.2025574
- Liu, Y., Xie, X., Hou, X., Shen, J., Shi, J., Chen, H., et al. (2020). Functional oral nanoparticles for delivering silibinin and cryptotanshinone against breast cancer lung metastasis. *J. Nanobiotechnology* 18 (1), 83–15. doi:10.1186/s12951-020-00638-x
- Mahdinloo, S., Kiaie, S. H., Amiri, A., Hemmati, S., Valizadeh, H., and Zakeri-Milani, P. (2020). Efficient drug and gene delivery to liver fibrosis: Rationale, recent advances, and perspectives. *Acta Pharm. Sin. B* 10 (7), 1279–1293. doi:10.1016/j.apbsb.2020.03.007
- Mateen, S., Raina, K., and Agarwal, R. (2013). Chemopreventive and anti-cancer efficacy of silibinin against growth and progression of lung cancer. *Nutr. cancer* 65, 3–11. doi:10.1080/01635581.2013.785004
- Melim, C., Magalhães, M., Santos, A. C., Campos, E. J., and Cabral, C. (2022). Nanoparticles as phytochemical carriers for cancer treatment: News of the last decade. *Expert Opin. Drug Deliv.* 19 (2), 179–197. doi:10.1080/17425247.2022.2041599
- Mishra, A., Ahmad, R., Singh, V., Gupta, M. N., and Sardar, M. (2013a). Preparation, characterization and biocatalytic activity of a nanoconjugate of alpha amylase and silver nanoparticles. *J. Nanosci. Nanotechnol.* 13 (7), 5028–5033. doi:10.1166/jnn.2013.7593
- Mishra, A., Kaushik, N. K., Sardar, M., and Sahal, D. (2013b). Evaluation of antiplasmodial activity of green synthesized silver nanoparticles. *Colloids Surfaces B Biointerfaces* 111, 713–718. doi:10.1016/j.colsurfb.2013.06.036
- Mogheri, F., Jokar, E., Afshin, R., Akbari, A. A., Dadashpour, M., Firouzi-amandi, A., et al. (2021). Co-delivery of metformin and silibinin in dual-drug loaded nanoparticles synergistically improves chemotherapy in human non-small cell lung cancer A549 cells. *J. Drug Deliv. Sci. Technol.* 66, 102752. doi:10.1016/j.jddst.2021.102752
- Nikdouz, A., Namavari, N., Shayan, R. G., and Hosseini, A. (2022). Comprehensive comparison of theranostic nanoparticles in breast cancer. *Am. J. Clin. Exp. Immunol.* 11 (1), 1–27.
- Pirker, R., and Zhou, C. (2022). Editorial: Lung cancer: Continuous progress in diagnosis and treatment. *Curr. Opin. Oncol.* 34 (1), 29–31. doi:10.1097/cco.0000000000000809
- Pucci, C., Martinelli, C., and Ciofani, G. (2019). Innovative approaches for cancer treatment: Current perspectives and new challenges. *Ecancermedicalscience* 13, 961. doi:10.3332/ecancer.2019.961
- Rao, N., and Wei, S. (2022). *Mesothelioma*. United States: Cytojournal, 19.
- Raval, M., Patel, P., Airao, V., Bhatt, V., and Sheth, N. (2021). Novel silibinin loaded chitosan-coated PLGA/PCL nanoparticles based inhalation formulations with improved cytotoxicity and bioavailability for lung cancer. *Bionanoscience* 11 (1), 67–83. doi:10.1007/s12668-020-00797-z
- Sadaf, A., Ahmad, R., Ghorbal, A., Elfalleh, W., and Khare, S. K. (2020). Synthesis of cost-effective magnetic nano-biocomposites mimicking peroxidase activity for remediation of dyes. *Environ. Sci. Pollut. Res.* 27 (22), 27211–27220. doi:10.1007/s11356-019-05270-3
- Singh, R. P., Deep, G., Chittethazh, M., Kaur, M., Dwyer-Nield, L. D., Malkinson, A. M., et al. (2006). Effect of silibinin on the growth and progression of primary lung tumors in mice. *JNCI J. Natl. Cancer Inst.* 98 (12), 846–855. doi:10.1093/jnci/djj231
- Singh, S. P., Mishra, A., Shyanti, R. K., Singh, R. P., and Acharya, A. (2021). Silver nanoparticles synthesized using Carica papaya leaf extract (AgNPs-PL) causes cell cycle arrest and apoptosis in human prostate (DU145) cancer cells. *Biol. Trace Elem. Res.* 199 (4), 1316–1331. doi:10.1007/s12011-020-02255-z
- Srivastava, S., Ahmad, R., and Khare, S. K. (2021). Alzheimer's disease and its treatment by different approaches: A review. *Eur. J. Med. Chem.* 216, 113320. doi:10.1016/j.ejmech.2021.113320
- Takke, A., and Shende, P. (2019). Nanotherapeutic silibinin: An insight of phytomedicine in healthcare reformation. *Nanomedicine Nanotechnol. Biol. Med.* 21, 102057. doi:10.1016/j.nano.2019.102057
- Tian, X., Gu, T., Lee, M.-H., and Dong, Z. (2022). Challenge and countermeasures for EGFR targeted therapy in non-small cell lung cancer. *Biochimica Biophysica Acta - Rev. Cancer* 1877 (1), 188645. doi:10.1016/j.bbcan.2021.188645
- Tyagi, A., Singh, R. P., Ramasamy, K., Raina, K., Redente, E. F., Dwyer-Nield, L. D., et al. (2009). Growth inhibition and regression of lung tumors by silibinin: Modulation of angiogenesis by macrophage-associated cytokines and nuclear factor-κB and signal transducers and activators of transcription 3. *Cancer Prev. Res.* 2 (1), 74–83. doi:10.1158/1940-6207.capr-08-0095
- Verdura, S., Cuyàs, E., Ruiz-Torres, V., Micol, V., Joven, J., Bosch-Barrera, J., et al. (2021). Lung cancer management with silibinin: A historical and translational perspective. *Pharmaceuticals* 14 (6), 559. doi:10.3390/ph14060559
- Wang, B., Chen, S., Xiao, H., Zhang, J., Liang, D., Shan, J., et al. (2022). Analysis of risk factors and gene mutation characteristics of different metastatic sites of lung cancer. *Cancer Med.* 11 (1), 268–280. doi:10.1002/cam4.4424
- Wuithschick, M., Birnbaum, A., Witte, S., Sztucki, M., Vainio, U., Pinna, N., et al. (2015). Turkevich in new robes: Key questions answered for the most common gold nanoparticle synthesis. *ACS Nano* 9 (7), 7052–7071. doi:10.1021/acsnano.5b01579



OPEN ACCESS

EDITED BY

Wansong Chen,
Central South University, China

REVIEWED BY

Ali Bumajdad,
Kuwait University, Kuwait
Mohammad Ehtisham Khan,
Jazan University, Saudi Arabia

*CORRESPONDENCE

Sirikanjana Thongmee,
fscisjn@ku.ac.th
Sougata Ghosh,
ghoshsibb@gmail.com

SPECIALTY SECTION

This article was submitted to
Nanoscience,
a section of the journal
Frontiers in Chemistry

RECEIVED 06 August 2022

ACCEPTED 11 October 2022

PUBLISHED 31 October 2022

CITATION

Bloch K, Mohammed SM, Karmakar S,
Shukla S, Asok A, Banerjee K,
Patil-Sawant R, Mohd Kaus NH,
Thongmee S and Ghosh S (2022),
Catalytic dye degradation by novel
phytofabricated silver/zinc
oxide composites.
Front. Chem. 10:1013077.
doi: 10.3389/fchem.2022.1013077

COPYRIGHT

© 2022 Bloch, Mohammed, Karmakar,
Shukla, Asok, Banerjee, Patil-Sawant,
Mohd Kaus, Thongmee and Ghosh. This
is an open-access article distributed
under the terms of the [Creative
Commons Attribution License \(CC BY\)](#).
The use, distribution or reproduction in
other forums is permitted, provided the
original author(s) and the copyright
owner(s) are credited and that the
original publication in this journal is
cited, in accordance with accepted
academic practice. No use, distribution
or reproduction is permitted which does
not comply with these terms.

Catalytic dye degradation by novel phytofabricated silver/zinc oxide composites

Khalida Bloch¹, Shahansha M. Mohammed², Srikanta Karmakar³,
Satyajit Shukla^{2,4}, Adersh Asok^{4,5}, Kaushik Banerjee⁶,
Reshma Patil-Sawant⁶, Noor Haida Mohd Kaus⁷,
Sirikanjana Thongmee^{8*} and Sougata Ghosh^{1,8*}

¹Department of Microbiology, School of Science, RK University, Rajkot, Gujarat, India, ²Functional Materials Section (FMS), Materials Science and Technology Division (MSTD), CSIR-National Institute for Interdisciplinary Science and Technology (NIIST), Council of Scientific and Industrial Research (CSIR), Thiruvananthapuram, Kerala, India, ³Department of Polymer Science and Technology, Calcutta University, Kolkata, West Bengal, India, ⁴Academy of Scientific and Innovative Research (AcSIR), Ghaziabad, India, ⁵Photosciences and Photonics Section, Chemical Sciences and Technology Division (CSTD), CSIR-National Institute for Interdisciplinary Science and Technology (NIIST), Council of Scientific and Industrial Research (CSIR), Thiruvananthapuram, Kerala, India, ⁶National Referral Laboratory, ICAR-National Research Centre for Grapes, Pune, India, ⁷School of Chemical Sciences, Universiti Sains Malaysia, Penang, Malaysia, ⁸Department of Physics, Faculty of Science, Kasetsart University, Bangkok, Thailand

Phytofabrication of the nanoparticles with exotic shape and size is an attractive area where nanostructures with noteworthy physicochemical and optoelectronic properties that can be significantly employed for photocatalytic dye degradation. In this study a medicinal plant, *Plumbago auriculata* leaf extract (PALE) was used to synthesize zinc oxide particles (ZnOPs) and silver mixed zinc oxide particles (ZnOAg1Ps, ZnOAg10Ps, ZnO10Ag1Ps) by varying the concentration of the metal precursor salts, i.e. zinc acetate and silver nitrate. The PALE showed significantly high concentrations of polyphenols, flavonoids, reducing sugar, starch, citric acid and plumbagin up to 314.3 ± 0.33 , 960.0 ± 2.88 , 121.3 ± 4.60 , 150.3 ± 3.17 , 109.4 ± 2.36 , and 260.4 ± 8.90 $\mu\text{g/ml}$, respectively which might play an important role for green synthesis and capping of the phytogenic nanoparticles. The resulting particles were polydispersed which were mostly irregular, spherical, hexagonal and rod like in shape. The pristine ZnOPs exhibited a UV absorption band at 352 nm which shifted around 370 nm in the Ag mixed ZnOPs with concomitant appearance of peaks at 560 and 635 nm in ZnO10Ag1Ps and ZnOAg1Ps, respectively. The majority of the ZnOPs, ZnOAg1Ps, ZnOAg10Ps, and ZnO10Ag1Ps were 407, 98, 231, and 90 nm in size, respectively. Energy dispersive spectra confirmed the elemental composition of the particles while Fourier transform infrared spectra showed the involvement of the peptide and methyl functional groups in the synthesis and capping of the particles. The composites exhibited superior photocatalytic degradation of methylene blue dye, maximum being 95.7% by the ZnOAg10Ps with a rate constant of 0.0463 s^{-1} following a first order kinetic model. The present result clearly highlights that Ag mixed ZnOPs synthesized using *Plumbago auriculata* leaf extract (PALE) can play a critical role in removal of hazardous dyes from effluents of textile and dye industries. Further expanding the application of these phytofabricated composites will promote a significant complementary and alternative strategy for treating refractory pollutants from wastewater.

KEYWORDS

Plumbago auriculata, zinc oxide particles, silver mixed composites, phytochemical, methylene blue, photocatalysis

1 Introduction

Recent industrial revolution has led to environmental pollution that has created a great concern. Several industries associated with dye, textiles, tanning of leather, paper and pulp are common sources of refractory pollutants in the water bodies. Discharge of the dye contaminated effluents cause soil, ground and surface water pollution (Mani and Bharagava, 2017; Din et al., 2021). Since 4000 years, textile dying technology exists although in ancient times, natural dyes were predominantly used. In 1856, first synthetic dye named “mauveine” was synthesized by William E. Perkin employing oxidation of impure aniline (Fagier, 2021). After the discovery of diazotization and azo coupling, majority of synthetic dyes were developed. Around thousand dyes are commercially available today. Approximately 10,000 different dyes and pigments are used which requires production of 0.7 million tons of synthetically generated dyes every year across the globe (Hashmi et al., 2021). These hazardous dyes cause majority of water pollution and inhibit the photosynthetic activity of aquatic plants due to reduction in the penetration of sunlight. It induces the toxic effect on aquatic life as dye contains aromatic, heavy metals and chloride (Saraf et al., 2015). The dye contaminated water also causes soil pollution and adversely affects the germination of seed (Kumar et al., 2015). The synthetic dyes show harmful effects on animals and humans. Evaporation of chemicals from the dye effluents into air leads to allergic reaction as they are absorbed by skin (Saleh and Djaja, 2014).

Several chemical and physical methods such as adsorption, precipitation, flocculation, electrolysis, oxidation, reduction, electrochemical treatment, ion exchange are used for the removal of dyes from polluted water (Gautam et al., 2017). But these methods are complicated, expensive and are not ecofriendly. Hence, removal of dyes by biological methods is considered as promising alternative due to their cost effective, less sludge producing and ecofriendly nature (Bloch et al., 2020). Several microbes such as bacteria, fungi and algae are also used to degrade wide range of dyes (Daneshvar et al., 2007). Nanotechnology driven solutions for dye removal are more efficient owing to the smaller size, significantly large ratio for surface area to volume and exotic physico-chemical and opto-electronic properties of nanoparticles (Mandeep and Shukla, 2020). Synthesis of nanomaterials includes various physical, chemical and biological methods (Nitnavare et al., 2022). Nanoparticles synthesized using chemical and physical methods have several disadvantages as compared to biological synthesis since, they employ toxic and corrosive chemicals for reduction and stabilization (Ghosh et al., 2016).

Microorganisms mediated syntheses of nanoparticles are slower and give only a limited number of morphological feature (Ghosh et al., 2022).

The use of medicinal plants for nanoparticles synthesis has acquired a great attention due to the ease in scaling up for larger production, apart from being cost effective and environmental friendly (Jamdade et al., 2019). Several nanoparticles composed of elemental gold, silver, copper, platinum, and palladium are synthesized using plants which show antimicrobial, antifungal, antibiofilm, cytotoxic, and photocatalytic properties (Shende et al., 2018). Novel nanocomposites of silver-loaded mesoporous zinc oxide and silver-titania are recently reported from extracts of *Lycium barbarum* L. for photocatalytic and therapeutic applications (Sharwani et al., 2021; Sharwani et al., 2022). Likewise, biogenic fabrication of silver nanoparticle-modified zeolitic imidazolate framework was reported as ideal for designing a non-enzymatic electrochemical sensor (Mohammad et al., 2022). Several carbon-based metal nanocomposites can also be used for photocatalytic degradation of hazardous dyes (Khan, 2021). In other studies biogenic zinc oxide nanoparticles (ZnONPs) synthesized from bulb and leaf extract of *Costus woodsonii* exhibited narrow band gap (Khan et al., 2019a,b).

On the basis of ethno botanical knowledge, *Plumbago auriculata* is widely used medicinal plant that possesses many secondary metabolites in its root and aerial parts (Govindan et al., 2020). Phytochemicals such as phenols, flavonoids, alkaloids, carbohydrates and saponins present in *P. auriculata* may help in synthesis of nanoparticles and may act as stabilizing and capping agent. The leaf and stem are rich in plumbagin, a naphthoquinone that possesses antimicrobial, antibiofilm, anticancer and antifungal activities (Singh et al., 2018). The present study attempted to synthesize zinc oxide particles (ZnOPs) and silver mixed zinc oxide particles (ZnOAgPs) using *P. auriculata* leaf extract (PALE) for photocatalytic dye degradation.

2 Materials and methods

2.1 Collection of plant material and plant extract preparation

The plant specimen of *P. auriculata* along with flower was collected from the campus of RK. University, Rajkot, India. The plant was authenticated by taxonomist of Department of Bioscience, Saurashtra University, Rajkot, India. The collected *P. auriculata* leaves were washed thoroughly and were shade dried at ambient temperature for 10 days. Dehydrated leaves

were pulverised to fine powder using electrical blender. A 5 g of dry leaf powder was added in deionized water (100 ml) and heated at 60°C for 20 min to prepare PALE. A Whatman no 1 filter paper was used for filtering the extract. The recovered filtrate was stored at 4°C and the same batch was used during all further experiments.

2.2 Phytochemical analysis

2.2.1 Total phenolic content

Folin-Ciocalteu reagent (0.5 ml) was added to PALE (3 ml) and incubated for 3 min at 25°C. Thereafter 2 ml of 7% sodium carbonate (Na_2CO_3) was added followed by incubation at 100°C for 1 min in a boiling water bath. The absorbance was recorded at 650 nm (Luximon-Ramma et al., 2002). A standard gallic acid curve with concentration ranging from 10 to 100 µg/ml was used to determine the total phenolic content of PALE.

2.2.2 Total flavonoid content

Initially 2% aluminium chloride (2 ml) dissolved in methanol was mixed with equal volume of PALE. The reaction mixture was incubated in darkness at 25°C for 10 min. The absorbance measured at 368 nm was extrapolated on a standard quercetin curve prepared in a range from 10 to 100 µg/ml for estimating the total flavonoid content (Wolfe et al., 2003).

2.2.3 Total reducing sugar content

The 3, 5-Dinitrosalicylic acid (DNSA) reagent was mixed with equal volume (1 ml) of PALE and incubated for 5 min at 100°C. Thereafter, 10 ml of deionized water was added followed by recording of the absorbance at 540 nm (Miller et al., 1959). A standard glucose curve prepared in a range from 100 to 1000 µg/ml was used to find the total reducing sugar in PALE.

2.2.4 Total starch content

Total starch content was estimated using anthrone reagent. PALE (1 ml) was added in anthrone reagent (4 ml) followed by incubation at 100°C for 8 min. After cooling the absorbance was recorded at 630 nm. The standard glucose curve (10–100 µg/ml) was used for the estimation of total starch content (Thayumanavan et al., 1984).

2.2.5 Total citric acid content

The citric acid was estimated as per protocol reported by Saffaran et al. (1948). In brief, 5% trichloroacetic acid and PALE were mixed in equal volume (0.5 ml) to which 4 ml of acetic anhydride was added followed by incubation at 60°C for 10 min. In the next step pyridine (0.5 ml) was mixed and incubated at 60°C for 40 min. Reaction mixture was further allowed to incubate in ice bath. After 5 min total citric acid content in PALE was evaluated by recording the absorbance 540 nm and extrapolating on a citric acid standard curve prepared in a range from 10 to 400 µg/ml.

2.2.6 Total ascorbic acid content

The PALE (4 ml) was initially brominated using 250 µL of bromine water followed by 250 µL of thiourea. Further 1 ml of 2, 4- Dinitrophenylhydrazine (DNPH) was added and was incubated at room temperature for 3 h. Then, 85% sulphuric acid (7 ml) was added and the absorbance was recorded at 540 nm. Standard ascorbic acid (1–10 µg/ml) was used to determine total ascorbic acid content (Sadasivam et al., 2008).

2.2.7 Total plumbagin content

Total plumbagin content was estimated by adding 10% alcoholic potassium hydroxide (KOH) into equal volume (0.5 ml) of PALE in which 1.5 ml of absolute alcohol was further added. Total plumbagin content was estimated by recording the absorbance at 520 nm and using a standard curve prepared by varying plumbagin concentration from 100 to 1000 µg/ml (Israni et al., 2010).

2.3 Synthesis of zinc oxide particles

At first, a stock solution of 10 mM of zinc acetate ($\text{ZnC}_4\text{H}_6\text{O}_4$) salt was prepared by mixing it in 100 ml of deionized water under stirring condition. Then, 5 ml of PALE was added to the 95 ml of $\text{ZnC}_4\text{H}_6\text{O}_4$ stock solution and stirred again at 150 rpm for 24 h at room temperature. After incubation, brown coloured pellets were collected by centrifuging the reaction mixture for 20 min at 10,000 rpm. The pellets were washed twice with distilled water by alternate centrifugation and redispersion for three times. The collected pellets were allowed to calcinate in muffle furnace at 400°C for 4 h (Naseer et al., 2020).

2.4 Synthesis of Ag mixed zinc oxide particles

Silver (Ag) mixed ZnOPs were fabricated by varying the concentration of AgNO_3 and $\text{ZnC}_4\text{H}_6\text{O}_4$. The salt solutions were mixed in identical concentration of 1 and 10 mM for the synthesis of ZnOAg1Ps and ZnOAg10Ps , respectively. For the synthesis of ZnO10Ag1Ps , 10 mM of $\text{ZnC}_4\text{H}_6\text{O}_4$ was mixed with 1 mM of AgNO_3 . Synthesis of respective particles was carried out by mixing 5 ml PALE into 95 ml of each reaction mixture under stirring condition (150 rpm for 24 h). The synthesized particles were recovered and washed similar to the process discussed above. The collected pellets were further calcinated at 400°C for 4 h in a muffle furnace (Thakur et al., 2020).

2.5 Characterization

At first, the UV-Vis. Absorption spectra of the bio-synthesized particles were analyzed by using UV-Visible

TABLE 1 Phytochemicals content of PALE.

Phenolic (μg/ml)	Flavonoid (μg/ml)	Reducing sugar (μg/ml)	Starch (μg/ml)	Citric acid (μg/ml)	Ascorbic acid (μg/ml)	Plumbagin (μg/ml)
314.30 ± 0.33	960.0 ± 2.88	121.30 ± 4.60	150.30 ± 3.17	109.40 ± 2.36	1.97 ± 1.55	260.40 ± 8.90

spectrometer (UV-1900, Shimadzu, Japan) operating at a resolution of 1 nm. The photoluminescence properties of the synthesized samples were recorded with Fluorescence Spectrophotometer (F-4700, Hitachi, Japan) at an excitation wavelength (λ_{ex}) of 340 nm (Jangir et al., 2017). The surface morphology of particles was determined using transmission electron microscopy (TEM, Tecnai G2 F30, Thermo Fisher, United States) operating at an accelerating voltage of 300 kV. Before that a droplet of the prepared sonicated sample was placed directly on the carbon-coated copper grid that was subsequently dried at 37°C (Basri et al., 2020). Further, energy dispersive X-ray analysis (EDAX) was employed for determining the elemental composition using Octane ELITE T70, EDAX, United States equipped in the TEM. Hydrodynamic size of the synthesized particles was estimated employing dynamic light scattering in a Particle Size/Zeta Potential Analyzer, Microtrac, United States (Salunke et al., 2014). The crystalline phases present were determined using the X-ray diffraction (XRD, EMPYREAN 3, Malvern Panalytical B.V. Netherlands). The broad-scan analysis was typically conducted within the range of 10–90° using the Cu K α (λ_{Cu} = 1.540 Å) X-radiation. The functional groups associated with the particles were characterized by Fourier-transform infrared (FT-IR) using ThermoNicolet FTIR spectrophotometer (Nicolet Instrument, Thermo scientific, United States). The washed particles sample (20 μ L) was mixed with 20 mg KBr and was dried at 50°C in hot air oven. The mixed powder was exposed to infrared source of 500–4500 cm⁻¹ (Brus, 1986).

2.6 GC-MS/MS analysis

The analysis was performed using an Agilent GC (7890A) equipped with a CTC Combipal (CTC Analytics, Switzerland) autosampler, connected to a triple quadrupole mass spectrometer (7000B, Agilent Technologies, Santa Clara, United States). The instrument was controlled by Mass Hunter software (ver. B.05.00.412). The multi-mode inlet (MMI) was operated in split mode. Later, 2 μ L of the PALE sample was injected into a gooseneck liner (78.5 × 6.5 mm, 4 mm). Two HP-5MS (5% phenylmethylpolysiloxane, Agilent Technologies, United States) capillary columns (15 m × 0.25 mm, 0.25 μ m) were connected through a purged ultimate union (Backflush-PUU). Ultra-pure grade helium (BOC India Ltd., Kolkata) was used as the carrier gas, with a constant 1.2 ml/min flow. The oven temperature was programmed to start at 90°C (1 min hold), then ramped at 40°C/min

to 170°C (0 min hold), followed by 15°C/min up to 290°C with a 6-min hold. This resulted in a total run time of 21 min. The temperatures of the ion source and transfer line were set to 230°C and 290°C respectively. Considering the number of molecules, it was important to optimise the chromatographic separation and mass spectrometric parameters to ensure the selectivity and sensitivity in analysis. The mass range was scanned from 50 to 550 amu. The identification of components was based on the comparison of their mass spectra with those of NIST mass spectral library.

2.7 Photocatalytic methylene blue dye degradation

The photocatalytic activity of ZnOPs and the ZnOAgPs was evaluated as the protocol reported earlier (Zachariah et al., 2008). In short, initially 0.4 g L⁻¹ of each particle sample was added to 125 ml of 7.5 μ M MB dye dissolved in distilled water with an initial neutral pH of 6.67. Thereafter, the resulting mixture was stirred to equilibrate stirring in the darkness (that is, without the UV irradiation) for 1 h in order to stabilize the adsorption of MB on the sample surface. The aqueous suspension was then subjected to UV irradiation in the photoreactor chamber (LZC-4X, Luzchem, Canada) using the 14 UVA lamps (6 top and 8 side lamps) with an emission peak intensity of 350 nm with concomitant magnetic stirring for 1 h. After each 10 min intervals, 8 ml aliquot was recovered and centrifuged (Hettich EBA 20, Sigma-Aldrich labware, Bengaluru, India). The supernatant was collected and examined using a UV-visible absorption spectrophotometer (UV-2401 PC, Shimadzu, Japan) to determine the residual MB concentration in the aqueous dye solution.

$$MB_{adsorbed} (\%) = \frac{C_{-60} - C_0}{C_{-60}} \times 100 = \frac{A_{-60} - A_0}{A_{-60}} \times 100 \quad (1)$$

where, C_{-60} and C_0 are the MB concentrations within the aqueous solution before (time (t) = 60 min) and after (t = 0 min) the adsorption experiment conducted in the dark condition; while, A_{-60} and A_0 are the corresponding absorbance values. The normalized concentration of MB remaining in the solution after stirring in the dark condition for 1 h is calculated using Eq. 2.

$$MB_{residual} (\%) = \frac{C_0}{C_{-60}} \times 100 = \frac{A_0}{A_{-60}} \times 100 \quad (2)$$

The normalized concentration of MB remaining in the solution under the UV irradiation is calculated using Eq. 3.

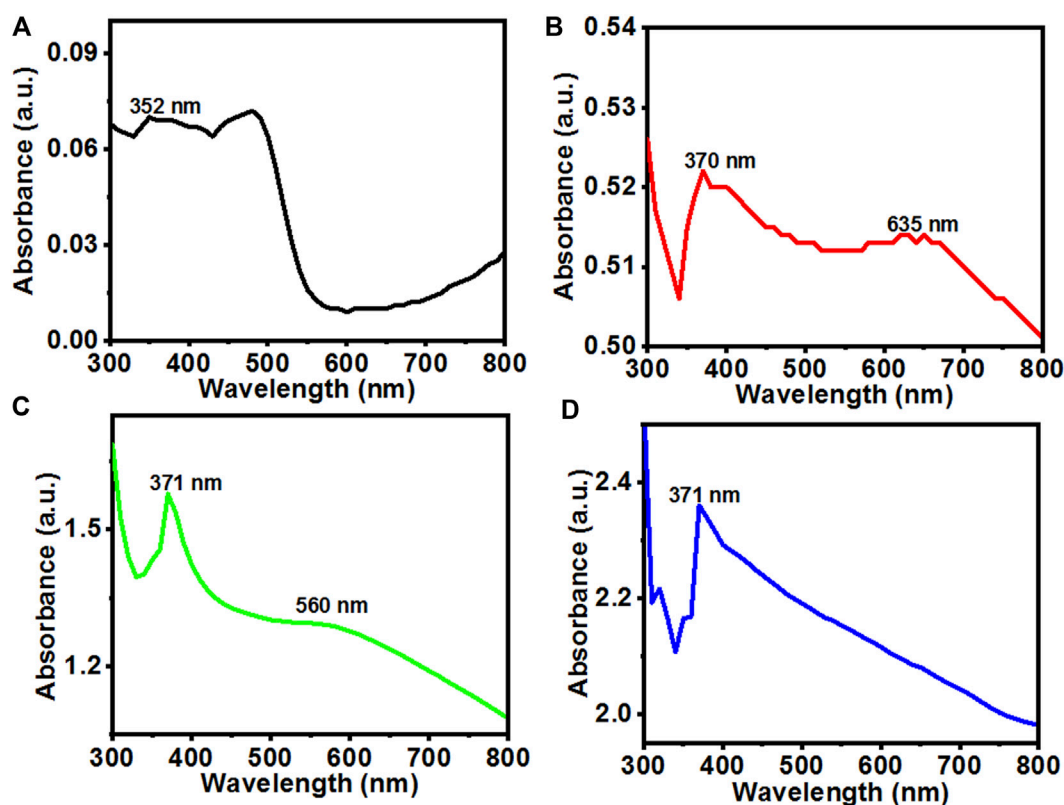


FIGURE 1

UV-Vis absorption spectra of the (A) ZnOPs; (B) ZnOAg1Ps; (C) ZnO10Ag1Ps; (D) ZnOAg10Ps synthesized by using PALE at room temperature.

$$MB_{residual} (\%) = \frac{C_t}{C_{-60}} \times 100 = \frac{A_t}{A_{-60}} \times 100 \quad (3)$$

where, C_t is the MB concentration remaining within the aqueous dye solution after the UV irradiation time of $t = t$ min; while, A_t is the corresponding absorbance value.

The first order kinetic constant (k) for the degradation of MB is calculated using Eq. 4

$$\ln \frac{C_0}{C_t} = kt \quad (4)$$

3 Results

3.1 Phytochemical analysis

The plants belonging to family of Plumbaginaceae are known to be a potential source of various phytochemicals such as phenols, flavonoids, naphthoquinone, alkaloids, and carbohydrates that might play an important role in formation of particles by redox reaction. Table 1 shows high flavonoid content ($960.0 \pm 2.88 \mu\text{g/ml}$) and phenolic content ($314.3 \pm 0.33 \mu\text{g/ml}$) in PALE. The *Plumbago* is

known to contain a naphthoquinone called plumbagin which showed its presence even in PALE at a concentration of $260.0 \mu\text{g/ml}$. Other phytochemicals such as citric acid, ascorbic acid and starch were also noted to be present in PALE. Hence, the presence of these phytochemicals may help in converting zinc acetate to ZnOPs.

3.2 UV-Visible absorption and photoluminescence spectroscopy analyses

Brown color precipitates were formed during reaction which converted to greyish white after calcination indicating synthesis of ZnOPs and ZnOAgPs. The UV-Vis absorption spectra of the synthesized particles were recorded as shown in Figures 1A–D. Figure 1A indicates the UV-Vis absorption spectrum of ZnOPs which showed a broad absorption in the range of 300–490 nm. The main characteristics peak of ZnOPs was observed at 352 nm. The slightly blue shifted peak position of ZnONPs with respect to bulk ZnO was observed implying lower particle size of ZnONPs in comparison to bulk ZnO.

On silver doping, the UV-Vis absorption spectrum of the ZnOAg1Ps revealed two characteristics peaks at 370 nm and

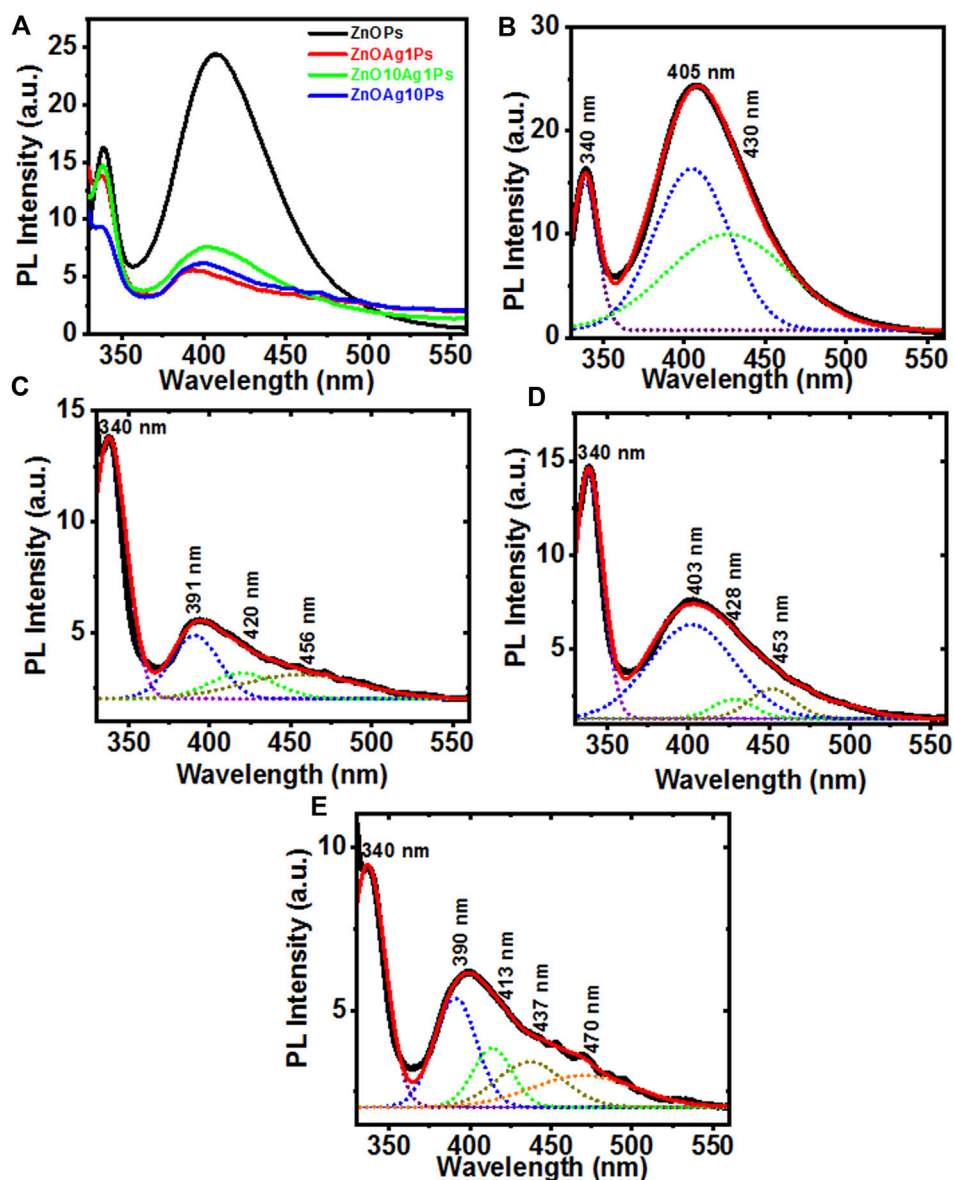


FIGURE 2

(A) Photoluminescence emission spectra of ZnOPs, ZnOAg1Ps, ZnOAg10Ps, ZnO10Ag1Ps; (B–E) the Gaussian fitted PL emission spectra of ZnOPs, ZnOAg1Ps, ZnOAg10Ps, ZnO10Ag1Ps, respectively.

635 nm, respectively as revealed in Figure 1B. Further, with the increase of the concentration of salts in ZnO10Ag1Ps, the absorbance peak became prominent at ~560 nm as evident in Figure 1C and blue shifted in comparison to that of ZnOAg1Ps. This blue shift may have arisen due to the decrease of optical scattering caused by grain growth and the reduction of grain boundary density (Lv et al., 2011). The UV-Vis absorbance spectrum of ZnOAg10Ps showed only the main characteristics peak of ZnOPs at 371 nm while there is no sharp peak observed for silver except some enhancement of visible absorbance as seen in Figure 1D. Here, the peak of ZnOPs is predominant over the

peak of silver because during the preparation of the sample, the concentration of the zinc acetate was much higher as compared to that of silver nitrate. It is interesting to observe that the relative visible absorbance in the UV-Vis spectra of ZnOAg1Ps, ZnOAg10Ps, and ZnO10Ag1Ps increased significantly compared to that of pure ZnOPs. This increased visible absorbance indicates that these samples will be highly active in visible light thereby having promising photocatalytic dye degrading ability which is evaluated in the subsequent section.

Further, the movement, separation, and recombination of photo-generated electron and hole (e^-h^+) pairs in the

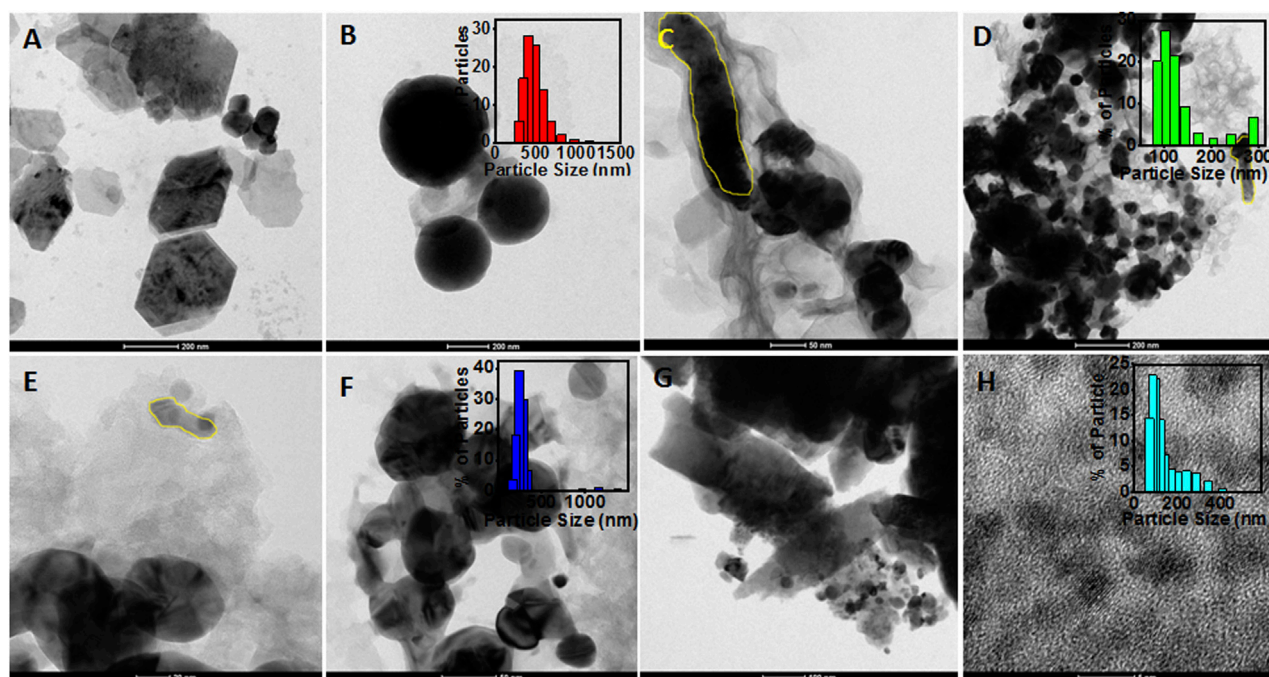


FIGURE 3

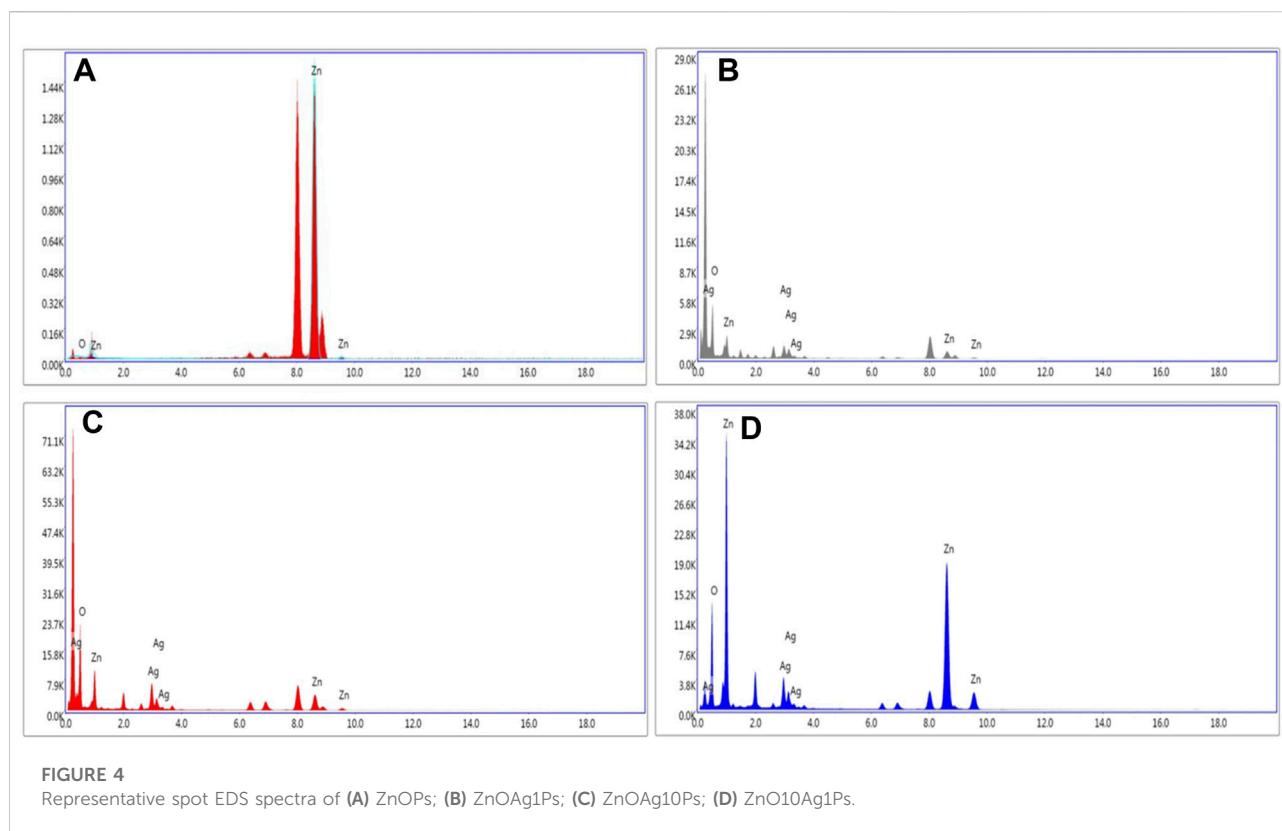
HRTEM images of particles synthesized using PALE. (A) ZnOPs with hexagonal shape (scale: 200 nm); (B) spherical shaped ZnOPs (scale: 200 nm) and inset showed the bar diagram of DLS data; (C) Rod shaped ZnOAg1Ps (scale: 50 nm); (D) Spherical ZnOAg1Ps (scale: 200 nm) and inset showed the bar diagram of DLS data; (E) Rod shaped ZnOAg10Ps (scale: 20 nm) and inset showed the bar diagram of DLS data; (F) spherical shaped ZnOAg10Ps (scale: 50 nm); (G) Rod shaped ZnO10Ag1Ps (scale: 100 nm) (H) spherical shaped ZnO10Ag1Ps (scale: 5 nm), and inset showed the bar diagram of DLS data.

synthesized particles were measured by recording the room temperature PL emission spectra at 300 nm excitation which are shown in Figure 2A. The PL intensity of the ZnOAgPs decreased as compared to that of the ZnOPs which indicated an effective transfer of the interfacial charge from ZnO to Ag, serving as an electron sink that doesn't allow the photo-induced carriers to recombine. Hence, the ZnOAgPs are estimated to show improved photocatalytic dye degradation performance than that of the pristine ZnOPs (Kadam et al., 2018). The Gaussian fitted PL emission spectra of the synthesized samples are shown in Figures 2B–E, respectively. It was observed that ZnOPs show a strong near band edge emission band that was centered at ~340 nm in all samples. The Gaussian fitted deconvoluting PL emission spectra of the synthesized particles showed some additional bands at ~405, ~420, ~456 and ~470 nm wavelengths, that are specific to oxygen vacancy states (V_o^+ and V_o^{++}) which was singly and doubly charged as well as defects in ZnOPs (Saoud et al., 2015).

3.3 HRTEM image, DLS, and XRD analyses

The morphology of the synthesized particles was determined using HRTEM images, as shown in Figure 3. The HRTEM image

of ZnOPs clearly showed two anisotropic microstructures of hexagonal and spherical (Figures 3A,B) shapes. The size and diameter of the observed hexagonal and spherical structures were observed to be 350 and 500 nm, respectively. It should be noted that the mentioned size of the particles are specific to the ones seen in the HRTEM image and not an average of several particles. The particle size of ZnOPs was also found by DLS analysis and the corresponding bar diagram is shown in the inset of Figure 3B. The size of ZnOPs was ranging from 289 to 1635 nm with maximum number of particles of size 407 nm. A nanorod of diameter ~40 nm and length ~350 nm was observed in ZnOAg1Ps sample (Figure 3C). There were some polydispersed spherical particles of size ~50–200 nm as observed in ZnOAg1Ps also (Figure 3D). The particle size distribution of ZnOAg1Ps were in a range from 85 to 409 nm with majority of size ~98 nm as seen in the inset of Figure 3D. Similar rods were also spotted for ZnOAg10Ps that were ~50 × ~10 nm in dimension as evident from Figure 3E. Apart from the rods, there were some spherical particles of size ~30 nm as well. The size of the ZnOAg10Ps was ~171–1635 nm with majority being around 231 nm as shown in inset of Figure 3F. A similar trend was also observed for ZnO10Ag1Ps where the rod shaped particles were larger in size (~758 nm) as seen in Figures 3G,H.



The size of the particles ranged from 72 to 687 nm most of which were around 90 nm.

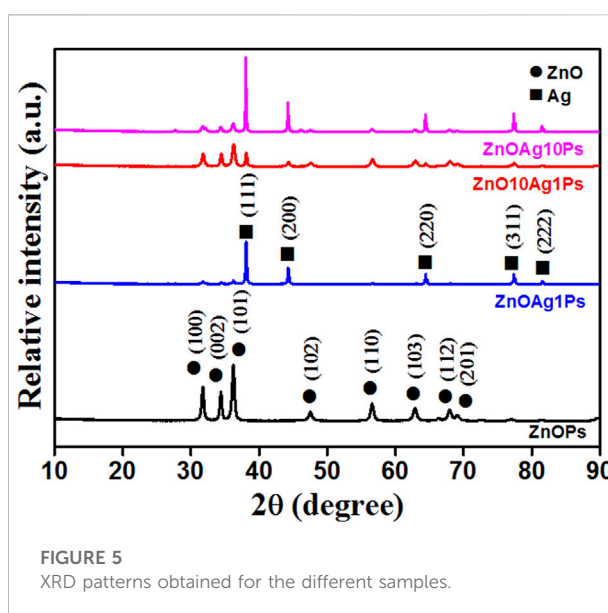
The elemental zinc (Zn), oxygen (O), and silver (Ag) in the composites were confirmed by EDAX spectra as shown in Figure 4. The purity of ZnOPs was confirmed by the presence of Zn and O in Figure 4A. Figure 4B indicated the presence of Zn and Ag up to 16.8% and 16.6%, respectively in ZnOAg1Ps. Figure 4C showed 25.3% Zn and 24.6% Ag in ZnOAg10 whereas ZnO10Ag1Ps exhibited 57.2% Zn and 8.5% Ag as evident from Figure 4D.

The XRD pattern obtained for the samples ZnOPs, ZnOAg1Ps, ZnO10Ag1Ps, and ZnOAg10Ps are presented in Figure 5. The obtained diffraction angle, the identified diffracting planes, the corresponding phases of ZnO (JCPDS file No.36-1451) and silver (JCPDS file No: 01-087-0597) are tabulated in Table 2. The planes of Ag are marked by * (star) for better clarification.

Hence, the XRD pattern analyses of the synthesized samples confirmed the presence of ZnO and silver (Ag) nanoparticles in our synthesized samples.

3.4 FTIR spectroscopy analysis

The PALE comprises different phytochemicals such as phenolic, flavonoid, reducing sugar, starch, citric acid, ascorbic



acid, plumbagin, *etc.*, that played a significant role for reducing Ag^+ and Zn^{2+} ions and stabilizing the synthesized particles. The PALE showed numerous characteristic bands in the FTIR spectra as depicted in Figures 6A,B. The peak at 3550 cm^{-1} is corresponding to the peptide linkage associated N–H stretch vibrations (Kannan and John, 2008), while the peak at 2994 cm^{-1} is specific to the stretching vibration of methyl groups (Li et al.,

TABLE 2 Analysis of XRD patterns presented in Figure 5.

Sample	2θ (deg.)	Diffracting plane
ZnOPs	31.8	(100)
	34.4	(002)
	36.2	(101)
	47.5	(102)
	56.5	(110)
	62.8	(103)
	67.9	(112)
	69.1	(201)
ZnOAg1Ps	31.8	(100)
	34.5	(002)
	36.2	(101)
	38.1	*(111)
	44.3	*(200)
	56.5	(110)
	64.4	*(220)
	77.9	*(311)
	81.5	*(222)
ZnO10Ag1Ps	31.8	(100)
	34.4	(002)
	36.2	(101)
	38.1	*(111)
	44.3	*(200)
	47.5	(102)
	56.6	(110)
	62.8	(103)
	64.4	*(220)
	67.9	(112)
	69.1	(201)
	77.3	*(311)
	81.4	*(222)
ZnOAg10Ps	31.8	(100)
	34.4	(002)
	36.2	(101)
	38.1	*(111)
	44.3	*(200)
	56.6	(110)
	62.8	(103)
	64.4	(220)
	77.3	(311)
	81.4	(222)

2007). The peak at 1395 cm^{-1} is attributed to germinal methyl group (Tripathy et al., 2010). The peak at 1067 cm^{-1} is attributed to the bending vibration of C–OH groups and the antisymmetric stretching band of polysaccharides and/or chlorophyll associated

C–O–C groups (Jain et al., 2011). These peaks indicated the presence of different phytochemicals in the PALE extract. The FTIR spectra of the synthesized ZnOAgPs composites by PALE are shown in Figure 6B. The peak at 3550 cm^{-1} , which is associated to the N–H stretch vibrations from the peptide linkages is slightly blue shifted for ZnAg1Ps and ZnAg10Ps while it remains at the same position for Zn10Ag1Ps. The main characteristic peaks of Zn–O vibration at 584 cm^{-1} was observed for all three samples (Mahalakshmi et al., 2020). Additionally, there are some other peaks observed at 2166, 2042, 1573, 1383, 1203, 1075, and 640 cm^{-1} which may be originated from the different vibrational bands of phenolic, flavonoid, sugar, starch, citric acid, ascorbic acid, and plumbagin (Jyoti et al., 2016).

3.5 GC-MS/MS analysis

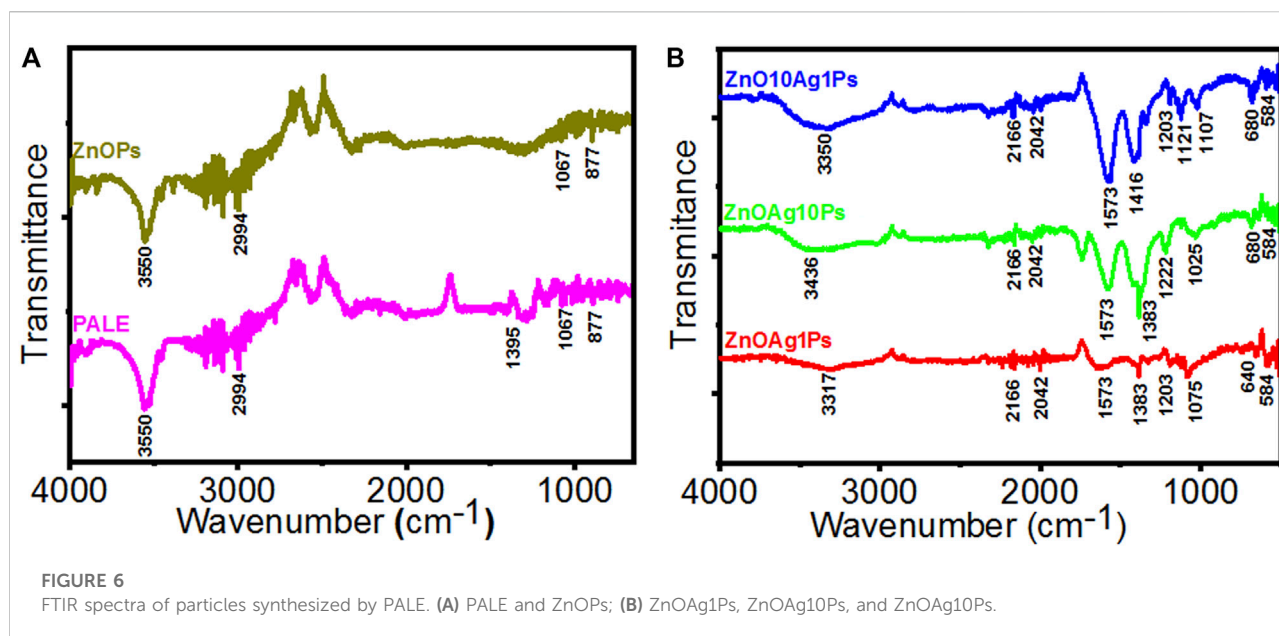
The major phytochemicals detected in PALE were dodecanoic acid, methyl ester, benzene, (3-octylundecyl)-, methyl stearate, methyl tetradecanoate, palmitic acid, methyl ester and others as evident from Table 3. These phytochemicals might have played a significant role in synthesis of the composites and their stabilization.

3.6 Photocatalytic dye degradation

In order to investigate the photocatalytic degradation of MB dye, phytochemical ZnOPs and ZnOAgPs were mixed with MB dye solution and reacted for various time intervals. The photocatalytic activity of ZnOPs and ZnOAgPs is shown in Figure 7. The degradation of MB under UV irradiation in presence of ZnOPs and ZnOAgPs synthesized by PALE was monitored using an UV-visible spectrophotometer. The absorption maxima of MB was centered at 664 nm and shoulder peak at 614 nm in visible region (Figure 7). The main absorption peak steadily decreased and eventually approached the base line when treated with the particles as clearly evident from Figures 7A–D. The plot of $\ln(C_0/C)$ vs. time for the catalytic degradation of MB is shown in Figure 8 while the visible colour change indicating dye degradation can be seen in Figure 8C. The experimental data fits well with the first order kinetic model with variable rate constants (k_1) as given in Table 4. ZnOAg10Ps showed the maximum MB dye adsorption (12.5%), followed by ZnO10Ag1Ps and others. ZnO10Ag1Ps showed maximum MB dye degradation of 95.7% with a rate constant of 0.0463 s^{-1} followed by others.

4 Discussion

Recently, ZnOPs have drawn much attention as promising photocatalyst which is mainly attributed to their attractive



properties that include high UV light absorption, high exciton binding energy (60 meV), high electron mobility, tunable morphology, easy availability, economical production and nontoxic nature (Ansari et al., 2017; Kim and Jo, 2017). However, the chemical and physical methods of ZnOPs synthesis involve hazardous reaction conditions and toxic chemicals for reduction and stabilization (Adersh et al., 2015). Hence, PALE mediated biofabrication is a green route for synthesis of ZnOPs with photocatalytic properties (Kitture et al., 2015). However, the photocatalytic potential of ZnOPs is often limited due to fast recombination of photo-excited electron-hole pairs in the single-phase semiconductor and a low quantum yield. This further limits the application and commercialization potential of pristine ZnO for photocatalytic degradation process (Saravanam et al., 2015a; Lee et al., 2015). One of the prominent solutions to deal with this bottleneck is to dope noble metals in the ZnOPs for synergistic enhancement of the photocatalytic activity (Saravanam et al., 2015b; Ansari et al., 2013; Ansari et al., 2015). Hence, we have attempted to mix Ag in the biogenic ZnOPs at various concentrations that might offer several advantages. Ag was selected because of its attractive properties such as, high electrical and thermal conductivity, high work function, and cost effectiveness (Zeng et al., 2017; Gami et al., 2022). Although some of the studies give an account on the chemically synthesized core shell ZnO/Ag photocatalysts, there are no reports on Ag mixed ZnOPs from *P. auriculata* (Andrade et al., 2017; Gupta et al., 2017; Rafaie et al., 2017; Sampaio et al., 2017). The advantage of phytofabricated ZnOAgPs is the stable deposition of the Ag on the semiconductor's active surface which is protected by the

phytochemicals unlike the chemical methods where the leaching of Ag from the composite system can pollute the water apart from affecting the photocatalytic reactions due to reduction in active surface. Also, the biogenic stable ZnOAgPs might be resistant to photo-chemical corrosion that often results under adverse or extreme abiotic conditions (Li et al., 2013; Ma et al., 2017). These phytofabricated composites enhance the proximity of the interface between semiconductor and Ag which is important for transfer of charge and optimization of plasmon-exciton interactions (Das et al., 2015).

Kadam et al. (2018) reported that this strategy accelerates Fermi level equilibrium and can reduce the band gap energy that in turn can promote separation of the interfacial charge and accelerate electron transfer. Additionally, this can prevent interaction from harsh chemicals and hence restrict agglomeration and degradation of the metal particles (Ansari et al., 2014). Nanostructured noble metals serve as active reaction sites and efficient electron traps that oppose the charge carriers to recombine (Guy and Ozacar, 2016).

In our study, the UV-Vis peak of ZnOPs was prominent in the ZnOAgPs indicating the higher amount of ZnO in the composites. It is important to note that the absorption spectra of ZnOAgPs didn't show superposition with the individual single-component particles which might be attributed to the strong electronic coupling between the Ag and ZnO (Satter et al., 2014). Ag mixed in the ZnO increased separation of charge, while the high ZnO content in the vicinity resulted in the increase in the refractive index of the surrounding medium which resulted in the shifting of the SPR band (Karmakar

TABLE 3 Main compounds detected in PALE by GC-MS/MS.

Sr.No	Name of compound	Rt (min)	Molecular formula	Molecular mass (g/mol)	Retention index	Area (%)
1	Benzene, (3-octylundecyl)-	3.317	C ₂₅ H ₄₄	344.62	2501	15.7
2	Disilicic acid (H6-Si2-O7), hexamethyl ester	4.252	C ₁₂ H ₃₀ O ₇ Si ₂	342.53	1200	1.8
4	1-Nitro-β-d-arabinofuranose, tetraacetate	4.887	C ₁₃ H ₁₇ NO ₁₁	363.27	1301	0.4
5	Melezitose	5.124	C ₁₈ H ₃₂ O ₁₆	504.438	1801	1.3
6	trans-Isoeugenol	6.073	C ₁₀ H ₁₂ O	164.2011	1000	0.4
7	1,4-Benzenedicarboxylic acid, dimethyl ester	7.008	C ₁₀ H ₁₀ O	194.18	1001	6.5
8	Dodecanoic acid, methyl ester	7.066	C ₁₃ H ₂₆ O	214.3443	1301	27.3
9	Benzenemethanimine, α-phenyl-	8.092	C ₁₃ H ₁₁ N	181.2331	1300	2.0
10	Methyl tetradecanoate	8.532	C ₁₅ H ₃₀ O	242.3975	1501	6.5
11	2-Propenoic acid, 3-(4-hydroxyphenyl)-, methyl ester	8.892	C ₁₀ H ₁₀ O ₃	178.1846	1000	2.0
13	Nicotinamide, 2,6-dimethoxy-4-methyl-	9.743	C ₉ H ₁₂ N	196.203	900	0.7
14	1,4-benzenedicarboxylic acid, 2-hydroxyethyl methyl ester	9.846	C ₁₁ H ₁₂ O ₅	224.21	1101	0.6
15	(+)-Asarinin	10.074	C ₂₀ H ₁₈ O ₆	354.4	2001	0.5
16	Palmitic acid, methyl ester	10.566	C ₁₇ H ₃₄ O ₂	270.45	1700	8.3
17	2,3-Dimethyl-5-(trifluoromethyl)-1,4-benzenediol #	11.047	C ₉ H ₉ F ₃ O ₂	206.16	901	0.6
18	16β-Hydroxyboldenone	11.258	C ₁₉ H ₂₆ O ₂	286.4	1900	0.6
19	Androsta-1,4-dien-3-one, 17-hydroxy-17-methyl-, (17α)-	11.544	C ₂₀ H ₂₈ O ₂	300.4	2001	0.5
20	(6-Isocodeine)/Morphinan, 7,8-didehydro-4,5-epoxy-3,6-bis [(trimethylsilyl)oxy]-, (5α,6α)-	11.687	C ₁₈ H ₂₁ NO ₃	299.4	1800	0.4
21	Methyl petroselinat	12.368	C ₁₉ H ₃₆ O ₂	296.5	1901	1.1
22	Oleic acid, methyl ester	12.424	C ₁₉ H ₃₆ O ₂	296.5	1900	0.6
23	8-Methylnonanoic acid, methyl ester	12.601	C ₁₁ H ₂₂ O	186.2912	1101	3.2
24	Methyl stearate	12.68	C ₁₉ H ₃₈ O ₂	298.5	1900	11.8
26	Nonanoic acid, 9-(o-propylphenyl)-, methyl ester	12.869	C ₁₉ H ₃₀ O ₂	290.45	1901	0.4
27	10,13-Octadecadiynoic acid, methyl ester	13.019	C ₁₉ H ₃₄ O ₂	294.5	1900	0.4
28	Carnegine (6,7-dimethoxy-1,2-dimethyl-3,4-dihydro-1H-isoquinoline)	13.195	C ₁₃ H ₁₉ NO ₂	221.29	1301	0.3
29	Benzene, 2-(1-decylundecyl)-1,4-dimethyl-	13.328	C ₂₉ H ₅₂	400.7232	2900	0.3
30	Dihydroxanthin	14.066	C ₁₇ H ₂₄ O ₅	308.4	1701	0.3
31	n-Hexadecylsuccinic anhydride	14.466	C ₂₀ H ₃₆ O ₃	324.5	2002	0.3

et al., 2020; Robkhob et al., 2020). Further, PL spectra provided strong scientific evidence of the distinct quenching of the emission in ZnOAgPs which was attributed to the efficient charge transfer from ZnO to Ag interface (Misra et al., 2014). Morphological analysis using HRTEM showed anisotropy among variously mixed structures. Spheres, rods, hexagons were observed. Our results are well in agreement with the ZnONPs synthesized using *Salvia officinalis* leaf extract (Abomuti et al., 2021). Ahmed et al. (2020) also synthesized similar Au/ZnO nanoparticles by using *Carya illinoensis* leaf extract for enhanced photocatalytic degradation of Rhodamine B dye. In another study, ZnONPs synthesized by *Ziziphus jujuba* leaves extract also formed irregular agglomerated particles with variable shape and size where irregular flake-shape

composites were formed with very small particles with an average particle size of 20 nm. Some particles were well-defined with spherical shape having an average particle size of 15 nm (Alharthi et al., 2021). The FTIR spectra confirmed the involvement of the active functional groups of the phytochemicals present in PALE for the synthesis and stabilization of the particles. Ameen et al. (2021) also reported similar involvement of the functional groups during synthesis of ZnONPs from *Acremonium potronii*.

Both ZnOPs and ZnOAgPs exhibited promising photocatalytic MB dye degradation which was found to be a function of reaction time. Phytogenic ZnONPs from aqueous extract of *Vitis rotundifolia* showed malachite green dye degradation after 150 min where the initial strong absorption peak visible at 620 nm gradually decreased with

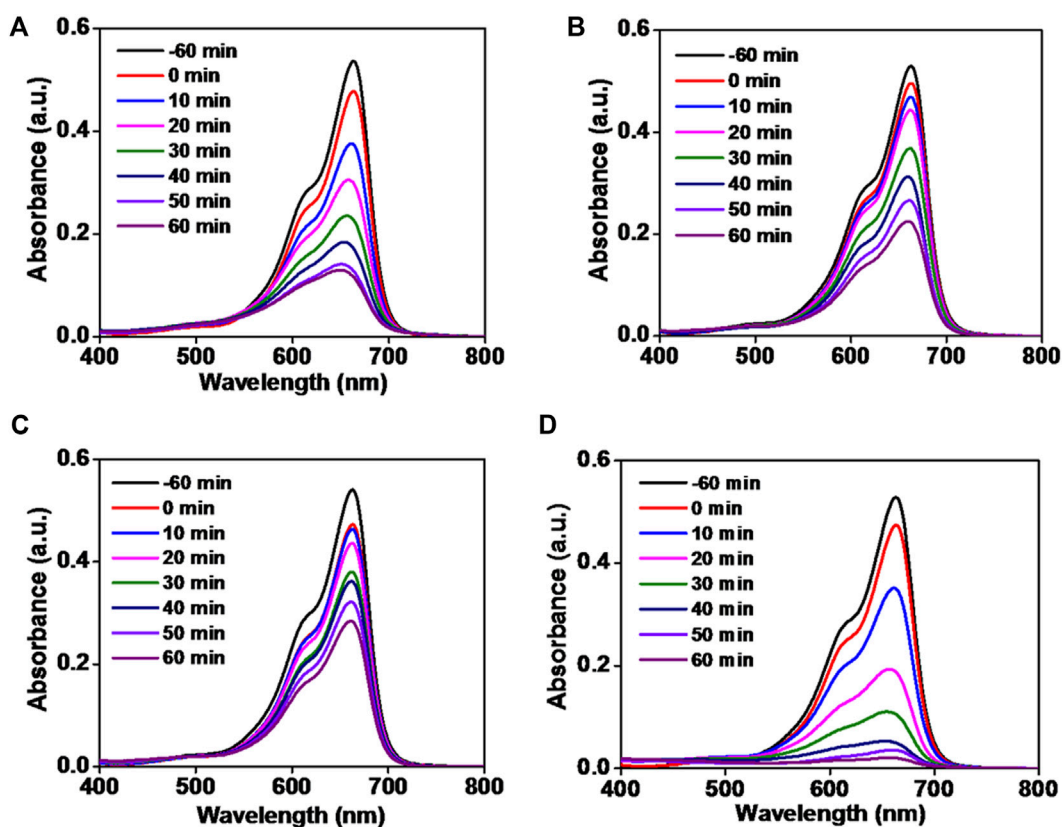


FIGURE 7

Absorption spectra of reduction of methylene blue dye by particles. (A) ZnOPs; (B) ZnOAg1Ps; (C) ZnOAg10Ps; (D) ZnO10Ag1Ps.

time (Brindhadevi et al., 2020). However, in case of ZnO10Ag1Ps the degradation of the MB was 95.7% within 60 min which was comparatively faster. Davar et al. (2015) reported photocatalytic degradation of methyl orange, methyl red and methylene blue dyes by the ZnONPs synthesized using lemon juice. On mixing with Ag the photocatalytic activity of ZnOPs against MB was increased which is in close agreement where AgNPs synthesized using Gongura leaves were decorated on to ZnONPs fabricated by hydrothermal route. The 5% AgNPs containing ZnO composites photodegraded (MB) dye up to 99.21% within 75 min under UV light irradiation (Jadav et al., 2020). The concentration of MB decreased with the increase in time which was due to redox reaction. The superior photocatalytic activity in mixed ZnOPs might be attributed to the creation of additional energy levels positioned between the VB, and CB of the ZnO, that resulted in the dopant incorporation mediated extension of the light absorption range (Chaudhari et al., 2022). Moreover, creating more defect levels within ZnO helps to produce efficient traps of e^- , which in turn decreases the possibility of the recombination rate resulting in the rapid formation of active radicals (Karthik et al., 2022). Previous reports

establish the mechanism for the same which indicate light absorption mediated VB to CB transfer of the photoexcited electrons upon irradiation. Therefore, the transit of the photoexcited VB electrons to the CB/impurity energy levels from the host lattice results in the generation of high amount of O_2 —associated with $d-d$ transitions. During this time, transfer of the VB photoexcited holes to the surface occurs that interrelate with water molecules, eventually generating large amount of $\bullet OH$ oxidative radical species. During the oxidation, the organic pollutants can catch the photoexcited holes. Hence, being tough and non selective, the generated reactive oxygen species can result in promising dye degradation at the surface of the photocatalyst. Similar results were noted with ZnO based nanocomposites synthesized using *S. lycopersicum*, coconut husk, *Allium cepa* L, *Syzygium cumini*, *Ruellia tuberosa*, *Artocarpus heterophyllus* for degradation of chemical dyes such as, Congo red, methylene blue, metanil yellow, crystal violet, and malachite green (Vidya et al., 2017; Rajkumar et al., 2019; Preethi et al., 2020; Sadiq et al., 2021; Vasantharaj et al., 2021; Priyadharshini et al., 2022). In view of the background, it is evident that Ag mixed phyto-genic ZnOPs

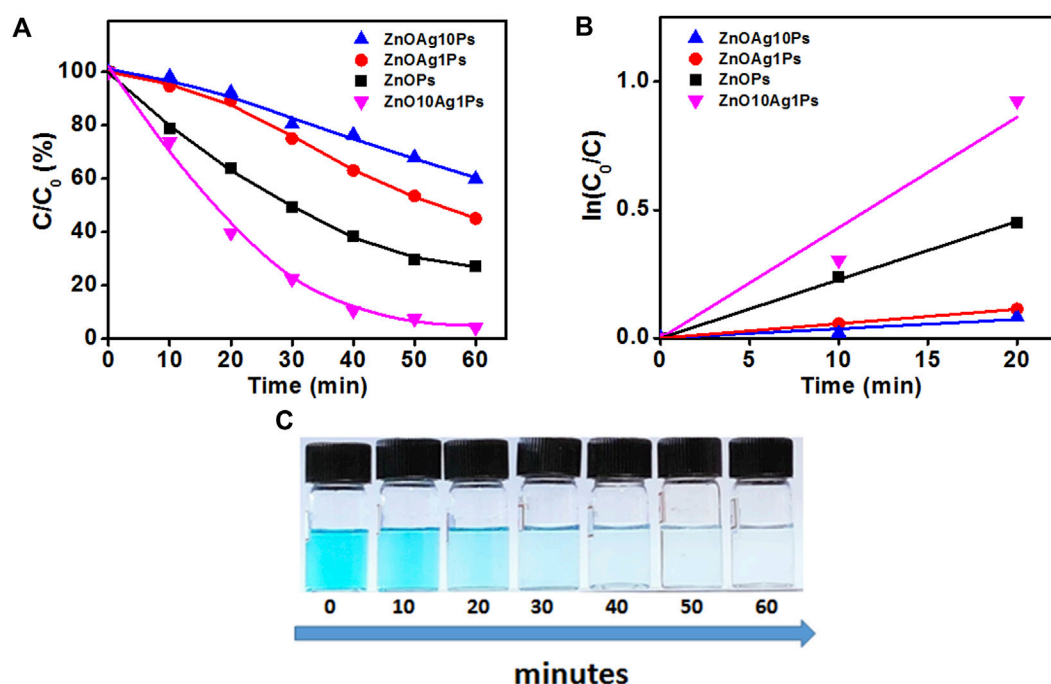


FIGURE 8

Degradation of MB in presence of particles. (A) Photocatalytic MB degradation by ZnOPs and ZnOAgPs under the UV light; (B) First-order kinetic constant for the degradation of MB under UV-light; (C) Visible colour change indicating MB degradation with time.

TABLE 4 Percentage of adsorption of MB and first order kinetic constant of particles.

Nanoparticles	Adsorption (%)	Degradation (%)	k_1 (s^{-1})
ZnOAg10Ps	12.5	40.4	0.0036
ZnOAg1Ps	6.5	55.1	0.0056
ZnO10Ag1Ps	10.3	95.7	0.0463
ZnOPs	10.99	72.7	0.0228

mediated dye removal can be a powerful strategy for dye contaminated wastewater treatment.

5 Conclusion

The current study reports the facile synthesis of pristine and Ag-mixed ZnOPs employing an environmentally benign, rapid and efficient route using *P. auriculata* leaf extract. The concentrations of the precursor metal salt concentrations were varied to get three different composites denoted as ZnOAg1Ps, ZnOAg10Ps, and ZnO10Ag1Ps. The particles were polydispersed with spherical, rod, hexagonal and irregular shapes. The phytochemical analysis revealed significant amount of polyphenols, flavonoids, starch,

reducing sugar, citric acid and plumbagin in PALE that might play a critical role in the synthesis and the stabilization of the nanoparticles. The structural and optical analysis confirmed the formation of crystalline pure ZnOPs as well as Ag doping. Both phytofabricated ZnOPs and ZnOAgPs showed superior photocatalytic MB dye degrading ability. Maximum MB dye degradation up to 95.7% with a rate constant of $0.0463\ s^{-1}$ was exhibited by ZnO10Ag1Ps. Hence, phytofabricated Ag mixed ZnOPs can help to develop promising strategy for treating hazardous dye contaminated industrial effluents to ensure clean environment.

Data availability statement

The original contributions presented in the study are included in the article/supplementary material, further inquiries can be directed to the corresponding authors.

Author contributions

ST and SG contributed to drafting the manuscript. AA and SS prepared the figures. KB, SM, and RPS performed the experiments and acquired the data. SK and KB prepared the figures and

interpreted the data. NHMK drafted the revised manuscript. All authors approved the final submission to Frontiers in Chemistry.

Funding

KB is thankful to Student Startup & Innovation Policy (SSIP) of Government of Gujarat and RK. University for funding (U-0647/SSIP/RKU/SOS/2021-22/13). SK is very much thankful to the UGC D.S. Kothari Post-Doctoral Fellowship Scheme for maintaining fellowship. SG acknowledges Kasetsart University, Bangkok, Thailand for Post Doctoral Fellowship and funding under Reinventing University Program (Ref. No. 6501.0207/10870 dated 9th November, 2021 and Ref. No. 6501.0207/9219 dated 14th September, 2022). ST is thankful to National Research Council of Thailand (NRCT) and Kasetsart University for funding (N42A650277).

Acknowledgments

The authors thank Sophisticated Analysis Instrumentation Facilities (SAIF), IIT Bombay TEM and SEM facilities. The authors acknowledge Department of Pharmaceutical Sciences, Saurashtra University, Rajkot for

References

- Abomuti, M. A., Danish, E. Y., Firoz, A., Hasan, N., and Malik, M. A. (2021). Green synthesis of zinc oxide nanoparticles using *Salvia officinalis* leaf extract and their photocatalytic and antifungal activities. *Biology* 10, 1075. doi:10.3390/biology10111075
- Adersh, A., Kulkarni, A. R., Ghosh, S., More, P., Chopade, B. A., and Gandhi, M. N. (2015). Surface defect rich ZnO quantum dots as antioxidant inhibiting α -amylase and α -glucosidase: A potential anti-diabetic nanomedicine. *J. Mat. Chem. B* 3, 4597–4606. doi:10.1039/C5TB00407A
- Ahmad, M., Rehman, W., Khan, M. M., Qureshi, M. T., Gul, A., Haq, S., et al. (2020). Phytogenic fabrication of ZnO and gold decorated ZnO nanoparticles for photocatalytic degradation of rhodamine B. *J. Environ. Chem. Eng.* 9, 104725. doi:10.1016/j.jece.2020.104725
- Alharthi, M. N., Ismail, I., Bellucci, S., and Salam, M. A. (2021). Green synthesis of zinc oxide nanoparticles by *Ziziphus jujuba* leaves extract: Environmental application, kinetic and thermodynamic studies. *J. Phys. Chem. Solids* 158, 110237. doi:10.1016/j.jpcs.2021.110237
- Ameen, F., Dowoud, T., and Alnadhari, S. (2021). Ecofriendly and low cost synthesis of ZnO nanoparticles from *Acremonium potronii* for the photocatalytic degradation of azo dyes. *Environ. Res.* 202, 111700. doi:10.1016/j.envres.2021.111700
- Andrade, G. R. S., Nascimento, C. C., Lima, Z. M., Neto, E. T., Costa, L. P., and Gimenez, I. F. (2017). Star-shaped ZnO/Ag hybrid nanostructures for enhanced photocatalysis and antibacterial activity. *Appl. Surf. Sci.* 399, 573–582. doi:10.1016/j.apsusc.2016.11.202
- Ansari, S. A., Ansari, S. G., Foad, H., and Cho, M. H. (2017). Facile and sustainable synthesis of carbon-doped ZnO nanostructures towards the superior visible light photocatalytic performance. *New J. Chem.* 41, 9314–9320. doi:10.1039/C6NJ04070E
- Ansari, S. A., Khan, M. M., Ansari, M. O., Lee, J., and Cho, M. H. (2013). Biogenic synthesis, photocatalytic, and photoelectrochemical performance of Ag–ZnO nanocomposite. *J. Phys. Chem. C* 117, 27023–27030. doi:10.1021/jp410063p
- Ansari, S. A., Khan, M. M., Ansari, M. O., Lee, J., and Cho, M. H. (2015). Gold nanoparticles-sensitized wide and narrow band gap TiO₂ for visible light applications: A comparative study. *New J. Chem.* 39, 4708–4715. doi:10.1039/C5NJ00556F
- Ansari, S. A., Khan, M. M., Lee, J., and Cho, M. H. (2014). Highly visible light active Ag@ZnO nanocomposites synthesized by gel-combustion route. *J. Ind. Eng. Chem.* 20, 1602–1607. doi:10.1016/j.jiec.2013.08.006
- the DLS and FTIR facilities. The work disclosed in this manuscript is part of the filed patent entitled “Bloch K.M., Ghosh S. (2022) A process of preparing silver doped zinc oxide nanoparticles using *Plumbago auriculata* leaf extract. Indian Patent (Filed) Application number IN 202221044985.”
- ## Conflict of interest
- The authors declare that the research was conducted in the absence of any commercial or financial relationships that could be construed as a potential conflict of interest.
- ## Publisher's note
- All claims expressed in this article are solely those of the authors and do not necessarily represent those of their affiliated organizations, or those of the publisher, the editors and the reviewers. Any product that may be evaluated in this article, or claim that may be made by its manufacturer, is not guaranteed or endorsed by the publisher.
- Basri, H. H., Talib, R. A., Sukor, R., Othman, S. H., and Ariffin, H. (2020). Effect of synthesis temperature on the size of ZnO nanoparticles derived from pineapple peel extract and antibacterial activity of ZnO–starch nanocomposite films. *Nanomaterials* 10, 1061. doi:10.3390/nano10061061
- Bloch, K., Webster, T. J., and Ghosh, S. (2020). “Mycogenic synthesis of metallic nanostructures and their use in dye degradation,” in *Photocatalytic degradation of dyes: Current trends and future*. Editors S. Dave, J. Das, and M. Shah (Amsterdam, Netherlands: Elsevier), 509–525. doi:10.1016/B978-0-12-823876-9.00014-7
- Brindhadevi, K., Samuel, M. S., Verma, T. N., Vasantharaj, S., Sathiyavimal, S., Saravanan, M., et al. (2020). Zinc oxide nanoparticles (ZnONPs)-induced antioxidants and photocatalytic degradation activity from hybrid grape pulp extract (HGPE). *Biocatal. Agric. Biotechnol.* 124, 101730. doi:10.1016/j.bcab.2020.101730
- Brus, L. (1986). Electronic wave functions in semiconductor clusters: Experiment and theory. *J. Phys. Chem.* 90, 2555–2560. doi:10.1021/j100403a003
- Chaudhari, A., Kaida, T., Desai, H. B., Ghosh, S., Bhatt, R. P., and Tanna, A. R. (2022). Dye degradation and antimicrobial applications of manganese ferrite nanoparticles synthesized by plant extracts. *Chem. Phys. Impact* 5, 100098. doi:10.1016/j.chphi.2022.100098
- Daneshvar, N., Ayazloo, M., Khataee, A. R., and Pourhassan, M. (2007). Biological decolorization of dye solution containing malachite green by microalgae *Cosmarium* sp. *Bioresour. Technol.* 98, 1176–1182. doi:10.1016/j.biortech.2006.05.025
- Das, S., Sinha, S., Suar, M., Yun, S., Mishra, A., and Tripathy, S. K. (2015). Solar-photocatalytic disinfection of *Vibrio cholerae* by using Ag@ZnO core-shell structure nanocomposites. *J. Photochem. Photobiol. B Biol.* 142, 68–76. doi:10.1016/j.jphotobiol.2014.10.021
- Davar, F., Majedi, A., and Mirzaei, A. (2015). Green synthesis of ZnO nanoparticles and its application in the degradation of some dyes. *J. Am. Ceram. Soc.* 98, 1739–1746. doi:10.1111/jace.13467
- Din, M. I., Khalid, R., Najeeb, J., and Hussain, Z. (2021). Fundamentals and photocatalysis of methylene blue dye using various nanocatalytic assemblies- a critical review. *J. Clean. Prod.* 298, 126567. doi:10.1016/j.jclepro.2021.126567
- Fagier, M. A. (2021). Plant-mediated biosynthesis and photocatalysis activities of zinc oxide nanoparticles: A prospect towards dyes mineralization. *J. Nanotechnol.* 2021, 1–15. doi:10.1155/2021/6629180

- Gami, B., Bloch, K., Mohammed, S. M., Karmakar, S., Shukla, S., Asok, A., et al. (2022). *Leucophyllum frutescens* mediated synthesis of silver and gold nanoparticles for catalytic dye degradation. *Front. Chem.* 10, 932416. doi:10.3389/fchem.2022.932416
- Gautam, S., Kaithwas, G., Bharagava, R. N., and Saxena, G. (2017). "Pollutants in tannery wastewater, their pharmacological effects and bioremediation approaches for human health protection and environmental safety," in *Environmental pollutants and their bioremediation approaches*. Editor R. N. Bharagava (Boca Raton, FL, USA: CRC Press, Taylor & Francis Group), 369–396. doi:10.1201/9781315173351-14
- Ghosh, S., Gurav, S. P., Harke, A. N., Chacko, M. J., Joshi, K. A., Dhepe, A., et al. (2016a). *Dioscorea oppositifolia* mediated synthesis of gold and silver nanoparticles with catalytic activity. *J. Nanomed. Nanotechnol.* 7, 1000398. doi:10.4172/2157-7439.1000398
- Ghosh, S., Sarkar, B., Kaushik, A., and Mostafavi, E. (2022). Nanobiotechnological prospects of probiotic microflora: Synthesis, mechanism and applications. *Sci. Total Environ.* 838, 156212. doi:10.1016/j.scitotenv.2022.156212
- Govindan, L., Ambazhagan, S., Altemimi, B. A., Lakshminarayanan, K., Kuppan, S., Pratap-Singh, A., et al. (2020). Efficacy of antimicrobial and larvicidal activities of green synthesized silver nanoparticles using leaf extract of *Plumbago auriculata* Lam. *Plants* 9, 1577. doi:10.3390/plants9111577
- Gupta, J., Mohapatra, J., and Bahadur, D. (2017). Visible light driven mesoporous Ag-embedded ZnO nanocomposites: Reactive oxygen species enhanced photocatalysis, bacterial inhibition and photodynamic therapy. *Dalton Trans.* 46, 685–696. doi:10.1039/C6DT03713E
- Guy, N., and Ozacar, M. (2016). The influence of noble metals on photocatalytic activity of ZnO for Congo red degradation. *Int. J. Hydrogen Energy* 41, 20100–20112. doi:10.1016/j.ijhydene.2016.07.063
- Hashmi, S. S., Shah, M., Muhammad, W., Ahmad, A., Ullah, M. A., Nadeem, M., et al. (2021). Potentials of phyto-fabricated nanoparticles as ecofriendly agents for photocatalytic degradation of toxic dyes and waste water treatment, risk assessment and probable mechanism. *J. Indian Chem. Soc.* 98, 100019. doi:10.1016/j.jics.2021.100019
- Israni, S. A., Kapadia, N. S., Lahiri, S. K., Yadav, G., and Shah, M. B. (2010). An UV-Vis spectrophotometric method for the estimation of plumbagin. *Int. J. ChemTech. Res.* 2, 856–859.
- Jadav, P., Shinde, S., Suryawanshi, S. S., Teli, S. B., Patil, P. S., Ramteke, A. A., et al. (2020). Green AgNPs decorated ZnO nanocomposites for dye degradation and antimicrobial applications. *Eng. Sci.* 12, 79–94. doi:10.30919/es8d1138
- Jain, N., Bharagava, A., Majumdar, S., Tarafdar, J. C., and Panwar, J. (2011). Extracellular biosynthesis and characterization of silver nanoparticles using *Aspergillus flavus* NJP08: A mechanism perspective. *Nanoscale* 3, 635–641. doi:10.1039/c0nr00656d
- Jamdade, D. A., Rajpali, D., Joshi, K. A., Kitture, R., Kulkarni, A. S., Shinde, V. S., et al. (2019). *Gnidia glauca*- and *Plumbago zeylanica*-mediated synthesis of novel copper nanoparticles as promising antidiabetic agents. *Adv. Pharmacol. Sci.* 2019, 1–11. doi:10.1155/2019/9080279
- Jangir, L. K., Kumari, Y., Kumar, A., Kumar, M., and Awasthi, K. (2017). Investigation of luminescence and structural properties of ZnO nanoparticles, synthesized with different precursors. *Mat. Chem. Front.* 7, 1413–1421. doi:10.1039/C7QM00058H
- Jyoti, K., Baunthiyal, M., and Singh, A. (2016). Characterization of silver nanoparticles synthesized using *Urtica dioica* Linn. leaves and their synergistic effects with antibiotics. *J. Radiat. Res. Appl. Sci.* 9, 217–227. doi:10.1016/j.jrras.2015.10.002
- Kadam, A. N., Bhopate, D. P., Kondalkar, V. V., Majhi, S. M., Bathula, C. D., Tran, A. V., et al. (2018). Facile synthesis of Ag-ZnO core-shell nanostructures with enhanced photocatalytic activity. *J. Ind. Eng. Chem.* 61, 78–86. doi:10.1016/j.jiec.2017.12.003
- Kannan, P., and John, S. A. (2008). Synthesis of mercaptothiadiazole-functionalized gold nanoparticles and their self-assembly on Au substrates. *Nanotechnology* 19, 085602. doi:10.1088/0957-4484/19/8/085602
- Karmakar, S., Ghosh, S., and Kumbhakar, P. (2020). Enhanced sunlight driven photocatalytic and antibacterial activity of flower-like ZnO@MoS₂ nanocomposite. *J. Nanopart. Res.* 22, 11. doi:10.1007/s11051-019-4710-3
- Karthik, K. V., Raghu, A. V., Reddy, K. R., Ravishankar, R., Sangeeta, M., Shetti, N. P., et al. (2022). Green synthesis of Cu-doped ZnO nanoparticles and its application for the photocatalytic degradation of hazardous organic pollutants. *Chemosphere* 287, 132081. doi:10.1016/j.chemosphere.2021.132081
- Khan, M. E. (2021). State-of-the-art developments in carbon-based metal nanocomposites as a catalyst: Photocatalysis. *Nanoscale Adv.* 3 (7), 1887–1900. doi:10.1039/d1na00041a
- Khan, M. M., Saadah, N. H., Khan, M. E., Harunsani, M. H., Tan, A. L., and Cho, M. H. (2019a). Phyto-genic synthesis of band gap-narrowed ZnO nanoparticles using the bulb extract of *Costus woodsonii*. *Bionanoscience* 9, 334–344. doi:10.1007/s12668-019-00616-0
- Khan, M. M., Saadah, N. H., Khan, M. E., Harunsani, M. H., Tan, A. L., and Cho, M. H. (2019b). Potentials of *Costus woodsonii* leaf extract in producing narrow band gap ZnO nanoparticles. *Mat. Sci. Semicond. Process* 91, 194–200. doi:10.1016/j.mssp.2018.11.030
- Kim, M., and Jo, W. K. (2017). Purification of aromatic hydrocarbons using Ag-multiwall carbon nanotube-ZnO nanocomposites with high performance. *J. Ind. Eng. Chem.* 47, 94–101. doi:10.1016/j.jiec.2016.11.018
- Kitture, R., Chordiya, K., Gaware, S., Ghosh, S., More, P. A., Kulkarni, P., et al. (2015). ZnO nanoparticles-red sandalwood conjugate: A promising anti-diabetic agent. *J. Nanosci. Nanotechnol.* 15, 4046–4051. doi:10.1166/jnn.2015.10323
- Kumar, R., Rashid, J., and Barakat, M. A. (2015). Zero valent Ag deposited TiO₂ for the efficient photocatalysis of methylene blue under UV-C light irradiation. *Colloids Interface Sci. Commun.* 5, 1–4. doi:10.1016/j.colcom.2015.05.001
- Lee, H. J., Kim, J. H., Park, S. S., Hong, S. S., and Lee, G. D. (2015). Degradation kinetics for photocatalytic reaction of methyl orange over Al-doped ZnO nanoparticles. *J. Ind. Eng. Chem.* 25, 199–206. doi:10.1016/j.jiec.2014.10.035
- Li, J., Cushing, S. K., Bright, J., Meng, F., Senty, T. R., Zheng, P., et al. (2013). Ag@Cu₂O core-shell nanoparticles as visible-light plasmonic photocatalysts. *ACS Catal.* 3, 47–51. doi:10.1021/cs300672f
- Li, S., Shen, Y., Xie, A., Yu, X., Qiu, L., Zhnag, L., et al. (2007). Green synthesis of silver nanoparticles using *Capsicum annum* L. extract. *Green Chem.* 9, 852–858. doi:10.1039/B615357G
- Luximon-Ramma, A., Baharun, T., Soobrattee, M. A., and Aruoma, O. I. (2002). Antioxidant activities of phenolic, proanthocyanidin, and flavonoid components in extracts of *Cassia fistula*. *J. Agric. Food Chem.* 50, 5042–5047. doi:10.1021/jf0201172
- Lv, J., Gong, W., Huang, K., Zhu, J., Meng, F., Song, X., et al. (2011). Effect of annealing temperature on photocatalytic activity of ZnO thin films prepared by sol-gel method. *Superlattices Microstruct.* 50, 98–106. doi:10.1016/j.spmi.2011.05.003
- Ma, X., Li, H., Liu, T., Du, S., Qiang, Q., Wang, Y., et al. (2017). Comparison of photocatalytic reaction-induced selective corrosion with photocorrosion: Impact on morphology and stability of Ag-ZnO. *Appl. Catal. B Environ.* 201, 348–358. doi:10.1016/j.apcatb.2016.08.029
- Mahalakshmi, S., Hema, N., and Vijaya, P. P. (2020). *In vitro* biocompatibility and antimicrobial activities of zinc oxide nanoparticles (ZnONPs) prepared by chemical and green synthetic route- A comparative study. *Bionanoscience* 10, 112–121. doi:10.1007/s12668-019-00698-w
- Mandeep and Shukla, P. (2020). Microbial nanotechnology for bioremediation of industrial wastewater. *Front. Microbiol.* 11, 590631. doi:10.3389/fmicb.2020.590631
- Mani, S., and Bharagava, R. N. (2017). Isolation, screening and biochemical characterization of bacteria capable of crystal violet dye decolorization. *Int. J. Adv. Sci. Res.* 2, 70–75.
- Miller, G. L. (1959). Use of dinitrosalicylic acid reagent for determination of reducing sugar. *Anal. Chem.* 31, 426–428. doi:10.1021/ac60147a030
- Misra, M., Kapur, P., Nayak, M., and Singla, M. (2014). Synthesis and visible photocatalytic activities of a Au@Ag@ZnO triple layer core-shell nanostructure. *New J. Chem.* 38, 4197–4203. doi:10.1039/C4NJ00569D
- Mohammad, A., Karim, M. R., Khan, M. E., AlSukaibi, A. K. D., and Yoon, T. (2022). Eco-benign fabrication of silver nanoparticle-modified zeolitic imidazolate framework and construction of a non-enzymatic electrochemical sensor. *Mater. Today Sustain.* 19, 100182. doi:10.1016/j.mtsust.2022.100182
- Naseer, M., Aslam, U., Khalid, B., and Chen, B. (2020). Green route to synthesize zinc oxide nanoparticles using leaf extracts of *Cassia fistula* and *Melia azadarach* and their antibacterial potential. *Sci. Rep.* 10, 9055. doi:10.1038/s41598-020-65949-3
- Nitinavare, R., Bhattacharya, J., Thongmee, S., and Ghosh, S. (2022). Photosynthetic microbes in nanobiotechnology: Applications and perspectives. *Sci. Total Environ.* 841, 156457. doi:10.1016/j.scitotenv.2022.156457
- Preethi, S., Abrana, K., Nithyasri, M., Kishore, P., Deepika, K., Ranjithkumar, R., et al. (2020). Synthesis and characterization of chitosan/zinc oxide nanocomposite for antibacterial activity onto cotton fabrics and dye degradation applications. *Int. J. Biol. Macromol.* 164, 2779–2787. doi:10.1016/j.ijbiomac.2020.08.047
- Priyadharshini, S. S., Shubha, J. P., Shivalingappa, J., Adil, S. F., Kuniyil, M., Hatshan, M. R., et al. (2022). Photocatalytic degradation of methylene blue and metanil yellow dyes using green synthesized zinc oxide (ZnO) nanocrystals. *Crystals* 12, 22–16. doi:10.3390/cryst12010022

- Rafaie, H. A., Nor, R. M., Azmina, M. S., Ramli, N. I. T., and Mokamed, R. (2017). Decoration of ZnO microstructures with Ag nanoparticles enhanced the catalytic photodegradation of methylene blue dye. *J. Environ. Chem. Eng.* 5, 3963–3972. doi:10.1016/j.jece.2017.07.070
- Rajkumar, K. S., Arun, S., Babu, M. D., Balaji, P., Sivasubramanian, S., Vignesh, V., et al. (2019). Facile biofabrication, characterization, evaluation of photocatalytic, antipathogenic activity and *in vitro* cytotoxicity of zinc oxide nanoparticles. *Biocatal. Agric. Biotechnol.* 22, 101436. doi:10.1016/j.bcab.2019.101436
- Robkhob, P., Ghosh, S., Bellare, J., Jamdade, D., Tang, I. M., and Thongmee, S. (2020). Effect of silver doping on antidiabetic and antioxidant potential of ZnO nanorods. *J. Trace Elem. Med. Biol.* 58, 126448. doi:10.1016/j.jtemb.2019.126448
- Sadasivam, S., and Manickam, A. (2008). *Biochemical methods*. 3rd ed. New Delhi, India: New Age International.
- Sadiq, H., Sher, F., Sehar, S., Lima, E. C., Zhuang, S., Iqbal, H. M. N., et al. (2021). Green synthesis of ZnO nanoparticles from *Syzygium cumini* leaves extract with robust photocatalysis applications. *J. Mol. Liq.* 335, 116567. doi:10.1016/j.molliq.2021.116567
- Saffran, M., and Denstedt, O. F. (1948). A rapid method for the determination of citric acid. *J. Biol. Chem.* 175, 849–855. doi:10.1016/s0021-9258(18)57202-1
- Saleh, R., and Djaja, N. F. (2014). UV light photocatalytic degradation of organic dyes with Fe-doped ZnO nanoparticles. *Superlattices Microstruct.* 74, 217–233. doi:10.1016/j.spmi.2014.06.013
- Salunke, G. R., Ghosh, S., Kumar, R. J. S., Khade, S., Vashisth, P., Kale, T., et al. (2014). Rapid efficient synthesis and characterization of silver, gold and bimetallic nanoparticles from the medicinal plant *Plumbago zeylanica* and their application in biofilm control. *Int. J. Nanomedicine* 4, 2635–2653. doi:10.2147/IJN.S59834
- Sampaio, M. J., Lima, M. J., Baptistata, D. L., Silva, A. M. T., Silva, C. G., and Faria, J. L. (2017). Ag-loaded ZnO materials for photocatalytic water treatment. *Chem. Eng. J.* 318, 95–102. doi:10.1016/j.cej.2016.05.105
- Saoud, K., Alsoubaihi, R., Bensalah, N., Bora, T., Bertino, M., and Dutta, J. (2015). Synthesis of supported silver nano-spheres on zinc oxide nanorods for visible light photocatalytic applications. *Mat. Res. Bull.* 63, 134–140. doi:10.1016/j.materresbull.2014.12.001
- Saraf, R., Shivakumara, C., Behera, S., Nagabhushana, H., and Dhananjaya, N. (2015). Facile synthesis of PbWO₄: Applications in photoluminescence and photocatalytic degradation of organic dyes under visible light. *Spectrochimica Acta Part A Mol. Biomol. Spectrosc.* 136, 348–355. doi:10.1016/j.saa.2014.09.038
- Saravanam, R., Khan, M. M., Gupta, V. K., Mosquera, E., Gracia, F., Narayanan, V., et al. (2015a). ZnO/Ag/CdO nanocomposite for visible light-induced photocatalytic degradation of industrial textile effluents. *J. Colloid Interface Sci.* 452, 126–133. doi:10.1016/j.jcis.2015.04.035
- Saravanam, R., Khan, M. M., Gupta, V. K., Mosquera, E., Gracia, F., Narayanan, V., et al. (2015b). ZnO/Ag/Mn₂O₃ nanocomposite for visible light-induced industrial textile effluent degradation, uric acid and ascorbic acid sensing and antimicrobial activity. *RSC Adv.* 5, 34645–34651. doi:10.1039/c5ra02557e
- Satter, S. S., Hoque, M., Rahman, M. M., Yousuf, M., Mollah, A., and Susan, M. (2014). An approach towards the synthesis and characterization of ZnO@Agcore@shell nanoparticles in water-in-oil microemulsion. *RSC Adv.* 4, 20612–20615. doi:10.1039/C4RA01046A
- Sharwani, A. A., Narayanan, K. B., Khan, M. E., and Han, S. S. (2022). Photocatalytic degradation activity of goji berry extract synthesized silver loaded mesoporous zinc oxide (Ag@ZnO) nanocomposites under simulated solar light irradiation. *Sci. Rep.* 12, 10017. doi:10.1038/s41598-022-14117-w
- Sharwani, A. A., Narayanan, K. B., Khan, M. E., and Han, S. S. (2021). Sustainable fabrication of silver-titania nanocomposites using goji berry (*Lycium barbarum* L.) fruit extract and their photocatalytic and antibacterial applications. *Arab. J. Chem.* 14 (12), 103456. doi:10.1016/j.arabjc.2021.103456
- Shende, S., Joshi, K. A., Kulkarni, A. S., Charolkar, C., Shinde, V. S., Parihar, V. S., et al. (2018). *Platanus orientalis* leaf mediated rapid synthesis of catalytic gold and silver nanoparticles. *J. Nanomed. Nanotechnol.* 9, 1000494. doi:10.4172/2157-7439.1000494
- Singh, K., Naidoo, Y., and Baijnath, H. (2018). A comprehensive review on the genus *Plumbago* with focus on *Plumbago auriculata* (Plumbaginaceae). *Afr. J. Tradit. Complement. Altern. Med.* 15, 199–215. doi:10.21010/ajcam.v15i1.21
- Thakur, D., Sharma, A., Rana, D. S., Thakur, N., Singh, D., Tamulevicius, T., et al. (2020). Facile synthesis of silver-doped zinc oxide nanostructures as efficient scaffolds for detection of p-nitrophenol. *Chemosensors* 8 (4), 108. doi:10.3390/chemosensors8040108
- Thayumanavan, B., and Sadasivam, S. (1984). Physicochemical basis for the preferential uses of certain rice varieties. *Plant Food. Hum. Nutr.* 34, 253–259. doi:10.1007/BF0126554
- Tripathy, A., Raichur, A. M., Chandrasekaran, N., Prathna, T. C., and Mukherjee, A. (2010). Process variables in biomimetic synthesis of silver nanoparticles by aqueous extract of *Azadirachta indica* (Neem) leaves. *J. Nanopart. Res.* 12, 237–246. doi:10.1007/s11051-009-9602-5
- Vasantharaj, S., Sathiyavimal, S., Senthilkumar, P., Kalpana, V. N., Rajalakshmi, G., Alsehli, M., et al. (2021). Enhanced photocatalytic degradation of water pollutants using bio-green synthesis of zinc oxide nanoparticles (ZnONPs). *J. Environ. Chem. Eng.* 9, 105772. doi:10.1016/j.jece.2021.105772
- Vidya, C., Manjunatha, C., Chandrababha, M. N., Rajshekar, M., and Antony, R. M. A. L. (2017). Hazard free green synthesis of ZnO nano-photocatalyst using *Artocarpus heterophyllus* leaf extract for the degradation of Congo red dye in water treatment applications. *J. Environ. Chem. Eng.* 5, 3172–3180. doi:10.1016/j.jece.2017.05.058
- Wolfe, K., Wu, X., and Liu, R. H. (2003). Antioxidant activity of apple peels. *J. Agric. Food Chem.* 51, 609–614. doi:10.1021/jf020782a
- Zachariah, A., Baiju, K. V., Shukla, S., Deepa, K. S., James, J., and Warriar, K. G. K. (2008). Synergistic effect in photocatalysis as observed for mixed-phase nanocrystalline titania processed via sol-gel solvent mixing and calcination. *J. Phys. Chem. C* 112, 11345–11356. doi:10.1021/jp712174y
- Zeng, C., Yuan, L., Li, X., Goa, C., and Wang, H. (2017). Fabrication of urchin-like Ag/ZnO hierarchical nano/microstructures based on galvanic replacement mechanism and their enhanced photocatalytic properties. *Surf. Interface Anal.* 49, 599–606. doi:10.1002/sia.6198



OPEN ACCESS

EDITED BY

Sudip Mukherjee,
Rice University, United States

REVIEWED BY

Debabrata Chowdhury,
Stanford University, United States
Arindam Pramanik,
University of Leeds, United Kingdom
Susheel Kumar Nethi,
Iowa State University, United States

*CORRESPONDENCE

Karishma Pardesi,
karishma@unipune.ac.in,
karishmapardesi@gmail.com

SPECIALTY SECTION

This article was submitted to
Nanoscience, a
section of the journal
Frontiers in Chemistry

RECEIVED 26 August 2022

ACCEPTED 14 October 2022

PUBLISHED 09 November 2022

CITATION

Tawre MS, Shiledar A, Satpute SK,
Ahire K, Ghosh S and Pardesi K (2022),
Synergistic and antibiofilm potential of
Curcuma aromatica derived silver
nanoparticles in combination with
antibiotics against multidrug-
resistant pathogens.
Front. Chem. 10:1029056.
doi: 10.3389/fchem.2022.1029056

COPYRIGHT

© 2022 Tawre, Shiledar, Satpute, Ahire,
Ghosh and Pardesi. This is an open-
access article distributed under the
terms of the [Creative Commons
Attribution License \(CC BY\)](#). The use,
distribution or reproduction in other
forums is permitted, provided the
original author(s) and the copyright
owner(s) are credited and that the
original publication in this journal is
cited, in accordance with accepted
academic practice. No use, distribution
or reproduction is permitted which does
not comply with these terms.

Synergistic and antibiofilm potential of *Curcuma aromatica* derived silver nanoparticles in combination with antibiotics against multidrug-resistant pathogens

Madhumita S. Tawre¹, Aishwarya Shiledar¹, Surekha K. Satpute¹,
Kedar Ahire², Sougata Ghosh³ and Karishma Pardesi ^{1*}

¹Department of Microbiology, Savitribai Phule Pune University, Pune, Maharashtra, India, ²Department of Zoology, Savitribai Phule Pune University, Pune, Maharashtra, India, ³Department of Microbiology, School of Science, RK University, Rajkot, Gujarat, India

Hospital acquired infections caused due to ESKAPE pathogens pose a challenge for treatment due to their growing antimicrobial resistance. *Curcuma aromatica* (CA) is traditionally known for its antibacterial, wound healing and anti-inflammatory properties. The present study highlights the biogenic synthesis of silver nanoparticles (CAAgNPs) capped and stabilized by the compounds from CA rhizome extract, also further demonstrating their antibacterial, antibiofilm and synergistic effects against multidrug-resistant (MDR) pathogens. CAAgNPs were synthesized using aqueous rhizome extract of CA (5 mg/ml) and AgNO₃ (0.8 mM) incubated at 60°C up to 144 h. UV-vis spectroscopy, field emission scanning electron microscopy (FESEM), transmission electron microscopy (TEM), energy dispersive spectroscopy (EDS) and X-ray diffraction (XRD) revealed CAAgNPs with characteristic peak at 430 nm, 13 ± 5 nm size of spherical shape, showing presence of silver and crystalline nature, respectively. Dynamic light scattering (DLS) and zeta potential confirmed their monodispersed nature with average diameter of 77.88 ± 48.60 nm and stability. Fourier transform infrared spectroscopic (FTIR) analysis demonstrated the presence of phenolic -OH and carbonyl groups possibly involved in the reduction and stabilization of CAAgNPs. The minimum inhibitory concentrations (MICs), minimum bactericidal concentrations (MBCs) and minimum biofilm inhibitory concentrations (MBICs) of CAAgNPs against *Pseudomonas aeruginosa*, NCIM 5029 and PAW1, and, *Staphylococcus aureus*, NCIM 5021 and S8 were in range from 8 to 128 µg/ml. Almost 50% disruption of pre-formed biofilms at concentrations 8–1,024 µg/ml was observed. Fluorescence microscopy and FESEM analysis confirmed cell death and disruption of pre-formed biofilms of *P. aeruginosa* PAW1 and *S. aureus* S8. Checkerboard assay demonstrated the synergistic effect of CAAgNPs (0.125–4 µg/ml) in combination with various antibiotics (0.063–1,024 µg/ml) against planktonic and biofilm forms of *P. aeruginosa* PAW1. The study confirms the antibacterial and antibiofilm activity of CAAgNPs alone and in combination

with antibiotics against MDR pathogens, thus, reducing the dose as well as toxicity of both. CAAgNPs have the potential to be used in wound dressings and ointments, and to improve the performances of medical devices and surgical implants. *In vivo* toxicity of CAAgNPs however needs to be tested further using mice models.

KEYWORDS

silver nanoparticles, *Curcuma aromatica*, antibiotics, synergy, multidrug-resistant, biofilms

1 Introduction

Pseudomonas aeruginosa and *Staphylococcus aureus* are amongst the six pathogens belonging to the “ESKAPE” group (*Enterococcus faecium*, *Staphylococcus aureus*, *Klebsiella pneumoniae*, *Acinetobacter baumannii*, *Pseudomonas aeruginosa*, and *Enterobacter* spp.) that are commonly associated with the hospital acquired nosocomial infections. *P. aeruginosa* and *S. aureus* exhibit multidrug-resistance (MDR) and virulence traits boosting the difficulty level of the treatment. The mounting antibiotic resistance has led the requisite for developing alternative strategies which can act on planktonic as well as biofilm forms of the MDR pathogens (Mulani et al., 2019). Moreover, biofilm formation by MDR pathogens contributes for the tolerance towards antibiotics making the treatment challenging (Gaidhani et al., 2014; Kamble and Pardesi, 2020; Tawre et al., 2021).

Medicinal plants or phytochemicals derived from them have been used as traditional medicines for treating bacterial infections. Plants contain a wide range of phytochemicals namely flavonoids, alkaloids, tannins, and terpenoids as their bioactive constituents which are accountable for their biological activity. Few important constituents from the plant extracts are insoluble in water which limits their usage in clinical practice. These constituents are less absorbed due to their inability to cross the lipid membranes of the cells and are highly sensitive to the acidic pH of the stomach, thereby reducing their bioavailability and efficacy (Gafur et al., 2020).

Other alternative strategies such as nanoparticles (NPs), antimicrobial peptides, phage therapy and photocatalytic therapy have been reported against MDR pathogens (Mulani et al., 2019). Advances in nanotechnology has created a benchmark in the field of biomedicine. The biological methods utilize an ecofriendly approach for the synthesis of NPs, over the physical and chemical methods requiring harsh reaction conditions that generate toxic and hazardous by-product (Altinsoy et al., 2019; Ansar et al., 2020; Mostafavi et al., 2022). Amongst the biogenic sources, synthesis of NPs using medicinal plants is widely explored. The phytochemicals from plants serve as reducing, stabilizing and capping agents for the synthesis of NPs hence offering diverse biomedical applications (Mohanta et al., 2020; Ghosh et al., 2021; Javed et al., 2021).

Amongst NPs, silver nanoparticles (AgNPs) are reconnoitered as potential antimicrobial agents and widely accepted for medical applications such as coating of medical devices and surgical implants, preparation of wound dressings and gels (Rai et al., 2009). Medicinal plant-mediated synthesis of AgNPs has attracted researchers due to their promising antibacterial and antibiofilm properties. NPs therefore offer a promising therapeutic platform for the development of innovative biofilm impellers (Koo et al., 2017; Pardesi et al., 2019; Singh et al., 2021). The factors influencing the biological activity of NPs include size distribution, morphology, surface charge, surface chemistry and capping agents (Cheon et al., 2019; Fahimirad et al., 2019). AgNPs synthesized using extracts of *Foeniculum vulgare* (Talank et al., 2022), *Picea abies* and *Pinus nigra* (Macovei et al., 2022), *Zataria multiflora* (Barabadi et al., 2021), *Punica granatum* (Swilam and Nematallah, 2020), *Lysiloma acapulcensis* (Garibo et al., 2020), *Gardenia resinifera* (Parit et al., 2020), *Brassica oleracea* (Ansar et al., 2020), *Piper betle* (Shah et al., 2019), *Prosopis juliflora* (Arya et al., 2019), *Rumex hastatus* (Rashid et al., 2019), *Galega officinalis* (Manosalva et al., 2019) and *Terminalia mantaly* (Majoumou et al., 2019) have been known to exhibit enhanced antimicrobial activity against *P. aeruginosa* and *S. aureus*. Biofilm inhibition by AgNPs synthesized using extracts of *Zataria multiflora* (Barabadi et al., 2021), *Piper betle* (Shah et al., 2019) *Rhodiola rosea* (Singh et al., 2018a), and *Cannabis sativa* (Singh et al., 2018b) have been reported in *P. aeruginosa* and *S. aureus*. AgNPs have been reported for their cytotoxicity by inducing oxidative stress caused due to the generation of reactive oxygen species (ROS) and free radicals and finally leading to cell death (Tripathi and Goshisht, 2022). Ag⁺ ions disrupts the mechanism of cell division leading to morphological changes in the cell and sudden death (Woo et al., 2008).

Curcuma aromatica (CA), a perennial herb, belonging to the Zingiberaceae family is mostly found in India and China. The germacrone component from the hexane extract of CA has been reported for its antimicrobial activity against Gram-positive bacteria (Revathi and Malathy, 2013). Despite the widespread use of CA in traditional medicine for treating various disorders, only sparse literature has scientifically evaluated and validated its therapeutic efficacy. We have previously reported the anticancer

activity of AgNPs synthesized using aqueous rhizome extract of CA (CAAgNPs) (Nadhe et al., 2020). These CAAgNPs were found to be less cytotoxic ($IC_{50} > 200 \mu\text{g/ml}$) against peripheral blood mononuclear cells (PBMCs) proposing their suitability for biomedical applications. Another study has reported the antimicrobial and antibiofilm potential of AgNPs synthesized using CA rhizome extract (Thomas et al., 2018). These AgNPs were incorporated in polymethyl methacrylate thin films which were used against the cariogenic bacterium *Streptococcus mutans*. Considering the limited data available for synthesis, characterization, and applications of CAAgNPs, we present a detailed information on the synthesis and characterization of CAAgNPs using aqueous rhizome extract of CA. The present study also demonstrates the antibacterial and antibiofilm potential of CAAgNPs against representative ESKAPE pathogens (*P. aeruginosa* and *S. aureus*) which are a major challenge to treat any wound infections. Since CA has been traditionally used to treat wound infections, we proposed that the synthesized AgNPs were stabilized by phytochemicals from CA extract offering a novel strategy for treating wound infections. We further tested the synergistic effect of CAAgNPs in combination with antibiotics belonging to different classes against planktonic and biofilm forms of an extensively drug-resistant (XDR) clinical isolate.

2 Materials and methods

2.1 Plant material and extract preparation

The dried rhizomes of CA were purchased from the local market based in Pune, Maharashtra, India and identified by a botanist from Botanical Survey of India (Western Regional Centre), Pune, Maharashtra, India (Identification No. 1603220017147). CA rhizomes were washed with distilled water, surface sterilized with 70% ethanol and dried under the shade followed by pulverization into fine powder. Aqueous rhizome extract was prepared by heating 0.5 g% (w/v) of CA powder for 1 h. The extract was filtered using Whatman filter paper no. 1 and the filtrate was stored at 4°C until further use.

2.2 Microorganisms used

Pseudomonas aeruginosa NCIM 5029 (ATCC 27853), *Staphylococcus aureus* NCIM 5021 (ATCC 25923), *Pseudomonas aeruginosa* PAW1 (clinical wound isolate) and *Staphylococcus aureus* S8 (clinical pus wound isolate) were used for antibacterial studies. *P. aeruginosa* PAW1 was concluded as an extensively drug-resistant (XDR) pathogen, resistant to ≥ 5 classes of antibiotics recommended by Clinical and Laboratory Standards Institute (CLSI, United States, 2018) except for polymyxin B, gentamicin and netilmicin (Tawre et al.,

2021). S8 was referred to as MDR pathogen, resistant to ≥ 3 antibiotic classes (Kamble and Pardesi, 2020).

2.3 Synthesis of *Curcuma aromatica* silver nanoparticles

Silver nitrate salt (AgNO_3 , 99.9%) (SRL, India) was procured and used without any further purification. Aqueous stock solution of silver nitrate (100 mM) was prepared in a stoppered volumetric flask and stored in amber colored bottle. CAAgNPs were synthesized using 0.5 g% (w/v) aqueous rhizome extract of CA with varying concentrations of AgNO_3 (0.4–1 mM) to optimize the parameters for the synthesis. The mixture was incubated at 50°C and was monitored daily for up to 144 h. Color change from yellow to brown was observed by spectral analysis using UV-vis spectroscopy (Spectra Max M2, Molecular Devices, United States). AgNO_3 concentration showing maximum peak for the synthesis of CAAgNPs was chosen and further optimization at different temperatures viz, 50, 60, and 70°C for 144 h was done. The maximum peak for the synthesis of CAAgNPs was read using UV-vis spectroscopy. Synthesized CAAgNPs were concentrated in a freeze drier (approximately 10 mg/ml) and stored at 4°C until further use.

2.4 Characterization of *Curcuma aromatica* silver nanoparticles

The surface morphology and particle size of CAAgNPs were analyzed using field emission scanning electron microscopy (FESEM) (FEI Nova Nano SEM 450, Netherlands) and transmission electron microscopy (TEM) (Tecnai G² 20U FEI, Netherlands). A drop of CAAgNPs was dried on glass slide and copper grid for FESEM and TEM analysis respectively (Singh et al., 2018b). Thin CAAgNPs films on glass slides were prepared for analysis of phase formation using X-ray diffractometer (XRD) (D8 Advanced Brucker, Germany) with a Cu K α (1.5 Å) source (Ghosh et al., 2012). The presence of silver ions in the CAAgNPs was detected by energy dispersive spectrometer (EDS) (JED-2300; JEOL) equipped with TEM at an energy range 0–20 keV. The functional groups present in the CAAgNPs were identified using Fourier-transform infrared (FTIR) spectroscopy (Jasco FT/IR-6100, Japan). CAAgNPs powder was mixed with potassium bromide and exposed to an infrared source of 400–4,000 cm^{-1} . Similarly, aqueous rhizome extract of CA was concentrated in a freeze drier and the powder was processed for FTIR analysis (Ghosh et al., 2012). The hydrodynamic diameter and zeta potential of the CAAgNPs were measured using dynamic light scattering (DLS) analysis (Nano-ZS90, Malvern, United Kingdom) (Barabadi et al., 2021).

2.5 Antibacterial studies

2.5.1 Effect of *Curcuma aromatica* silver nanoparticles on MDR/XDR pathogens

2.5.1.1 Minimum inhibitory concentrations (MICs) and minimum bactericidal concentrations (MBCs)

MICs of synthesized CAAgNPs (10 mg/ml stock solution) were tested against *P. aeruginosa*, NCIM 5029 and PAW1 and, *S. aureus*, NCIM 5021 and S8 using broth microdilution method (CLSI, United States, 2021). Briefly, O.D. adjusted culture having 10^5 CFU/ml in Luria Bertani (LB) broth was added to the microtiter plate. CAAgNPs were added to the microtiter plate at concentrations ranging from 2 to 1,024 μ g/ml by serial dilution. The aqueous rhizome extract of CA (100 mg/ml; concentrated in a freeze drier) was also tested at concentrations ranging from 2 to 4,000 μ g/ml. The wells having LB medium alone and culture inoculated LB medium were considered as negative and positive controls respectively. The plates were read at 540 nm using a microplate reader at 0 h and incubated at 37°C to note the readings after 24 h. MBCs were determined by spotting 10 μ l of the medium from each well of the microtitre plates on to LB agar plates. The minimum concentration at which there was no growth was considered as MBC. The experiment was performed in triplicates.

2.5.2 Effect of *Curcuma aromatica* silver nanoparticles on biofilms formed by MDR/XDR pathogens

The effect of CAAgNPs on biofilms was evaluated through biofilm inhibition and disruption assays against *P. aeruginosa*, NCIM 5029 and PAW1 and, *S. aureus*, NCIM 5021 and S8. Minimum biofilm inhibitory concentrations (MBICs) of CAAgNPs were determined using crystal violet staining assay (Gaidhani et al., 2014). Briefly, LB containing 10^5 CFU/ml of the test isolate was added to the wells of the microtiter plate. CAAgNPs were then added at concentrations ranging from 2 to 1,024 μ g/ml. Similarly, MBICs of CA rhizome extract were determined at concentrations ranging from 2 to 4,000 μ g/ml. The wells having LB medium alone and culture inoculated LB medium were considered as negative and positive controls respectively. Plates were incubated for 24 h at 37°C. After incubation, the bacterial cell suspension was slowly aspirated without disturbing the biofilm to remove the planktonic cells and wells were washed twice with phosphate-buffered saline (PBS). Biofilms were stained with 0.1% crystal violet at 37°C for 10 min. The wells were then washed with PBS and allowed to air dry. The stained biofilms were then solubilized in 33% acetic acid. The biofilm formation was measured at 590 nm using a microtiter plate reader. The experiment was performed in triplicates.

Similarly, biofilm disruption assay was performed using O.D. adjusted culture as mentioned above. Plates were incubated at

37°C for 24 h to allow the biofilm formation. CAAgNPs were then added to the pre-formed biofilms at varying concentrations (2 to 1,024 μ g/ml) and plates were further incubated at 37°C for 24 h. The treated biofilms were measured using the protocol as described above. The experiment was performed in triplicates. Percent biofilm inhibition or disruption was calculated as follows.

Percent biofilm inhibition or disruption

$$= \frac{(A_{590\text{nm}} \text{ without CAAgNPs} - A_{590\text{nm}} \text{ with CAAgNPs})}{A_{590\text{nm}} \text{ without CAAgNPs}} \times 100$$

where A stands for absorbance.

2.5.3 Live/dead staining of *Curcuma aromatica* silver nanoparticles treated pre-formed biofilms of MDR/XDR pathogens

Fluorescence microscopic analysis was performed for the qualitative estimation of the cell viability in the pre-formed biofilms of *P. aeruginosa* PAW1 and *S. aureus* S8 treated with and without CAAgNPs using LIVE/DEAD BacLight™ Bacterial viability kit (Invitrogen, California). Briefly, biofilm was allowed to form on the sterile cover slips for 24 h at 37°C (Tawre et al., 2021). Further, the pre-formed biofilm was treated with CAAgNPs at their respective MBICs for 24 h at 37°C. Untreated biofilm was kept as control. The cover slips were then removed from the medium and washed twice with PBS. The biofilms were stained with BacLight dye mixture and incubated for 15 min under dark conditions. The biofilms were then washed twice with PBS to remove the excess stain. The fluorescence from live (green) and dead (red) cells was observed using filters with excitation wavelength of 450–490 nm and 545–570 nm respectively under fluorescence microscope (Zeiss Axioscope A1, Germany) with 100× objective. The images were processed using ImageJ software.

2.5.4 Field emission scanning electron microscopy of *Curcuma aromatica* silver nanoparticles treated pre-formed biofilms of MDR/XDR pathogens

Effect of CAAgNPs on pre-formed biofilms of *P. aeruginosa* PAW1 and *S. aureus* S8 was observed under FESEM at $\times 30,000$ magnification. Briefly, LB containing 10^5 CFU/ml of culture was dispensed in 12 well plates. Sterile glass slides of approximately 5 \times 5 mm in size were placed in each well. The plates were incubated at 37°C for 24 h and biofilm was allowed to form on the surface of the slide. Further, the pre-formed biofilm was treated with CAAgNPs at their respective MBICs for 8 h at 37°C. Untreated biofilm was kept as control. Glass slides containing biofilm were then removed from the medium, washed twice with PBS and processed for FESEM analysis (Tawre et al., 2021). Briefly, the biofilms were fixed with 2.5% glutaraldehyde at 4°C for overnight and then washed with PBS.

Further, biofilms were washed with a series of ethanol gradations 20, 40, 60, 80 and 90% for 15 min each, and twice with absolute ethanol. The slides were air-dried, coated with gold, and observed under FESEM at 30,000× magnification.

2.5.5 Synergistic effect of *Curcuma aromatica* silver nanoparticles in combination with antibiotics against planktonic and biofilm forms of *P. aeruginosa* PAW1

The synergistic effect of CAAgNPs in combination with antibiotics was evaluated using the checkerboard assay using an XDR *P. aeruginosa* PAW1 isolate. Seventeen antibiotics were selected for the synergy assays against *P. aeruginosa* PAW1 as per our earlier report (Tawre et al., 2021). Briefly, O.D. adjusted culture (10^5 CFU/ml) in LB broth was added to the microtiter plate. Checkerboard assay was performed using each antibiotic (0.0625–1,024 µg/ml) tested in combination with CAAgNPs (0.25–8 µg/ml) (Berenbaum, 1978). Antibiotics alone and CAAgNPs alone were also tested. Antibiotics were serially diluted from higher to lower concentrations and CAAgNPs were added to each well of a row at selected concentration. The wells having LB medium alone and culture inoculated LB medium were considered as negative and positive controls respectively. Plates were incubated at 37°C for 24 h and O.D. was read at 540 nm. The experiment was performed in triplicates. Percent viability for each combination was determined and fractional inhibitory concentration (FIC) index was calculated as follows:

$$\text{FIC}_A = \frac{\text{MICs}_A \text{ in combination}}{\text{MICs}_A}$$

$$\text{FIC}_N = \frac{\text{MICs}_N \text{ in combination}}{\text{MICs}_N}$$

$$\sum \text{FIC} = \text{FIC}_A + \text{FIC}_N$$

where A indicates antibiotics; N indicates CAAgNPs.

The interaction was described as synergistic if FIC index value was ≤ 0.5 , additive if $0.5 < \text{FIC} \leq 1$, indifferent if $1 < \text{FIC} < 2$ and antagonistic if $\text{FIC} \geq 2$. The effect of the combination on *P. aeruginosa* PAW1 viability was represented in the form of heat plots indicating the interactions as synergistic, additive, or antagonistic (Habash et al., 2017).

Biofilm inhibition assay was performed using checkerboard assay as described above using a combination of CAAgNPs with antibiotics. Crystal violet staining assay was performed as described above and percent biofilm inhibition was determined. The experiment was performed in triplicates.

2.6 Statistical analysis

All the experiments were replicated three times for each assay and the results were determined as means \pm SD. Statistical

analysis using one-way ANOVA was carried out followed by Tukey's HSD post hoc test for biofilm inhibition and disruption assays. Differences were considered statistically significant at $p < 0.01$ or $p < 0.05$. Graphical analysis of the data was performed using Graph pad prism 9.

3 Results

3.1 Synthesis and characterization of *Curcuma aromatica* silver nanoparticles

Gradual color change from yellow to brown was observed during CAAgNPs synthesis with a strong surface plasmon resonance (SPR) band within an average of λ_{max} 430 nm (Figure 1A). Optimization study revealed that 0.5 g% (w/v) aqueous rhizome extract of CA and 0.8 mM of AgNO_3 incubated at 60°C for 144 h gave the maximum synthesis of CAAgNPs (Figures 1B,C). Spectrum analysis displayed the maximum peak of CAAgNPs at 0.8 mM concentration of AgNO_3 (Figure 1D).

TEM analysis revealed that the CAAgNPs were monodispersed with spherical shape and 13 ± 5 nm in size analyzed using ImageJ software (Figures 2A,B). The peak at 3 KeV was observed in EDS analysis confirming the presence of elemental silver (Figure 2C). FESEM analysis endorsed spherical morphology and uniformity in the shape of CAAgNPs (Figure 3A). Elemental mapping conducted through EDS demonstrated the presence of silver (Figure 3B). It was also evident that elements of C, O, and N were uniformly distributed on the surface of CAAgNPs suggesting the presence of phytochemicals involved in the stabilization of CAAgNPs. XRD analysis showed diffraction peaks at 38.0° , 44.86° , 64.70° , and 77.4° and these corresponds to (111), (200), (220), and (311) planes of a face-centered cubic (fcc) structure of silver crystals (Figure 4A). The data was matched with the standard Joint Committee for Powder Diffraction Set (card 040783) confirming a face-centered cubic structure for CAAgNPs. Functional groups associated with aqueous rhizome extract of CA and CAAgNPs were identified by FTIR (Figure 4B). The FTIR analysis of aqueous rhizome extract of CA indicated peaks at $1,214 \text{ cm}^{-1}$ related to aromatic CO stretching vibration, $1,361 \text{ cm}^{-1}$ related the olefin bending vibration of the CC group bound to the benzene ring of the curcumin, $1,596 \text{ cm}^{-1}$ related to C=C double-bond stretching, and $2,977 \text{ cm}^{-1}$ related to C-H stretching. The FTIR results of CAgNPs indicated peaks at $1,404 \text{ cm}^{-1}$ related to the presence of C-C, in which CH_3 bending occurred; $1,660 \text{ cm}^{-1}$ related to C=O with carbonyl stretching and the existence of amide-1 ($-\text{NHCO}$ of amide), where the proteins are bent; $2,921 \text{ cm}^{-1}$ for the extension of the C-H bond with alkanes vibration and aldehyde C-H stretching. DLS illustrated the average hydrodynamic diameter of CAAgNPs to be 77.88 ± 48.60 nm (Figure 4C) and the -23.8 mV of zeta potential (Figure 4D).

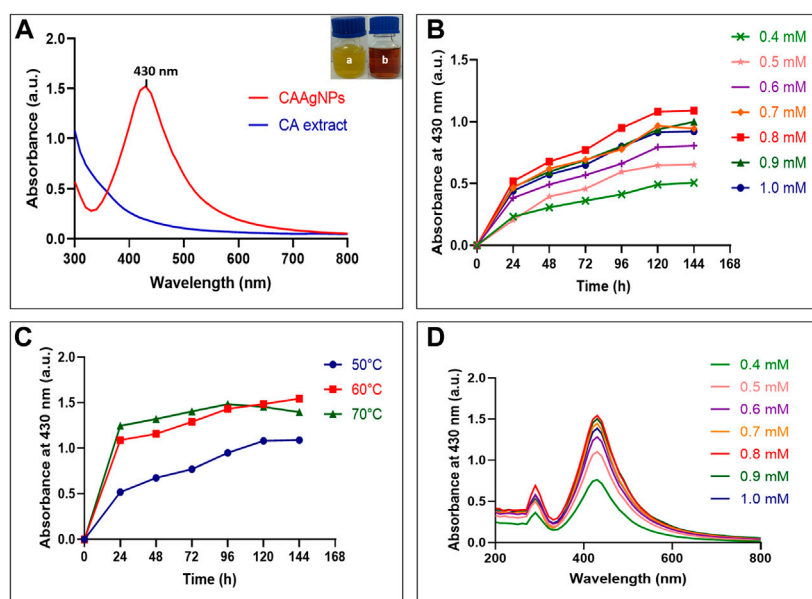


FIGURE 1

Optimization of CAgNPs synthesis (A) UV-visible spectrum for aqueous CA rhizome extract and synthesized CAgNPs (maximum peak at 430 nm). "a" in the inset indicates yellow colored aqueous CA rhizome extract before synthesis and "b" indicates brown colored CAgNPs after synthesis. Time course of CAgNPs synthesis at (B) 0.4, 0.5, 0.6, 0.7, 0.8, 0.9, and 1 mM concentration of AgNO_3 , and (C) 50, 60, and 70°C temperatures. (D) UV-visible spectrum for CAgNPs synthesis using range of concentrations of AgNO_3 at 144 h.

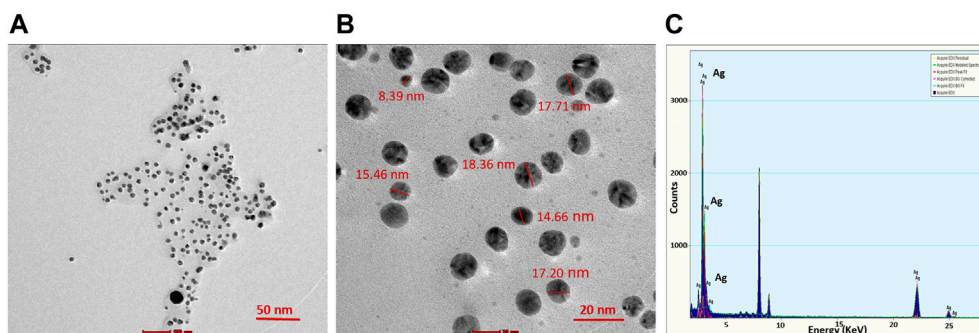


FIGURE 2

TEM imaging of CAgNPs at (A) 50 nm and (B) 20 nm scales revealed the spherical shape and size in the range of 13 ± 5 nm. (C) EDS analysis indicated the peak for the presence of Ag^+ at 3 KeV.

3.2 Antibacterial and antibiofilm activity of *Curcuma aromatica* silver nanoparticles

MICs of CAgNPs against *P. aeruginosa*, NCIM 5029 and PAW1 were 16 and 8 $\mu\text{g}/\text{ml}$ respectively, whereas those for *S. aureus*, NCIM 5021 and S8 were 32 and 64 $\mu\text{g}/\text{ml}$ respectively (Table 1). MBCs of CAgNPs against *P. aeruginosa*, NCIM 5029 and PAW1 was 32 $\mu\text{g}/\text{ml}$, whereas those for *S. aureus*, NCIM 5021 and S8 was 128 $\mu\text{g}/\text{ml}$ (Table 1). MICs, MBCs and

MBICs of the aqueous rhizome extract of CA against all four isolates were 3 mg/ml, >3 mg/ml and 3 mg/ml respectively. MBICs of CAgNPs against all four isolates was the same as their MICs against planktonic cells. Biofilm inhibition was observed in a dose-dependent manner for all the isolates tested (Figures 5A,B). Different letters on the bars indicate that mean values of the treatments are significantly different at $p < 0.01$ according to Tukey's post hoc test. Error bars indicates the standard deviation from the three biological replicates.

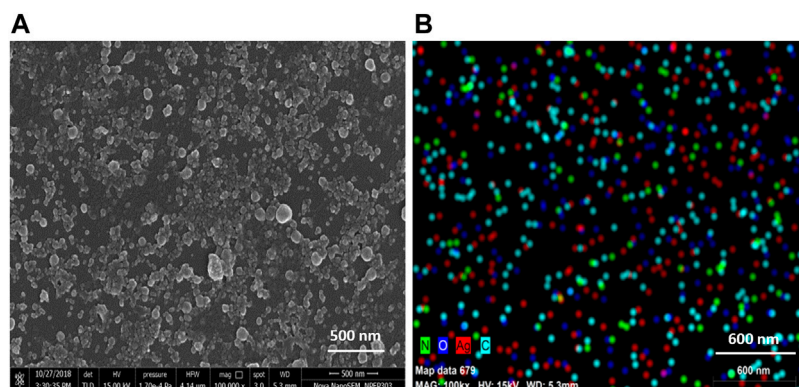


FIGURE 3

(A) SEM imaging of CAgNPs revealed spherical and uniform shape observed under 1,00,000 × magnification at 500 nm scale. (B) Elemental mapping of silver (red color) in CAgNPs using EDS at 600 nm scale. Uniform distribution of C, O, and Ag elements on the surface of CAgNPs indicating successful coating.

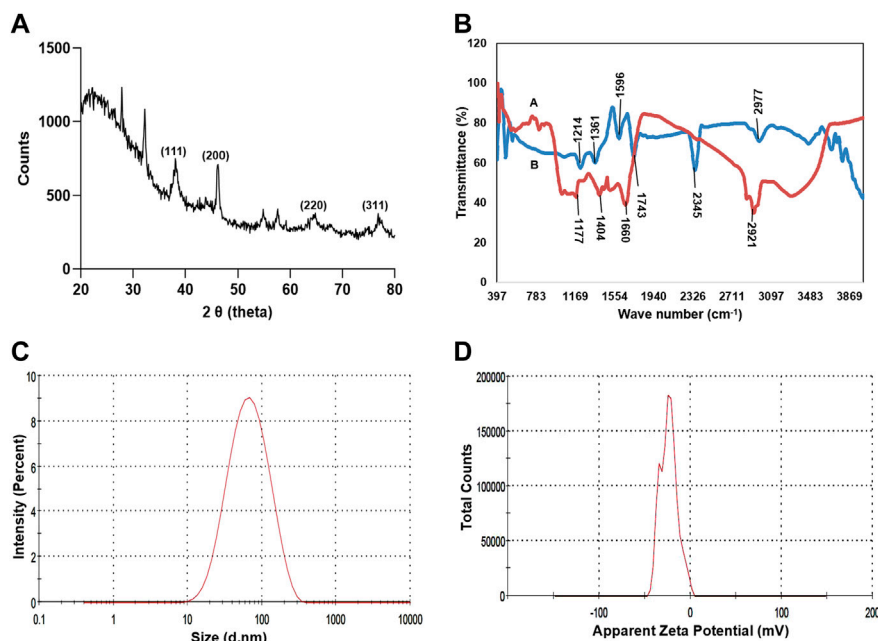


FIGURE 4

Characterization of CAgNPs (A) XRD analysis showed diffraction peaks at 38°, 44.86°, 64.70°, and 77.4° corresponding to (111), (200), (220) and (311) planes of a face-centered cubic (fcc) structure of silver crystals revealing crystalline nature. (B) FTIR analysis of CAgNPs represented by "A (red line)" indicates a peak at 1,404 cm^{-1} related to the presence of C-C, 1,660 cm^{-1} related to C=O and 2,921 cm^{-1} for the extension of the C-H bond with alkanes vibration and aldehyde C-H stretching. FTIR analysis of CA rhizome extract represented by "B (blue line)" indicates a peak at 1,214 cm^{-1} related to aromatic CO stretching vibration, 1,361 cm^{-1} related the olefin bending vibration of the CC group bound to the benzene ring of the curcumin, 1,596 cm^{-1} related to C=C double-bond stretching, and 2,977 cm^{-1} related to C-H stretching (C) DLS analysis confirmed the uniformity and average hydrodynamic diameter of CAgNPs to be 77.88 ± 48.60 nm. (D) Zeta potential at -23.8 mV indicated stability of CAgNPs.

3.3 Biofilm disruption by *Curcuma aromatica* silver nanoparticles

The treatment of 24 h old biofilms with CAgNPs resulted in disruption of biofilms, varying between

34.08%–76.60% (*P. aeruginosa* NCIM 5029), 36.21%–67.79% (*P. aeruginosa* PAW1), 10.76%–78.94% (*S. aureus* NCIM 5021) and 22.48%–69.12% (*S. aureus* S8). Different letters on the bars indicate that mean values of treatments are significantly different at $p < 0.01$ or $p < 0.05$ (indicated with

TABLE 1 Antibacterial and antibiofilm activity of CAAgNPs against MDR/XDR pathogens.

Microorganisms	MICs ($\mu\text{g/ml}$)	MBCs ($\mu\text{g/ml}$)	MBICs ($\mu\text{g/ml}$)
<i>P. aeruginosa</i> NCIM 5029	16	32	16
<i>P. aeruginosa</i> PAW1	8	32	8
<i>S. aureus</i> NCIM 5021	32	128	32
<i>S. aureus</i> S8	64	128	64

Note: MICs-Minimum inhibitory concentrations; MBCs-Minimum bactericidal concentrations; MBICs-Minimum biofilm inhibitory concentrations.

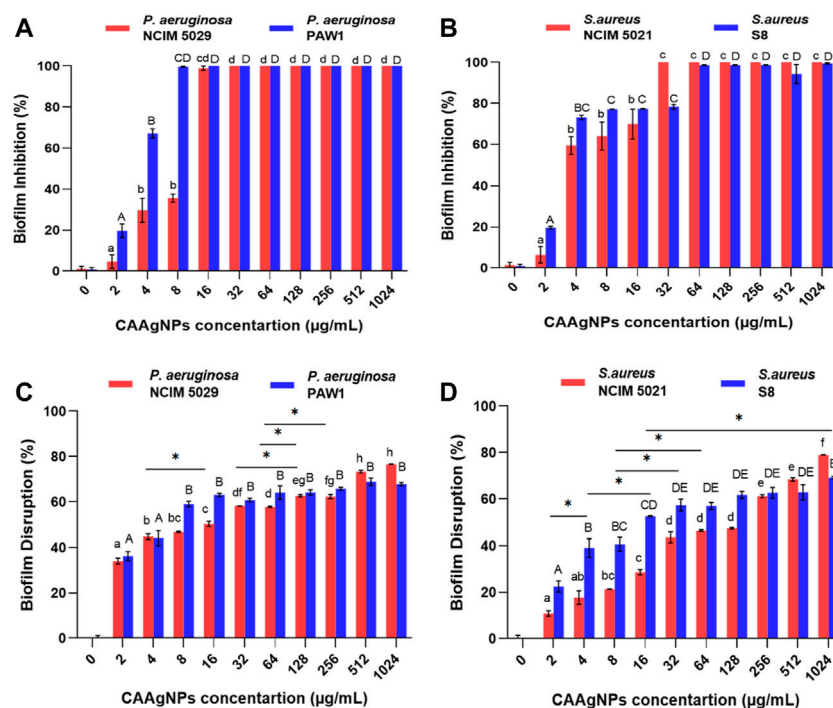


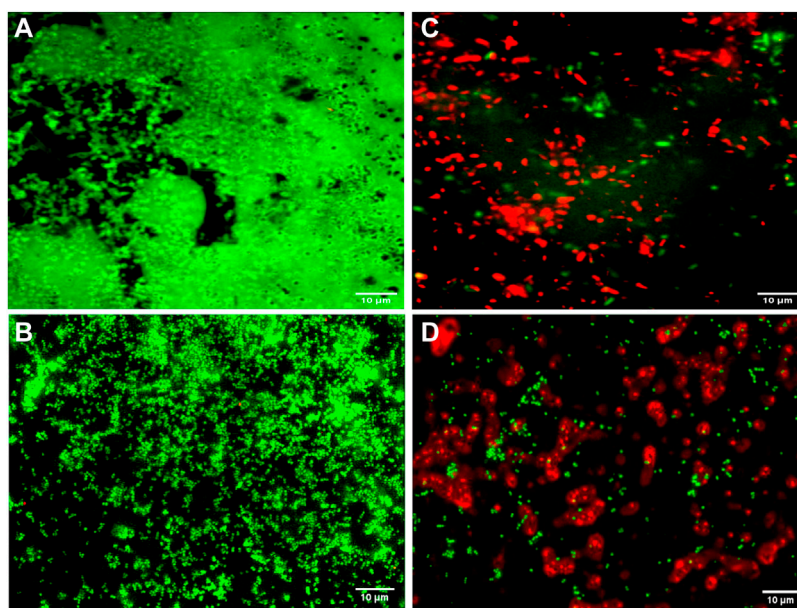
FIGURE 5

Percent biofilm inhibition of (A) *P. aeruginosa*, NCIM 5029 and PAW1 and (B) *S. aureus*, NCIM 5021 and S8 after treatment with CAAgNPs at concentrations ranging from 2 to 1,024 $\mu\text{g/ml}$. Error bars indicate standard deviation from three biological replicates. Different alphabets on top of the bars indicates differences considered statistically significant at $p < 0.01$. Percent biofilm disruption of (C) *P. aeruginosa*, NCIM 5029 and PAW1 and (D) *S. aureus*, NCIM 5021 and S8 after treatment with CAAgNPs at a concentration ranging from 2 to 1,024 $\mu\text{g/ml}$. Error bars indicate standard deviation from three biological replicates. Different alphabets on top of the bars indicates differences considered statistically significant at $p < 0.01$. Single "*" (asterisk) indicates differences considered statistically significant at $p < 0.05$.

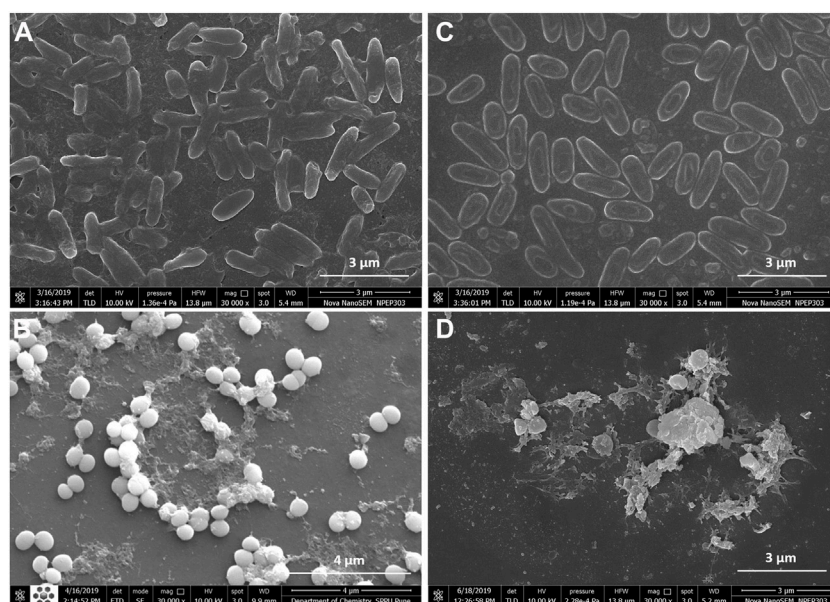
asterisk) according to Tukey's post hoc test. Error bars indicate the standard deviation from the three biological replicates. Percent disruption in MDR clinical isolates (*P. aeruginosa* PAW1 and *S. aureus* S8) was less as compared to the antibiotic sensitive standard isolates (*P. aeruginosa* NCIM 5029 and *S. aureus* NCIM 5021). Complete eradication of biofilm was not observed in any of the four isolates tested even at CAAgNP concentrations as high as 1,024 $\mu\text{g/ml}$ (Figures 5C,D).

Fluorescence microscopic images revealed that the untreated pre-formed biofilms of *P. aeruginosa* PAW1 and

S. aureus S8 have a greater number of viable cells indicated by green color obtained at 528 nm for SYTO9 signal (Figures 6A,B). Comparatively, greater number of dead cells indicated by red color obtained at 645 nm for PI signal were observed for CAAgNPs treated pre-formed biofilms (Figures 6C,D). The cells which were about to die were indicated by yellow-orange color. FESEM analysis revealed that the untreated biofilms of *P. aeruginosa* PAW1 as well as *S. aureus* S8, were intact without any alterations in the cell morphology (Figures 7A,B). Comparatively, disruption of the cells and extracellular matrix in 24 h old biofilm of *P. aeruginosa* PAW1 and *S.*

**FIGURE 6**

Fluorescence microscopic analysis of 24 h pre-formed biofilms under 100 x objective. Untreated pre-formed biofilms of (A) *P. aeruginosa* PAW1 and (B) *S. aureus* S8 with greater number of viable cells (green) obtained at 528 nm for SYTO9 signal. CAAgNPs treated pre-formed biofilms of (C) *P. aeruginosa* PAW1 and (D) *S. aureus* S8 with greater number of dead cells (red) obtained at 645 nm for PI signal. Few cells indicated by yellow-orange color were about to die.

**FIGURE 7**

FESEM images of 24 h pre-formed biofilms at 30,000 x magnification. Untreated biofilms of (A) *P. aeruginosa* PAW1 and (B) *S. aureus* S8; CAAgNPs treated biofilms of (C) *P. aeruginosa* PAW1 and (D) *S. aureus* S8. Disruption of extracellular matrix and cell morphology was observed in treated biofilms at respective MICs.

TABLE 2 FICi values of combination of CAAgNPs with antibiotics against planktonic and biofilm forms of *P. aeruginosa* PAW1.

Antibiotics	MICs (μg/ml) Planktonic cells			FICi	MBICs (μg/ml) Biofilm forms		FICi
	A	B	C		D	E	
Penicillins							
Piperacillin	128 ^R	0.125	1	0.126	0.125	2	0.251
Monobactams							
Aztreonam	16 ^I	0.125	2	0.258	4	2	0.500
Lipopeptides							
Colistin	16 ^I	0.25	0.5	0.078	0.5	1	0.125
Aminoglycosides							
Gentamicin	0.25 ^S	0.0625	0.25	0.281	0.0625	0.25	0.313
Tobramycin	64 ^R	0.25	0.5	0.066	0.125	1	0.127
Amikacin	64 ^R	1	0.25	0.047	0.25	1	0.129
Netilmicin	0.5 ^S	0.0625	0.25	0.156	0.0625	0.5	0.188
Cephems							
Cefepime	>1024 ^R	0.125	1	0.125	1	4	0.500
Ceftazidime	>1024 ^R	0.125	1	0.125	0.5	4	0.500
Fluoroquinolones							
Ciprofloxacin	256 ^R	0.125	1	0.125	0.25	2	0.251
Norfloxacin	512 ^R	0.25	1	0.125	0.25	2	0.250
Levofloxacin	512 ^R	0.25	1	0.125	2	2	0.254
Ofloxacin	>1024 ^R	0.125	1	0.125	0.125	2	0.250
Gatifloxacin	256 ^R	0.125	1	0.125	4	1	0.141
Carbapenems							
Doripenem	1024 ^R	0.125	2	0.250	0.125	4	0.500
Meropenem	1024 ^R	0.125	2	0.250	0.25	2	0.250
Imipenem	1024 ^R	0.125	2	0.250	1	4	0.500

Note: A: MICs of antibiotics, B: lowest effective concentration of antibiotics (μg/ml) in combination with CAAgNPs; C: lowest effective concentration of CAAgNPs (μg/ml) in combination with antibiotics. S: sensitive; I: intermediate; R: resistant. FICi, represents-Synergistic: FIC_i ≤ 0.5; Additive: 0.5 < FIC_i ≤ 1; Indifferent: 1 < FIC_i < 2; Antagonistic: FIC_i ≥ 2.

aureus S8 at their respective MICs of CAAgNps was observed (Figures 7C,D).

3.4 Synergistic activities of *Curcuma aromatica* silver nanoparticles in combination with antibiotics against planktonic and biofilm forms of *P. aeruginosa* PAW1

MICs for antibiotics against *P. aeruginosa* PAW1 were adopted from our published work (Tawre et al., 2021). Synergistic effect was observed for all combinations of CAAgNPs with antibiotics since FICi was <0.5 (Table 2). The percent viability calculated for each combination of CAAgNPs with antibiotics was represented in the form of a heat plots (Figures 8A–D; Figures 9A–E; Figures 10A–E; and Figures 11A–C). Heat plots gave a better understanding of synergistic behavior of combination of CAAgNPs with antibiotics like

isobologram plots of drug-drug interaction (Tallarida, 2016). FICi value < 0.5 for each combination (indicated by an asterisk) was lying below the dashed line (passing through the respective MICs of CAAgNPs and antibiotics) which indicated synergistic interaction.

Interestingly, two classes of antibiotics namely cepheims (ceftazidime and cefepime) and carbapenems (meropenem, dorepenem, imipenem) in combination with CAAgNPs showed antagonistic effect at higher concentrations. Conversely, they showed synergistic effect at lower concentrations.

The FICi values for all combinations of CAAgNPs with antibiotics were ≤0.5 against *P. aeruginosa* PAW1 biofilm (Table 2) indicating a synergistic interaction.

4 Discussion

The emergence of antibiotic resistance has created a threat making it empirical to develop alternative treatment strategies

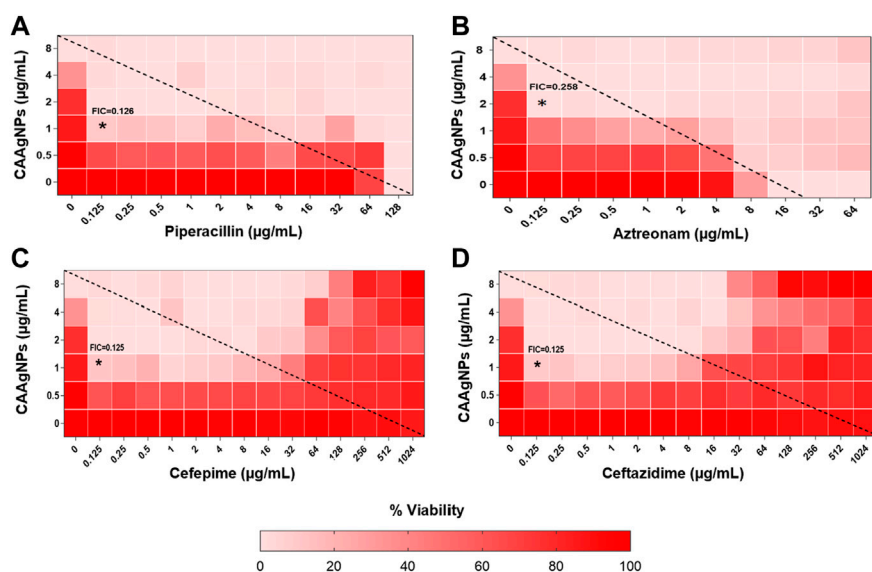


FIGURE 8

Heat plots demonstrating synergistic effect of CAAgNPs in combination with antibiotics against *P. aeruginosa* PAW1. Representation of normalized values of percent viability after treatment of CAAgNPs (0–8 µg/ml) with (A) Piperacillin (0–128 µg/ml), (B) Aztreonam (0–64 µg/ml), (C) Cefepime (0–1,024 µg/ml) and (D) ceftazidime (0–1,024 µg/ml) respectively. Untreated cells with hundred percent viability indicated by darker red boxes. Lighter red boxes indicate reduced cell viability. Dashed line passes through the MICs and “*” (asterisk) below it represents the FIC_i values suggesting a synergistic effect.

against infections caused due to MDR pathogens. AgNPs have explicitly substantiated their role in the field of biomedicine due to their properties. Numerous medicinal plants have been employed to synthesize AgNPs and are reported for their antibacterial and antibiofilm properties against MDR pathogens (Siddiqi et al., 2018; Fahimirad et al., 2019).

Since ancient times the medicinal value of CA has been acknowledged for antibacterial and wound healing properties. The proteases from turmeric species have procoagulant and fibrinogenolytic activity. This provides a scientific basis for the traditional use of turmeric to stop bleeding and promote wound healing processes (Shivalingu et al., 2016). In the present study, it was proposed that the phytochemicals from the aqueous rhizome extract of CA may be involved in the stabilization of the CAAgNPs, and also enhancing their wound healing and antimicrobial properties.

The nature of the plant extract, its concentration, concentration of the metal salt, and other parameters such as pH, temperature and time of incubation certainly influence the yield and other characteristics of the synthesized NPs (Akhtar et al., 2013; Fahimirad et al., 2019). The phytochemicals present in the plant extract reduce the Ag^+ ions to Ag^0 , followed by capping and stabilization of newly synthesized AgNPs (Fahimirad et al., 2019). Maximum rate of CAAgNPs synthesis was observed at 0.8 mM AgNO_3 concentration as compared to the lower concentrations. Reduction in the rate of synthesis was seen at higher concentrations. Similarly, it has

been reported that with increased concentration of AgNO_3 it gets deposited on the surface of AgNPs by forming unclear surfaces (Fahimirad et al., 2019). There was increase in the rate of CAAgNPs synthesis with rising temperatures till 60°C with increasing incubation period till 144 h. The optimized parameters for the maximal synthesis of CAAgNPs were 0.5% (w/v) of aqueous rhizome extract of CA treated with 0.8 mM AgNO_3 solution, incubated at 60°C for 144 h. These CAAgNPs were found to be stable, even after one year. The optimization studies certainly suggested that the experimental parameters such as concentration of AgNO_3 , temperature and reaction time have an overall impact on the synthesis of CAAgNPs. TEM technique assured the size (13 ± 5 nm) and spherical shape of the CAAgNPs. Earlier studies with AgNPs derived using CA have documented its spherical shape with few rods and triangles ranging in size of 20–40 nm (Thomas et al., 2018). Detailed characterization of CAAgNPs was not documented in the earlier report. Our study confirms the characteristics of CAAgNPs thoroughly. FESEM also confirmed the spherical shape of CAAgNPs. Further elemental mapping and EDS analysis displayed the presence of silver. XRD validated the crystalline nature of CAAgNPs. DLS revealed that the average hydrodynamic diameter of CAAgNPs was 77.88 ± 48.60 nm which was higher than the size measured using TEM. Since TEM measures the core size of CAAgNPs and DLS measures the hydrodynamic radius of CAAgNPs, which includes the coating on its surface. Earlier studies have suggested similar reports with

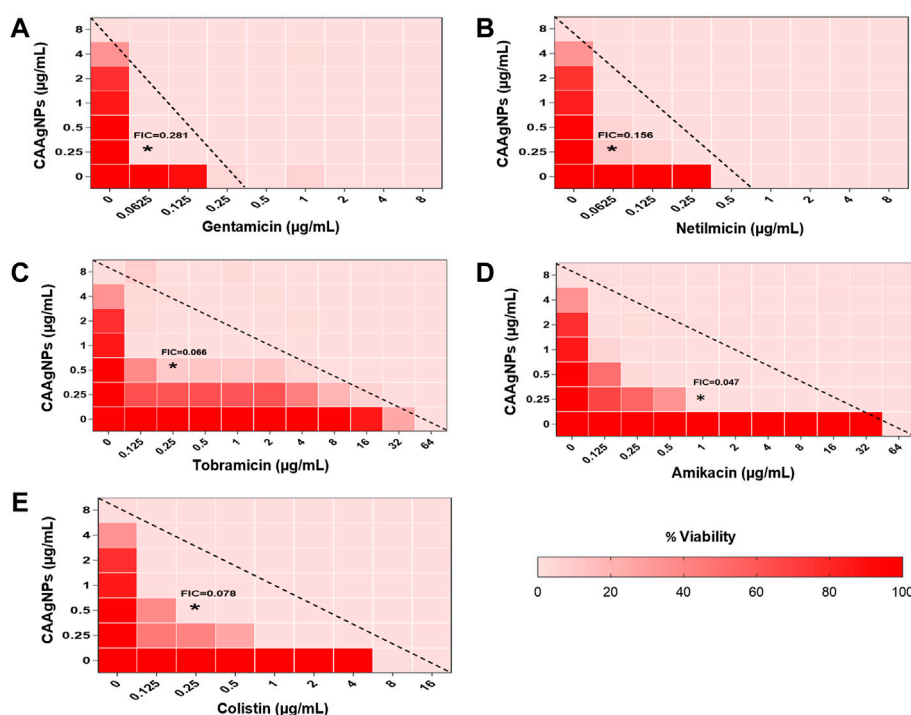


FIGURE 9

Heat plots demonstrating synergistic effect of CAAgNPs in combination with antibiotics against *P. aeruginosa* PAW1. Representation of normalized values of percent viability after treatment of CAAgNPs (0–8 µg/ml) with (A) Gentamicin (0–8 µg/ml), (B) Netilmicin (0–8 µg/ml), (C) Tobramycin (0–64 µg/ml), (D) Amikacin (0–64 µg/ml), and (E) Colistin (0–16 µg/ml) respectively. Untreated cells with hundred percent viability indicated by darker red boxes. Lighter red boxes indicate reduced cell viability. Dashed line passes through the MICs and “*” (asterisk) below it represents the FICi values suggesting a synergistic effect.

differences in size measurement using TEM and DLS analysis (Ansar et al., 2020). Zeta potential confirmed the negative charge on CAAgNPs which keeps the particles monodispersed and prevents agglomeration. NPs with negative zeta potential values suggest there are strong repulsive forces between the NPs, that prevent the agglomeration of the NPs in solution (Majoumouo et al., 2019).

Plants and their parts contain carbohydrates, fats, proteins, nucleic acids, pigments and several types of secondary metabolites which act as reducing agents to produce nanoparticles from metal salts without producing any toxic by-product (Siddiqi et al., 2018). The phytochemical constituents of CA reported in literature include germacrone, curdione, curcumin, dehydrocurdione, zederone, curcumenol, zedoarondiol and β -sitosterol (Pintatum et al., 2020; Umar et al., 2020). These phytochemicals are known for various biological activities and therefore may act as reducing agents involved in synthesis of CAAgNPs and also play a role in their capping and stabilization. The FTIR absorption spectra of CA rhizome extract and CAAgNPs demonstrated shifts in peak from 1,596 cm^{-1} to 1,660 cm^{-1} which correlates with the involvement of phenolic -OH and carbonyl groups as

stabilizing and reducing agent in the formation of CAAgNPs. Shift in peak from 1,214 cm^{-1} to 1,177 cm^{-1} correlates with the involvement of aromatic CO group. The presence of these functional groups confirmed that the CAAgNPs are capped with compounds from CA rhizome extract suggesting their involvement in stabilization. These results are consistent with the earlier studies reported for medicinal plants (Mohanta et al., 2020; Muniyappan et al., 2021).

The antibacterial activity of AgNPs is certainly dependent on their shape and size; the smaller the size higher is the activity (Dakal et al., 2016; Duran et al., 2016). Ag^+ ions are released from AgNPs which then penetrate through the bacterial cell wall, rupturing it and leading to denaturation of proteins and leading to cell death (Siddiqi et al., 2018). Through the present study, we focused on antibacterial and antibiofilm activities of CAAgNPs against MDR pathogens. Lower MICs were observed against *P. aeruginosa*, NCIM 5029 (16 µg/ml) and PAW1 (8 µg/ml) as compared to *S. aureus*, NCIM 5021 (32 µg/ml) and S8 (64 µg/ml) suggesting that Gram-negative bacteria are more sensitive to CAAgNPs than Gram-positive bacteria. Comparable results were observed with AgNPs synthesized using *Cannabis sativa* in an

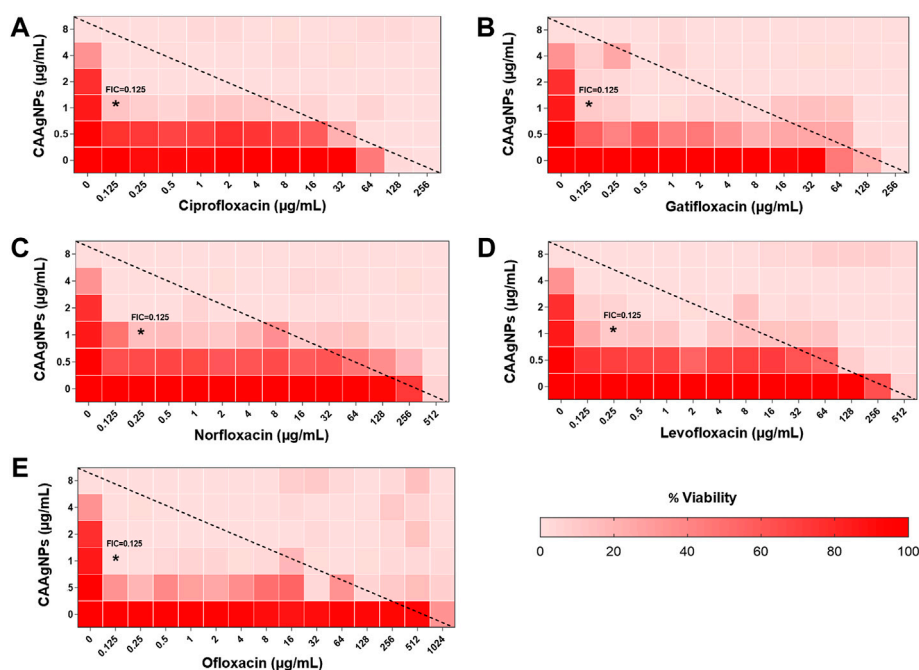


FIGURE 10

Heat plots demonstrating synergistic effect of CAAgNPs in combination with antibiotics against *P. aeruginosa* PAW1. Representation of normalized values of percent viability after treatment of CAAgNPs (0–8 µg/ml) with (A) Ciprofloxacin (0–256 µg/ml), (B) Gatifloxacin (0–256 µg/ml), (C) Norfloxacin (0–512 µg/ml), (D) Levofloxacin (0–512 µg/ml) and (E) Ofloxacin (0–1,024 µg/ml) respectively. Untreated cells with hundred percent viability indicated by darker red boxes. Lighter red boxes indicate reduced cell viability. Dashed line passes through the MICs and “*” (asterisk) below it represents the FICi values suggesting a synergistic effect.

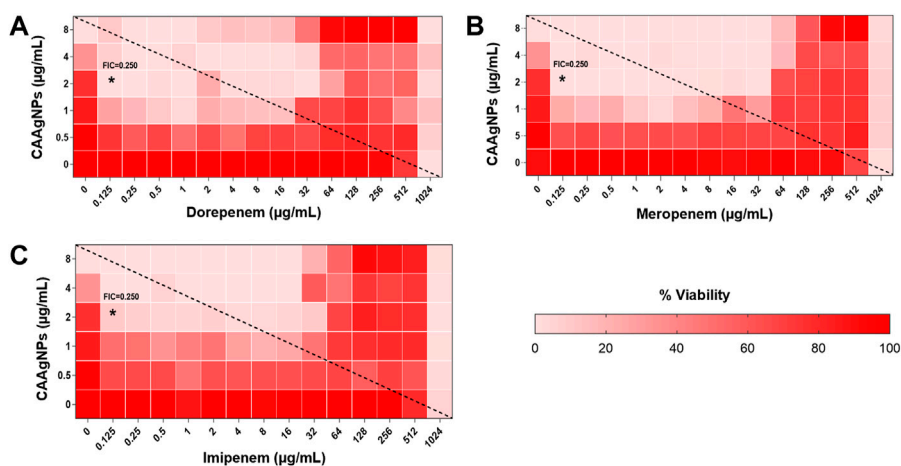


FIGURE 11

Heat plots demonstrating synergistic effect of CAAgNPs in combination with antibiotics against *P. aeruginosa* PAW1. Representation of normalized values of percent viability after treatment of CAAgNPs (0–8 µg/ml) with (A) dorepenem (0–1,024 µg/ml), (B) meropenem (0–1,024 µg/ml) and (C) imipenem (0–1,024 µg/ml) respectively. Untreated cells with hundred percent viability indicated by darker red boxes. Lighter red boxes indicate reduced cell viability. Dashed line passes through the MICs and “*” (asterisk) below it represents the FICi values suggesting a synergistic effect.

earlier study (Singh et al., 2018b). The antibacterial studies of AgNPs against *P. aeruginosa* PAO1 have demonstrated the MIC of 12.5 µg/ml (Shah et al., 2019). In an earlier report, MICs of synthesized AgNPs against *S. aureus* were 8 µg/ml (Talank et al., 2022) and 4 µg/ml (Barabadi et al., 2021). These observations also suggest that smaller size of the AgNPs in the range 8–20 nm display lower MICs as compared to the large size AgNPs. The difference in susceptibility pattern is attributed to the thin cell wall and double cell membrane of Gram-negative bacteria through which AgNPs can penetrate (Pal et al., 2007). Contrary, penetration of AgNPs is prevented in Gram-positive bacteria due to thick cell wall with negatively charged peptidoglycan resulting in weaker antibacterial effect (Feng et al., 2000). The aqueous rhizome extract of CA displayed very high MICs, MBCs and MBICs as compared to the CAAgNPs. The antibacterial and antibiofilm activity of CAAgNPs can be attributed to the functional groups such as phenolic and aromatic from the aqueous rhizome extract of CA present on the surface of CAAgNPs. There is a possibility that these phytochemicals may be involved in the stabilization of CAAgNPs which deserve merit to be further explored. These observations are well supported with earlier studies on AgNPs derived from *Camellia sinensis*, suggesting that polyphenols of plant extract present onto the surface of AgNPs pose antimicrobial activity (Onitsuka et al., 2019). Our previous work demonstrated the potential of curcumin functionalized iron oxide nanoparticles by displaying improved inhibition of *Agrobacterium tumefaciens* when compared to bare iron oxide nanoparticles (Kitture et al., 2012). Hence, the superior antibacterial activity of CAAgNPs found in this study is well in agreement with the previous report.

One of the major reasons for acquiring drug resistance by pathogenic bacteria is biofilm formation. Elimination of biofilms becomes a major concern while treating such infections, as the pathogens do not respond to the antibiotic therapy making it imperative to develop innovative strategies. Consequently, new agents should effectively aid in inhibiting planktonic as well as biofilm forms of the pathogen (Paradesi et al., 2019). AgNPs synthesized from medicinal plants are well reported to inhibit biofilms formed by *P. aeruginosa* (Singh et al., 2018a; Singh et al., 2018b; Arya et al., 2019). The AgNPs synthesized using CA rhizome extract have also been reported to be incorporated in polymethyl methacrylate thin films which displayed antimicrobial and antibiofilm (inhibition up to 94%) activity against the cariogenic bacterium *Streptococcus mutans*. Similarly, in the present study, CAAgNPs were effective in complete biofilm inhibition of *P. aeruginosa*, NCIM 5029 and PAW1, *S. aureus*, NCIM 5021 and S8 at their respective MICs. In an earlier study, 91.02% inhibition of *S. aureus* biofilm was observed after treatment of AgNPs synthesized using *Z. multiflora* (Barabadi et al., 2021). In another study, treatment with

three types of AgNPs displayed >99% of biofilm inhibition at 100, 50 and 60 µg/ml concentrations for *P. aeruginosa* and at 90, 60 and 60 µg/ml concentrations for *S. aureus* (Mohanta et al., 2020). Although biofilm disruption assay demonstrated around 50% reduction in the biofilm mass at the respective MICs, however, >1,024 µg/ml of concentration was required for the complete disruption of biofilm. Live/Dead staining of CAAgNPs treated pre-formed biofilms of *P. aeruginosa* PAW1 and *S. aureus* S8 revealed that very few cells were viable (green) and greater number of the cells were dead (dead). Disruption of pre-formed biofilms matrix of *P. aeruginosa* PAW1 and *S. aureus* S8 observed through FESEM analysis also demonstrated the antibiofilm potential of CAAgNPs. Reduction in the cell numbers and disruption of the cell surface morphology as compared to untreated control was observed. Comparable results were observed in earlier studies after treatment of pre-formed biofilms of *P. aeruginosa* and *S. aureus* with AgNPs (Singh et al., 2018b; Singh et al., 2019a; Singh et al., 2019b). These findings suggest a possibility that Ag⁺ ions are released from CAAgNPs that adhere to the cell membrane, internalize through cell membrane, damage the cell components, and consequently leads to the cell death.

Repeated use of antibiotics has developed resistance towards the existing antibiotics and currently no new antibiotics are in the pipeline (Mulani et al., 2019). Similarly, it is conveyed in an earlier study that repeated exposure to AgNPs may develop resistance in the organisms (Panacek et al., 2018). Consequently, alternate strategies such as combination therapies involving antibiotics with AgNPs to treat MDR pathogens should come into play. Such combination therapy will reduce the dosage of antibiotic and AgNPs well below their MICs which otherwise required a high amount to exhibit the inhibitory effects on MDR pathogens. Reduced dosage will minimize any toxic effects on the host cells.

Representation of percent viability of *P. aeruginosa* PAW1 treated with CAAgNPs in combination with antibiotics using heat plots gives a better understanding of synergism. In the present study, the combination of CAAgNPs with antibiotics from class, penicillins, monobactams, aminoglycosides and fluoroquinolones suggested synergistic effects (FIC_i <0.5). Similar results were obtained in another study where AgNPs were used in combination with aztreonam and tobramycin against *P. aeruginosa* PAO1 biofilms. Smaller size AgNPs (10 and 20 nm) were found to be more effective at lower concentrations as compared to larger size AgNPs (40, 60 and 100 nm). The study also suggests that the antimicrobial activity of AgNPs can be affected by the factors such as strain dependent differences, source of AgNPs synthesis and surface modifications. (Habash et al., 2014; Habash et al., 2017). The efficacy of polymyxin B in combination with AgNPs was enhanced as compared to polymyxin B alone (Salman et al., 2019). AgNPs synthesized using *D. bulbifera* tuber extract have displayed

synergistic effect in combination with antibiotics against *P. aeruginosa* (Ghosh et al., 2012). Earlier report has demonstrated non-specific synergistic activity of antibiotics with AgNPs against *P. aeruginosa* and *S. aureus* (Panacek et al., 2015). Interestingly, synergistic effect was also observed with two classes of antibiotics namely cepheims (ceftazidime and cefepime) and carbapenems (meropenem, imipenem or dorepenem) at lower concentrations when in combination with CAAgNPs, however, an antagonistic effect was observed at higher concentrations.

Earlier reports have suggested the role of AgNPs in altering the cell membrane integrity, leading to increase in the cell permeability thereby allowing the entry of antibiotics inside the cell (Vazquez-Munoz et al., 2019). Further studies to understand the mechanistic action of CAAgNPs therefore needs to be investigated. Antagonistic interactions indicate a possibility that high antibiotic concentrations (of cepheims and carbapenem class) just below the MIC values hinder the CAAgNPs activity. This observation also needs to be further investigated to understand the mechanism that leads to antagonistic effects.

Complete inhibition of biofilm was observed with CAAgNPs in combination with antibiotics which occurred at concentrations much below their individual MICs and displayed synergistic effect. In earlier reports, the synergistic effect of AgNPs with polymyxin B has been reported against *P. aeruginosa* biofilm. This further affirms the role of CAAgNPs as an effective antibacterial and antibiofilm agent. FIC_i of CAAgNPs in combination with antibiotics obtained using MBICs indicated their synergistic effect on biofilm forms of *P. aeruginosa* PAW1.

The use of AgNPs as antibiofilm coatings in surgical implants, antimicrobial agents in topical applications, or as formulations in wound dressings has shown promising results in animal models (Mulani et al., 2019). However, there is a thin line in between the *in vitro* studies being performed and execution of these findings into the clinical trials. There is a noteworthy advancement where AgNPs were incorporated in topical gel for antimicrobial activity in a phase I trial (Clinical Trial Registration: NCT03752424). More such agents should be clinically tested in terms of their efficacy and safety to be made commercially available in the market. Therefore, before employing AgNPs in medicine, their biocompatibility becomes a crucial factor (Qing et al., 2018). Low toxicity of AgNPs derived using *Lysiloma acapulcensis* towards human peripheral blood lymphocytes has been documented (Garibo et al., 2020). In an earlier report, the effect of AgNPs on PBMCs was tested considering the possibility that AgNPs may penetrate the skin and enter the bloodstream. AgNPs were found to be nontoxic towards PBMCs (Banasiuk et al., 2016). In our earlier study,

CAAgNPs were tested for their toxic effects on PBMC's (Nadhe et al., 2020) and showed IC₅₀ > 200 µg/ml which is much higher than the MICs against MDR pathogens reported in the present study. These findings suggests that CAAgNPs have the potential to be used for therapeutic applications against MDR pathogens as they exhibit low toxic effects on PBMCs. *In vivo* safety and efficacy studies of CAAgNPs concerning mice models becomes imperative before the execution of CAAgNPs for further biomedical applications. Forthcoming studies focusing on mechanistic action of CAAgNPs such as inhibition of efflux pump activity, membrane permeabilization and change in membrane potential of bacterial cells needs to be investigated.

5 Conclusion

Overall, CAAgNPs are promising candidates to be used as antibacterial as well as antibiofilm agents against MDR pathogens (singly or in combination with antibiotics). Combination studies revealed that the required concentrations of antibiotics and CAAgNPs can be further lowered, thereby, reducing the toxic effects caused, if any. The low toxicity of CAAgNPs observed against PBMCs suggests their potential use in biomedical applications. We recommend possible uses of CAAgNPs in the preparation of wound dressings, gels or ointments, and coating of medical devices, catheters, and dental and orthopedic implants.

Data availability statement

The original contributions presented in the study are included in the article, further inquiries can be directed to the corresponding author.

Author contributions

MST: conceptualization, methodology, formal analysis and investigation, writing—original draft preparation; AS: methodology; SKS: writing—review and editing; KA: writing—review and editing; SG: writing—review and editing; KP: conceptualization, writing—review and editing, funding acquisition, resources, supervision.

Funding

The work was supported by financial grant received under the UPE-Phase II program (UGC-262-A-2) and Rashtriya Uchchatar Shiksha Abhiyan (RUSA-CBS-TH-3.2).

Acknowledgments

MST acknowledges SARTHI for providing Chief Minister Special Research Fellowship (CMSRF). SG acknowledges the Department of Science and Technology (DST), Ministry of Science and Technology, Government of India and Jawaharlal Nehru Centre for Advanced Scientific Research, India for funding under Post-doctoral Overseas Fellowship in Nano Science and Technology (Ref. JNC/AO/A.0610.1(4) 2019–2260 dated August 19, 2019). The authors acknowledge the support received from Department of Physics, SPPU, for TEM, XRD, and FTIR analysis; Central Instrumentation Facility, SPPU, for FESEM, and EDS analysis and Institute of Bioinformatics and Biotechnology, SPPU, for DLS analysis.

References

- Akhtar, M. S., Panwar, J., and Yun, Y. S. (2013). Biogenic synthesis of metallic nanoparticles by plant extracts. *ACS Sustain. Chem. Eng.* 1, 591–602. doi:10.1021/SC300118U
- Altinsoy, B. D., Şeker Karatoprak, G., and Ocsoy, I. (2019). Extracellular directed ag NPs formation and investigation of their antimicrobial and cytotoxic properties. *Saudi Pharm. J.* 27, 9–16. doi:10.1016/j.jpsps.2018.07.013
- Ansar, S., Tabassum, H., Aladwan, N. S. M., Naiman Ali, M., Almaarik, B., AlMahrouqi, S., et al. (2020). Eco friendly silver nanoparticles synthesis by *Brassica oleracea* and its antibacterial, anticancer and antioxidant properties. *Sci. Rep.* 10, 18564–18612. doi:10.1038/s41598-020-74371-8
- Arya, G., Kumari, R. M., Sharma, N., Gupta, N., Kumar, A., Chatterjee, S., et al. (2019). Catalytic, antibacterial and antibiofilm efficacy of biosynthesised silver nanoparticles using *Prosopis juliflora* leaf extract along with their wound healing potential. *J. Photochem. Photobiol. B Biol.* 190, 50–58. doi:10.1016/j.jphotobiol.2018.11.005
- Banasik, R., Frackowiak, J. E., Krychowiak, M., Matuszewska, M., Kawiak, A., Ziabka, M., et al. (2016). Synthesis of antimicrobial silver nanoparticles through a photomediated reaction in an aqueous environment. *Int. J. Nanomedicine* 11, 315–324. doi:10.2147/IJN.S93611
- Barabadi, H., Mojab, F., Vahidi, H., Marashi, B., Talank, N., Hosseini, O., et al. (2021). Green synthesis, characterization, antibacterial and biofilm inhibitory activity of silver nanoparticles compared to commercial silver nanoparticles. *Inorg. Chem. Commun.* 129, 108647. doi:10.1016/j.inoc.2021.108647
- Berenbaum, M. C. (1978). A method for testing for synergy with any number of agents. *J. Infect. Dis.* 137, 122–130. doi:10.1093/infdis/137.2.122
- Cheon, J. Y., Kim, S. J., Rhee, Y. H., Kwon, O. H., and Park, W. H. (2019). Shape-dependent antimicrobial activities of silver nanoparticles. *Int. J. Nanomedicine* 14, 2773–2780. doi:10.2147/IJN.S196472
- Dakal, T. C., Kumar, A., Majumdar, R. S., and Yadav, V. (2016). Mechanistic basis of antimicrobial actions of silver nanoparticles. *Front. Microbiol.* 7, 1831. doi:10.3389/fmicb.2016.01831
- Duran, N., Duran, M., de Jesus, M. B., Seabra, A. B., Favaro, W. J., and Nakazato, G. (2016). Silver nanoparticles: A new view on mechanistic aspects on antimicrobial activity. *Nanomedicine Nanotechnol. Biol. Med.* 12, 789–799. doi:10.1016/j.nano.2015.11.016
- Fahimirad, S., Ajalloueian, F., and Ghorbanpour, M. (2019). Synthesis and therapeutic potential of silver nanomaterials derived from plant extracts. *Ecotoxicol. Environ. Saf.* 168, 260–278. doi:10.1016/j.ecoenv.2018.10.017
- Feng, Q. L., Wu, J., Chen, G. Q., Cui, F. Z., Kim, T. N., and Kim, J. O. (2000). A mechanistic study of the antibacterial effect of silver ions on *Escherichia coli* and *Staphylococcus aureus*. *J. Biomed. Mat. Res.* 52, 662–668. doi:10.1002/1097-4636(20001215)52:4<662::AID-JBM10>3.0.CO;2-3
- Gafur, A., Sukamdani, G. Y., Kristi, N., Maruf, A., Xu, J., Chen, X., et al. (2020). From bulk to nano-delivery of essential phytochemicals: Recent progress and strategies for antibacterial resistance. *J. Mat. Chem. B* 8, 9825–9835. doi:10.1039/D0TB01671C
- Gaidhani, S. V., Raskar, A. V., Poddar, S., Gosavi, S., Sahu, P. K., Pardesi, K. R., et al. (2014). Time dependent enhanced resistance against antibiotics & metal salts by planktonic & biofilm form of *Acinetobacter haemolyticus* MMC 8 clinical isolate. *Indian J. Med. Res.* 140, 665–671. Available: /pmc/articles/PMC4311322/?report = abstract
- Garibo, D., Borbon-Nunez, H. A., de Leon, J. N. D., Garcia Mendoza, E., Estrada, I., Toledano-Magana, Y., et al. (2020). Green synthesis of silver nanoparticles using *Lysiloma acapulcensis* exhibit high-antimicrobial activity. *Sci. Rep.* 10, 12805–12811. doi:10.1038/s41598-020-69606-7
- Ghosh, S., Patil, S., Ahire, M., Kitture, R., Kale, S., Pardesi, K., et al. (2012). Synthesis of silver nanoparticles using *Dioscorea bulbifera* tuber extract and evaluation of its synergistic potential in combination with antimicrobial agents. *Int. J. Nanomedicine* 483, 483–496. doi:10.2147/ijn.s24793
- Ghosh, S., Bloch, K., and Webster, T. J. (2021). Functionalized biogenic nanoparticles and their applications. *Nanobiotechnology* 2021, 303–322. doi:10.1016/B978-0-12-822878-4.00019-5
- Habash, M. B., Goodyear, M. C., Park, A. J., Surette, M. D., Vis, E. C., Harris, R. J., et al. (2017). Potentiation of tobramycin by silver nanoparticles against *Pseudomonas aeruginosa* biofilms. *Antimicrob. Agents Chemother.* 61, e00415–e00417. doi:10.1128/AAC.00415-17
- Habash, M. B., Park, A. J., Vis, E. C., Harris, R. J., and Khursigara, C. M. (2014). Synergy of silver nanoparticles and aztreonam against *Pseudomonas aeruginosa* PAO1 Biofilms. *Antimicrob. Agents Chemother.* 58, 5818–5830. doi:10.1128/AAC.03170-14
- Javed, B., Ikram, M., Farooq, F., Sultana, T., Mashwani, Z.-U.-R., Naveed, I. R., et al. (2021). Biogenesis of silver nanoparticles to treat cancer, diabetes, and microbial infections: A mechanistic overview. *Appl. Microbiol. Biotechnol.* 105, 2261–2275. doi:10.1007/s00253-021-11171-8
- Kamble, E., and Pardesi, K. (2020). Antibiotic tolerance in biofilm and stationary-phase planktonic cells of *Staphylococcus aureus*. *Microb. Drug Resist.* 00, 3–12. doi:10.1089/mdr.2019.0425
- Kitture, R., Ghosh, S., Kulkarni, P., Liu, X. L., Maity, D., Patil, S. I., et al. (2012). Fe 3O 4-citrate-curcumin: Promising conjugates for superoxide scavenging, tumor suppression and cancer hyperthermia. *J. Appl. Phys.* 111, 064702. doi:10.1063/1.3696001
- Koo, H., Allan, R. N., Howlin, R. P., Stoodley, P., and Hall-Stoodley, L. (2017). Targeting microbial biofilms: Current and prospective therapeutic strategies. *Nat. Rev. Microbiol.* 15, 740–755. doi:10.1038/nrmicro.2017.99
- Macovei, I., Luca, S. V., Skalicka-Wozniak, K., Sacarescu, L., Pascariu, P., Ghilan, A., et al. (2022). Phyto-functionalized silver nanoparticles derived from conifer bark extracts and evaluation of their antimicrobial and cytogenotoxic effects. *Molecules* 27, 217. doi:10.3390/MOLECULES27010217
- Majoumou, M. S., Sibuyi, N. R. S., Tincho, M. B., Mbekou, M., Boyom, F. F., and Meyer, M. (2019). Enhanced anti-bacterial activity of biogenic silver nanoparticles synthesized from *Terminalia mantaly* extracts. *Int. J. Nanomedicine* 14, 9031–9046. doi:10.2147/IJN.S223447

Conflict of interest

The authors declare that the research was conducted in the absence of any commercial or financial relationships that could be construed as a potential conflict of interest.

Publisher's note

All claims expressed in this article are solely those of the authors and do not necessarily represent those of their affiliated organizations, or those of the publisher, the editors and the reviewers. Any product that may be evaluated in this article, or claim that may be made by its manufacturer, is not guaranteed or endorsed by the publisher.

- Manosalva, N., Tortella, G., Cristina Diez, M., Schalchli, H., Seabra, A. B., Durán, N., et al. (2019). Green synthesis of silver nanoparticles: Effect of synthesis reaction parameters on antimicrobial activity. *World J. Microbiol. Biotechnol.* 35, 88. doi:10.1007/s11274-019-2664-3
- Mohanta, Y. K., Biswas, K., Jena, S. K., Hashem, A., AbdAllah, E. F., and Mohanta, T. K. (2020). Anti-biofilm and antibacterial activities of silver nanoparticles synthesized by the reducing activity of phytoconstituents present in the Indian medicinal plants. *Front. Microbiol.* 11, 1143. doi:10.3389/fmicb.2020.01143
- Mostafavi, E., Zarepour, A., Barabadi, H., Zarrabi, A., Truong, L. B., and Medina-Cruz, D. (2022). Antineoplastic activity of biogenic silver and gold nanoparticles to combat leukemia: Beginning a new era in cancer theragnostic. *Biotechnol. Rep. (Amst)*. 34, e00714. doi:10.1016/J.BTRE.2022.E00714
- Mulani, M. S., Kamble, E. E., Kumkar, S. N., Tawre, M. S., and Pardesi, K. R. (2019). Emerging strategies to combat ESKAPE pathogens in the era of antimicrobial resistance: A review. *Front. Microbiol.* 10, 539. doi:10.3389/fmicb.2019.00539
- Muniyappan, N., Pandeewaran, M., and Amalraj, A. (2021). Green synthesis of gold nanoparticles using *Curcuma pseudomontana* isolated curcumin: Its characterization, antimicrobial, antioxidant and anti-inflammatory activities. *Environ. Chem. Ecotoxicol.* 3, 117–124. doi:10.1016/J.ENCECO.2021.01.002
- Nadhe, S. B., Tawre, M. S., Agrawal, S., Chopade, B. A., Sarkar, D., and Pardesi, K. (2020). Anticancer potential of AgNPs synthesized using *Acinetobacter* sp. and *Curcuma aromatica* against HeLa cell lines: A comparative study. *J. Trace Elem. Med. Biol.* 62, 126630. doi:10.1016/J.JTEMB.2020.126630
- Onitsuka, S., Hamada, T., and Okamura, H. (2019). Preparation of antimicrobial gold and silver nanoparticles from tea leaf extracts. *Colloids and Surfaces B: Biointerfaces* 173, 242–248. doi:10.1016/j.colsurfb.2018.09.055
- Pal, S., Tak, Y. K., and Song, J. M. (2007). Does the antibacterial activity of silver nanoparticles depend on the shape of the nanoparticle? A study of the Gram-negative bacterium *Escherichia coli*. *Appl. Environ. Microbiol.* 73, 1712–1720. doi:10.1128/AEM.02218-06
- Panacek, A., Kvitek, L., Smekalova, M., Vecerova, R., Kolar, M., Roderova, M., et al. (2018). Bacterial resistance to silver nanoparticles and how to overcome it. *Nat. Nanotechnol.* 13, 65–71. doi:10.1038/s41565-017-0013-y
- Panacek, A., Smekalova, M., Kilianova, M., Prucek, R., Bogdanova, K., Vecerova, R., et al. (2015). Strong and nonspecific synergistic antibacterial efficiency of antibiotics combined with silver nanoparticles at very low concentrations showing no cytotoxic effect. *Molecules* 21, 26. doi:10.3390/molecules21010026
- Pardesi, K. R., Pable, A. A., Bhagat, D. D., and Satpute, S. K. (2019). “Applications of metal nanoparticles to combat biofilm forming ESKAPE pathogens,” in *Recent advances in Biotechnology* (Nova Science Publisher).
- Parit, S. B., Karade, V. C., Patil, R. B., Pawar, N. V., Dhavale, R. P., Tawre, M., et al. (2020). Bioinspired synthesis of multifunctional silver nanoparticles for enhanced antimicrobial and catalytic applications with tailored SPR properties. *Mat. Today Chem.* 17, 100285. doi:10.1016/J.MTCHEM.2020.100285
- Pintatam, A., Maneerat, W., Logie, E., Tuenter, E., Sakavitsi, M. E., Pieters, L., et al. (2020). *In vitro* anti-inflammatory, anti-oxidant, and cytotoxic activities of four *Curcuma* species and the isolation of compounds from *Curcuma aromatica* rhizome. *Biomolecules* 10, 799. doi:10.3390/Biom10050799
- Qing, Y., Cheng, L., Li, R., Liu, G., Zhang, Y., Tang, X., et al. (2018). Potential antibacterial mechanism of silver nanoparticles and the optimization of orthopedic implants by advanced modification technologies. *Int. J. Nanomedicine* 13, 3311–3327. doi:10.2147/IJN.S165125
- Rai, M., Yadav, A., and Gade, A. (2009). Silver nanoparticles as a new generation of antimicrobials. *Biotechnol. Adv.* 27, 76–83. doi:10.1016/j.biotechadv.2008.09.002
- Rashid, S., Azeem, M., Khan, S. A., Shah, M. M., and Ahmad, R. (2019). Characterization and synergistic antibacterial potential of green synthesized silver nanoparticles using aqueous root extracts of important medicinal plants of Pakistan. *Colloids and Surfaces B: Biointerfaces* 179, 317–325. doi:10.1016/j.colsurfb.2019.04.016
- Revathi, S., and Malathy, N. S. (2013). Antibacterial activity of rhizome of *Curcuma aromatica* and partial purification of active compounds. *Indian J. Pharm. Sci.* 75, 732–735.
- Salman, M., Rizwana, R., Khan, H., Munir, I., Hamayun, M., Iqbal, A., et al. (2019). Synergistic effect of silver nanoparticles and polymyxin B against biofilm produced by *Pseudomonas aeruginosa* isolates of pus samples *in vitro*. *Artif. Cells Nanomed. Biotechnol.* 47, 2465–2472. doi:10.1080/21691401.2019.1626864
- Shah, S., Gaikwad, S., Nagar, S., Kulshrestha, S., Vaidya, V., Nawani, N., et al. (2019). Biofilm inhibition and anti-quorum sensing activity of phytosynthesized silver nanoparticles against the nosocomial pathogen *Pseudomonas aeruginosa*. *Biofouling* 35, 34–49. doi:10.1080/08927014.2018.1563686
- Shivalingu, B. R., Vivek, H. K., Priya, B. S., Soujanya, K. N., and Nanjunda Swamy, S. (2016). Purification and characterization of novel fibrin(ogen)olytic protease from *Curcuma aromatica* Salisb. Role in hemostasis. *Phytomedicine* 23, 1691–1698. doi:10.1016/j.phymed.2016.09.007
- Siddiqi, K. S., Husen, A., and Rao, R. A. K. (2018). A review on biosynthesis of silver nanoparticles and their biocidal properties. *J. Nanobiotechnology* 16, 14–28. doi:10.1186/s12951-018-0334-5
- Singh, B. P., Ghosh, S., and Chauhan, A. (2021). Development, dynamics and control of antimicrobial-resistant bacterial biofilms: A review. *Environ. Chem. Lett.* 19, 1983–1993. doi:10.1007/s10311-020-01169-5
- Singh, N., Paknikar, K. M., and Rajwade, J. (2019a). RNA-sequencing reveals a multitude of effects of silver nanoparticles on *Pseudomonas aeruginosa* biofilms. *Environ. Sci. Nano* 6, 1812–1828. doi:10.1039/C8EN01286E
- Singh, N., Rajwade, J., and Paknikar, K. M. (2019b). Transcriptome analysis of silver nanoparticles treated *Staphylococcus aureus* reveals potential targets for biofilm inhibition. *Colloids and Surfaces B: Biointerfaces* 175, 487–497. doi:10.1016/J.COLSURFB.2018.12.032
- Singh, P., Pandit, S., Beshay, M., Mokkapat, V. R. S. S., Garnaes, J., Olsson, M. E., et al. (2018a). Anti-biofilm effects of gold and silver nanoparticles synthesized by the *Rhodiola rosea* rhizome extracts. *Artif. Cells Nanomed. Biotechnol.* 46, S886–S899. doi:10.1080/21691401.2018.1518909
- Singh, P., Pandit, S., Garnaes, J., Tunjic, S., Mokkapat, V. R. S. S., Sultan, A., et al. (2018b). Green synthesis of gold and silver nanoparticles from *Cannabis sativa* (Industrial hemp) and their capacity for biofilm inhibition. *Int. J. Nanomedicine* 13, 3571–3591. doi:10.2147/IJN.S157958
- Swilam, N., and Nematallah, K. A. (2020). Polyphenols profile of pomegranate leaves and their role in green synthesis of silver nanoparticles. *Sci. Rep.* 10, 14851–14911. doi:10.1038/s41598-020-71847-5
- Talank, N., Morad, H., Barabadi, H., Mojab, F., Amidi, S., Kobarfard, F., et al. (2022). Bioengineering of green-synthesized silver nanoparticles: *In vitro* physicochemical, antibacterial, biofilm inhibitory, anticoagulant, and antioxidant performance. *Talanta* 243, 123374. doi:10.1016/J.TALANTA.2022.123374
- Tallarida, R. J. (2016). Drug combinations: Tests and analysis with isoboles. *Curr. Protoc. Pharmacol.* 72, 9191. doi:10.1002/0471141755.PH0919S72
- Tawre, M. S., Kamble, E. E., Kumkar, S. N., Mulani, M. S., and Pardesi, K. R. (2021). Antibiofilm and antipersister activity of acetic acid against extensively drug resistant *Pseudomonas aeruginosa* PAW1. *PLoS One* 16, e0246020. doi:10.1371/JOURNAL.PONE.0246020
- Thomas, R., Snigdha, S., Bhavitha, K. B., Babu, S., Ajith, A., and Radhakrishnan, E. K. (2018). Biofabricated silver nanoparticles incorporated polymethyl methacrylate as a dental adhesive material with antibacterial and antibiofilm activity against *Streptococcus mutans*. *3 Biotech* 38, 404. doi:10.1007/s13205-018-1420-y
- Tripathi, N., and Goshisht, M. K. (2022). Recent advances and mechanistic insights into antibacterial activity, antibiofilm activity, and cytotoxicity of silver nanoparticles. *ACS Appl. bio Mat.* 5, 1391–1463. doi:10.1021/ACSABM.2C00014
- Umar, N. M., Parumasivam, T., Aminu, N., and Toh, S.-M. (2020). Phytochemical and pharmacological properties of *Curcuma aromatica* Salisb (wild turmeric). *J. Appl. Pharm. Sci.* 10, 180–194. doi:10.7324/JAPS.2020.1010018
- Vazquez-Munoz, R., Meza-Villezas, A., Fournier, P. G. J., Soria-Castro, E., Juarez-Moreno, K., Gallego-Hernandez, A. L., et al. (2019). Enhancement of antibiotics antimicrobial activity due to the silver nanoparticles impact on the cell membrane. *PLoS One* 14, e0224904. doi:10.1371/JOURNAL.PONE.0224904
- Woo, K. J., Hye, C. K., Ki, W. K., Shin, S., So, H. K., and Yong, H. P. (2008). Antibacterial activity and mechanism of action of the silver ion in *Staphylococcus aureus* and *Escherichia coli*. *Appl. Environ. Microbiol.* 74, 2171–2178. doi:10.1128/AEM.02001-07



OPEN ACCESS

EDITED BY

Sougata Ghosh,
RK University, India

REVIEWED BY

Ravindra Pratap Singh,
Indira Gandhi National Tribal University,
India
Anuja Shreeram Kulkarni,
The Ohio State University, United States

*CORRESPONDENCE

Karen Pillay,
✉ muthusamy@ukzn.ac.za

SPECIALTY SECTION

This article was submitted to
Nanoscience,
a section of the journal
Frontiers in Chemistry

RECEIVED 25 November 2022

ACCEPTED 22 February 2023

PUBLISHED 07 March 2023

CITATION

Ngcongco K, Krishna SBN and Pillay K
(2023), Biogenic metallic nanoparticles as
enzyme mimicking agents.
Front. Chem. 11:1107619.
doi: 10.3389/fchem.2023.1107619

COPYRIGHT

© 2023 Ngcongco, Krishna and Pillay.
This is an open-access article distributed
under the terms of the [Creative
Commons Attribution License \(CC BY\)](#).
The use, distribution or reproduction in
other forums is permitted, provided the
original author(s) and the copyright
owner(s) are credited and that the original
publication in this journal is cited, in
accordance with accepted academic
practice. No use, distribution or
reproduction is permitted which does not
comply with these terms.

Biogenic metallic nanoparticles as enzyme mimicking agents

Khanyisile Ngcongco¹, Suresh Babu Naidu Krishna² and
Karen Pillay^{1*}

¹School of Life Sciences, University of KwaZulu-Natal, Durban, South Africa, ²Department of Biomedical and Clinical Technology, Durban University of Technology, Durban, South Africa

The use of biological systems such as plants, bacteria, and fungi for the synthesis of nanomaterials has emerged to fill the gap in the development of sustainable methods that are non-toxic, pollution-free, environmentally friendly, and economical for synthesizing nanomaterials with potential in biomedicine, biotechnology, environmental science, and engineering. Current research focuses on understanding the characteristics of biogenic nanoparticles as these will form the basis for the biosynthesis of nanoparticles with multiple functions due to the physicochemical properties they possess. This review briefly describes the intrinsic enzymatic mimetic activity of biogenic metallic nanoparticles, the cytotoxic effects of nanoparticles due to their physicochemical properties and the use of capping agents, molecules acting as reducing and stability agents and which aid to alleviate toxicity. The review also summarizes recent green synthetic strategies for metallic nanoparticles.

KEYWORDS

biogenic metallic nanoparticles, nanozymes, capping agents, toxicity, green synthesis

1 Introduction

Recent advances in nanotechnology have allowed researchers to develop devices with promising potential for use in a wide variety of applications in biomedicine, biotechnology, environmental science, and engineering (Bundschuh et al., 2018; Dan, 2020). Nanoparticles are the basic fundamental component in nanotechnology with sizes that range from 1 to 100 nm (Alavi and Karimi, 2018; Khan et al., 2019; Speranza, 2021). These structures offer major advantages due to their unique physicochemical properties such as their small sizes and diverse morphologies, large surface area to volume ratio, and in the case of metallic nanoparticles, their magnetization (Bundschuh et al., 2018). These physicochemical properties can be exploited for a broad spectrum of applications and present possible solutions to emerging global issues such as antimicrobial resistance, environmental pollution, and energy and food production (Ealias and Saravanakumar, 2017).

There is thus a need for more sustainable methods of synthesizing nanoparticles that are non-toxic, pollution free and more environmentally friendly when compared to the conventional chemical and physical methods for nanoparticle synthesis (Alavi and Karimi, 2018; Huynh et al., 2020; Bahrulolum et al., 2021; Ying et al., 2022). Recent studies focused on the use of biological organisms including plants, bacteria, yeast, fungi, lichens or algae to synthesize nanoparticles; in a method referred to as biological synthesis (Patil and Chandrasekaran, 2020; Nguyen et al., 2021; Ying et al., 2022). Proteins, enzymes, phenolic compounds, amines, alkaloids and pigments are some of the molecules in plants and microorganisms that can synthesize nanoparticles due to their reduction capability (Nadaroglu et al., 2017). The chemical and physical methods of synthesizing nanoparticles

involve the use of reducing agents and stabilizing agents for the reduction of metal ions and to prevent agglomeration of the nanoparticles, however, these agents tend to be toxic to the environment and significantly contributes to nanoparticle toxicity which is highly unfavourable especially in the biomedical field (de Lima et al., 2012; Qu et al., 2019; Huynh et al., 2020; Nayak et al., 2021). In biological synthetic methods, biological organisms can produce biomolecules that act as reducing and stabilizing agents (Bahrulolum et al., 2021). These agents are not harmful to the environment, and maintain the stability of the synthesized nanoparticles thereby rendering them non-toxic (Nadaroglu et al., 2017).

Earlier reviews have highlighted the nanozyme activity of various types of nanoparticles (Ragg et al., 2015; Wu et al., 2019; Wang et al., 2020b; Ge et al., 2022). Some excellent review articles have also highlighted the biogenic strategies of metallic nanoparticles and advances in their role for biomedical application (Singh et al., 2021a; Nayak et al., 2021; Srivastava et al., 2021; Nayak et al., 2022). This mini review is different in that it provides an up to date overview of various biogenic strategies for metallic nanoparticle production, the role of biogenic synthesis as capping agents and up to date use of biogenic metallic nanoparticles as nanozymes.

2 Biogenic metallic nanoparticles

Many different biological organisms have been found to have an ability to synthesize a variety of metallic nanoparticles, with the most recent (2018–2022) studies presented in Supplementary Table S1 in the Supplementary Information. Although Supplementary Table S1 covers plants, bacteria, fungi and lichen as systems that can be used for metallic nanoparticle production, it should be noted that Bryophytes also have an inherent ability to produce metallic nanoparticles. To the best of our knowledge, bryophytes have not been used to produce metallic nanoparticles from 2018, and thus a review by Srivastava et al. (2021) gives a good overview of the bryophytes used for metallic nanoparticle production (Srivastava et al., 2021).

Plants are promising candidates for nanoparticle synthesis because they detox and reduce the accumulation of metals as they alter the chemical composition of metals making them non-toxic and thus producing nanoparticles as a by-product (Nadaroglu et al., 2017; Zhang et al., 2020). Plant extracts such as sugars, flavonoids, saponin, proteins, enzymes, tannins, phenolics, alkaloids, steroids, and organic acids, can be obtained from plant parts, such as leaves, stems, roots, fruit, bark, flowers, seeds and buds (Moodley et al., 2018; Yulizar et al., 2020). The extracts act as reducing agents which result in the production of nanoparticles. Recently, plant extracts from *Citrus sinensis*, *Lawsonia inermis*, *Artemisia haussknechtii*, *Cochlospermum gossypium* and *Juglans regia* have been reported for their use in nanoparticle synthesis (Alavi and Karimi, 2018; Kredy, 2018; Srivastava et al., 2019).

Bacteria are also target candidates in nanoparticle production because of their rapid growth, cost-effectiveness, easy culturing, and since their growth conditions and environment can be easily controlled and manipulated (Nadaroglu et al., 2017). The

emergence of resistance mechanisms in bacteria as a means of overcoming the harmful effects of metals also contributes to their ability to biosynthesize metallic nanoparticles. These mechanisms include transitions in the redox state, the operation of efflux systems, the buildup of metals inside the cell, intracellular precipitation, and extracellular creation of complexes (Figure 1A) (Moodley et al., 2021). These nanoparticles were believed to be formed through a method involving the NADH-dependent reductase enzyme, which goes through oxidation to create NAD^+ and potentially, the lost free electron could turn Ag^+ into AgNPs (Gurunathan et al., 2009; Sintubin et al., 2009).

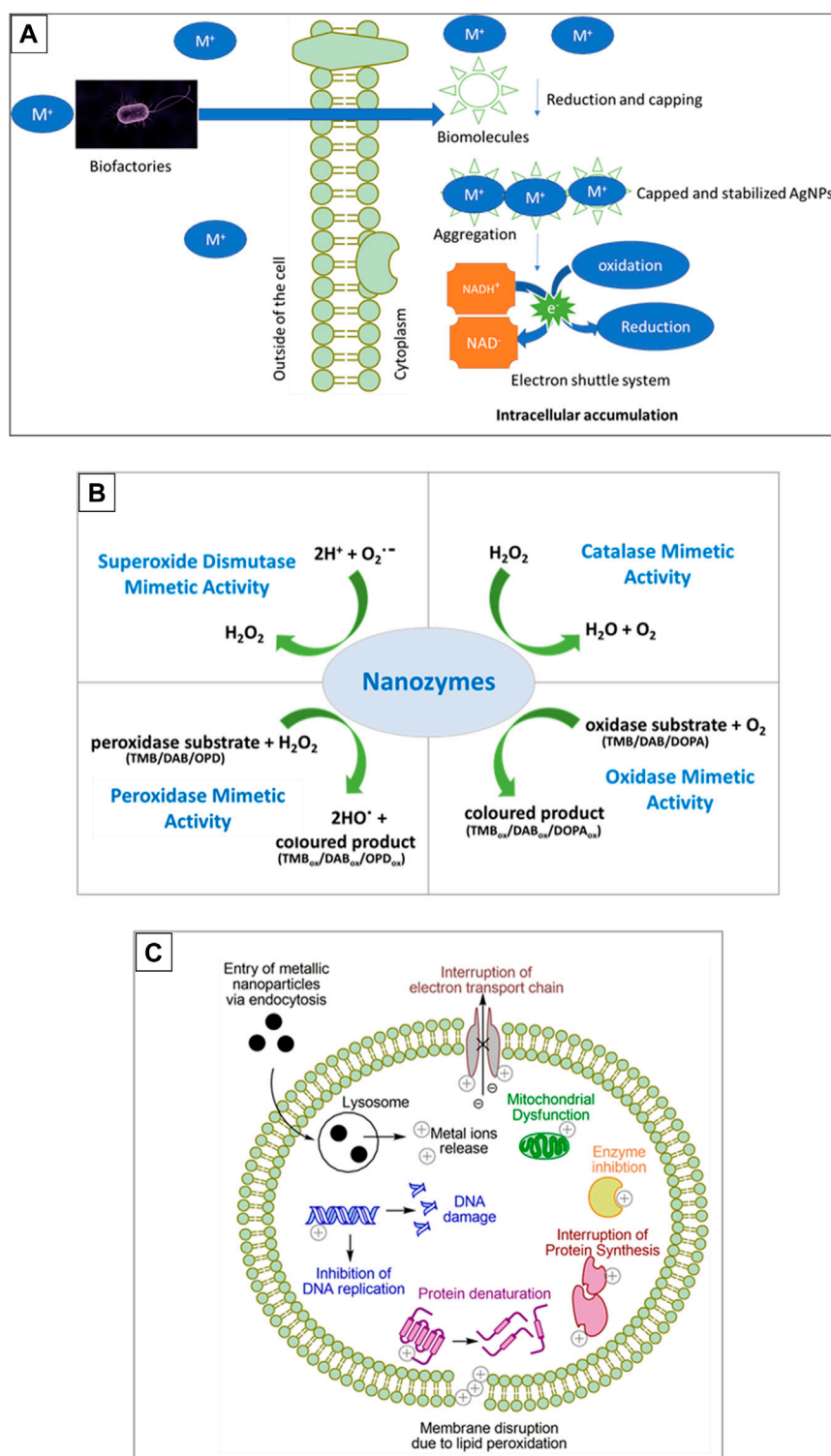
Bacteria have the ability to convert heavy metal ions into nanoparticles by reducing them (Capuzzo, 2021). These advantages can therefore be exploited for nanoparticle synthesis. Bacteria including *Pseudomonas stutzeri*, *Desulfovibrio alaskensis*, *Morganella psychrotolerans* and *Lactobacillus casei* were recently reported to synthesize a variety of nanoparticles (Xu et al., 2018; Capeness et al., 2019).

Fungi are also ideal candidates for nanoparticle synthesis as their growth is easy and cost effective for laboratories and also at the industrial scale (Molnár et al., 2018). These organisms secrete a large number of enzymes and they have a large surface area due to their mycelia which play a vital role in rapidly forming nanoparticles as these characteristics causes metal precursor salts to be quickly converted to metallic nanoparticles (Khandel and Shahi, 2018; Li et al., 2021). Fungi such as *Ganoderma lucidum*, *Lignosus rhinocerotis*, *Trichoderma longibrachiatum*, and *Penicillium corylophilum* were recently used for the synthesis of metallic nanoparticles (Elamawi et al., 2018; Katas et al., 2019; Fouda et al., 2020; Nguyen et al., 2021).

3 The intrinsic enzyme mimetic activity of biogenic metallic nanoparticles

Nanoparticles are known to be multifunctional and among the functions that they possess is the ability to catalyse reactions. Initially, the catalytic activity of nanoparticles was a result of the conjugation of catalysts or enzymes to the shell of the nanoparticles and therefore the nanoparticles would provide magnetic properties while the catalyst or enzyme on the surface of the nanoparticles provided the catalytic activity (Gao et al., 2007). This drew the interest of researchers to other possible intrinsic enzyme-like activities that nanoparticles may possess.

Nanoparticles exhibiting enzyme-like catalytic activities, referred to as nanozymes, act as mimic enzymes that can replace natural enzymes because natural enzymes have disadvantages in their catalytic functions due to the high cost of production, the time consuming process for production, denaturation in harsh environmental conditions and therefore must have suitable pH and temperature, and specific substrates (Ragg et al., 2015; Ahmed et al., 2019; Singh, 2019; Rastogi et al., 2021). Since nanozymes are easy to produce with low cost, have high stability, and good robustness; they are suitable candidates for applications requiring catalytic functions and were found to possess enzymatic activity identical to that of peroxidase, haloperoxidase, oxidase, catalase, hydrolase, and superoxide dismutase as summarized in Figure 1B (Ragg et al., 2015;

**FIGURE 1**

Synthesis, enzyme function and toxicity of metallic nanoparticles. (A) Is a schematic representation of biosynthesis of metal nanoparticles by microorganisms, (B) depicts the enzyme mimetic activity of biogenic nanoparticles and (C) shows the mechanisms of nanoparticle toxicity. Substrates used are 3, 3', 5, 5'-Tetramethylbenzidine (TMB), 3, 3'-Diaminobenzidine (DAB), o-phenylenediamine (OPD), or 3,4-dihydroxyphenylalanine (DOPA).

Ahmed et al., 2019). To date, there are more than 300 types of nanomaterials that have been found to possess the intrinsic enzyme-like activity (Gao and Yan, 2016).

Ferrihydrite nanoparticles synthesized from the bacteria *Comamonas testosteroni* exhibited peroxidase-like activity similar to that of horseradish peroxidase (HRP), and these nanoparticles

were able to catalyze reactions of the peroxidase chromogenic agents 3, 3', 5, 5'-Tetramethylbenzidine (TMB), 3, 3'-Diaminobenzidine (DAB), and o-phenylenediamine (OPD) in the presence of H₂O₂ (Ahmed et al., 2019). This peroxidase-like activity displayed by the bacteria was exploited to develop a colorimetric method for the detection of H₂O₂ and glucose which was used for successfully detecting glucose in human serum (Ahmed et al., 2019). Magnetic nanoparticles referred to as magnetosomes, synthesized from *Magnetospirillum gryphiswaldense* (magnetotactic bacteria) also exhibit intrinsic peroxidase-like activity indicated by their ability to catalyze TMB *in vitro* in the presence of H₂O₂ (Guo et al., 2012). The peroxidase-like activity of magnetosomes plays a role in reducing enhanced intracellular reactive oxygen species (ROS) levels generated under conditions having low oxygen and high iron concentration (Guo et al., 2012; Lin et al., 2019). ROS are very reactive chemical molecules containing oxygen, generated in cell organelles including the endoplasmic reticulum (ER), peroxisomes and the mitochondria (Yu et al., 2020b). This ROS elimination role is thought to be significant for the survival of magnetotactic bacteria growing under similar conditions (Guo et al., 2012; Lin et al., 2019). The peroxidase mimetic activity of magnetosomes has been used for the detection of H₂O₂ and glucose (Hu et al., 2010).

Plant extracts contain products that comprise functional groups including phenolic acids, proteins, polyphenol, bioactive alkaloids, terpenoids and sugars, which reduce metal ions in the synthetic mechanism for nanoparticles (Das et al., 2022a). These functional groups can stabilize the synthesized nanoparticles and improve their catalytic efficiency (Das et al., 2022a). Palladium nanoparticles synthesized using gum kondagogu, a tree gum from *C. gossypium*, were used for developing a colorimetric assay for quantifying cholesterol from human serum based on the peroxidase-like activity exhibited by the synthesized nanoparticles (Rastogi et al., 2021). This study showed the potential application of the intrinsic peroxidase mimicking properties of the palladium nanoparticles for diagnostic, detection and quantification purposes (Rastogi et al., 2021).

Prunus nepalensis fruit extract was used for synthesizing gold nanoparticles exhibiting peroxidase-like catalytic activity (Das et al., 2022a). The catalytic activity of the gold nanoparticles was confirmed by the ability to catalyze the oxidation of the substrate TMB in the presence of H₂O₂ (Das et al., 2022a). It was found that the gold nanoparticles exhibited a higher maximum reaction velocity and affinity for TMB compared to natural horse radish peroxidase (Das et al., 2022a). The improved catalytic efficiency of the gold nanoparticles is said to have been a result of the functional groups present in the fruit extract (Das et al., 2022a). This peroxidase-like activity of the gold nanoparticles was exploited for a potential colorimetric immuno-sensing assay for the detection of *Mycobacterium bovis*, a bovine tuberculosis transmitted from cattle to humans through the "consumption of unpasteurized milk" (Smith et al., 2004; Das et al., 2022a). Silver nanoparticles synthesized from *Cucumis sativus* and *Aloe vera* extracts, with the *A. vera* extract used as a capping agent, catalyzed the reduction of methyl orange dye and *para*-nitrophenol (Riaz et al., 2022). This indicated the potential of these nanoparticles in the degradation of nitro-phenols that are found in industrial waste.

Ferrihydrite nanoparticles from *Trichoderma guizhouense* synthesized during interaction of the fungus with hematite, whereby fungi take up minerals to form nanoparticles, also exhibited peroxidase-like activity (Yu et al., 2020a). Fungi interact with minerals and biomineralize them into nanoparticles, and this interaction is known as fungus-mineral interaction. The interaction is important in the transformation of rocks, minerals and metals, the degradation of rhizospheric organic matter and phosphate fixation. The generation of ROS was observed during fungal growth and therefore, the concentration of these species must be maintained at sub-toxic levels (Yu et al., 2020a). The peroxidase-like activity of the synthesized ferrihydrite nanoparticles reduced the generated ROS, lowering their toxic effects. It was suggested that the production of the nanoparticles caused the ROS generated during fungal growth to decrease, therefore maintaining the concentration of the ROS at sub-toxic levels.

The enzymatic activity of biogenic nanoparticles similar to natural enzymes presents a platform whereby they can be exploited for developing several methods for diagnostic, detection and biosensing applications. To date, there are numerous patent applications and patents that have been granted for nanozyme production and nanozyme systems which highlights the importance of these small molecules. A list of these patents and patent applications are listed in Table 1, together with a summary of various applications of biogenic nanoparticles that have recently been evaluated, highlighting the versatility of these nano molecules.

4 Toxicity of nanoparticles and the role of capping agents

Nanoparticle toxicity presents a challenge, especially in areas such as biomedicine, cosmetics, agriculture and the food science, and thus there is a need for the development of nanoparticles with low cytotoxicity. The main physicochemical properties that determine toxicity of nanoparticles are size, shape, surface chemistry, surface composition, surface area to volume ratio and stability (Aillon et al., 2009; Sukhanova et al., 2018). The primary mechanisms of toxicity of metallic nanoparticles stem from them entering the cell *via* endocytosis, which places them within an acidic lysosome resulting in oxidation and release of metal ions. The intracellular metal ions can then exert a myriad of toxic effects as summarised in Figure 1C (Repetto et al., 2010; Carrillo-Carrion et al., 2014).

Fortunately, encapsulation strategies have recently been on the radar of researchers in a bid to reduce the toxic effects of nanoparticles as it could provide stability to the nanoparticle and reduce its susceptibility to release metal ions.

Capping agents are molecules that play an essential role in the growth, aggregation, and physicochemical properties of nanoparticles by regulating their size, shape, geometry, and surface chemistry (Javed et al., 2022; Sidhu et al., 2022). Capping agents can firmly adsorb on the nanoparticle surface forming a single or multilayer protective coating thus providing long term nanoparticle stability (Javed et al., 2022). Capping agents can consist of proteins, carbohydrates, amino acids, and lipids (Bulgarini et al., 2021) and can prevent aggregation of nanoparticles (Sidhu et al., 2022).

TABLE 1 List of Nanozyme Patent Applications and Summary of Recent Nanoparticle applications.

Invention	Inventors	Application number	Year	Country	References
Nanozymes, methods of making nanozymes, and methods of using nanozymes	Cao, Y.C., Liu, C., Liu, H., Wang, Z., and YangS.H.	WO2011133504-A2	2011	WIPO (PCT)	Cao et al. (2011)
Synthesis method of enzyme-mimic magnetic nanocatalysts, and enzyme-mimic magnetic nanocatalysts thereby	Jang, J., Lee, S., and Lee, J	KR101350722B1	2014	South Korea	Jang et al. (2014)
Nanozymes, methods of making nanozymes, and methods of using nanozymes	Cao, Y.C., and Liu, C	WO2015023715A1	2015	WIPO (PCT)	Cao and Liu (2015)
Nanozymes, methods of making nanozymes, and methods of using nanozymes	Cao, Y.C., and Liu, C	US20160215279A1	2016	United States	Cao and Liu (2016)
Nanoparticle-attached enzyme cascades for accelerated multistep biocatalysis	Medintz, I.L., Vranish, J.N., Ancona, M., Susumu, K., and DiazS.A.	US20180171325A1	2017	United States	Medintz et al. (2017)
Stabilized polymeric nanocapsules, dispersions comprising the nanocapsules, and methods for the treatment of bacterial biofilms	Rotello, V.M., Landis, R.F., Gupta, A., and LeeY.W.	WO2017040024A1	2017	United States	Rotello et al. (2017)
PD-IR nanoparticles used as peroxidase mimics	Xia, X	20,170,199,179	2017	United States	Xia (2017)
Nanozymes, methods of making nanozymes, and methods of using nanozymes	Cao, Y.C., Liu, C., Liu, H., Wang, Z., and YangS.H.	US 10,081,542 B2	2018	United States	Cao et al. (2018)
Ig E detection and allergy diagnostic method using enzyme-mimetic nanozyme-based immunoassay	Lee, S., Lee, S., Kim, M., Shin, S., Lee, J., and Kim, M	WO2018084340A1	2018	WIPO (PCT)	Lee et al. (2018)
Enzyme-encapsulated nanoparticle platform	Ortac, I., Esener, S.C., Yayla, I.G., and Messmer, B	US10300152B2	2019	United States	Ortac et al. (2019)
RNA silencing nanozymes	Cao, Y.C., and Jiang, T	20210139873	2021	United States	Cao and Jiang (2020)

Application	Function	References
Antimicrobial Agents	Activity against bacterial and fungal growth	Dong et al. (2019), Akpinar et al. (2021), Sarwer et al. (2022), Soliman et al. (2022)
Bioremediation	Degradation of heavy metals, pesticides, insecticides, herbicides and dyes from polluted environments	Tripathi et al. (2018), López-Miranda et al. (2019), Chaudhari et al. (2022), Gami et al. (2022), Salama et al. (2022)
Delivery Systems	Delivery of cancer targeting genes and therapeutic drugs	Abolhasani Zadeh et al. (2022)
Enzyme Immobilization	Immobilization of enzymes from reaction mixtures	Fotiadou et al. (2021)
MRI Contrast Agents	Molecular imaging, diagnosis and treatment of diseases	Cai et al. (2019), Nan et al. (2021), Wei et al. (2021)

Capping agents are found in biological organisms, and they can act as reducing and stability agents, an advantage that is noteworthy for biogenic nanoparticles (Guilger-Casagrande et al., 2021), (Javed et al., 2022). In addition, capping agents from biological organisms can be introduced to the chemical synthetic strategies and this has become an essential strategy in lowering the cytotoxic effects of chemically synthesized nanoparticles (Sidhu et al., 2022).

The encapsulation of nanoparticles with capping agents forms a barrier between the inner core of the nanoparticle and the surrounding environment, improving nanoparticle solubility, reactivity, interactions with biomolecules, preventing aggregation and inducing their biological functions (Weingart et al., 2013). A study by Guilger-Casagrande et al. (2021) evaluated the effects and functions of capping agents on the stability of silver nanoparticles synthesized by the fungal strain *Trichoderma harzianum* by comparing the stability of the nanoparticles with and without capping agents. It was found that when capping agents were removed from nanoparticles, the diameter of the nanoparticles

increased and it was proposed that the reason for this may be “subsequent aggregation of the nanoparticles” (Guilger-Casagrande et al., 2021).

Soliman et al. (2022) suggested that extracellular enzymes and proteins from *Trichoderma saturnisporum* acted as capping agents in the synthesis of silver and gold nanoparticles. Puri and Patil (2022) confirmed the presence of phytochemicals by screening *Tinospora cordifolia* extract used for synthesizing selenium nanoparticles. Among the phytochemicals present in the extract were phenolics and flavonoids and the hydroxyl groups of these biomolecules were proposed to act as capping agents (Puri and Patil, 2022). Highly stable, negatively charged, spherically shaped and nano-sized selenium nanoparticles were synthesized from the plant extracts and it was suggested that the stability of the nanoparticles was due to the phytochemicals detected in the extract (Puri and Patil, 2022). Silver nanoparticles synthesized using yeast extract were capped by biomolecules from the extract, and the resulting silver

nanoparticles exhibited shapes, sizes and surface chemistry that exhibited good long-term stability (Shu et al., 2020).

Biogenic nanoparticles thus present a promising potential for a variety of applications with the added advantage of low toxicity due to their inherent capping potential, a feature that is lacking in physicochemical synthetic strategies that are reliant on addition of synthetic capping agents resulting in labor intensive multi-step processes (de Lima et al., 2012).

5 Current scenarios and challenges

The emergence of nanotechnology has seen nanoparticles having widespread application and being the molecule of choice, resulting in them being in high demand. Although there are numerous synthetic strategies for nanoparticle production, the physical and chemical routes pose many challenges such as the need for expensive equipment, capping agents and harmful chemicals, and production of monodisperse nanoparticles with similar morphology is not so straight forward. Green synthetic methods, using inherent biological machinery and phytochemicals as capping and stabilization agents, is therefore seen as the preferred method for nanoparticle production. However, large scale production is still seen as a challenge and researchers are daily evaluating new strategies for scaling up. One of the novel methods that could be explored for large scale production of nanoparticles is investigating the role of soil microbes in influencing plant growth and uptake of nutrients. This could have importance in nanoparticle production as soil microbes could directly affect how metals and nutrients are taken up by plants before being packaged into nanoparticles (Das et al., 2022b).

6 Conclusion and future prospects

The use of biological organisms for synthesizing nanoparticles is increasing as these organisms produce their own reducing and stabilizing agents that are involved in reducing metal ions to nanoparticles and also providing encapsulation. The biogenic nanoparticles thus have the important benefit of reduced toxicity and have immense application in a wide variety of biotechnology and biomedical fields such as drug delivery systems, scanning techniques, cosmetics, and assay systems. There is thus huge potential for exploiting biogenic nanoparticles for our advancement, however the scaling up of nanoparticle production is still an area that requires more research. An exciting area of

research that could possibly result in an effective scaling up mechanism could be the role of soil microbes in plant growth as a symbiotic relationship could potentially be manipulated to allow improved metal and nutrient uptake by the plants thereby resulting in increased nanoparticle production.

Author contributions

KN and KP have conceptualized and prepared the manuscript. SBNK edited and critically reviewed the manuscript. All authors contributed to the article and approved the submitted version.

Funding

This work is based on the research supported by the National Research Foundation of South Africa (Grant number 107539). The opinions, findings and conclusions or recommendations is that of the authors and the NRF accepts no liability whatsoever in this regard.

Conflict of interest

The authors declare that the research was conducted in the absence of any commercial or financial relationships that could be construed as a potential conflict of interest.

Publisher's note

All claims expressed in this article are solely those of the authors and do not necessarily represent those of their affiliated organizations, or those of the publisher, the editors and the reviewers. Any product that may be evaluated in this article, or claim that may be made by its manufacturer, is not guaranteed or endorsed by the publisher.

Supplementary material

The Supplementary Material for this article can be found online at: <https://www.frontiersin.org/articles/10.3389/fchem.2023.1107619/full#supplementary-material>

References

- Abdullah, S. M., Kolo, K., and Sajadi, S. M. (2020). Greener pathway toward the synthesis of lichen-based ZnO@TiO₂@SiO₂ and Fe₃O₄@SiO₂ nanocomposites and investigation of their biological activities. *Food Sci. Nutr.* 8 (8), 4044–4054. doi:10.1002/fsn3.1661
- Abolhasani Zadeh, F., Abdalkareem Jasim, S., Atakhanova, N. E., Majidi, H. S., Abed Jawad, M., Khudair Hasan, M., et al. (2022). Drug delivery and anticancer activity of biosynthesized mesoporous Fe(2) O(3) nanoparticles. *IET Nanobiotechnol* 16 (3), 85–91. doi:10.1049/nbt2.12080
- Ahmed, A., Abagana, A., Cui, D., and Zhao, M. (2019). De novo iron oxide hydroxide, ferrihydrite produced by *Comamonas testosteroni* exhibiting intrinsic peroxidase-like activity and their analytical applications. *BioMed Res. Int.* 2019, 1–14. doi:10.1155/2019/7127869
- Aillon, K. L., Xie, Y., El-Gendy, N., Berkland, C. J., and Forrest, M. L. (2009). Effects of nanomaterial physicochemical properties on *in vivo* toxicity. *Adv. Drug Deliv. Rev.* 61 (6), 457–466. doi:10.1016/j.addr.2009.03.010
- Akpınar, I., Unal, M., and Sar, T. (2021). Potential antifungal effects of silver nanoparticles (AgNPs) of different sizes against phytopathogenic *Fusarium oxysporum f. sp. radicle-lycopersici* (FORL) strains. *SN Appl. Sci.* 3 (4), 506–514. doi:10.1007/s42452-021-04524-5
- Al-Sheddi, E. S., Farshori, N. N., Al-Oqail, M. M., Al-Massarani, S. M., Saquib, Q., Wahab, R., et al. (2018). Anticancer potential of green synthesized silver nanoparticles using extract of *nepeta deflersiana* against human cervical cancer cells (HeLa). *Bioinorg. Chem. Appl.* 2018, 1–12. doi:10.1155/2018/9390784

- Alavi, M., and Karimi, N. (2018). Characterization, antibacterial, total antioxidant, scavenging, reducing power and ion chelating activities of green synthesized silver, copper and titanium dioxide nanoparticles using *Artemisia haussknechtii* leaf extract. *Artif. Cells Nanomed Biotechnol.* 46 (8), 2066–2081. doi:10.1080/21691401.2017.1408121
- Alavi, M., Karimi, N., and Valadbeigi, T. (2019). Antibacterial, antibiofilm, anti-quorum sensing, antimotility, and antioxidant activities of green fabricated Ag, Cu, TiO₂, ZnO, and Fe₃O₄ NPs via protoparmeliopsis muralis lichen aqueous extract against multi-drug-resistant bacteria. *ACS Biomaterials Sci. Eng.* 5 (9), 4228–4243. doi:10.1021/acsbomaterials.9b00274
- Bahrulolum, H., Nooraei, S., Javanshir, N., Tarrahimofrad, H., Mirbagheri, V. S., Easton, A. J., et al. (2021). Green synthesis of metal nanoparticles using microorganisms and their application in the agrifood sector. *J. Nanobiotechnology* 19 (1), 86–26. doi:10.1186/s12951-021-00834-3
- Bulgarini, A., Lampis, S., Turner, R. J., and Vallini, G. (2021). Biomolecular composition of capping layer and stability of biogenic selenium nanoparticles synthesized by five bacterial species. *Microb. Biotechnol.* 14 (1), 198–212. doi:10.1111/1751-7915.13666
- Bundschuh, M., Filser, J., Lüderwald, S., McKee, M. S., Metreveli, G., Schaumann, G. E., et al. (2018). Nanoparticles in the environment: Where do we come from, where do we go to? *Environ. Sci. Eur.* 30 (1), 6–17. doi:10.1186/s12302-018-0132-6
- Cai, X., Zhu, Q., Zeng, Y., Zeng, Q., Chen, X., and Zhan, Y. (2019). <p>Manganese oxide nanoparticles as MRI contrast agents in tumor multimodal imaging and therapy</p>. *Int. J. Nanomedicine* 14, 8321–8344. doi:10.2147/ijn.s218085
- Cao, Y. C., Liu, C., Liu, H., Wang, Z., and Yang, S. H. (2011). *Nanozymes, methods of making nanozymes, and methods of using nanozymes*. PCT/US2011/032980.
- Cao, Y. C., Liu, C., Liu, H., Wang, Z., and Yang, S. H. (2018). *Nanozymes, methods of making nanozymes, and methods of using nanozymes*. United States of America patent application US10081542B2.
- Cao, Y. C., and Jiang, T. (2020). *RNA silencing nanozymes*. 20210139873.
- Cao, Y. C., and Liu, C. (2015). *Nanozymes, methods of making nanozymes, and methods of using nanozymes*. WO2015023715A1.
- Cao, Y. C., and Liu, C. (2016). *Nanozymes, methods of making nanozymes, and methods of using nanozymes*. United States of America patent application US20160215279A1. Florida.
- Capeness, M. J., Echavarri-Bravo, V., and Horsfall, L. E. (2019). Production of biogenic nanoparticles for the reduction of 4-nitrophenol and oxidative laccase-like reactions. *Front. Microbiol.* 10, 997–999. doi:10.3389/fmicb.2019.00997
- Capuzzo, A. (2021). Bacterial synthesis of nanoparticles: Current trends in biotechnology and biomedical fields. *Ann. Adv. Biomed. Sci.* 4, 1–18. doi:10.20944/preprints202103.0358.v1
- Carrillo-Carrion, C., Nazarenus, M., Paradinas, S. S., Carregal-Romero, S., Almendral, M. J., Fuentes, M., et al. (2014). Metal ions in the context of nanoparticles toward biological applications. *Curr. Opin. Chem. Eng.* 4, 88–96. doi:10.1016/j.coch.2013.11.006
- Chaudhari, A., Kaida, T., Desai, H. B., Ghosh, S., Bhatt, R. P., and Tanna, A. R. (2022). Dye degradation and antimicrobial applications of manganese ferrite nanoparticles synthesized by plant extracts. *Chem. Phys. Impact* 5, 1–6. doi:10.1016/j.chphi.2022.100098
- Ciplak, Z., Gokalp, C., Getiren, B., Yildiz, A., and Yildiz, N. (2018). Catalytic performance of Ag, Au and Ag-Au nanoparticles synthesized by lichen extract. *Green Process. Synthesis* 7 (5), 433–440. doi:10.1515/gps-2017-0074
- Dan, D. (2020). Nanotechnology, nanoparticles and nanoscience: A new approach in chemistry and life sciences. *Soft Nanosci. Lett.* 10, 17–26. doi:10.4236/snsl.2020.102002
- Das, B., Lou-Franco, J., Gilbride, B., Ellis, M. G., Stewart, L. D., Grant, I. R., et al. (2022a). Peroxidase-mimicking activity of biogenic gold nanoparticles produced from *Prunus nepalensis* fruit extract: Characterizations and application for the detection of *Mycobacterium bovis*. *ACS Appl. Bio Mater.* 5 (6), 2712–2725. doi:10.1021/acsbm.2c00180
- Das, P. P., Singh, K. R., Nagpure, G., Mansoori, A., Singh, R. P., Ghazi, I. A., et al. (2022b). Plant-soil-microbes: A tripartite interaction for nutrient acquisition and better plant growth for sustainable agricultural practices. *Environ. Res.* 214 (1), 113821. doi:10.1016/j.envres.2022.113821
- de Lima, R., Seabra, A. B., and Duran, N. (2012). Silver nanoparticles: A brief review of cytotoxicity and genotoxicity of chemically and biogenically synthesized nanoparticles. *J. Appl. Toxicol.* 32 (11), 867–879. doi:10.1002/jat.2780
- Dong, Y., Zhu, H., Shen, Y., Zhang, W., and Zhang, L. (2019). Antibacterial activity of silver nanoparticles of different particle size against *Vibrio Natriegens*. *PLOS ONE* 14 (9), 1–12. doi:10.1371/journal.pone.0222322
- Ealias, A. M., and Saravanakumar, M. P. (2017). A review on the classification, characterisation, synthesis of nanoparticles and their application. *IOP Conf. Ser. Mater. Sci. Eng.* 263, 1–16. doi:10.1088/1757-899X/263/3/032019
- Elamawi, R. M., Al-Harbi, R. E., and Hendi, A. A. (2018). Biosynthesis and characterization of silver nanoparticles using *Trichoderma longibrachiatum* and their effect on phytopathogenic fungi. *Egypt. J. Biol. Pest Control* 28 (1), 28–11. doi:10.1186/s41938-018-0028-1
- Fotiadiou, R., Chatzikonstantinou, A. V., Hammami, M. A., Chalmes, N., Moschovas, D., Spyrou, K., et al. (2021). Green synthesized magnetic nanoparticles as effective nanosupport for the immobilization of lipase: Application for the synthesis of lipophenols. *Nanomater. (Basel)* 11 (2), 1–20. doi:10.3390/nano11020458
- Fouda, A., Salem, S. S., Wassel, A. R., Hamza, M. F., and Shaheen, T. I. (2020). Optimization of green biosynthesized visible light active CuO/ZnO nano-photocatalysts for the degradation of organic methylene blue dye. *Heliyon* 6 (9), 1–13. doi:10.1016/j.heliyon.2020.e04896
- Gami, B., Bloch, K., Mohammed, S. M., Karmakar, S., Shukla, S., Asok, A., et al. (2022). *Leucophyllum frutescens* mediated synthesis of silver and gold nanoparticles for catalytic dye degradation. *Front. Chem.* 10, 1–14. doi:10.3389/fchem.2022.932416
- Gandhi, A. D., Murugan, K., Umamahesh, K., Babujanathanam, R., Kavitha, P., and Selvi, A. (2019). Lichen *Parmelia sulcata* mediated synthesis of gold nanoparticles: An eco-friendly tool against *Anopheles stephensi* and *Aedes aegypti*. *Environ. Sci. Pollut. Res.* 26 (23), 23886–23898. doi:10.1007/s11356-019-05726-6
- Gandhi, A. D., Miraclin, P. A., Abilash, D., Sathiyaraj, S., Velmurugan, R., Zhang, Y., et al. (2021). Nanosilver reinforced *Parmelia sulcata* extract efficiently induces apoptosis and inhibits proliferative signalling in MCF-7 cells. *Environ. Res.* 199, 111375. doi:10.1016/j.envres.2021.111375
- Gao, L., and Yan, X. (2016). Nanozymes: An emerging field bridging nanotechnology and biology. *Sci. China Life Sci.* 59 (4), 400–402. doi:10.1007/s11427-016-5044-3
- Gao, L., Zhuang, J., Nie, L., Zhang, J., Zhang, Y., Ning, G., et al. (2007). Intrinsic peroxidase-like activity of ferromagnetic nanoparticles. *Nat. Nanotechnol.* 2, 577–583. doi:10.1038/nnano.2007.260
- Ge, X., Cao, Z., and Chu, L. (2022). The antioxidant effect of the metal and metal-oxide nanoparticles. *Antioxidants* 11 (4), 791. doi:10.3390/antiox11040791
- Guilger-Casagrande, M., Germano-Costa, T., Bilecky-José, N., Pasquato-Stigliani, T., Carvalho, L., Fraceto, L. F., et al. (2021). Influence of the capping of biogenic silver nanoparticles on their toxicity and mechanism of action towards *Sclerotinia sclerotiorum*. *J. Nanobiotechnology* 19 (1), 53–18. doi:10.1186/s12951-021-00797-5
- Guo, F. F., Yang, W., Jiang, W., Geng, S., Peng, T., and Li, J. L. (2012). Magnetosomes eliminate intracellular reactive oxygen species in *Magnetospirillum gryphiswaldense* MSR-1. *Environ. Microbiol.* 14 (7), 1722–1729. doi:10.1111/j.1462-2920.2012.02707.x
- Gurunathan, S., Kalishwaralal, K., Vaidyanathan, R., Venkataraman, D., Pandian, S. R., Muniyandi, J., et al. (2009). Biosynthesis, purification and characterization of silver nanoparticles using *Escherichia coli*. *Colloids Surf. B Biointerfaces* 74 (1), 328–335. doi:10.1016/j.colsurfb.2009.07.048
- Hu, L., Song, T., Ma, Q., Chen, C., Pan, W., Xie, C., et al. (2010). in *Bacterial magnetic nanoparticles as peroxidase mimetics and application in immunoassay*. Editors U. Häfeli, W. Schütt, and M. Zborowski, 369–374.
- Huynh, K. H., Pham, X. H., Kim, J., Lee, S. H., Chang, H., Rho, W. Y., et al. (2020). Synthesis, properties, and biological applications of metallic alloy nanoparticles. *Int. J. Mol. Sci.* 21 (14), 1–29. doi:10.3390/ijms211415174
- Jang, J., Lee, S., and Lee, J. (2014). *Synthesis method of enzyme-mimic magnetic nanocatalysts, and enzyme-mimic magnetic nanocatalysts thereby*. South Korea patent application. KR102120002401A.
- Javed, R., Sajjad, A., Naz, S., Sajjad, H., and Ao, Q. (2022). Significance of capping agents of colloidal nanoparticles from the perspective of drug and gene delivery, bioimaging, and biosensing: An insight. *Int. J. Mol. Sci.* 23 (18), 10521–10528. doi:10.3390/ijms231810521
- Katas, H., Lim, C. S., Nor Azlan, A. Y. H., Buang, F., and Mh Busra, M. F. (2019). Antibacterial activity of biosynthesized gold nanoparticles using biomolecules from *Lignosus rhinocerotis* and chitosan. *Saudi Pharm. J. SPJ official Publ. Saudi Pharm. Soc.* 27 (2), 283–292. doi:10.1016/j.jsps.2018.11.010
- Khan, I., Saeed, K., and Khan, I. (2019). Nanoparticles: Properties, applications and toxicities. *Arabian J. Chem.* 12 (7), 908–931. doi:10.1016/j.arabjc.2017.05.011
- Khandel, P., and Shahi, S. K. (2018). Mycogenic nanoparticles and their bio-prospective applications: Current status and future challenges. *J. Nanostructure Chem.* 8 (4), 369–391. doi:10.1007/s40097-018-0285-2
- Khorrami, S., Zarrabi, A., Khaleghi, M., Danaei, M., and Mozafari, M. R. (2018). Selective cytotoxicity of green synthesized silver nanoparticles against the MCF-7 tumor cell line and their enhanced antioxidant and antimicrobial properties. *Int. J. Nanomedicine* 13, 8013–8024. doi:10.2147/ijn.s189295
- Kredy, H. (2018). The effect of pH, temperature on the green synthesis and biochemical activities of silver nanoparticles from *Lawsonia inermis* extract. *J. Pharm. Sci. Res.* 10, 2022–2026.
- Lee, S., Lee, S., Kim, M., Shin, S., Lee, J., and Kim, M. (2018). *Ig e detection and allergy diagnostic method using enzyme-mimetic nanozyme-based immunoassay*. WO2018084340A1.
- Li, Q., Liu, F., Li, M., Chen, C., and Gadd, G. M. (2021). Nanoparticle and nanomineral production by fungi. *Fungal Biol. Rev.* 41, 31–44. doi:10.1016/j.fbr.2021.07.003
- Lin, W., Kirschvink, J. L., Paterson, G. A., Bazylinski, D. A., and Pan, Y. (2019). On the origin of microbial magnetoreception. *Natl. Sci. Rev.* 7 (2), 472–479. doi:10.1093/nsr/nwz065
- López-Miranda, J. L., Esparza, R., Rosas, G., Perez, R., and Estevez-Gonzalez, M. (2019). Catalytic and antibacterial properties of gold nanoparticles synthesized by a

- green approach for bioremediation applications. *3 Biotech.* 9 (4), 135–139. doi:10.1007/s13205-019-1666-z
- Medintz, I. L., Vranish, J. N., Ancona, M., Susumu, K., and Diaz, S. A. (2017). *Nanoparticle-attached enzyme cascades for accelerated multistep biocatalysis*. US20180171325A1.
- Molnár, Z., Bodai, V., Szakacs, G., Erdelyi, B., Fogarassy, Z., Safran, G., et al. (2018). Green synthesis of gold nanoparticles by thermophilic filamentous fungi. *Sci. Rep.* 8 (1), 1–12. doi:10.1038/s41598-018-22112-3
- Moodley, J. S., Krishna, S. B. N., Pillay, K., Sershen, N., and Govender, P. (2018). Green synthesis of silver nanoparticles from Moringa oleifera leaf extracts and its antimicrobial potential. *Adv. Nat. Sci. Nanosci. Nanotechnol.* 9 (1), 015011–015019. doi:10.1088/2043-6254/aaabb2
- Moodley, J. S., Krishna, S. B. N., Pillay, K., and Govender, P. (2021). “Green synthesis of metal nanoparticles for antimicrobial activity,” in *Novel nanomaterials*. Editor K. Krishnamoorthy (London: IntechOpen), 253–278.
- Nadaroglu, H., Alayli, A., and Ince, S. (2017). Synthesis of nanoparticles by green synthesis method. *Int. J. Innovative Res. Rev.* 1, 6–9.
- Nadhe, S. B., Singh, R., Wadhvani, S. A., and Chopade, B. A. (2019). *Acinetobacter* sp. mediated synthesis of AgNPs, its optimization, characterization and synergistic antifungal activity against *C. albicans*. *J. Appl. Microbiol.* 127 (2), 445–458. doi:10.1111/jam.14305
- Nan, X., Lai, W., Li, D., Tian, J., Hu, Z., and Fang, Q. (2021). Biocompatibility of bacterial magnetosomes as mri contrast agent: A long-term *in vivo* follow-up study. *Nanomater. (Basel)* 11 (5), 1235. doi:10.3390/nano11051235
- Nayak, V., Singh, K. R., Singh, A. K., and Singh, R. P. (2021). Potentialities of selenium nanoparticles in biomedical science. *New J. Chem.* 45 (6), 2849–2878. doi:10.1039/d0nj05884j
- Nayak, V., Singh, K. R. B., Verma, R., Pandey, M. D., Singh, J., and Singh, R. P. (2022). Recent advancements of biogenic iron nanoparticles in cancer theranostics. *Mater. Lett.* 313, 131769. doi:10.1016/j.matlet.2022.131769
- Nguyen, V. P., Le Trung, H., Nguyen, T. H., Hoang, D., and Tran, T. H. (2021). Synthesis of biogenic silver nanoparticles with eco-friendly processes using *Ganoderma lucidum* extract and evaluation of their theranostic applications. *J. Nanomater.* 2021, 1–11. doi:10.1155/2021/6135920
- Ortaç, I., Esener, S. C., Yayla, I. G., and Messmer, B. (2019). *Enzyme-encapsulated nanoparticle platform*. US10300152B2.
- Patil, S., and Chandrasekaran, R. (2020). Biogenic nanoparticles: A comprehensive perspective in synthesis, characterization, application and its challenges. *J. Genet. Eng. Biotechnol.* 18 (1), 67–23. doi:10.1186/s43141-020-00081-3
- Pugazhendhi, A., Prabhu, R., Muruganathan, K., Shanmuganathan, R., and Natarajan, S. (2019). Anticancer, antimicrobial and photocatalytic activities of green synthesized magnesium oxide nanoparticles (MgONPs) using aqueous extract of *Sargassum wightii*. *J. Photochem Photobiol. B* 190, 86–97. doi:10.1016/j.jphotobiol.2018.11.014
- Puri, A., and Patil, S. (2022). *Tinospora cordifolia* stem extract-mediated green synthesis of selenium nanoparticles and its biological applications. *Pharmacogn. Res.* 14 (3), 289–296. doi:10.5530/pres.14.3.42
- Qu, Y., Li, X., Lian, S., Dai, C., Jv, Z., Zhao, B., et al. (2019). Biosynthesis of gold nanoparticles using fungus *Trichoderma* sp. WL-Go and their catalysis in degradation of aromatic pollutants. *IET Nanobiotechnol.* 13 (1), 12–17. doi:10.1049/iet-nbt.2018.5177
- Ragg, R., Tahir, M., and Tremel, W. (2015). Solids go bio: Inorganic nanoparticles as enzyme mimics. *Eur. J. Inorg. Chem.* 2016, 1896–1915. doi:10.1002/ejic.201600408
- Rastogi, L., Dash, K., and Sashidhar, R. B. (2021). Selective and sensitive detection of cholesterol using intrinsic peroxidase-like activity of biogenic palladium nanoparticles. *Curr. Res. Biotechnol.* 3, 42–48. doi:10.1016/j.crbiot.2021.02.001
- Repetto, M. G., Ferrarotti, N. F., and Boveris, A. (2010). The involvement of transition metal ions on iron-dependent lipid peroxidation. *Archives Toxicol.* 84 (4), 255–262. doi:10.1007/s00204-009-0487-y
- Riaz, M., Sharafat, U., Zahid, N., Ismail, M., Park, J., Ahmad, B., et al. (2022). Synthesis of biogenic silver nanocatalyst and their antibacterial and organic pollutants reduction ability. *ACS Omega* 7 (17), 14723–14734. doi:10.1021/acsomega.1c07365
- Rotello, V. M., Landis, R. F., Gupta, A., and Lee, Y. W. (2017). *Stabilized polymeric nanocapsules, dispersions comprising the nanocapsules, and methods for the treatment of bacterial biofilms*. WO2017040024A1.
- Salama, A. M., Behaery, M. S., Elaal, A. E. A., and Abdelaal, A. (2022). Influence of cerium oxide nanoparticles on dairy effluent nitrate and phosphate bioremediation. *Environ. Monit. Assess.* 194 (5), 326. doi:10.1007/s10661-022-10003-0
- Saleh, M., and Alwan, S. (2020). Bio-synthesis of silver nanoparticles from bacteria *Klebsiella pneumoniae*: Their characterization and antibacterial studies. *J. Phys. Conf. Ser.* 1664, 012115. doi:10.1088/1742-6596/1664/1/012115
- Sarwer, Q., Amjad, M. S., Mehmood, A., Binish, Z., Mustafa, G., Farooq, A., et al. (2022). Green synthesis and characterization of silver nanoparticles using myrsine africana leaf extract for their antibacterial, antioxidant and phytotoxic activities. *Molecules* 27 (21), 7612. doi:10.3390/molecules27217612
- Shu, M., He, F., Li, Z., Zhu, X., Ma, Y., Zhou, Z., et al. (2020). Biosynthesis and antibacterial activity of silver nanoparticles using yeast extract as reducing and capping agents. *Nanoscale Res. Lett.* 15 (1), 14–19. doi:10.1186/s11671-019-3244-z
- Siddiqi, K. S., Rashid, M., Rahman, A., TajuddinHusen, A., and Rehman, S. (2018). Biogenic fabrication and characterization of silver nanoparticles using aqueous-ethanolic extract of lichen (*Usnea longissima*) and their antimicrobial activity. *Biomater. Res.* 22, 23. doi:10.1186/s40824-018-0135-9
- Sidhu, A. K., Verma, N., and Kaushal, P. (2022). Role of biogenic capping agents in the synthesis of metallic nanoparticles and evaluation of their therapeutic potential. *Front. Nanotechnol.* 3, 1–17. doi:10.3389/fnano.2021.801620
- Singh, K. R., Nayak, V., Singh, J., Singh, A. K., and Singh, R. P. (2021a). Potentialities of bioinspired metal and metal oxide nanoparticles in biomedical sciences. *RSC Adv.* 11 (40), 24722–24746. doi:10.1039/d1ra04273d
- Singh, P., Singh, K. R., Singh, J., Das, S. N., and Singh, R. P. (2021b). Tunable electrochemistry and efficient antibacterial activity of plant-mediated copper oxide nanoparticles synthesized by *Annona squamosa* seed extract for agricultural utility. *RSC Adv.* 11 (29), 18050–18060. doi:10.1039/d1ra02382a
- Singh, S. (2019). Nanomaterials exhibiting enzyme-like properties (nanozymes): Current advances and future perspectives. *Front. Chem.* 7, 46–10. doi:10.3389/fchem.2019.00046
- Sintubin, L., De Windt, W., Dick, J., Mast, J., van der Ha, D., Verstraete, W., et al. (2009). Lactic acid bacteria as reducing and capping agent for the fast and efficient production of silver nanoparticles. *Appl. Microbiol. Biotechnol.* 84 (4), 741–749. doi:10.1007/s00253-009-2032-6
- Smith, R. M., Drobniowski, F., Gibson, A., Montague, J. D., Logan, M. N., Hunt, D., et al. (2004). *Mycobacterium bovis* infection, United Kingdom. *Emerg. Infect. Dis.* 10 (3), 539–541. doi:10.3201/eid1003.020819
- Soliman, M. K. Y., Salem, S. S., Abu-Elghait, M., and Azab, M. S. (2022). Biosynthesis of silver and gold nanoparticles and their efficacy towards antibacterial, antibiofilm, cytotoxicity, and antioxidant activities. *Appl. Biochem. Biotechnol.* 195, 1158–1183. doi:10.1007/s12010-022-04199-7
- Speranza, G. (2021). Carbon nanomaterials: Synthesis, functionalization and sensing applications. *Nanomater. (Basel, Switz.)* 11 (4), 967–999. doi:10.3390/nano11040967
- Srivastava, V., Pandey, S., Mishra, A., and Choubey, A. K. (2019). Green synthesis of biogenic silver particles, process parameter optimization and application as photocatalyst in dye degradation. *SN Appl. Sci.* 1 (12), 1722. doi:10.1007/s42452-019-1762-z
- Srivastava, S., Usmani, Z., Atanasov, A. G., Singh, V. K., Singh, N. P., Abdel-Azeem, A. M., et al. (2021). Biological nanofactories: Using living forms for metal nanoparticle synthesis. *Mini Rev. Med. Chem.* 21 (2), 245–265. doi:10.2174/1389557520999201116163012
- Sukhanova, A., Bozrova, S., Sokolov, P., Berestovoy, M., Karaulov, A., and Nabiev, I. (2018). Dependence of nanoparticle toxicity on their physical and chemical properties. *Nanoscale Res. Lett.* 13 (1), 44–21. doi:10.1186/s11671-018-2457-x
- Tripathi, S., Sanjeevi, R., Jayaraman, A., Chauhan, D., and Rathoure, D. A. (2018). *Nano-Bioremediation: Nanotechnology and bioremediation*, 202–219.
- Wang, D., Cui, L., Chang, X., and Guan, D. (2020a). Biosynthesis and characterization of zinc oxide nanoparticles from *Artemisia annua* and investigate their effect on proliferation, osteogenic differentiation and mineralization in human osteoblast-like MG-63 Cells. *J. Photochem Photobiol. B* 202, 111652. doi:10.1016/j.jphotobiol.2019.111652
- Wang, P., Wang, T., Hong, J., Yan, X., and Liang, M. (2020b). Nanozymes: A new disease imaging strategy. *Front. Bioeng. Biotechnol.* 8, 15–10. doi:10.3389/fbioe.2020.00015
- Wei, H., Wiśniowska, A., Fan, J., Harvey, P., Li, Y., Wu, V., et al. (2021). Single-nanometer iron oxide nanoparticles as tissue-permeable MRI contrast agents. *Proc. Natl. Acad. Sci. U. S. A.* 118 (42), e2102340118–8. doi:10.1073/pnas.2102340118
- Weingart, J., Vabbilisetty, P., and Sun, X.-L. (2013). Membrane mimetic surface functionalization of nanoparticles: Methods and applications. *Adv. colloid interface Sci.* 197–198, 68–84. doi:10.1016/j.cis.2013.04.003
- Wu, J., Wang, X., Wang, Q., Lou, Z., Li, S., Zhu, Y., et al. (2019). Nanomaterials with enzyme-like characteristics (nanozymes): Next-generation artificial enzymes (II). *Chem. Soc. Rev.* 48, 1004–1076. doi:10.1039/C8CS00457A
- Xia, X. (2017). *PD-IR nanoparticles used as peroxidase mimics*. US20170199179 A1.
- Xu, C., Guo, Y., Qiao, L., Ma, L., Cheng, Y., and Roman, A. (2018). Biogenic synthesis of novel functionalized selenium nanoparticles by *Lactobacillus casei* ATCC 393 and its protective effects on intestinal barrier dysfunction caused by enterotoxigenic *Escherichia coli* K88. *Front. Microbiol.* 9, 1–13. doi:10.3389/fmicb.2018.01129
- Yassin, M. A., Elgorban, A. M., El-Samawaty, A., and Almunqedhi, B. M. A. (2021). Biosynthesis of silver nanoparticles using *Penicillium verrucosum* and

analysis of their antifungal activity. *Saudi J. Biol. Sci.* 28 (4), 2123–2127. doi:10.1016/j.sjbs.2021.01.063

Ying, S., Guan, Z., Ofoegbu, P. C., Clubb, P., Rico, C., He, F., et al. (2022). Green synthesis of nanoparticles: Current developments and limitations. *Environ. Technol. Innovation* 26, 1–20. doi:10.1016/j.eti.2022.102336

Yu, G.-H., Chi, Z.-L., Kappler, A., Sun, F.-S., Liu, C.-Q., Teng, H. H., et al. (2020a). Fungal nanophase particles catalyze iron transformation for oxidative stress removal and iron acquisition. *Curr. Biol.* 30 (15), 2943–2950.e4. doi:10.1016/j.cub.2020.05.058

Yu, Z., Li, Q., Wang, J., Yu, Y., Wang, Y., Zhou, Q., et al. (2020b). Reactive oxygen species-related nanoparticle toxicity in the biomedical field. *Nanoscale Res. Lett.* 15 (1), 115. doi:10.1186/s11671-020-03344-7

Yulizar, Y., Kusriani, E., Apriandanu, D. O. B., and Nurdini, N. (2020). *Datura metel* L. Leaves extract mediated CeO₂ nanoparticles: Synthesis, characterizations, and degradation activity of DPPH radical. *Surfaces Interfaces* 19, 1–6. doi:10.1016/j.surfin.2020.100437

Zhang, D., Ma, X.-L., Gu, Y., Huang, H., and Zhang, G.-w. (2020). Green synthesis of metallic nanoparticles and their potential applications to treat cancer. *Front. Chem.* 8, 1–18. doi:10.3389/fchem.2020.00799



OPEN ACCESS

EDITED BY

Sirikanjana Thongmee,
Kasetsart University, Thailand

REVIEWED BY

Surekha K. Satpute,
Savitribai Phule Pune University, India
Alok Prasad Das,
Rama Devi Women's University, India

*CORRESPONDENCE

Muhammad Rajaei Ahmad Mohd Zain,
✉ rajaei@usm.my
Rina Rani Ray,
✉ raypumicro@gmail.com

SPECIALTY SECTION

This article was submitted to Nanoscience,
a section of the journal
Frontiers in Chemistry

RECEIVED 07 December 2022

ACCEPTED 30 January 2023

PUBLISHED 07 March 2023


CITATION

Ghosh S, Mondol S, Lahiri D, Nag M,
Sarkar T, Pati S, Pandit S, Alarfaj AA,
Mohd Amin MF, Edinur HA,
Ahmad Mohd Zain MR and Ray RR (2023),
Biogenic silver nanoparticles (AgNPs) from
Tinosporacordifolia leaves: An effective
antibiofilm agent against *Staphylococcus*
aureus ATCC 23235.
Front. Chem. 11:1118454.
doi: 10.3389/fchem.2023.1118454

COPYRIGHT

© 2023 Ghosh, Mondol, Lahiri, Nag, Sarkar,
Pati, Pandit, Alarfaj, Mohd Amin, Edinur,
Ahmad Mohd Zain and Ray. This is an
open-access article distributed under the
terms of the [Creative Commons
Attribution License \(CC BY\)](https://creativecommons.org/licenses/by/4.0/). The use,
distribution or reproduction in other
forums is permitted, provided the original
author(s) and the copyright owner(s) are
credited and that the original publication in
this journal is cited, in accordance with
accepted academic practice. No use,
distribution or reproduction is permitted
which does not comply with these terms.

Biogenic silver nanoparticles (AgNPs) from *Tinosporacordifolia* leaves: An effective antibiofilm agent against *Staphylococcus aureus* ATCC 23235

Sreejita Ghosh¹, Somdutta Mondol¹, Dibyajit Lahiri², Moupriya Nag²,
Tanmay Sarkar ³, Siddhartha Pati^{4,5}, Soumya Pandit⁶,
Abdullah A. Alarfaj⁷, Mohamad Faiz Mohd Amin⁸,
Hisham Atan Edinur⁹, Muhammad Rajaei Ahmad Mohd Zain^{10*} and
Rina Rani Ray^{1*}

¹Department of Biotechnology, MaulanaAbulKalam Azad University of Technology, Kolkata, West Bengal, India, ²Department of Biotechnology, University of Engineering and Management, Kolkata, West Bengal, India, ³Department of Food Processing Technology, Malda Polytechnic, West Bengal State Council of Technical Education, Govt. of West Bengal, Malda, India, ⁴Skills innovation and Academic network (SIAN) Institute-ABC, Balasore, Odisha, India, ⁵NatNov Private Limited, Greater Noida, Odisha, India, ⁶Department of Life Science, Sharda University, Noida, India, ⁷Department of Botany and Microbiology, College of Science, King Saud University, Riyadh, Saudi Arabia, ⁸Environmental Technology Division, School of Industrial Technology, UniversitiSains Malaysia, Penang, Malaysia, ⁹Renewable Biomass Transformation Cluster, School of Industrial Technology, UniversitiSains Malaysia, Penang, Malaysia, ¹⁰School of Health Sciences, UniversitiSains Malaysia, Health Campus, Kelantan, Malaysia

Medicinal plants are long known for their therapeutic applications. *Tinospora cordifolia* (commonly called gulancha or heart-leaved moonseed plant), a herbaceous creeper widely has been found to have antimicrobial, anti-inflammatory, anti-diabetic, and anti-cancer properties. However, there remains a dearth of reports regarding its antibiofilm activities. In the present study, the anti-biofilm activities of phytoextract of *T. cordifolia* and the silver nanoparticles made from this phytoextract were tested against the biofilm of *S. taphylococcus aureus*, one of the major nosocomial infection-producing bacteria taking tetracycline antibiotic as control. Both phytoextract from the leaves of *T. cordifolia*, and the biogenic AgNPs from the leaf extract of *T. cordifolia*, were found successful in reducing the biofilm of *Staphylococcus aureus*. The biogenic AgNPs formed were characterized by UV- Vis spectroscopy, Field emission Scanning Electron Microscopy (FE- SEM), and Dynamic light scattering (DLS) technique. FE- SEM images showed that the AgNPs were of size ranging between 30 and 50 nm and were stable in nature, as depicted by the zeta potential analyzer. MIC values for phytoextract and AgNPs were found to be 180 mg/mL and 150 µg/mL against *S. aureus* respectively. The antibiofilm properties of the AgNPs and phytoextract were analyzed using the CV assay and MTT assay for determining the reduction of biofilms. Reduction in viability count and revival of the *S. aureus* ATCC 23235 biofilm cells were analyzed followed by the enfeeblement of the EPS matrix to quantify the reduction in the contents of carbohydrates, proteins and eDNA. The SEM analyses clearly indicated that although the phytoextracts could destroy the biofilm network of *S. aureus* cells yet the biogenically synthesized AgNPs were more effective in biofilm disruption. Fourier Transformed Infrared Radiations (FT- IR) analyses revealed that the AgNPs could bring about more exopolysaccharide (EPS) destruction in comparison to the phytoextract. The

antibiofilm activities of AgNPs made from the phytoextract were found to be much more effective than the non-conjugated phytoextract, indicating the future prospect of using such particles for combatting biofilm-mediated infections caused by *S. aureus*.

KEYWORDS

Tinospora cordifolia, phytoextract, green synthesis, biogenic silver nanoparticles, biofilms, *Staphylococcus aureus*, biofilm

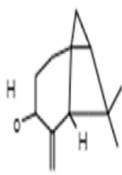
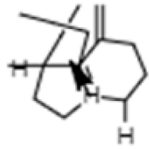
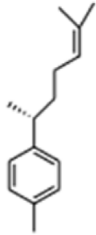
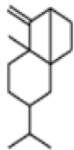
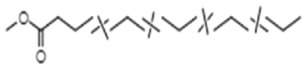
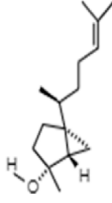
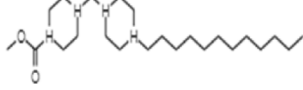
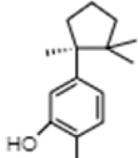
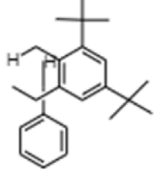
1 Introduction

Development of biofilm is a natural tendency of bacteria, to survive adversities (Donlan, 2002). It is a syntrophic cluster of sessile bacterial cells, remaining shielded by a self-secreted extracellular polymeric substance (EPS). With the help of such polymeric substances, the bacterial cells can spread over biotic and abiotic surfaces and their binding with such surfaces plays a significant role in spreading the pathogenicity and virulence of the respective bacteria (Haiko and Westerlund-Wikström, 2013). The diversity of the biochemical constitution of the EPS matrix leads to different capacities of surface adherence with the substratum, which in turn causes a wide range of adaptations to adverse environmental conditions (Kostakioti et al., 2013). The EPS prevents the penetrance of antibiotics and other drugs resulting in the development of antibiotic resistance and multi-drug resistance. In today's clinical point of view, biofilm-associated chronic and acute infections are the most challenging to treat, and day by day these infections start to threaten human health globally. *Staphylococcus aureus* is one of the predominant bacteria responsible for causing community-acquired and nosocomial infections and such infections often become life-threatening (Silva-Santana et al., 2020). *S. aureus* is a Gram-positive bacterium and it is a human commensal that continuously colonizes the frontal niches of about 20%–25% of fit adult communities and 60% remain occasionally colonized (Ellis et al., 2014). The attachment of *S. aureus* to the surfaces of medical implants and host tissues results in the development of matured biofilm resulting in the persistence of chronic infections (Foster et al., 2014). The development of biofilm and their residence in the EPS matrix lessens their susceptibilities to different antibiotics and host immunity, which makes these infections difficult to eradicate (Chatterjee et al., 2014). The biofilms of *Staphylococcus aureus* are known to cause infections such as bacteremia, endocarditis, multiple sclerosis and sepsis (Sheykhsaran et al., 2022). Various parameters lead to the development of biofilms. These factors include particular gene expressions and communication among proteins that help in adherence of the biofilm to the substrate. During more advanced stages of the infections caused by *Staphylococcus aureus* biofilms, bacterial cells get dispersed from the biofilms and get spread to the secondary sites thereby worsening the infection. The World Health Organization (WHO) has classified a list of antibiotic-resistant pathogens, based on the priority of finding new alternative therapies for treating those infections, which can no longer be treated with the available antibiotic therapeutic strategies. There are three stages of priority list pathogens: Priority 1 (critical), priority 2 (high) and priority 3

(medium). Among the priority list of pathogens, WHO has considered *S. aureus* in the second priority group (high priority) because *S. aureus* is resistant against a wide class of antibiotics including methicillin and vancomycin. Vancomycin was one of the last resort antibiotics to eradicate the methicillin-resistant *S. aureus* (MRSA) infections. Prolonged or suboptimal exposure to vancomycin has led to the development of decreased vulnerability of the *S. aureus* associated infections. This decreased susceptibility can be also due to the thickening of the EPS matrix and various antibiotic inactivating enzymes present in the EPS matrix (Al-Marzoqi et al., 2020).

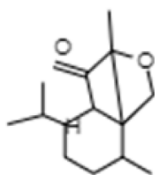
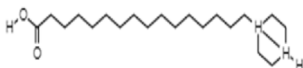
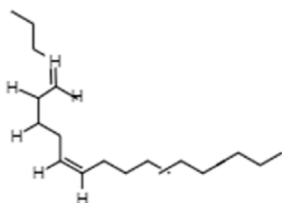
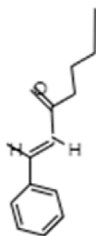
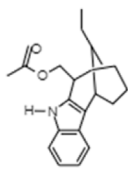
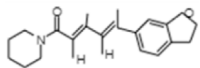
Silver is an antimicrobial substance with antiseptic, antibacterial, and anti-inflammatory properties (Fong et al., 2005). When silver is in a soluble state, such as Ag^+ or Ag^0 clusters, it is physiologically active. Ag^+ is the ionic version of silver in silver sulfadiazine, silver nitrate, as well as other ionic silver compounds. Silver is used as an ingredient in various ointments, creams, medicines, and medical instruments. Nanoparticles of silver have unique characteristics attributed to their very small size, which helps in enhancing their bioavailability and efficacy. Silver nanoparticles (AgNPs) possess inhibitory actions on bacterial, fungal, and viral growth (Jeong et al., 2005). AgNPs are increasingly explored by researchers because of their cytotoxic and antibacterial potential due to their easy attachment with the bacterial cell walls. This adherence impacts the cellular respiration and permeability leading to cell death. Moreover, AgNPs can easily enter the cells and bind with the biomolecules, including protein and DNA through their phosphorous and sulfur groups, respectively (Abed and Mohammed, 2021). Besides, their antimicrobial properties, their biosynthesis process is comparatively cost-effective (Capek, 2004). Physical and chemical methods of AgNPs synthesis involve the use of toxic reagents and result in a very low yield of AgNPs. However, the biogenic method of AgNPs synthesis is environment-friendly, readily-scalable, simple and involves only natural reagents, so they are free from potential toxicities and also biocompatible (Emeka et al., 2014). Hence, the biological methods for the preparation of nanoparticles have more advantages over chemical and physical methods of AgNP synthesis, via processes like ultrathin film procedure, thermal evaporation, synthesis through diffusion flame, lithographic process, electrodeposition, sol-gel technique, chemical solution and vapor deposition, catalytic process, hydrolysis and method of co-precipitation (Hu et al., 2020). However, the exact mechanism of anti-biofilm activities of AgNPs is not yet clearly understood. It is being presumed that their extremely small sizes lead to the increase in oxidative stress within the bacterial cells through the generation of reactive oxygen species (ROS) or through denaturation of the fatty acids present

TABLE 1 GC-MS analysis of phytoextract of *T. cordifolia*

Sl No	Rt	Name of the compounds	Molecular formula	Molecular Wt (g/mol)	Structure
1	4.94	Isopinocarveol	C ₁₀ H ₁₆ O	152.23	
2	8.60	Caryophyllene	C ₁₅ H ₂₄	204.35	
3	9.38	Benzene, 1-(1,5-dimethyl-4-hexenyl)-4-methyl	C ₁₅ H ₂₂	202.34	
4	10.45	(+)-Sativene	C ₁₅ H ₂₄	204.35	
5	10.78	Methyl 4,7,10,13-hexadecatetraenoate	C ₁₇ H ₂₆ O ₂	262.4	
6	11.70	7-epi-cis-sesquisabinene hydrate	C ₁₅ H ₂₆ O	222.37	
7	12.13	2,5-Octadecadiynoic acid, methyl ester	C ₁₉ H ₃₀ O ₂	290.4	
8	12.71	Phenol, 2-methyl-5-(1,2,2-trimethylcyclopentyl)-, (S)-	C ₁₅ H ₂₂ O	218.33	
9	13.33	Phenol, 2,4-bis(1,1-dimethylethyl)	C ₂₂ H ₃₀ O	310	

(Continued on following page)

TABLE 1 (Continued) GC-MS analysis of phytoextract of *T. cordifolia*

Sl No	Rt	Name of the compounds	Molecular formula	Molecular Wt (g/mol)	Structure
10	14.97	5-Isopropyl-2,8-dimethyl-9-oxatricyclo [4.4.0.0 (2,8)] decan-7-one	C ₁₄ H ₂₂ O ₂	222.32	
11	17.79	17-Octadecynoic acid	C ₁₈ H ₃₂ O ₂	280.4	
12	17.96	Z,Z,Z-4,6,9-Nonadecatriene	C ₁₉ H ₃₄	262.5	
13	20.51	n-Propyl cinnamate	C ₁₂ H ₁₄ O ₂	190.24	
14	26.71	Dasycarpidan-1-methanol, acetate (ester)	C ₂₀ H ₂₆ N ₂ O ₂	326.4	
15	28.86	Piperine	C ₁₇ H ₁₉ NO ₃	285.34	

inside the cell membrane and increasing peroxidation of lipids. Once, the AgNPs penetrate the cells they destabilize the intracellular biomolecules and structures leading to the death of the bacterial cells (Rozhin et al., 2021). Table 1 below describes about the potential applications of AgNPs in different fields.

In this study, we threw light on the green synthesis of AgNP from the leaf extracts of *T. cordifolia* and tested the efficacies of the phytoextract alone as well as biogenic AgNPs as antibiofilm agents against the biofilms formed by *S. aureus*. This study also investigated the antibacterial properties of the AgNP nanoconjugates biogenically synthesized from *T. cordifolia* leaf extract along with investigation of anti-biofilm activity. The leaf extracts of *T. cordifolia* are generally enriched with diterpenoids, sterols, aliphatics and alkaloids. These bioactive compounds can potentially act as reducing agents in the biosynthesis of AgNPs. Pertinent to the increased resistance against the available antibiotics, AgNP nanoconjugates have been synthesized to overcome the problem of antibiotic resistance as well as to punctuate the persistence of acute and chronic biofilm-associated infections caused by *S. aureus* since biofilms are extremely

impermeable to the penetration of antibiotics or other antibacterial agents due to the presence of multiple drug efflux pumps and antibiotic inactivating enzymes. The nanoconjugates of silver synthesized from the leaf extract of *T. cordifolia* can penetrate deeper and reach the sessile bacterial cells residing within the biofilms of *S. aureus* due to their small sizes.

2 Materials and methods

2.1 Preparation of *Tinospora cordifolia* leaf extract

The leaves of *T. cordifolia* were collected from the local gardens of West Bengal under the guidance of Botanist, India and they were washed with double distilled water and dried. After that, the leaves were crushed with 95% methanol followed by incubation for 16–24 h at room temperature (Quave et al., 2012). Then the phytoextract was sieved using a gauge cloth followed by centrifugation at 5000 rpm for

Field of application	Utility of the AgNPs in the field	References
Anaesthetics	Breathing mask coating and coating of endotracheal tubes for mechanical support of ventilation	Mocanu et al. (2013)
Diagnostics	Pyramids made of nanosilver to enhance the process of biological detection. Ultrafast and ultrasensitive platforms for clinical diagnosis of myocardial infarction. Fluorescence associated sensing of RNA with turntable coated with AgNPs having plasmonic properties	Lee and Jun (2019)
Drug therapy	Remote controlled LASER light associated microcapsule opening	Ivanova et al. (2018)
Optics	Coating of contact lens	Nguyen et al. (2021)
Imaging	Dendrimer and silver nanoconjugate to label cells. Silver sand nanoconjugates as fluorescent core shell nanoballs used in molecular and cellular imaging of the malignant cells	Homan et al. (2010)
Neurology	Catheter coating for drainage of cerebrospinal fluid (CSF)	Wallace et al. (2017)
Orthopaedics	Bone cement additive used in implantable substances manufactured with layers of clay and AgNP stabilized with starch. Intramedullary nail coating used in fractures of long bones. Implant coating in orthopaedic stockings for replacement of joints.	Poon et al. (2021)
Patient care	AgNP used as superabsorbent nanogel for incontinence substances	Shen et al. (2018)
Pharmaceutical	Dermatitis treatment. AgNPs inhibit the replication of HIV-I, helps in treating ulcerative colitis, wound healing characteristics	Mathur et al. (2018)
Biomedical	Anti-fungal, anti-bacteria, anti-inflammatory, anti-viral, anti-cancer and anti-angiogenic agent	Burdusel et al. (2018)
Textiles	Medicinal devices and textiles, textile coating to block UV rays	Mirzaei et al. (2021)
Food industries	Food processing and packaging using AgNP coatings	Zorraquin- Pena et al. (2020)
Environmental applications	Water and air disinfection, disinfection of groundwater, drinking water and biological wastewater	Jaffri and Ahmad (2018)

10 min and the supernatant was collected and stored at 4°C for further use. The methanol used was of analytical grade and purchased from HiMedia.

2.1.1 Synthesis of biogenic AgNP preparation using leaf extract of *Tinospora cordifolia*

10% w/v of properly washed and dried *T. cordifolia* leaves were crushed in 20 mL of double distilled water. The aqueous extract was then sieved with a gauge cloth followed by centrifugation at 5,000 rpm for 10 min and the supernatant was collected. 90 mL of 1 mM silver nitrate solution was prepared, to which, 10 mL of phytoextract was added dropwise while stirring with a magnetic stirrer (Jalal et al., 2016). The biosynthesis of AgNPs was confirmed by the change in color from white to reddish brown. This reaction mixture was further centrifuged at 5000 rpm for 10 min and the pellets were collected followed by washing twice with distilled water and re-suspended in phosphate buffered saline (PBS).

2.2 Characterization of the biologically synthesized AgNPs

The biogenically synthesized AgNPs were characterized using various techniques such as UV-Vis spectroscopy, Field Emission Scanning Electron Micrograph (FE- SEM), Dynamic Light Scattering (DLS) and measurement of zeta potential, which are all listed below.

2.2.1 Characterization using UV-Vis spectroscopy

The synthesis and stability of biogenic AgNPs can be detected by the UV-Visible spectra of the AgNP solution (Sharma et al., 2020). Double distilled water was used as blank. The absorbance spectra of

the reddish brown AgNP solution were recorded at wavelengths ranging from 300 to 700 nm by using Lasany LI- 294/ 296 Microprocessor single beam UV-Vis spectrophotometer.

2.2.2 Characterization by using Field Emission Scanning Electron Microscope (FE- SEM)

The biogenically synthesized AgNPs were dropped cast on a cover slip and oven-dried (Jalal et al., 2016). Then the dried sample of AgNPs was visualized under JEOL JSM- 7600F Field Emission Scanning Electron Microscope at a voltage of 15 kV to determine the surface morphology of the biogenic AgNPs.

2.2.3 Characterization by using Dynamic Light Scattering (DLS) and zeta potential measurement

The hydrodynamic diameter, zeta potential (surface charge), and particle distribution intensity (polydispersity index/PdI) of AgNPs can be examined using DLS by the process of measuring the dynamic variations of the intensity of light scattering caused by Brownian motion of the particles (Elamawi et al., 2018). All the measurements were performed in triplicate with 1 min of equilibration time at 25°C temperature in a Zetasizer Nanoseries (Nano- ZS). The mode of data processing was set to high multi-modal resolution.

2.3 Cultivation of the *Staphylococcus aureus* ATCC 23235 working strain and development of biofilm

Biofilm forming strain of *Staphylococcus aureus* ATCC 23235 was grown in Luria Bertani broth (SRL) overnight at a

temperature of 37°C at pH 7.4. The bacterial strains that were used in this study were cultured within an Erlenmeyer flask of 100 mL containing 50 mL of Luria Bertani broth at pH seven and were incubated for 24 h at 37°C. The biofilm formation by the working bacterial strain was analyzed by the use of the microplate assay method. Biofilm growth depends on the synergistic activities of the concentrations of sugar and salt. The optimal concentration for the formation of biofilms was found by adding various concentrations of glucose (0.25%–10% w/v) and NaCl (0.5%–7% w/v) in the culture broth. All the experimental setups were incubated at 37°C for a period of 72 h.

2.4 Study of antimicrobial activities of phytoextract and biogenic AgNPs

Antimicrobial activities of phytoextract from *T. cordifolia* and biogenic AgNPs and standard antibiotics were detected by analyzing the diameter (in millimeters) of the inhibition zones obtained by agar well diffusion method. Various agar plates containing the test bacterial strain were treated with phytoextracts, AgNPs, and antibiotics at different concentrations in wells, punctured on the plates. The plates were incubated at 37°C for 24 h and observed for inhibition zones in accordance with the specifications made by the National Committee for Clinical Laboratory Standards (Patra et al., 2014).

2.5 Determination of minimum inhibitory concentration (MIC)

The MIC values of the phytoextract from *T. cordifolia* and the biogenic AgNPs were determined against *S. aureus* ATCC 23235 by the technique of microdilution (Jeyaseelan and Jashothan, 2012). 10 µL of *S. aureus* ATCC 23235 was inoculated in 5 mL of LB broth and treated with phytoextract (concentrations ranging from 10 to 50 µg/mL) and biogenic AgNPs (concentrations ranging between 1 and 50 µg/mL), except in the control tubes. The test tubes were incubated at 37°C for a period of 24 h and the bacterial growth intensity was measured spectrophotometrically at 660 nm.

2.6 Determination of minimum biofilm eradication concentration

The minimum biofilm eradication concentration was calculated using an MTT assay (Baishya et al., 2016). In 96-well plates, added 100 µL of LB broth and 2 µL of *S. aureus* ATCC 23235 was added to each well and incubated at 37°C for 72 h. The LB broth was discarded after 72 h at 37°C to remove the planktonic cells, and 20 µL of phytoextract and biogenic AgNPs was added to all of the wells except the control (untreated microbe) followed by the addition of MTT reagent and mixing it well with the help of cyclomixer including control and incubated at 37°C for 4 h and the absorbance was measured at 550 nm using Thermo Scientific Multiskan Sky ELISA plate reader.

2.7 Determination of reduction of biofilm formation by *Staphylococcus aureus* ATCC 23235 on treatment with phytoextract and biogenic AgNPs

The microtiter plate technique was used to estimate biofilm formation quantitatively (Lahiri et al., 2021b). In this method, six-well plates were used and each well was filled with 5 mL LB Broth a single coverslip was dropped in each of the wells, and 20 µL of *S. aureus* ATCC 23235 cells was added to all the wells. After 72 h of incubation at 37°C, 100 µL of treatment was added and kept in the incubator for 24 h at 37°C. The planktonic cells were gently removed and the coverslip was taken out and stained with crystal violet dye (0.1% w/v in acetic acid) for 1 min. After discarding the excess crystal violet dye, the stained cells were treated with acetic acid for 1 min and absorbance of the acetic acid from the coverslip was measured at 540 nm spectrophotometrically. A sterile growing medium only and a functioning solution were employed as negative and positive controls, respectively, in the assay. The following formula was used to compute the percentage of biofilm inhibition:

$$\begin{aligned} &\text{Percentage (\% of biofilm inhibition)} \\ &= \frac{(\text{OD at 540 nm of non-treated cells}) - (\text{OD at 540 nm of treated cells})}{(\text{OD at 540 nm of non-treated cells})} \times 100 \quad (1) \end{aligned}$$

2.8 Detection of viability and revival count of the sessile bacterial cells

The bacterial cells were grown in an LB broth containing chitin flakes (0.1% w/v) for a period of 72 h and then the broth was discarded to remove the planktonic cells and the chitin flakes were washed with sterile double distilled water. Followed by washing, fresh LB broth was added followed by the addition of 240 µL of phytoextract, AgNPs, and standard antibiotic (tetracycline). The bacterial growth was spectrophotometrically determined at 660 nm at regular time intervals of 2 h (Ding et al., 2015). After measuring the viability count of the sessile biofilm cells, the remaining broth from the test tubes was discarded and the sessile cells, which were attached to the chitin flakes were washed with sterilized double distilled water to eliminate any planktonic cells before being refilling with 5 mL of fresh LB broth in each test tube. The density of these cells was spectrophotometrically measured at 660 nm to detect any revival of the biofilm-forming cells after withdrawing the treatment.

2.9 Enfeeblement of extracellular polymeric substances (EPS)

The mechanism of extraction of EPS associated with the biofilm-forming bacterial cells, 30 µL of *S. aureus* ATCC 23235 inoculum was added to 15 mL of LB broth containing chitin flakes and grown for a period of 72 h at a temperature of 37°C. After 72 h, the LB broth was discarded to eliminate the planktonic cells and the chitin flakes were washed with sterile double-distilled water. Then 240 µL of phytoextract and AgNPs were added to the respective conical flasks, except for the control, and incubated for a period of 1 h. 5 mL of phosphate-buffered saline (PBS) at pH 7.2 was added in each conical flask and cyclospinned for 2–3 min for breakage of the

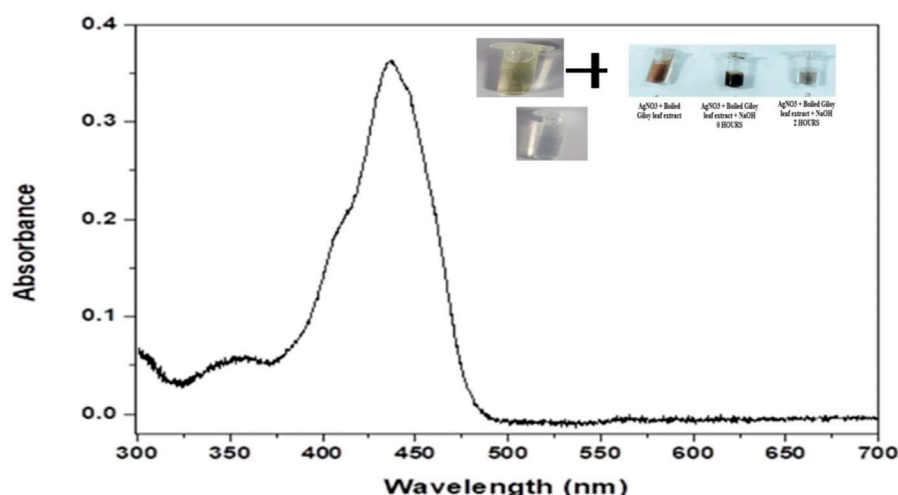


FIGURE 1

Graphical representation UV-Visible absorption spectra of AgNPs from leaf extract of *Tinospora cordifolia* showing absorbance peak at the wavelength of 430 nm.

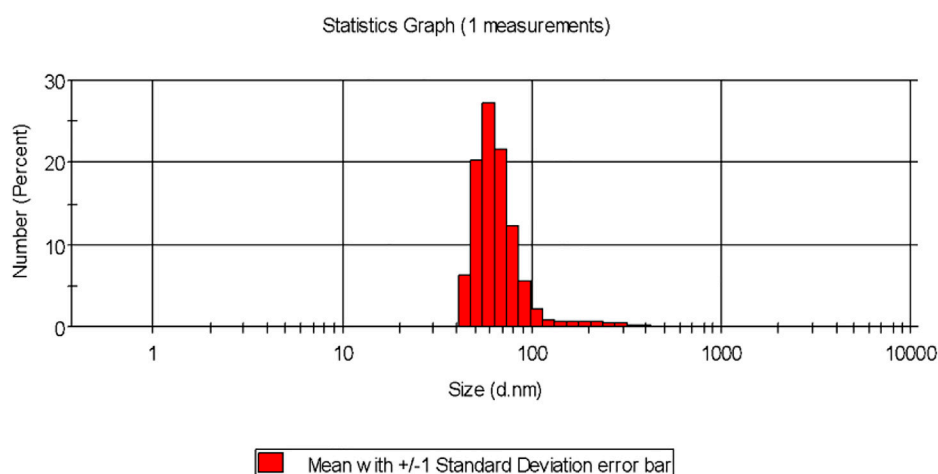


FIGURE 2

Particle size distribution of the biogenic AgNP solution synthesized from the leaf extract of *Tinospora cordifolia*.

biofilm by hindering the interactions and keeping the EPS components together within the matrix. The PBS was then transferred to 15 mL flacon tubes followed by centrifugation at 6000rpm for 15 min s at 4°C. The pellet was re-suspended in 2.5 mL of 10 mM TrisHCl (at pH 7.8). 20mM beta-mercaptoethanol (BME) and 1 mM phenylmethylsulfonyl fluoride (PMSF) was added to the above suspension in a ratio of 1:1. The cell suspension was provided with heat shock by placing it between hot water and ice for 5 min each and the process was repeated for 4–5 times for all the samples. The suspensions were then centrifuged at 5000 rpm for 30 min at 4°C and the supernatant was transferred in fresh tubes followed by the addition of 1 mL of 10% Trichloroacetic acid (TCA) in acetone and incubated for at least 72 h at 4°C. After 72 h, the suspensions were again centrifuged at 5000 rpm for 30 min at 4°C followed by the washing of the protein pellet with 90% acetone and air drying. The pellet was dissolved in 500 µL of rehydration buffer (Teanpaisan et al., 2017).

2.9.1 Reduction in total carbohydrate content of EPS

The content of carbohydrates present in the EPS was quantified using the Anthrone method (Meade et al., 1982). In this method, to each of the EPS samples, 50 µL of 80% phenol was added and mixed completely for 2 mins using vortex followed by the addition of 2 mL of concentrated sulfuric acid and the color turned to deep red. The mixture was incubated at room temperature for 10 min before being measured spectrophotometrically for a reduction in carbohydrate content in EPS at 490 nm.

2.9.2 Reduction in total protein content of EPS

Protein content was estimated by using Bradford assay, which is the shortest sensitive method of simple dye binding assay and was developed by Marion M. Bradford in 1976. In this method, 2 µL of samples were loaded in a 96-well plate with 100 µL of Bradford reagent followed by incubation at room temperature for 5 min, and the

TABLE 2 Size of the particle and zeta Potential analysis.

Type of NPs	Polydispersity index (PDI)	Size of the particle (nm)	Zeta potential (mV)
Green-synthesized AgNPs	0.201 ± 0.005	43.82 ± 1.02–91.28 ± 1.12	−11.37 mV

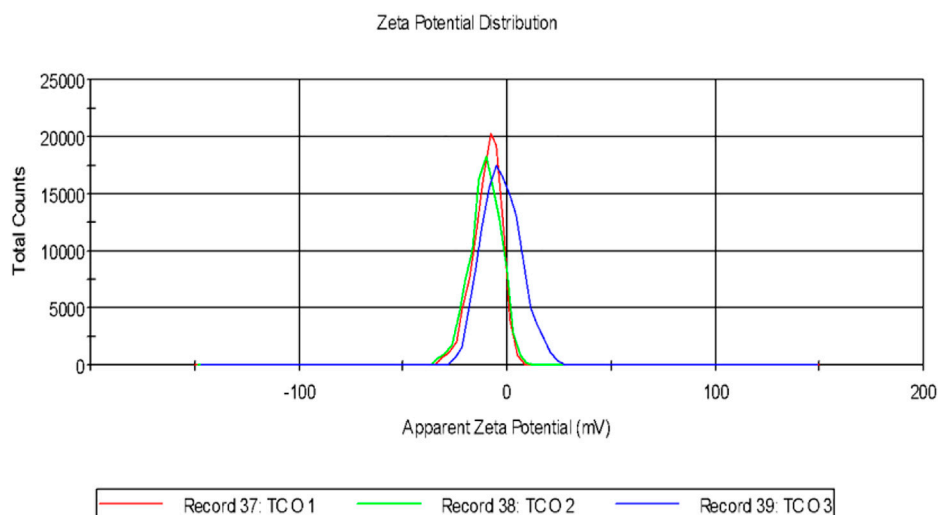


FIGURE 3
Zeta potential of AgNPs biosynthesized from the leaf extract of *Tinospora cordifolia*.

absorbance of protein content in the EPS was measured using Thermo Scientific Multiskan Sky ELISA plate reader at 595 nm.

2.9.3 Reduction in total eDNA content of EPS

For estimating the eDNA content of EPS, the EPS samples were diluted with cold 100% ethanol in a 1:3 ratio followed by incubation at 4°C for 2 h and spectrophotometrically measured at a wavelength of 560 nm.

2.10 FTIR analysis of the EPS matrix after treatment

Biofilm produced by *S. aureus* ATCC 23235 on chitin flakes in LB broth for 72 h at 37°C was treated separately with phytoextract of *T. cordifolia* and the biogenic AgNPs followed by drying in a hot air oven. The FT-IR spectra were recorded in the range between 450 and 4000 cm^{−1} with a PerkinElmer FT-IR Spectrometer (Frontier) (Pati et al., 2020).

2.11 Detection of biofilm reduction by scanning electron microscopy (SEM)

Biofilms developed on chitin flakes in LB broth after incubation for 72 h at 37°C, were treated with the phytoextract as well as with the biogenic AgNPs and incubated for 2 h at 37°C. Thereafter, the broth was discarded and the chitin flakes were washed with 0.9% (w/v) NaCl for removing any leftover planktonic cells. The samples were then suspended in 2.5% glutaraldehyde for 20 mins followed by repeated dehydration using upgraded ethanol. The dried chitin flakes

containing the sessile colonies were visualized under a ZEISS EVO-MA 10 scanning electron microscope (Lahiri et al., 2021a).

2.12 Reagents and chemicals

All chemicals and reagents used in the experimentation are of analytical grade and were purchased from HiMedia and SRL.

2.13 Statistical analyses

All the experiments were performed in triplicate and the results were depicted as mean ± SD (standard deviation).

3 Results and discussion

3.1 Identification of the bioactive compounds from the phytoextract of *Tinospora cordifolia*

It was observed that the phytoextract of *T. cordifolia* comprised of different chromophoric groups such as -OH, phenolic, unsaturated carbonyls, etc. Mass spectrum interpretation through GC-MS of unidentified bioactive compounds and comparing them with the database stored in National Institute Standard and Technology (NIST) library verified the biochemical identity of 15 compounds from *T. cordifolia* extract. The molecular formula, name of the compounds, peak area, molecular weight, and bioactivity of the experimental materials were determined. The relative percentage

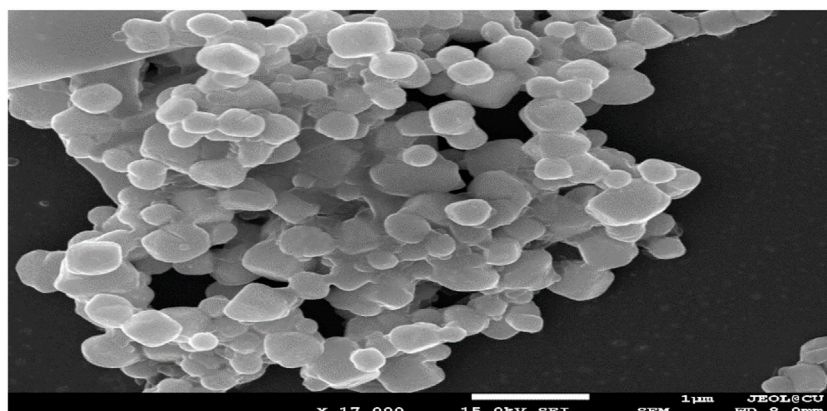


FIGURE 4
FE- SEM images of biogenic AgNPs from *T. cordifolia* leaves.

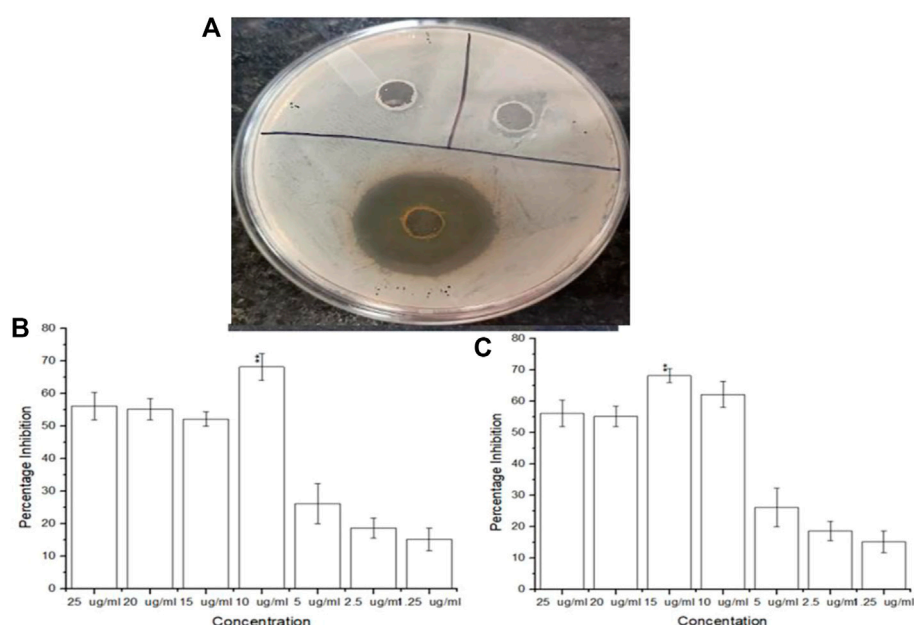


FIGURE 5
(A) Inhibitory zones on addition of AgNPs (B) Antimicrobial efficacy of biogenic AgNPs from *Tinospora cordifolia* and (C) Antimicrobial efficacy of the phytoextract of *Tinospora cordifolia*.

composition of each bioactive compound was calculated by comparison with the average peak area with respect to the total area (Table 1).

3.2 Characterization of the biogenic AgNPs

3.2.1 Determination of UV- Vis spectra of the biogenically synthesized AgNPs

UV-Vis spectroscopy acts as an important technique for the purpose to detect the synthesis of AgNPs with the monitoring of electronic structures and optical properties of the synthesized NPs.

The electron clouds undergo oscillation on the surface of the NPs possessing the ability to absorb the electromagnetic waves possessing a particular frequency. This mechanism is termed surface plasmon resonance (SPR) which in turn is being recorded by the use of a UV-Vis spectrophotometer (Smitha et al., 2008). The UV- Visible spectra of the biogenically synthesized AgNPs using the leaf extract of *T. cordifolia* presented a peak at 430 nm (Figure 1) in correspondence with the surface plasmon response of AgNPs. The peak was similar to the work performed by Marhaby and Seoudi 2016 which also depicted the AgNPs synthesized by 4-Nitrophenol fetched at a peak at 423 nm (Almarhaby and Seoudi, 2016). Another work showed the peak of biogenic AgNPs from *Clinacanthus nutans* at 450 nm (Mat Yusuf

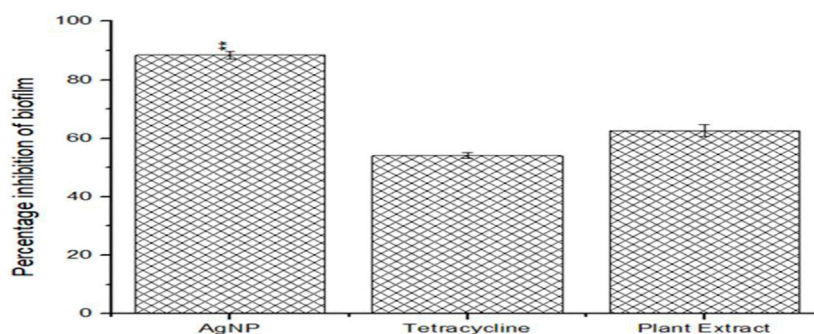


FIGURE 6

Anti-biofilm efficacies of biogenic AgNPs, phytoextract and antibiotic Tetracycline against *Staphylococcus aureus* ATCC 23235.

et al., 2020). Biogenic synthesis of AgNPs is based on conditions like the type of solvent being used, the reducing agent, and the non-toxic substance being used for the purpose of stabilizing the nanoparticles (Raveendran et al., 2003). The change in the intensity of the wavelength is based on the increase in the number of NPs that are formed as a result of the reduction of silver ions along with the biomolecules that are present within the system. It is usually observed that the SPR bands become sharper and undergoes a shift to shorter wavelengths with the rise in temperature indicating a decrease in the size of the particles. The reduction in the size of the NPs is due to an enhancement in the reduction time during the mechanism of synthesis. Consumption of silver ions takes place during the process thereby blocking the phenomenon of secondary reduction taking place on the surface of AgNPs (Yang and Li, 2013). It has been observed that NPs that absorb wavelengths between 400 and 900 nm are spherical in shape (Yusuf et al., 2020).

4 Particle size distribution and surface charge analysis of the biogenic AgNPs

Dynamic light scattering (DLS) is the technique used for the purpose of measuring the average size of the NPs within liquid suspension requiring fewer volumes of samples. The measurement of the size is based on the Brownian motion theory which denotes the random movement of the particles randomly in suspension or gas. The dynamic fluctuation from the intensity of light scattering is used for measuring the average size of the NPs (Murdock et al., 2008). The size of the biogenically synthesized AgNPs ranged between 43.82 ± 1.023 nm– 91.28 ± 1.12 nm (Figure 2). A considerable number of peaks appeared below 100 nm (Table 2).

It was observed that the calculated PDI was 0.201 ± 0.005 for the green-synthesized NPs which is within the range from 0–1 in which 0 signifies monodisperse and one is polydisperse (Murdock et al., 2008). Thus the result signifies that the synthesized AgNPs were present in the monodisperse phase and aggregations of particles were minimum. Experimental conditions have a direct influence on morphology, size, and stability (Ghorbani et al., 2011). The agglomeration of NPs sometimes occurs due to the presence of bioactive compounds present within the solution (Shameli et al., 2012). The charges of the moving particles under the impact of the electric field can be calculated with the help of Zeta Potential (Bhattacharjee, 2016). Negative charges

were observed around the particle which does not represent the actual surface charge (Figure 3). The presence of the negative charge is due to the absorption of bioactive compounds on the surface of AgNPs (Moldovan et al., 2016). Temperature plays a vital role in the regulation of the stability of the NPs and thereby increases the value of zeta potential. The high amount of zeta potential results in the development of repulsive forces thereby preventing aggregation of the particles (Priyadarshini et al., 2013).

4.1 FE- SEM analyses of the AgNPs

Green-synthesized AgNPs were studied under FE-SEM and it was observed that the NPs were spherical in shape (Figure 4) that was as per the SPR peak being observed in the UV-spectroscopy. The peak was observed at 430 nm which indicated the spherical nature of the NPs. In the presence of a protective agent, the sides of the NPs showed slightly elliptical or oval (Ahila et al., 2016). High surface tension and energy resulted in the agglomeration of the NPs (Wang et al., 2020).

4.2 Antimicrobial activity determination of the phytoextract and AgNPs against *Staphylococcus aureus* ATCC 23235

Amongst the phytoextract and the biogenic AgNPs, the biogenic AgNPs depicted zones of inhibition of 12–18 mm while that of the phytoextract was 10–15 mm (Figure 5A). A control setup was arranged using ethanol and tetracycline that did not show significant antimicrobial activity against *S. aureus* ATCC 23235 proving that the test bacteria developed resistance against ethanol as well as a tetracycline antibiotic. The biogenic AgNPs possessed a MIC value of as low as 10 μ g/mL (Figure 5B) while the phytoextract showed a MIC value of 15 μ g/mL (Figure 5C), which is quite higher in comparison to the AgNPs. This determines that the phytoextract along with AgNPs can have better effects against *Staphylococcus aureus* ATCC 23235 than phytoextract alone. This may be due to the higher penetration capacities of the AgNPs, which can penetrate deep within the bacterial cells and bring about their destruction. This observation was similar to the previously published work where the AgNPs exhibit an inhibitory effect within the range of 4–64 μ g/mL (Attallah et al., 2022).

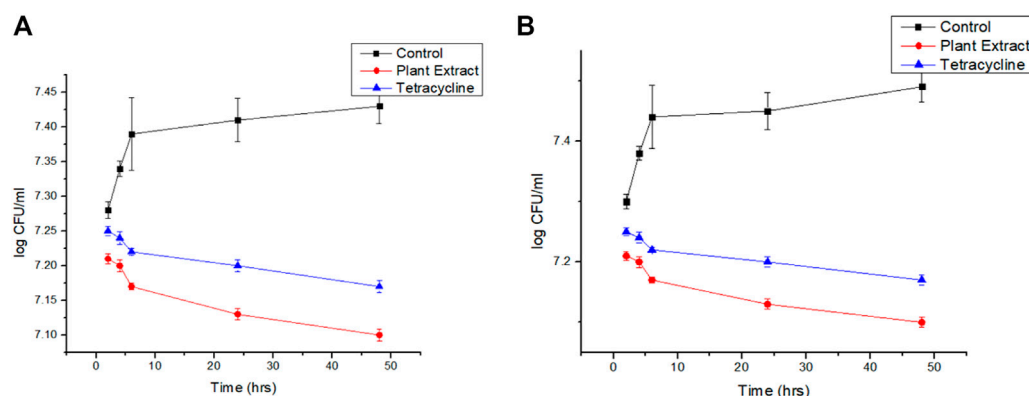


FIGURE 7

(A): Viability count reduction followed by treatment with phytoextract, AgNPs, and tetracycline and (B) Revival of the cells after withdrawal of the treatment.

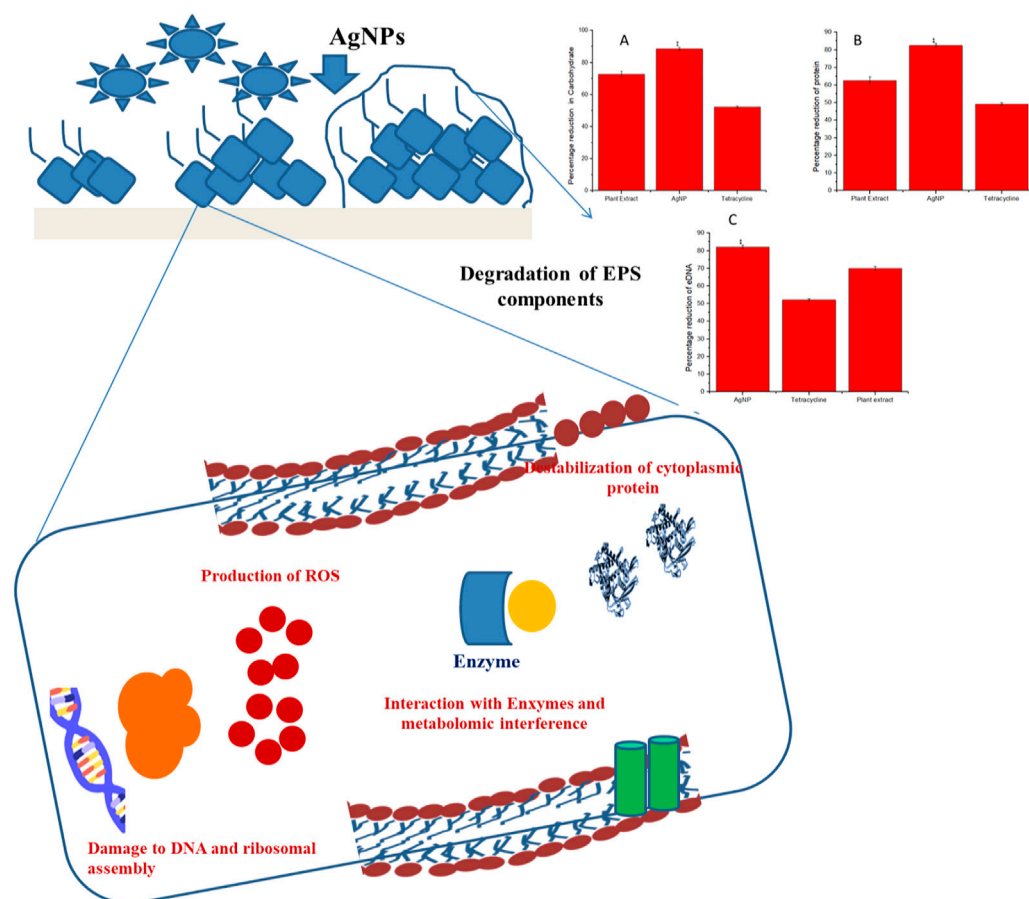


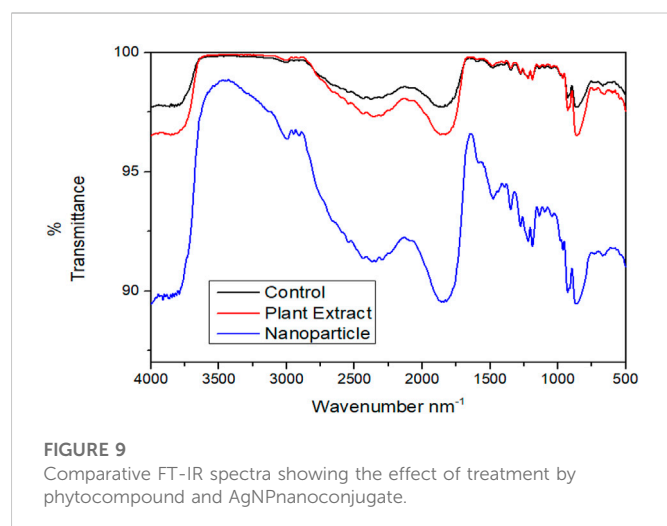
FIGURE 8

Probable mode of action involved in the eradication of biofilm matrix by biogenically synthesized AgNPs from *Tinospora cordifolia*.

4.3 Antibiofilm property determination of phytoextract and AgNPs

Both the phytoextract as well as the biogenic AgNPs demonstrated antibiofilm properties against *S. aureus* ATCC 23235 (Figure 6).

However, the biogenic AgNPs showed a percentage reduction of more than $83.14\% \pm 0.56\%$ of the biofilm, while that of the phytoextract and tetracycline were around $60.12\% \pm 1.23\%$ and $50.25\% \pm 0.87\%$ respectively. The reduction of biofilm by AgNPs were found to be statistically significant ($p < 0.01$) Figure 1. The



biosynthesized AgNPs exhibited greater efficacy of action due to the doped bioactive compounds from the plant source (Miškovská et al., 2022).

4.4 Reduction in viability and revival count of the sessile cells after treatment

It was found that the viability count of the sessile colonies of *Staphylococcus aureus* ATCC 23235 demonstrated the highest reduction in the presence of biogenic AgNP than the phytoextract and tetracycline (Figure 7A). The efficacy of the biofilm eradication was further validated by the negligible revival of the cells after the withdrawal of the respective treatments for 24 h (Figure 7B).

4.5 Reduction in the contents of the biofilm matrices of *Staphylococcus aureus* ATCC 23235 by biogenic AgNPs and phytoextract

Structural composition disruption of the biofilm matrices, namely carbohydrates, proteins, and eDNA leads to biofilm destabilization. It

was observed that the maximum reduction of carbohydrates, proteins, and eDNA of the EPS matrix was brought about due to the activity of the biogenically synthesized AgNPs than the phytoextract alone or tetracycline. Carbohydrate content was reduced by about $90.12\% \pm 0.56\%$ by the biogenic AgNPs while that with phytoextract and tetracycline were about $65\% \pm 1.03\%$ and $50\% \pm 0.98\%$ (Figure 8A). The content of protein was significantly reduced by around $85\% \pm 1.26\%$ by the biogenic AgNPs while that with phytoextract and tetracycline were around $65\% \pm 0.75\%$ and $45\% \pm 1.02\%$ (Figure 8B). The eDNA content was reduced to about $80\% \pm 1.23\%$ by the biogenic AgNPs in comparison to the phytoextract, which reduced the eDNA content by $65\% \pm 0.85\%$, and tetracycline, which decreased the content of eDNA by $50\% \pm 0.45\%$ (Figure 8C).

4.6 FTIR analysis of the EPS modification by the biogenic AgNPs and phytoextract

FT-IR was performed for analyzing the modifications in the functional groups of the EPS matrix of *S. aureus* ATCC 23235 after treating with the biogenically synthesized AgNPs and the phytoextract (Figure 9). Remarkable modifications in the spectral regions of polysaccharides ($890\text{--}1175\text{ cm}^{-1}$), lipids ($3,000\text{--}2800\text{ cm}^{-1}$), proteins ($1700\text{--}1500\text{ cm}^{-1}$), and nucleic acids ($1,300\text{--}900\text{ cm}^{-1}$) were analyzed in the FT-IR spectroscopy. The biogenic AgNPs brought about the highest reduction in peak intensities, shape alterations, and shifts in wavelengths of *S. aureus* ATCC 23235 in comparison with the control sample and sample treated with phytoextract. This suggests that the biogenic AgNPs could directly interact and decrease the concentration of various EPS constituents such as polysaccharides, lipids, and nucleic acids as evidenced by the reduced peak intensity data.

4.7 Photomicrographic analyses of the removal of biofilm by treatment with biogenic AgNPs and phytoextract

The best anti-biofilm activity was observed with the biogenic AgNPs than the phytoextract and this indicates that the phytoextract acts synergistically well when combined with NPs than phytoextract alone. AgNP- treated (Figure 10B) and

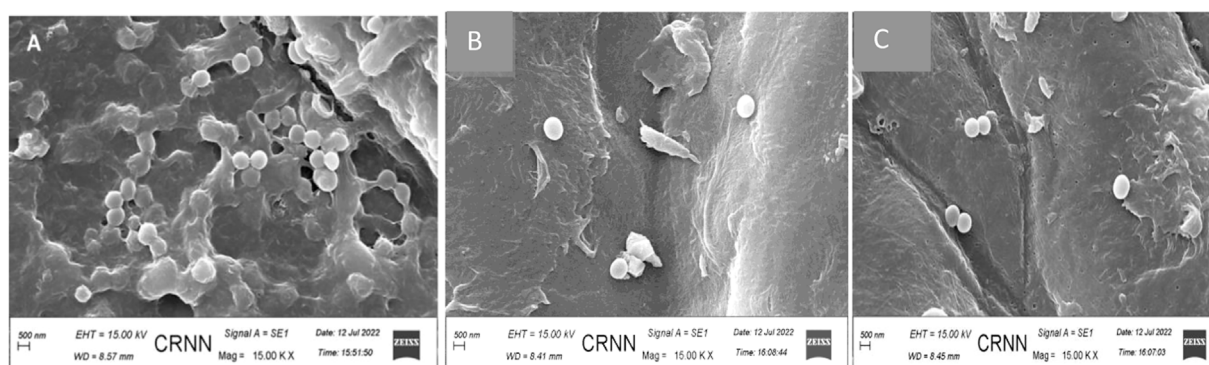


FIGURE 10
Scanning electron micrograph of *Staphylococcus aureus* (A) before and (B) after treatment with biogenic AgNPs (C) *Staphylococcus aureus* ATCC 23235 after treatment with phytoextract seen at a magnification of $\times 15000$.

phytoextract-treated (Figure 10C) bacterial sessile cells were observed under SEM, which depicted clear biofilm disruption of the sessile cells after treatment as compared with the control samples (Figure 10A).

5 Conclusion

The application of natural products for human welfare is time immemorial and their usage are getting enhanced with every passing day. *Tinospora cordifolia* is a widely available weed possessing numerous health-beneficial activities (Ahmad et al., 2021) and can be used successfully for irreversible disruption of the biofilm-associated cells of *S. aureus*. *T. cordifolia* can also be effectively used in the green synthesis of biogenic AgNPs from silver nitrate. Such kind of NP synthesis can be deemed to be environmentally friendly since it is free from any type of harmful chemicals or reducing substances since the entire NP synthesis process is biogenic. However, the exact mode of action of AgNPs on bacterial cells is yet to be known in detail. Some of the experimental results indicated that these NPs mainly interact with the cell surfaces of several bacteria (Mikhailova, 2020). On the surfaces of cells, the AgNPs get adhered to the cell wall and cell membrane of bacteria thereby penetrating deep inside the intracellular organelles and modifying the biomolecular signal transduction pathways. In the case of Gram-positive bacteria such as *S. aureus*, the AgNPs find their way to the cytoplasm by membrane property modification leading to the dissipation of proton motive force (PMF) and lead to the damage in the bacterial cell due to membrane destruction (Durán et al., 2016). The penetration of AgNPs lead to the development of oxidative stress within the cells leading to the generation of reactive oxygen species (ROS), which oxidize the double bonds of the membrane fatty acids allowing the production of free radicals and damage to the cell membrane (Vega-Baudrit et al., 2019). The preliminary step for the formation of biofilms gets inhibited by the presence of AgNPs. This is because the AgNPs can bind with the cellular surface thereby altering the adhesive compounds such as extra polymeric matrices, which are involved in the aggregation of bacterial cells and biofilm formation (Gurunathan et al., 2014).

The biologically synthesized AgNPs have demonstrated good anti-biofilm efficacy, suggesting that they could be employed as an antibiofilm weapon against the biofilm-associated infections caused by *S. aureus*. Experimental observations clearly indicated that biofilm removal is accomplished through irreversible denaturation of EPS matrices and subsequent inhibition of biofilm formation by *S. aureus*. The mode of action of these biogenic AgNPs synthesized

from the leaf extract of *T. cordifolia* is mainly by EPS matrix denaturation. Hence, these NPs can act as potential drug candidates for controlling chronic and persistent infections caused by the biofilms of *S. aureus*.

Data availability statement

The original contributions presented in the study are included in the article/supplementary material, further inquiries can be directed to the corresponding authors.

Author contributions

Conceptualization, SG, DL, MN, TS, SiP, SM, SoP, HE, and RR; writing—original draft preparation, DL, MN, TS, and RR; writing—review and editing, AA, SG, DL, MN, TS, SiP, SM, SoP, HE, and RR. All authors have read and agreed to the published version of the manuscript.

Acknowledgments

The authors extend their appreciation to the Researchers supporting Project number (RSP-2021/98) King Saud University, Riyadh, Saudi Arabia for financial support.

Conflict of interest

Author SiP was employed by the company NatNov Private Limited.

The remaining authors declare that the research was conducted in the absence of any commercial or financial relationships that could be construed as a potential conflict of interest.

Publisher's note

All claims expressed in this article are solely those of the authors and do not necessarily represent those of their affiliated organizations, or those of the publisher, the editors and the reviewers. Any product that may be evaluated in this article, or claim that may be made by its manufacturer, is not guaranteed or endorsed by the publisher.

References

- Abed, K., and Mohammed, A. E. (2021). Synergistic and antagonistic effects of biogenic silver nanoparticles in combination with antibiotics against some pathogenic microbes. *Front. Bioeng. Biotechnol.* 9, 652362. doi:10.3389/fbioe.2021.652362
- Ahila, N. K., Ramkumar, V. S., Prakash, S., Manikandan, B., Ravindran, J., Dhanalakshmi, P. K., et al. (2016). Synthesis of stable nanosilver particles (AgNPs) by the proteins of seagrass *Syringodium isoetifolium* and its biomedical properties. *Biomed. Pharmacother.* 84, 60–70. doi:10.1016/j.biopha.2016.09.004
- Ahmad, S., Zahiruddin, S., Parveen, B., Basist, P., Parveen, A., Parveen, R., et al. (2021). Indian medicinal plants and formulations and their potential against COVID-19—preclinical and clinical research. *Front. Pharmacol.* 11, 578970. doi:10.3389/fphar.2020.578970
- Al-Marzoqi, A. H., Kareem, S. M., Alhuchaimi, S., Hindi, N. K. K., and Ghasemian, A. (2020). Decreased vancomycin susceptibility among *Staphylococcus aureus* clinical isolates and postulated platforms to explore rational drugs. *Rev. Res. Med. Microbiol.* 31 (3), 111–116. doi:10.1097/RRM.0000000000000204
- Almarhaby, F., and Seoudi, R. (2016). Preparation and characterization of silver nanoparticles and their use in catalytic reduction of 4-nitrophenol. *World J. Nano Sci. Eng.* 06, 29–37. doi:10.4236/wjnse.2016.61003
- Attallah, N. G. M., Elekhawey, E., Negm, W. A., Hussein, I. A., Mokhtar, F. A., and Al-Fakhry, O. M. (2022). *Vivo* and *in vitro* antimicrobial activity of biogenic silver nanoparticles against *Staphylococcus aureus* clinical isolates. *Pharm. (Basel)* 15, 194. doi:10.3390/ph15020194

- Baishya, R., Bhattacharya, A., Mukherjee, M., Lahiri, D., and Banerjee, S. (2016). Establishment of a simple reproducible model for antibiotic sensitivity pattern study of biofilm forming *Staphylococcus aureus*. *Mat. Today Proc.* 3, 3461–3466. doi:10.1016/j.matpr.2016.10.028
- Bhattacharjee, S. (2016). DLS and zeta potential – what they are and what they are not? *J. Control. Release* 235, 337–351. doi:10.1016/j.jconrel.2016.06.017
- Burdusel, A. C., Gherasim, O., Grumezescu, A. M., Mogoantă, L., Ficai, A., and Andronescu, E. (2018). Biomedical applications of silver nanoparticles: An up-to-date overview. *Nanomaterials* 8 (9), 681. doi:10.3390/nano8090681
- Capek, I. (2004). Preparation of metal nanoparticles in water-in-oil (w/o) microemulsions. *Adv. Colloid Interface Sci.* 110, 49–74. doi:10.1016/j.cis.2004.02.003
- Chatterjee, S., Maiti, P., Dey, R., Kundu, A., and Dey, R. (2014). Biofilms on indwelling urologic devices: Microbes and antimicrobial management prospect. *Ann. Med. Health Sci. Res.* 4, 100–104. doi:10.4103/2141-9248.126612
- Ding, X., Peng, X.-J., Jin, B.-S., Xiao, M., Chen, J.-K., Li, B., et al. (2015). Spatial distribution of bacterial communities driven by multiple environmental factors in a beach wetland of the largest freshwater lake in China. *Front. Microbiol.* 6, 129. doi:10.3389/fmicb.2015.00129
- Donlan, R. M. (2002). Biofilms: Microbial life on surfaces. *Emerg. Infect. Dis.* 8, 881–890. doi:10.3201/eid0809.020063
- Durán, N., Durán, M., de Jesus, M. B., Seabra, A. B., Fávaro, W. J., and Nakazato, G. (2016). Silver nanoparticles: A new view on mechanistic aspects on antimicrobial activity. *Nanomedicine Nanotechnol. Biol. Med.* 12, 789–799. doi:10.1016/j.nano.2015.11.016
- Elamawi, R. M., Al-Harbi, R. E., and Hendi, A. A. (2018). Biosynthesis and characterization of silver nanoparticles using *Trichoderma longibrachiatum* and their effect on phytopathogenic fungi. *Egypt. J. Biol. Pest Control* 28, 28. doi:10.1186/s41938-018-0028-1
- Ellis, M. W., Schlett, C. D., Millar, E. V., Crawford, K. B., Cui, T., Lanier, J. B., et al. (2014). Prevalence of nasal colonization and strain concordance in patients with community-associated *Staphylococcus aureus* skin and soft-tissue infections. *Infect. Control Hosp. Epidemiol.* 35, 1251–1256. doi:10.1086/678060
- Emeka, E. E., Ojiefoh, O. C., Aleruchi, C., Hassan, L. A., Christiana, O. M., Rebecca, M., et al. (2014). Evaluation of antibacterial activities of silver nanoparticles green-synthesized using pineapple leaf (*Ananas comosus*). *Micron* 57, 1–5. doi:10.1016/j.micron.2013.09.003
- Fong, J., Wood, F., and Fowler, B. (2005). A silver coated dressing reduces the incidence of early burn wound cellulitis and associated costs of inpatient treatment: Comparative patient care audits. *Burns* 31, 562–567. doi:10.1016/j.burns.2004.12.009
- Foster, T. J., Geoghegan, J. A., Ganesh, V. K., and Höök, M. (2014). Adhesion, invasion and evasion: The many functions of the surface proteins of *Staphylococcus aureus*. *Nat. Rev. Microbiol.* 12, 49–62. doi:10.1038/nrmicro3161
- Ghorbani, H., Safekordi, A., Attar, H., and Rezayat, M. (2011). Biological and non-biological methods for silver nanoparticles synthesis. *Chem. Biochem. Eng. Q.* 25.
- Gurunathan, S., Han, J. W., Kwon, D.-N., and Kim, J.-H. (2014). Enhanced antibacterial and anti-biofilm activities of silver nanoparticles against Gram-negative and Gram-positive bacteria. *Nanoscale Res. Lett.* 9, 373. doi:10.1186/1556-276X-9-373
- Haiko, J., and Westerlund-Wikström, B. (2013). The role of the bacterial flagellum in adhesion and virulence. *Biol. (Basel)* 2, 1242–1267. doi:10.3390/biology2041242
- Homan, K. A., Shah, J., Gomez, S., Gensler, H., Karpouk, A. B., Brannon-Peppas, L., et al. (2010). Silver nanosystems for photoacoustic imaging and image-guided therapy. *J. Biomed. Opt.* 15 (2), 1. doi:10.1117/1.3365937
- Hu, D., Ogawa, K., Kajiyama, M., and Enomae, T. (2020). Characterization of self-assembled silver nanoparticle ink based on nanoemulsion method. *R. Soc. open Sci.* 7 (5), 200296. doi:10.1098/rsos.200296
- Ivanova, N., Gugleva, V., Dobрева, M., Pehlivanov, I., Stefanov, S., and Andonova, V. (2018). *Silver nanoparticles as multi-functional drug delivery systems*. London, UK: IntechOpen, 71–91. doi:10.5772/intechopen.80238
- Jaffri, S. B., and Ahmad, K. S. (2018). Phytofunctionalized silver nanoparticles: Green biomaterial for biomedical and environmental applications. *Rev. Inorg. Chem.* 38 (3), 127–149. doi:10.1515/revic-2018-0004
- Jalal, M., Ansari, M. A., Shukla, A. K., Ali, S. G., Khan, H. M., Pal, R., et al. (2016). Green synthesis and antifungal activity of Al₂O₃ NPs against fluconazole-resistant *Candida* spp isolated from a tertiary care hospital. *RSC Adv.* 6, 107577–107590. doi:10.1039/C6RA23365A
- Jeong, S. H., Yeo, S. Y., and Yi, S. C. (2005). The effect of filler particle size on the antibacterial properties of compounded polymer/silver fibers. *J. Mat. Sci.* 40, 5407–5411. doi:10.1007/s10853-005-4339-8
- Jeyaseelan, E. C., and Jashothan, P. T. J. (2012). *In vitro* control of *Staphylococcus aureus* (NCTC 6571) and *Escherichia coli* (ATCC 25922) by *Ricinus communis* L. *Asian pac. J. Trop. Biomed.* 2, 717–721. doi:10.1016/S2221-1691(12)60216-0
- Kostakioti, M., Hadjifrangiskou, M., and Hultgren, S. J. (2013). Bacterial biofilms: Development, dispersal, and therapeutic strategies in the dawn of the postantibiotic era. *Cold Spring Harb. Perspect. Med.* 3, a010306. doi:10.1101/cshperspect.a010306
- Lahiri, D., Nag, M., Dutta, B., Sarkar, T., and Ray, R. R. (2021a). Artificial neural network and response surface methodology-mediated optimization of bacteriocin production by rhizobium leguminosarum. *Iran. J. Sci. Technol. Trans. A Sci.* 45, 1509–1517. doi:10.1007/s40995-021-01157-6
- Lahiri, D., Nag, M., Sarkar, T., Dutta, B., and Ray, R. R. (2021b). Antibiofilm activity of α -amylase from *Bacillus subtilis* and prediction of the optimized conditions for biofilm removal by response surface methodology (RSM) and artificial neural network (ANN). *Appl. Biochem. Biotechnol.* 193, 1853–1872. doi:10.1007/s12010-021-03509-9
- Lee, S. H., and Jun, B. H. (2019). Silver nanoparticles: Synthesis and application for nanomedicine. *Int. J. Mol. Sci.* 20 (4), 865. doi:10.3390/ijms20040865
- Mat Yusuf, S. N. A., Mood, C., Ahmad, N., Sandai, D., Lee, C., and Lim, V. (2020). Optimization of biogenic synthesis of silver nanoparticles from flavonoid-rich *Clinalcanthus nutans* leaf and stem aqueous extracts. *R. Soc. Open Sci.* 7, 200065. doi:10.1098/rsos.200065
- Mathur, P., Jha, S., Ramteke, S., and Jain, N. K. (2018). Pharmaceutical aspects of silver nanoparticles. *Artif. cells, nanomedicine, Biotechnol.* 46, 115–126. doi:10.1080/21691401.2017.1414825
- Meade, H. M., Long, S. R., Ruvkun, G. B., Brown, S. E., and Ausubel, F. M. (1982). Physical and genetic characterization of symbiotic and auxotrophic mutants of *Rhizobium meliloti* induced by transposon Tn5 mutagenesis. *J. Bacteriol.* 149, 114–122. doi:10.1128/jb.149.1.114-122.1982
- Mikhailova, E. O. (2020). Silver nanoparticles: Mechanism of action and probable bio-application. *J. Funct. Biomater.* 11, 84. doi:10.3390/jfb11040084
- Mirzaei, M., Furxhi, I., Murphy, F., and Mullins, M. (2021). A supervised machine-learning prediction of textile's antimicrobial capacity coated with nanomaterials. *Coatings* 11 (12), 1532. doi:10.3390/coatings11121532
- Miškovská, A., Rabochová, M., Michailidu, J., Masák, J., Čejková, A., Lorinčík, J., et al. (2022). Antibiofilm activity of silver nanoparticles biosynthesized using viticultural waste. *PLoS One* 17, e0272844. doi:10.1371/journal.pone.0272844
- Mocanu, A., Pasca, R. D., Tomoaia, G., Garbo, C., Frangopol, P. T., Horovitz, O., et al. (2013). New procedure to synthesize silver nanoparticles and their interaction with local anesthetics. *Int. J. Nanomedicine* 8, 3867–3874. doi:10.2147/IJN.S51063
- Moldovan, B., David, L., Achim, M., Clichici, S., and Filip, G. A. (2016). A green approach to phytomediated synthesis of silver nanoparticles using *Sambucus nigra* L. fruits extract and their antioxidant activity. *J. Mol. Liq.* 221, 271–278. doi:10.1016/j.molliq.2016.06.003
- Murdock, R. C., Braydich-Stolle, L., Schrand, A. M., Schlager, J. J., and Hussain, S. M. (2008). Characterization of nanomaterial dispersion in solution prior to *in vitro* exposure using dynamic light scattering technique. *Toxicol. Sci.* 101, 239–253. doi:10.1093/toxsci/kfm240
- Nguyen, D. C. T., Dowling, J., Ryan, R., McLoughlin, P., and Fitzhenry, L. (2021). Pharmaceutical-loaded contact lenses as an ocular drug delivery system: A review of critical lens characterization methodologies with reference to ISO standards. *Contact Lens Anterior Eye* 44 (6), 101487. doi:10.1016/j.clac.2021.101487
- Patra, J. K., Kim, E. S., Oh, K., Kim, H.-J., Kim, Y., and Baek, K.-H. (2014). Antibacterial effect of crude extract and metabolites of *Phytolacca americana* on pathogens responsible for periodontal inflammatory diseases and dental caries. *BMC Complement. Altern. Med.* 14, 343. doi:10.1186/1472-6882-14-343
- Poon, T. K. C., Iyengar, K. P., and Jain, V. K. (2021). Silver Nanoparticle (AgNP) Technology applications in trauma and orthopaedics. *J. Clin. Orthop. Trauma* 21, 101536. doi:10.1016/j.jcot.2021.101536
- Priyadarshini, S., Gopinath, V., Meera Priyadarshini, N., MubarakAli, D., and Velusamy, P. (2013). Synthesis of anisotropic silver nanoparticles using novel strain, *Bacillus flexus* and its biomedical application. *Colloids Surf. B. Biointerfaces* 102, 232–237. doi:10.1016/j.colsurfb.2012.08.018
- Quave, C. L., Estévez-Carmona, M., Compadre, C. M., Hobby, G., Hendrickson, H., Beenken, K. E., et al. (2012). Ellagic acid derivatives from *Rubus ulmifolius* inhibit *Staphylococcus aureus* biofilm formation and improve response to antibiotics. *PLoS One* 7, e28737. doi:10.1371/journal.pone.0028737
- Raveendran, P., Fu, J., and Wallen, S. L. (2003). Completely “green” synthesis and stabilization of metal nanoparticles. *J. Am. Chem. Soc.* 125, 13940–13941. doi:10.1021/ja029267j
- Rozhin, A., Batasheva, S., Kruchkova, M., Cherednichenko, Y., Rozhina, E., and Fakhrullin, R. (2021). Biogenic silver nanoparticles: Synthesis and application as antibacterial and antifungal agents. *Micromachines* 12 (12), 1480. doi:10.3390/mi12121480
- Shameli, K., Bin Ahmad, M., Jaffar Al-Mulla, E. A., Ibrahim, N. A., Shabanzadeh, P., Rustaiyan, A., et al. (2012). Green biosynthesis of silver nanoparticles using *Callicarpa maingayi* stem bark extraction. *Molecules* 17, 8506–8517. doi:10.3390/molecules17078506
- Sharma, K., Guleria, S., and Razdan, V. K. (2020). Green synthesis of silver nanoparticles using ocimum gratissimum leaf extract: Characterization, antimicrobial activity and toxicity analysis. *J. Plant Biochem. Biotechnol.* 29, 213–224. doi:10.1007/s13562-019-00522-2
- Shen, J., Cui, C., Li, J., and Wang, L. (2018). *In situ* synthesis of a silver-containing superabsorbent polymer via a greener method based on carboxymethyl celluloses. *Molecules* 23 (10), 2483. doi:10.3390/molecules23102483

- Sheykhsaran, E., Abbasi, A., Baghi, H. B., Ghotaslou, R., Sharifi, Y., Sefidan, F. Y., et al. (2022). *Staphylococcus aureus*: A bacterial candidate for multiple sclerosis incidence and progression. *Rev. Res. Med. Microbiol.* 33 (4), 212–220. doi:10.1097/MRM.0000000000000321
- Silva-Santana, G., Cabral-Oliveira, G., Oliveira, D., Nogueira, B., Pereira-Ribeiro, P., and Mattos-Guaraldi, A. (2020). *Staphylococcus aureus* biofilms: An opportunistic pathogen with multidrug resistance. *Rev. Med. Microbiol.* 32, 12–21. doi:10.1097/MRM.0000000000000223
- Smitha, S. L., Nissamudeen, K. M., Philip, D., and Gopchandran, K. G. (2008). Studies on surface plasmon resonance and photoluminescence of silver nanoparticles. *Spectrochim. Acta Part A Mol. Biomol. Spectrosc.* 71, 186–190. doi:10.1016/j.saa.2007.12.002
- Teanpaisan, R., Kawsud, P., Pahumunto, N., and Puripattanavong, J. (2017). Screening for antibacterial and antibiofilm activity in Thai medicinal plant extracts against oral microorganisms. *J. Tradit. Complement. Med.* 7, 172–177. doi:10.1016/j.jtcme.2016.06.007
- Vega-Baudrit, J., Gamboa, S., Rojas, E., and Martinez, V. (2019). Synthesis and characterization of silver nanoparticles and their application as an antibacterial agent. *Int. J. Biosens. Bioelectron.* 5. doi:10.15406/ijbsbe.2019.05.00172
- Wallace, A., Albadawi, H., Patel, N., Khademhosseini, A., Zhang, Y. S., Naidu, S., et al. (2017). Anti-fouling strategies for central venous catheters. *Cardiovasc. Diagnosis Ther.* 7, S246–S257. doi:10.21037/cdt.2017.09.18
- Wang, F., Li, J., Tang, X., Huang, K., and Chen, L. (2020). Polyelectrolyte three layer nanoparticles of chitosan/dextran sulfate/chitosan for dual drug delivery. *Colloids Surfaces B Biointerfaces* 190, 110925. doi:10.1016/j.colsurfb.2020.110925
- Zorraquín-Peña, I., Cueva, C., Bartolomé, B., and Moreno-Arribas, M. V. (2020). Silver nanoparticles against foodborne bacteria. Effects at intestinal level and health limitations. *Microorganisms* 8 (1), 132. doi:10.3390/microorganisms8010132



OPEN ACCESS

EDITED BY

Sougata Ghosh,
RK University, India

REVIEWED BY

Cristina Satriano,
University of Catania, Italy
Raymond J. Turner,
University of Calgary, Canada

*CORRESPONDENCE

Ashwini Chauhan,
✉ ashwinichauhan@tripurauniv.ac.in

SPECIALTY SECTION

This article was submitted
to Nanoscience,
a section of the journal
Frontiers in Chemistry

RECEIVED 05 January 2023

ACCEPTED 02 March 2023

PUBLISHED 23 March 2023

CITATION

Malhotra A, Chauhan SR, Rahaman M,
Tripathi R, Khanuja M and Chauhan A
(2023), Phyto-assisted synthesis of zinc
oxide nanoparticles for developing
antibiofilm surface coatings on central
venous catheters.
Front. Chem. 11:1138333.
doi: 10.3389/fchem.2023.1138333

COPYRIGHT

© 2023 Malhotra, Chauhan, Rahaman,
Tripathi, Khanuja and Chauhan. This is an
open-access article distributed under the
terms of the [Creative Commons
Attribution License \(CC BY\)](#). The use,
distribution or reproduction in other
forums is permitted, provided the original
author(s) and the copyright owner(s) are
credited and that the original publication
in this journal is cited, in accordance with
accepted academic practice. No use,
distribution or reproduction is permitted
which does not comply with these terms.

Phyto-assisted synthesis of zinc oxide nanoparticles for developing antibiofilm surface coatings on central venous catheters

Akshit Malhotra^{1,2}, Suchitra Rajput Chauhan³, Mispaur Rahaman⁴,
Ritika Tripathi³, Manika Khanuja⁵ and Ashwini Chauhan^{1*}

¹Department of Microbiology, Tripura University, Suryamaninagar, Tripura, India, ²Invisiobiome, New Delhi, India, ³Centre for Advanced Materials and Devices (CAMD), School of Engineering and Technology, BML Munjal University, Gurgaon, Haryana, India, ⁴Central Instrumentation Centre, Tripura University, Suryamaninagar, Tripura, India, ⁵Centre for Nanoscience and Nanotechnology, Jamia Millia Islamia, New Delhi, India

Medical devices such as Central Venous Catheters (CVCs), are routinely used in intensive and critical care settings. In the present scenario, incidences of Catheter-Related Blood Stream Infections (CRBSIs) pose a serious challenge. Despite considerable advancements in the antimicrobial therapy and material design of CVCs, clinicians continue to struggle with infection-related complications. These complications are often due to colonization of bacteria on the surface of the medical devices, termed as biofilms, leading to infections. Biofilm formation is recognized as a critical virulence trait rendering infections chronic and difficult to treat even with 1,000x, the minimum inhibitory concentration (MIC) of antibiotics. Therefore, non-antibiotic-based solutions that prevent bacterial adhesion on medical devices are warranted. In our study, we report a novel and simple method to synthesize zinc oxide (ZnO) nanoparticles using ethanolic plant extracts of *Eupatorium odoratum*. We investigated its physio-chemical characteristics using Field Emission- Scanning Electron Microscopy and Energy dispersive X-Ray analysis, X-Ray Diffraction (XRD), Photoluminescence Spectroscopy, UV-Visible and Diffuse Reflectance spectroscopy, and Dynamic Light Scattering characterization methods. Hexagonal phase with wurtzite structure was confirmed using XRD with particle size of ~50 nm. ZnO nanoparticles showed a band gap 3.25 eV. Photoluminescence spectra showed prominent peak corresponding to defects formed in the synthesized ZnO nanoparticles. Clinically relevant bacterial strains, viz., *Proteus aeruginosa* PAO1, *Escherichia coli* MTCC 119 and *Staphylococcus aureus* MTCC 7443 were treated with different concentrations of ZnO NPs. A concentration dependent increase in killing efficacy was observed with 99.99% killing at 500 µg/mL. Further, we coated the commercial CVCs using green synthesized ZnO NPs and evaluated its *in vitro* antibiofilm efficacy using previously optimized *in situ* continuous flow model. The hydrophilic functionalized interface of CVC prevents biofilm formation by *P. aeruginosa*, *E. coli* and *S. aureus*. Based on our findings, we propose ZnO nanoparticles as a promising non-antibiotic-based preventive solutions to reduce the risk of central venous catheter-associated infections.

KEYWORDS

green synthesis, plant mediated synthesis, zinc oxide nanoparticles (ZnO NPs), nanoparticle coatings, anti-biofilm coatings, device associated infections, anti-microbial resistance, medical devices

1 Introduction

Intravascular catheters are indispensable in modern day critical care settings (Smith and Nolan, 2013). Annually, in US alone, implantation of 0.15 billion intravascular catheters has been witnessed (Shah et al., 2013). Intravascular catheters like peripherally inserted catheters, central venous catheters and totally implantable venous access ports (TIVAPs) are implanted in patients for various applications such as renal dialysis (Agarwal et al., 2019), nutritional support (Pittiruti et al., 2009), administration of chemotherapy (Kim et al., 2010) and hemodynamic monitoring (Huygh et al., 2016). Unfortunately, the use of central venous catheters is associated with high infection rates (Marco et al., 2018) besides other complications such as mechanical failure (Copetti and de Monte, 2005) and thrombosis (Lebeaux et al., 2014b). In clinics, ~5%–8% TIVAPs get contaminated by structurally complex microbial biofilm communities due to microbial adhesion upon their surface (Lebeaux et al., 2014a; Stressmann Franziska et al., 2017). Hence, clinicians are challenged with the combined mortality, morbidity and economic burden associated with the use of central venous catheters (Marco et al., 2018). Despite adoption of effective frontline procedures such as prophylactic and therapeutic antimicrobial lock solutions (Niyyar, 2012), aseptic care bundles (O'Grady et al., 2011) or use of next-generation catheter designs employing anti-fouling materials (Ricardo et al., 2020)) deleterious microbial contamination resulting in central-line associated bloodstream infections (CLABSI) remains an unmet problem (Chopra et al., 2013). CLABSI originating from biofilm lifestyle of microbes can be difficult to eradicate due to the multi-factorial recalcitrance of microbial biofilms (David et al., 2014; Singh et al., 2021). A recent health-care-associated infection (HAIs) surveillance network in India found *Klebsiella* spp., *Acinetobacter* spp., *Pseudomonas* spp., and *Escherichia* spp. to be the most important etiological agents for CLABSI infections indicating an alarming predominance of Gram-negative bacteria (Mathur et al., 2022). There is a strong need to develop effective strategies which can control infections in Central Venous Catheters caused by such bacterial pathogens, primarily, to avert the risk of bloodstream infections.

In order to prevent and/or treat CVC-associated bloodstream infections, there are no fool-proof solutions apart from removal of contaminated device which increases cost of patient care and associated trauma (LaBella and Tang, 2012). Clinical practice guidelines indicate administration of antibiotic lock therapy to treat catheter-related infections (Mermel et al., 2009). Several antimicrobial lock solutions like minocycline-EDTA (Ferreira Chacon et al., 2011), ethanol (Wolf et al., 2013) and vancomycin-based lock solutions (Safdar and Maki, 2006) are used to salvage CVCs and also maintain patency. Other than the strategies to treat biofilm associated occlusions in CVCs, clinicians choose insertion of the CVC consisting anti-infective surface modification technologies (Casimero et al., 2020). These surface modifications employ antibiotics like minocycline (Raad et al., 1996), rifampin (Hanna et al., 2004), biocides like polyhexanide (Krikava et al., 2011), silver salts (Corral et al., 2003) or noble metal alloy coating (Björling et al., 2018). Despite significant success in reduction of CLABSI rate by use of surface modified CVCs, there are certain limitations to these

coating designs. The drawbacks include the limited release kinetics of antimicrobials (Walder et al., 2002; Wang et al., 2018), emergence of antimicrobial resistance (Sampath et al., 2001), and regulatory and safety issues (Guleri et al., 2012).

ZnO shows high biocompatibility to human organs, recognized as safe and approved by FDA as food additive (Puspasari et al., 2022). ZnO NPs are well known for their anti-quorum sensing (Husain et al., 2020), broad spectrum antimicrobial and antibiofilm activity (Mahamuni-Badiger et al., 2020). ZnO NPs of different morphologies have been utilized as antibacterial coating materials in textile fibers (Verbič et al., 2019), anticorrosion coating for metals (Qing et al., 2015), protection coatings for heritage buildings (Cinteză and Tănase, 2020) and antifouling coatings for dental (Moradpoor et al., 2021) and orthopedic implants (Memarzadeh et al., 2015). Although silver NPs are used to develop antibacterial surfaces of CVCs, reports of limited efficacy (Antonelli et al., 2012) and bacterial resistance against Ag NPs (Stabryla et al., 2021) warrant for better solutions. Urinary catheters were functionalized using ZnO NP based formulations (Ivanova et al., 2021), however, there are no reports on development of antifouling coatings on central venous catheters. In this study, we report a novel and facile-green synthesis of ZnO Nanoparticles (ZnO NPs) using extract of *Eupatorium odoratum*, a traditional medicinal plant used by local tribal population of Tripura (Debbarma et al., 2017). We used ZnO NPs, synthesized using phyto-assisted precipitation method, to develop coatings on luminal and outer surfaces of Totally Implantable Venous Access Port (TIVAP, a type of CVC). Green synthesized ZnO NPs conferred antifouling characteristics to the modified surfaces of TIVAP against *Escherichia coli*, *Proteus aeruginosa* (Gram-negative) and *Staphylococcus aureus* (Gram-positive) bacterial species using *in vitro* CVC continuous flow model system (Chauhan et al., 2012).

2 Material and methods

2.1 Collection of plant leaves and preparation of ethanolic extract

The plant leaves of *E. odoratum* were collected, washed with distilled water and subsequently dried at room temperature in dark conditions. After this, the dried leaves were ground to powder and 10 g of powder sample was mixed with 100 mL of ethanol for continuous stirring at 150 rpm for 24 h. In order to remove solid sediments, the mixture was then centrifuged at 10,000 rpm for 10 min. The supernatant was filtered using Whatman filter paper No. 1 and later, concentrated using rotary evaporator to obtain crude extract which was further lyophilized and stored at 4°C.

2.2 Synthesis of zinc oxide nanoparticles (ZnO NPs)

Zinc Oxide nanoparticles were prepared using phyto-assisted precipitation (Ranpariya et al., 2021) method using highly concentrated Zn precursor, ZnCl₂. Briefly, 0.2 M ZnCl₂ was prepared with total reaction mixture volume as 100 mL. Initially, only 80 mL distilled water was mixed with ZnCl₂ powder using

magnetic stirring at 150 rpm at 70°C. After complete dissolution of ZnCl_2 crystals, the ethanolic extract of *E. odoratum* (10 mg/mL concentration) was added to the reaction mixture with a total volume of 5 mL and later, pH was adjusted to 6. After 1 h of continuous stirring, the mixture was transferred to centrifuge tubes for centrifugation at 15,000 rpm for 10 min at 4°C. The supernatant was discarded and the pellet was transferred to fresh tube and mixed with 50% ethanol (v/v in distilled water). The centrifugation cycle is repeated twice and the obtained pellet was kept in oven to dry for 12 h at 80°C.

2.3 Determining physico-chemical properties of synthesized nanoparticles by different characterization techniques

The crystallographic phase of NPs was confirmed by X-ray diffraction analysis (PANalytical, EMPYREAN). The operating voltage and current during XRD were 45 kV and 45 mA, respectively and, the diffraction pattern was recorded across the 2θ range of 20°–80° with Cu K α source (1.5406 Å). The peaks obtained in XRD analysis was corroborated with JCPDS database to determine the phase formation of ZnO nanoparticles. The surface morphological analysis of ZnO NPs was done by FE-SEM microscopy (FE-SEM, Sigma-300, Carl Zeiss) and elemental composition was investigated by EDAX spectroscopy. In order to find the band gap of synthesized ZnO NPs, diffuse reflectance spectroscopy was done (Lambda-365 UV-Vis Spectrophotometer Perkin Elmer) with the reflectance of light in 200–800 nm range. The photoluminescence emission spectrum was recorded at laser wavelength of 355 nm and 285 μW incident power using Witech Alpha 300 RA system. The hydrodynamic size and zeta potential of NPs was measured using Litesizer 500 (Anton Paar GmbH). ZnO NPs suspension in distilled water was passed through 0.22 μm nylon syringe filter and sonicated for 30 min at RT in ultrasonic cleaner (LMUC-3, Labman Scientific Instruments Pvt. Ltd., India) operating at 40 kHz.

2.4 Development of ZnO NP based coatings on totally implantable venous access ports (TIVAP)

The coating suspension consisted of 0.2% (w/v) HPMC and 5% (w/v) ZnO NPs in 81.25% ethanol. The coating solution was infused inside the lumens of TIVAP (2005ISP, Vygon, Ecouen, France) with the help of syringe and immersed in the coating solution. The tubings of TIVAP were in contact with coating solution for 6 h at 60°C under continuous orbital shaking at 150 rpm. After this, the excess solution was removed by immersing the catheter in 1x PBS, flushing the lumen of TIVAP by 1x PBS and therefore, ensuring no occlusion inside the lumen of TIVAP. The coated TIVAP was dried in oven at 80°C for 16 h. In order to confirm the coating of ZnO NPs on surfaces of TIVAP, FE-SEM and EDAX analysis was done (Sigma-300, Carl Zeiss) to further compare uncoated and coated TIVAP surfaces in terms of surface morphology and elemental composition. The catheters were sterilized as described elsewhere (Chauhan et al., 2014) in absolute ethanol.

2.5 Bacterial strains and growth media

S. aureus MTCC 7443 was grown in Tryptic Soy Broth (TSB) and Gram- *E. coli* MTCC 119 and *P. aeruginosa* PAO1 (kind gift received from Dr. Mohan C. Joshi, Jamia Milia Islamia, N. Delhi, India) were grown in Luria-Bertani broth (LB) at 37°C. For enumerating bacterial cell viability, serially diluted culture was spotted on sterile TSB agar (*S. aureus*) or LB agar (*E. coli* or *P. aeruginosa*) plates and kept for incubation at 37°C for 12–16 h.

2.6 Effect of *Eupatorium odoratum* mediated and chemically synthesized ZnO NPs on exponentially growing bacteria

The efficacy of *E. odoratum* mediated or chemically synthesized (kind gift from Dr. Khanuja, Jamia Milia Islamia, N. Delhi, India) ZnO NPs in inhibiting growth of *S. aureus*, *E. coli* or *P. aeruginosa* was checked by recording OD 600 nm at different time intervals using Shimadzu UV-Vis Spectrophotometer. Each treatment was replicated thrice and each experiment was carried out 3 times. The exponentially ($\text{OD}_{600} \approx 0.3\text{--}0.5$) grown bacterial culture of *S. aureus*, *E. coli* or *P. aeruginosa* was given treatment of different concentrations of ZnO NPs and allowed to incubate for 24 h at 37°C with continuous shaking at 150 rpm. The untreated wells were kept as controls. After the incubation, the colony forming units were estimated by plating the serial dilutions on LB agar or TSB agar media plates for Gram-negative and Gram-positive bacteria respectively, and incubated at 37°C for 12–16 h (Lebeaux et al., 2014a).

2.7 Evaluation of *in vitro* antibiofilm efficacy of surface modified TIVAP using continuous flow system

The antibiofilm efficacy of surface modified TIVAP was evaluated using continuous flow system described previously (Chauhan et al., 2012) with few modifications. Briefly, bacterial biofilms of *S. aureus*, *E. coli* or *P. aeruginosa* were allowed to form on the ZnO NPs coated, HPMC coated and uncoated TIVAP. Under sterile conditions in laminar airflow, the catheters were supplied with fresh media from reservoir bottles. The intraluminal sections of TIVAP were filled with *S. aureus*, *E. coli* or *P. aeruginosa* at a cell density 100 cells/50 μL and allowed to adhere on catheter's internal surface at 37°C for 3 h. Later, non-adherent bacteria were removed by flushing out 1x PBS for a duration of 10 min followed by continuous supply of media at a speed of 300 $\mu\text{L}/\text{min}$ for 48 h. The non-adherent cells and spent media were collected in the discard bottle from the catheters. After 48 h, the biofilm bacterial cells from intraluminal section of TIVAP were harvested by a vigorous process as described previously (Chauhan et al., 2012). The TIVAP catheter surface was wiped using 70% ethanol to remove any contaminants present on the outer lumen of the TIVAP catheter. Under sterile conditions, the lumen of the catheter was cut cross sectionally in small pieces followed by transversal cuts to expose the inner lumen of the catheter. The cut sections were immersed

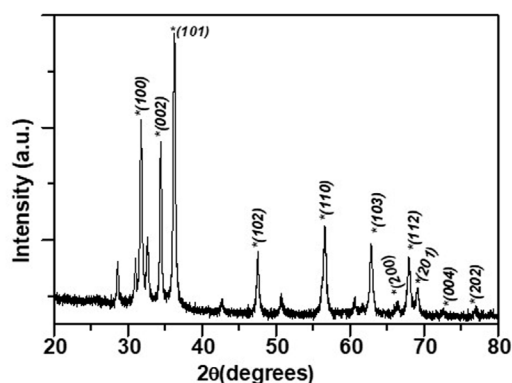


FIGURE 1
XRD pattern for the synthesized ZnO NPs.

in 1 mL 1xPBS containing tube and vortexed for 1 min. This was followed by sonication for 5 min using water bath ultrasonic cleaner (LMUC-3, Labman Scientific Instruments Pvt. Ltd., India) operating at 40 kHz followed by vortex mixing for 1 min. Later, the bacterial cells in the 1xPBS suspension were diluted serially and plated on TSB agar (*S. aureus*) or LB agar (*E. coli* or *P. aeruginosa*) for viable cell count estimation.

3 Results and discussion

3.1 Phyto assisted ZnO NPs show hexagonal phase with wurtzite structure

The phase of the ZnO NPs synthesized using ethanolic extracts of *E. odoratum* was identified with the help of X ray diffraction pattern as shown in Figure 1. A series of diffraction peaks due to (100), (002), (101), (102), (110), (103), (200), (112), (201), (004), (202) planes were observed from the synthesized ZnO NPs. A JCPDS file 36-1451 was used to identify the hexagonal phase with wurtzite structure in the synthesized ZnO NPs. Spurious low intensity peaks were also observed specifically between 20° and 35°. These peaks could be due to the intermediate product or impurities. Confirmation of multiphase or impurity was done by EDAX measurements. Only “Zn” and “O” signals were observed in sample indicating that unidentified peaks in observed XRD pattern corresponds to the intermediate phase only. Similar observation has been reported by Luković Golić et al. (2011), and others (Tokumoto et al., 2002).

Average crystallite size of the ZnO NPs have been determined from the Williamson-Hall plot (W-H plot) ($\beta \cos \theta$ versus $4 \sin \theta$) (Jeffery, 1957) after determining the FWHM of the XRD peaks and considering instrumental broadening.

$$\beta_{Total} = \beta_{Size} + \beta_{Strain} = \frac{0.9\lambda}{t \cos \theta} + \frac{4(\Delta d) \sin \theta}{d \cos \theta} \quad (1)$$

$$\beta_{Total} \cos \theta = \frac{0.9\lambda}{t} + \frac{4(\Delta d) \sin \theta}{d}$$

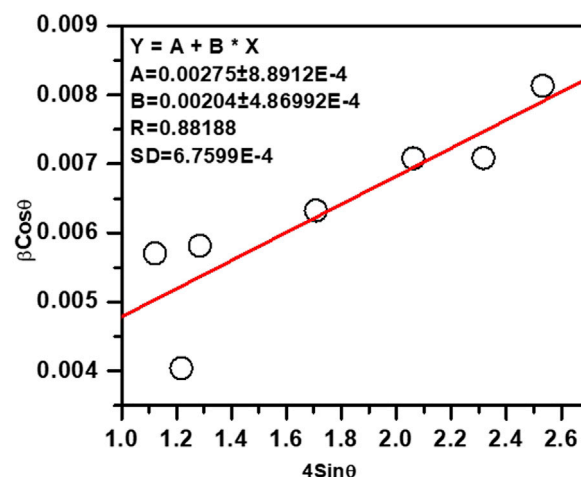


FIGURE 2
Williamson-Hall plot for the ZnO NPs, particle size was determined from the intercept.

Where, θ denotes the Bragg angle, t represents the crystal or particle size of ZnO NPs synthesized using ethanolic extracts of *E. odoratum*, d represents interplanar lattice spacing, β_{Size} and β_{Strain} represent the FWHM contributions pertaining to the size and strain, respectively. $\Delta d/d$ is the measure of strain. FWHM was obtained by fitting individual XRD peak to Lorentzian peak. Figure 2 shows the W-H plot yielding ZnO particle size = 50.4 nm.

The lattice parameters of synthesized ZnO NPs were obtained using an interactive powder diffraction data interpretation and indexing program (Wu, 1989). The indexing program yields lattice parameters by least square fitting to the positions of x ray diffraction peaks in 20–80° range. Lattice parameters $a = 3.25500 \pm 0 \text{ \AA}$ and $c = 5.21459 \pm 0.00091 \text{ \AA}$ were fitted at figure of merit, $F = 33.9$ and $R = 0.00011$. The low value of the R-factor ($\sim 10^{-3}$) and high value of $F > 10$ were indicative of the satisfactory estimate of the lattice parameters.

3.2 FE-SEM and EDAX spectroscopy analysis

The morphology of ZnO NPs was investigated using FE-SEM microscopy. The spherical and hexagonal morphologies were observed (Figure 3). The SEM micrographs reveal particle aggregation and homogenous morphology distribution in agreement with earlier reports (Chaudhuri and Malodia, 2017; Naseer et al., 2020; Faisal et al., 2021; Iqbal et al., 2021). However, in the previous studies green synthesis procedure has also resulted in irregular crystal growth of ZnO NPs (Ogunyemi et al., 2019; Priyadarshini et al., 2022). The average grain size of *E. odoratum* leaves' ethanolic extract mediated ZnO NPs was $34 \pm 7.98 \text{ nm}$ in our study which is in close agreement with XRD findings. As per previous findings, using SEM analysis different size ranges of bio-fabricated ZnO NPs have been reported such as 45–150 nm using cell free extract of *Bacillus megaterium* (Saravanan et al., 2018), 25–87 nm using fruit, seed and pulp extract of *Citrullus colocynthis* (Azizi et al., 2017), 10–20 nm (Doan Thi et al., 2020) using

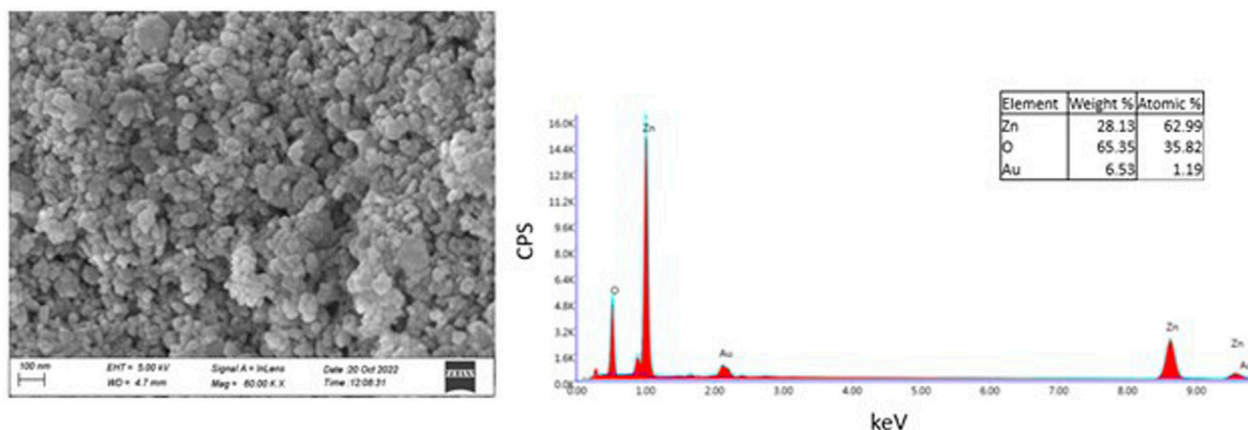


FIGURE 3

SEM and EDAX Analysis. Field Emission-Scanning Electron Microscopy Images of Zinc Oxide Nanoparticles synthesized using green synthesis showing spherical, hexagonal structures of Zinc Oxide. EDAX spectra reveals presence of Zn and O confirming pure synthesis of Zinc Oxide nanoparticles.

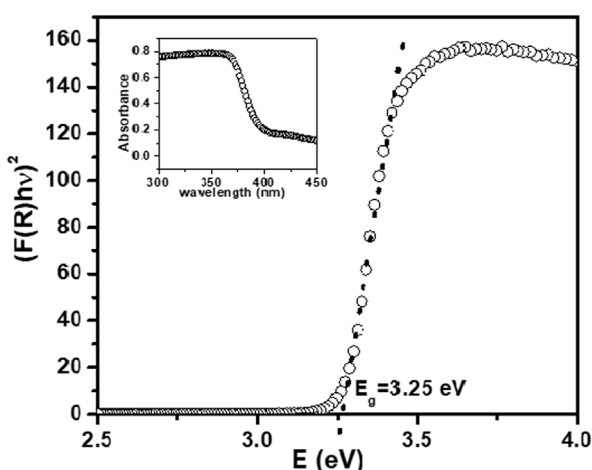


FIGURE 4

Kubelka-Munk function (KM) versus photon energy for ZnO NPs. Inset- Absorption spectra for synthesized ZnO NPs.

orange fruit peel extract, 30–43 nm using *Withania somnifera* root extract (Prasad et al., 2021), etc. In EDAX spectroscopy, the synthesized nanoparticles showed presence of Zn (65.35 wt%), O (28.13 wt%) and Au (6.53 wt%, due to gold sputter coating prior to SEM microscopy) indicating successful synthesis of ZnO nanoparticles.

3.3 UV-visible absorption and diffuse reflectance spectroscopy (DRS) analysis

DRS spectra for synthesized NPs showed strong reflection above 365 nm. Absorption spectra for the ZnO NPs synthesized using ethanolic extracts of *E. odoratum* is shown

in inset of Figure 4. The absorption peak for synthesized ZnO NPs was observed at 380.5 nm. Researchers have presented reports of both, the red shift due to defect incorporations with extended localized states within the band gap region (Marotti et al., 2006; Kamarulzaman et al., 2015) and the blue shift of E_g (Tan et al., 2005; Debanath and Karmakar, 2013).

The bandgap energy of ZnO NPs is calculated using Kubelka-Munk (KM) relation as described in Wetchakun et al. (2012) and Yan et al. (2021).

$$\frac{K}{S} = \frac{(1 - R_{\infty})^2}{2R_{\infty}} = F(R) \quad (2)$$

Where, $F(R)$ is the remission or Kubelka-Munk (KM) function. In parabolic band structure,

$$\alpha h\nu = C(h\nu - E_g)^{1/2} \quad (3)$$

where, α denotes linear absorption coefficient of the material; $h\nu$ denotes photon energy; C denoted proportionality constant.

For constant scattering coefficient (S) with wavelength, and using Eqs 1, 2,

$$[F(R)h\nu]^2 = B(h\nu - E_g) \quad (3a)$$

E_g was measured by extrapolating the linear portion of modified KM function and $h\nu$, as shown in Figure 4. The optical bandgap for the synthesized NPs was found to be 3.25 eV. The smaller bandgap value as compared to bulk ZnO (~3.3 eV) may be attributed to defects including, dislocations, stacking faults, zinc and oxygen vacancies, Zn and oxygen interstitial.

3.4 Photoluminescence (PL) spectroscopy analysis

To study the possible defects in the synthesized ZnO NPs, PL spectra was investigated at room temperature. PL spectra of the

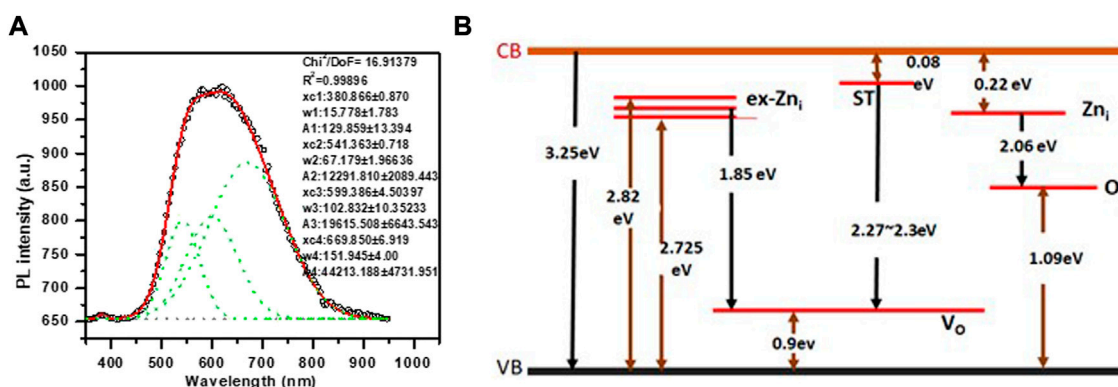


FIGURE 5

(A) Photoluminescence spectra measured at room temperature for green synthesized ZnO NPs. Dotted curve shows the fitted Gaussian peaks to obtain defect states in the ZnO NPs. (B) Energy level diagram of synthesized ZnO NPs showing defect states (Vempati et al., 2012) and the possible transition corresponding to observed defect states in PL spectra.

synthesized sample was recorded using excitation wavelength at 355 nm wavelength with 285 μ W power. Emission signal was recorded with CCD (charge Coupled Detector). Optical properties of synthesized ZnO NPs were investigated for its use as coatings in central venous catheter. The nanoparticle size (Choopun et al., 2005; Wang et al., 2005) and surface morphology (Ye et al., 2005; Zhao et al., 2016) as well as defects and synthesis process (Kumar Jangir et al., 2017) affect the PL properties of ZnO. Generally, room temperature PL of ZnO exhibits sharp transition in UV range and a broad transition in visible range. The sharp transition in UV range corresponds to optical transition between electrons in conduction band (CB) and holes in valence band (VB), including excitonic effect (band to band transition). PL originates due to recombination of surface states (Chestnoy et al., 1986). The broad emission is related to dopant/impurities or point defects such as zinc interstitial and oxygen vacancies (Kumar Jangir et al., 2017), etc. Figure 5A shows PL spectra of ZnO nanomaterial. The UV emission at 381.8 nm is attributed to near bandgap excitonic emission (band to band transition). Free exciton in ZnO occur when electron hole pair forms between CB and VB. Second observed peak corresponding to crystalline defects in PL spectra was fitted to Gaussian peak function to obtain corresponding energy level and to access types of defects present in the synthesized sample and their influence on the optical properties.

The number of fitted peaks (Figure 5A) indicate the presence of defect states. The parameters obtained from fitted peaks including peak position, FWHM, area under the curve, are shown in the Figure 5A. Figure 5B shows energy band diagram for the synthesized ZnO NPs. The PL spectra of NPs show intense red emission at 669.85 nm, along with orange and green emission at 599.3 nm and 541.3 nm, respectively. Green emission is attributed transition from surface traps (ST) to oxygen vacancy level (V_o). Orange emission is due to transition from Zn_i level to O_i level and red emission is attributed to transition from ex Zn_i level to V_o level.

3.5 Dynamic Light Scattering

The particle size distribution of green synthesized zinc oxide nanoparticles is moderately multimodal with polydispersity index as 0.26 and the hydrodynamic diameter is 142.82 nm. Moreover, d_{90} , i.e., 69.95 nm (Figure 6A) represents the size of 90% of particles in the suspension to be below the d_{90} value which is larger than the average particle size, i.e., 34 nm observed in SEM. This is possibly due to the bias of the characterization technique to measure bigger size particles or aggregates (Modena et al., 2019).

The correlogram of ZnO nanoparticles samples decays rapidly (Figure 6B) indicating the composition of NPs suspension by small sized particles, therefore, changing their relative positions rapidly and also, bringing about rapid intensity fluctuations (Figure 6C). The colloid suspensions with ζ -potential in range $\in (-\infty, -15] + [15, \infty)$ are known to be stable (Modena et al., 2019). The colloids are strongly stable if ζ -potential modulus is greater than 25 governed by adequate mutual repulsive forces (Zhou, 2012; Morais et al., 2013). The ζ -potential of ZnO NPs is -15.61 mV (Figure 6D), possessing anionic surface charge and can form a moderately stable colloid. There is a close relationship between the plant extract metabolites and ζ -potential (Lynch et al., 2009). Moreover, the presence of negative charge on NPs due to adsorption of plant extract metabolites reduces aggregation among particles making it a stable dispersion (Vimala et al., 2014).

3.6 SEM-EDAX analysis of ZnO NP-coated CVCs

The surface of TIVAP showed functionalization of ZnO nanoparticles using SEM-EDAX analysis (Figures 7A, B). The zinc oxide nanoparticles along with HPMC form polymer encapsulated nanoparticles coatings on catheter surfaces as

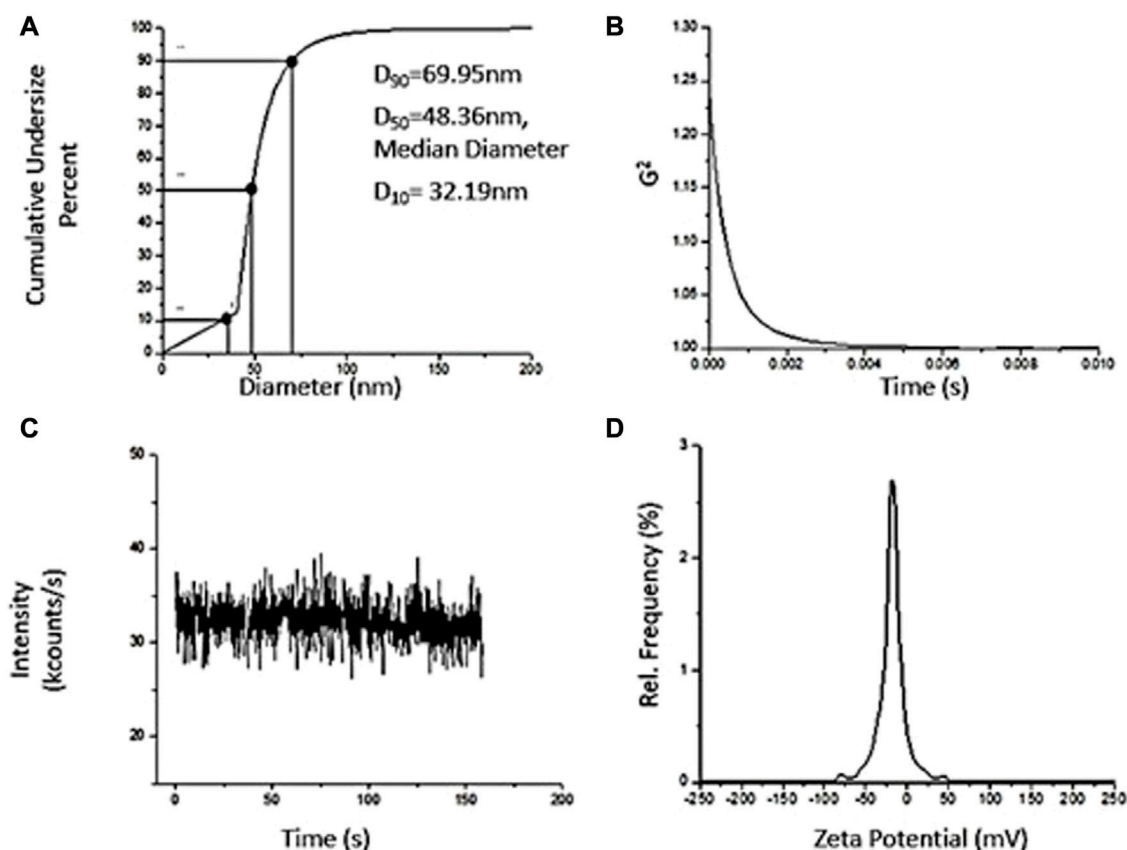


FIGURE 6

Dynamic Light Scattering Characterization of ZnO synthesized using Green Synthesis. (A) Particle Size Distribution, $D_{10} = 32.19$ nm, Median Diameter, $D_{50} = 48.36$ nm, $D_{90} = 69.95$ nm. (B) Correlogram. (C) Intensity Fluctuation Plot. (D) Zeta Potential distribution upon nanoparticles.

observed in SEM micrograph (Figure 7A). Recently, HPMC based films were developed incorporated with ZnO Nanoparticles for antibacterial wound dressing application (Pitpisutkul and Prachayawarakorn, 2022). Further, more detailed investigations are required to find exact mechanism of chemical interaction between HPMC, ZnO and PDMS surfaces.

3.7 ZnO NPs efficiently kill clinically relevant bacteria

ZnO exhibits improved antibacterial activity at the nanoscale (Padmavathy and Vijayaraghavan, 2008). The antibacterial properties of ZnO nanoparticles have been reported as a function of its characteristic features. ZnO Nanoparticles when doped with Fe results in significant antibacterial activity against Gram-negative bacteria like *P. aeruginosa*, *E. coli* (Kayani et al., 2018). ZnO nanoparticles consisting flower like morphology (hierarchical structures) make Gram-positive bacteria more susceptible than Gram-negative bacteria (Babayevska et al., 2022). The differential antimicrobial activities of ZnO NPs are due to influence of physical and chemical properties of ZnO NPs obtained by varying synthesis methods, modification of NP surface using doping with metals or capping agent (Gudkov et al., 2021; da Silva et al., 2019). To assess

the antibacterial efficacy of ZnO NPs synthesized using ethanolic extracts of *E. odoratum* or chemically synthesized ZnO NPs, exponentially growing bacteria were treated with different concentrations (50 $\mu\text{g/mL}$ to 750 $\mu\text{g/mL}$) of ZnO NPs for 24 h at 37°C. The viable cell count was estimated by plating the *S. aureus* on TSB agar plates, and *E. coli* and *P. aeruginosa* on LB agar plates. Untreated cultures were used as controls (Figures 8A–F; Supplementary Figure S1). Although a concentration dependent killing was observed upon exposure of all the bacterial strains to either *E. odoratum* mediated or chemically synthesized ZnO NPs, there was no significant difference in the antibacterial activity between the ZnO NPs synthesized by two methods. Although the growth of both Gram-positive as well as Gram-negative strains was inhibited significantly with increasing concentration, growth of *S. aureus* was inhibited up to 99.9% at a concentration of 250 $\mu\text{g/mL}$ *E. odoratum* mediated ZnO NPs. Maximum killing of 99.98% was seen in case of *S. aureus* at 500 $\mu\text{g/mL}$ ZnO NPs whereas 99.9% killing could be achieved only at higher concentration of 750 $\mu\text{g/mL}$ in case of Gram-negative bacteria. This could be due to presence of secondary metabolites (rich in phenols, saponins and tannins) (Inya-agma et al., 1987) in *E. odoratum* extracts, as previously reported, maybe specifically active against Gram-positive bacteria. The literature suggests broad spectrum antibacterial and antifungal activity of *E. odoratum* plant extract. Venkat Raman et al. (Venkata

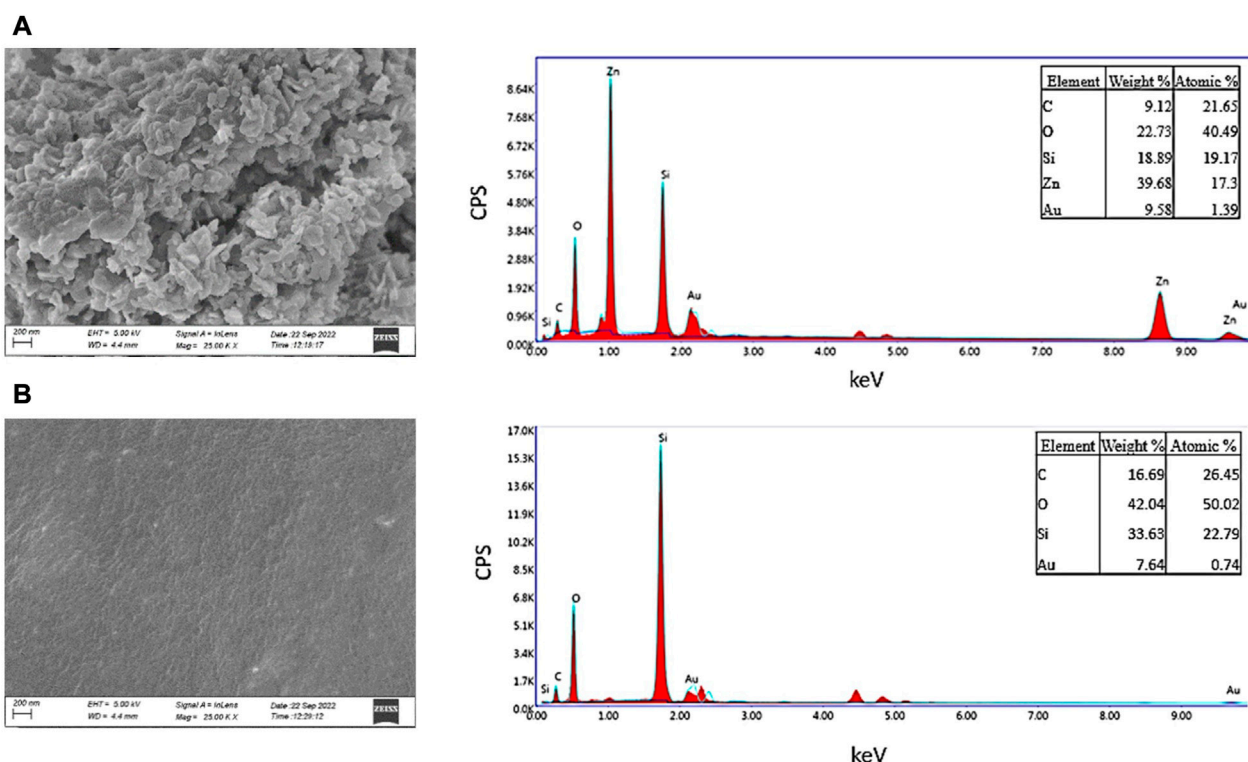


FIGURE 7

SEM and EDAX Analysis of surface morphology of coated and uncoated catheters. (A) Coated Surface of CVC. (B) Uncoated Surface of CVC.

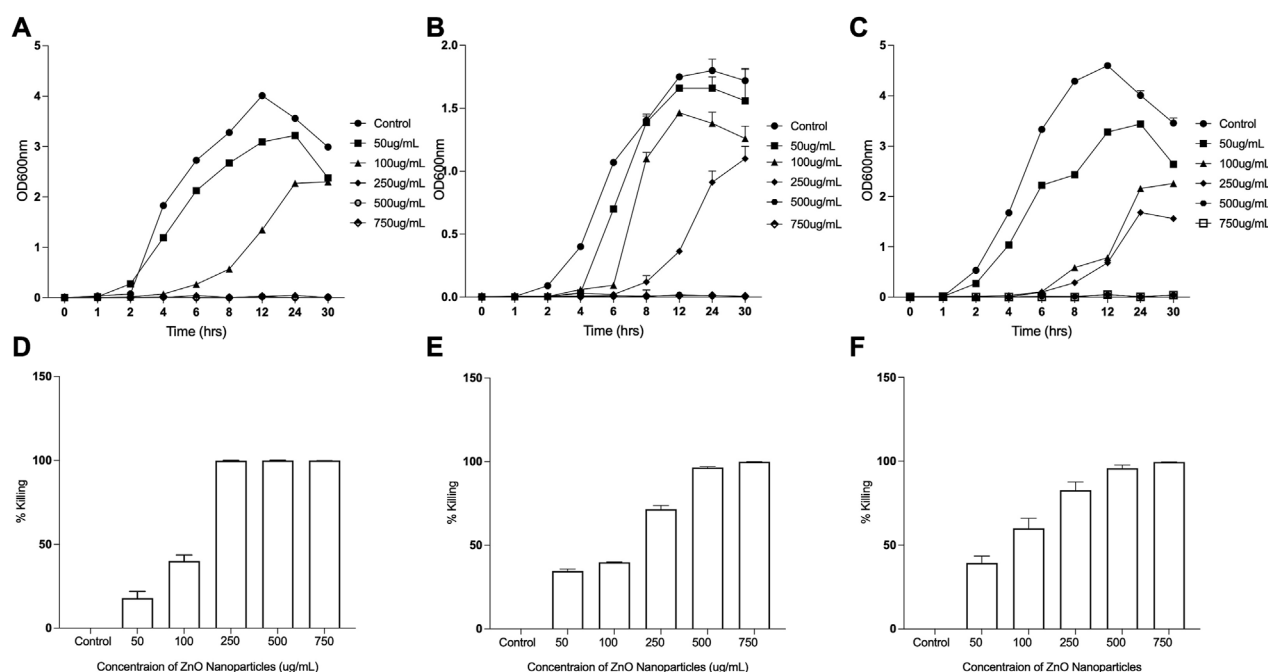


FIGURE 8

Antibacterial Efficacy of *Eupatorium odoratum* mediated ZnO NPs. Inhibition of: (A) *Staphylococcus aureus*, (B) *Escherichia coli*, and (C) *Proteus aeruginosa* growth in the presence of different concentrations of ZnO NPs; Percentage killing of: (D) *Staphylococcus aureus*, (E) *Escherichia coli*, and (F) *Proteus aeruginosa*, after 24 h of exposure to different concentrations of ZnO NPs.

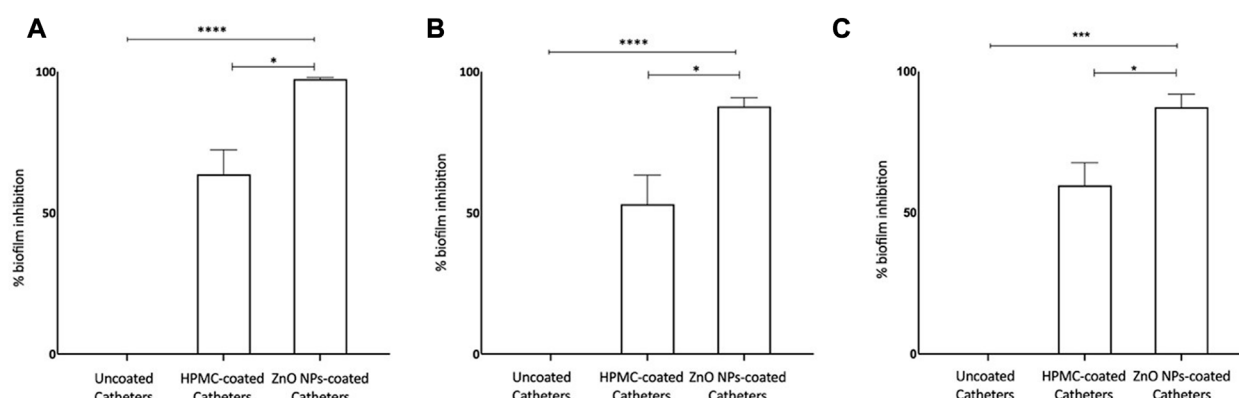


FIGURE 9

Antibiofilm Efficacy of ZnO NP coated CVCs. (A) Biofilm formation of *Staphylococcus aureus* is inhibited by >97%. (B) Biofilm formation of *Escherichia coli* is inhibited nearly by 90%. (C) Biofilm formation of *Proteus aeruginosa* is inhibited by >90%. ZnO-NPs Coated: ZnO NPs-HPMC composite coating. Statistical analysis was done by 1-way analysis of variance (unpaired t-test with Welch's correction) using GraphPad Prism software (version 8.0.1). Differences were considered significant at $p < 0.05^*$, $p < .0005^{***}$; $p < 0.0001^{****}$.

raman et al., 2012) have shown broad spectrum antibacterial activity against Gram-negative and Gram-positive bacteria including MTCC736 *Bacillus subtilis*, MTCC2807 *Corynebacterium glutamicum*, MTCC1572 *E. coli*, MTCC7028 *Klebsiella pneumoniae*, MTCC733 *Salmonella typhi*, MTCC87 *S. aureus*, MTCC1938 *Streptococcus thermophilus*, MTCC1771 *P. vulgaris*, MTCC451 *Vibrio parahaemolyticus*. *E. odoratum* extract shows significant ($p < 0.001$) antibacterial activity against all bacterial species excluding *Proteus vulgaris* and *S. typhi*. Besides, *E. odoratum* also show antifungal activity (Ramesh and Subramani, 2018). *Chromolaena odorata* (synonym of *E. odoratum*) extract in combination with antibiotics inhibit growth of *P. aeruginosa* isolated from wound infections. Moreover, *E. odoratum* mediated ZnO NPs are able to kill efficiently both the both the Gram-positive and Gram-negative bacteria, indicating the broad-spectrum activity of these NPs and further warrants the evaluation for probable application in clinical settings. Furthermore, as suggested by other research groups, focused studies are needed to compare the antibacterial efficacies of metal and/or metal oxide NPs using optimized techniques more relevant to nanoparticles (Kourmouli et al., 2018; Masri et al., 2022).

3.8 ZnO NPs coating on totally implantable venous access ports (TIVAP) reduce biofilm formation

Zinc oxide nanoparticles are well recognized antibacterial (Liu et al., 2009; El-Masry et al., 2022) and antibiofilm agents, and used to develop antifouling surfaces of medical devices, for example, modifying dental resins (Wang et al., 2019) and denture bases in dental implants (Cierniech et al., 2019) and deposition (Wang et al., 2021) and patterning of ZnO NPs on titanium (Ye et al., 2022) for orthopedic implants. We have developed coating of ZnO NPs, synthesized using ethanolic plant extract of *E. odoratum*, on silicone elastomer-based surface of the commercial TIVAP with help of hydroxypropyl methylcellulose (HPMC) as binding agent. ZnO-HPMC based coatings result in formation of hydrophilic surfaces (Rao et al., 2014). The ZnO NPs

coated CVCs showed more than 97% inhibition of *S. aureus* biofilm formation and up to 90% inhibition of *E. coli* and *P. aeruginosa* biofilm formation (Figure 9). Hydrophilic surfaces are known to reduce bacterial adhesion and biofilm formation (Lorenzetti et al., 2015; Verhorstert et al., 2020). ZnO NPs based coatings can be tuned to attain hydrophilic surfaces reducing bacterial colonization and inhibiting biofilm formation upon the surfaces (Yong et al., 2015; Kusworo et al., 2021). Our results demonstrated the application of ZnO NPs for the first-time and successful reduction in bacterial formation which can successfully reduce risk of central venous catheter associated infections. Further, *in vivo* studies would validate the antifouling ability in the presence of trilateral interaction between host, device and bacteria.

4 Conclusion

HPMC and ZnO are well recognised as safe materials and applied in coatings of food packaging products and wound applications. Zinc oxide nanoparticles were synthesized using plant extract of medicinal plant *E. odoratum* that showed excellent antibacterial activity up to 99.99% killing efficacy. ZnO NPs were coated on commercial TIVAPs using HPMC polymer. The coated CVCs prevented the bacterial biofilm formation of clinically relevant bacteria, viz., *E. coli*, *P. aeruginosa* and *S. aureus* in an *in situ* continuous flow system. Based on our findings, we propose application of green synthesized ZnO NPs (a non-antibiotic based) surface coatings on Central Venous Catheter which has immense potential of improving the patient outcome in clinical settings.

Data availability statement

The original contributions presented in the study are included in the article/Supplementary Material, further inquiries can be directed to the corresponding author.

Author contributions

AM and SC: Performed experiments, data analysis, writing original draft; MR: FE-SEM and EDAX experiments, RT: Writing and documentation; MK: Reviewing and editing of the manuscript, AC: Supervision, conceptualization, formal analysis, reviewing and editing of manuscript.

Funding

This research was funded by UGC-BSR [F.30-487/2019(BSR)], DST-Nanomission (DST/NM/NB/2018/203), ICMR (OMI/20/2020-ECD-1), and SERB-CRG (CRG/2021/001974).

Acknowledgments

AM would like to thank DST-Nanomission for the fellowship support. AC would like to thank Central Instrumentation Centre Facility, Tripura University for access to FE-SEM Microscopy (Sigma-300, Carl Zeiss) and Dr. Pratap Acharya, Department of Pharmacy, Tripura University for using Dynamic Light Scattering (Litesizer, Anton-Paar) facility. SC would like to acknowledge CAMD, BML Munjal University for using XRD, UV-Vis and DRS, and PL characterization facilities.

References

- Agarwal, A. K., Haddad, N. J., Vachharajani, T. J., and Asif, A. (2019). Innovations in vascular access for hemodialysis. *Kidney Int.* 95 (5), 1053–1063. doi:10.1016/j.kint.2018.11.046
- Antonelli, M., de Pascale, G., Ranieri, V. M., Pelaia, P., Tufano, R., Piazza, O., et al. (2012). Comparison of triple-lumen central venous catheters impregnated with silver nanoparticles (AgTive®) vs conventional catheters in intensive care unit patients. *J. Hosp. Infect.* 82 (2), 101–107. doi:10.1016/j.jhin.2012.07.010
- Azizi, S., Mohamad, R., and Mahdavi Shahri, M. (2017). Green microwave-assisted combustion synthesis of zinc oxide nanoparticles with *Citrullus colocynthis* (L.) schrad: Characterization and biomedical applications. *Molecules* 22 (2), 301. doi:10.3390/molecules22020301
- Babayevska, N., Przysiecka, Ł., Iatsunskyi, I., Nowaczyk, G., Jarek, M., Janiszewska, E., et al. (2022). ZnO size and shape effect on antibacterial activity and cytotoxicity profile. *Sci. Rep.* 12 (1), 8148. doi:10.1038/s41598-022-12134-3
- Björling, G., Johansson, D., Bergström, L., Strekalovsky, A., Sanchez, J., Frostell, C., et al. (2018). Evaluation of central venous catheters coated with a noble metal alloy—a randomized clinical pilot study of coating durability, performance and tolerability. *J. Biomed. Mater. Res. Part B: Appl. Biomater.* 106 (6), 2337–2344. doi:10.1002/jbm.b.34041
- Casimero, C., Ruddock, T., Hegarty, C., Barber, R., Devine, A., and Davis, J. (2020). Minimising blood stream infection: Developing new materials for intravascular catheters. *Medicines* 7 (9), 49. doi:10.3390/medicines7090049
- Chaudhuri, S. K., and Malodia, L. (2017). Biosynthesis of zinc oxide nanoparticles using leaf extract of *calotropis gigantea*: Characterization and its evaluation on tree seedling growth in nursery stage. *Appl. Nanosci.* 7 (8), 501–512. doi:10.1007/s13204-017-0586-7
- Chauhan, A., Lebeaux, D., Decante, B., Kriegel, I., Escande, M.-C., Ghigo, J.-M., et al. (2012). A rat model of central venous catheter to study establishment of long-term bacterial biofilm and related acute and chronic infections. *PLOS ONE* 7 (5), e37281. doi:10.1371/journal.pone.0037281
- Chauhan, A., Bernardin, A., Mussard, W., Kriegel, I., Estève, M., Ghigo, J.-M., et al. (2014). Preventing Biofilm Formation and associated occlusion by biomimetic glycolaldehyde polymer in central venous catheters. *J. Infect. Dis.* 210 (9), 1347–1356. doi:10.1093/infdis/jiu249
- Chestnoy, N., Harris, T. D., Hull, R., and Brus, L. E. (1986). Luminescence and photophysics of cadmium sulfide semiconductor clusters: The nature of the emitting electronic state. *J. Phys. Chem.* 90 (15), 3393–3399. doi:10.1021/j100406a018
- Choopun, S., Hongsith, N., Tanunchai, S., Chairuangsi, T., Krua-in, C., Singkarat, S., et al. (2005). Single-crystalline ZnO nanobelts by RF sputtering. *J. Cryst. Growth* 282 (3), 365–369. doi:10.1016/j.jcrysgro.2005.05.020
- Chopra, V., O'Horo, J. C., Rogers, M. A. M., Maki, D. G., and Safdar, N. (2013). The risk of bloodstream infection associated with peripherally inserted central catheters compared with central venous catheters in adults: A systematic review and meta-analysis. *Infect. Control Hosp. Epidemiol.* 34 (9), 908–918. doi:10.1086/671737
- Cierech, M., Wojnarowicz, J., Kolenda, A., Krawczyk-Balska, A., Prochwicz, E., Woźniak, B., et al. (2019). Zinc oxide nanoparticles cytotoxicity and release from newly formed PMMA–ZnO nanocomposites designed for denture bases. *Nanomaterials* 9 (9), 1318. doi:10.3390/nano9091318
- Cinteză, L. O., and Tănase, M. A. (2020). “Multifunctional ZnO nanoparticle: Based coatings for cultural heritage preventive conservation,” in *Thin films*. Editor A. E. Ares (IntechOpen). Ch. 6. doi:10.5772/intechopen.94070
- Copetti, R., and de Monte, A. (2005). Rapid echocardiographic diagnosis of suspected paradoxical gas embolism after central venous catheter placement in the upright position. *Echocardiography* 22 (8), 695–696. doi:10.1111/j.1540-8175.2005.40082.x
- Corral, L., Nolla-Salas, M., Ibañez-Nolla, J., León, M. A., Dí'az, R. M., Cruz Martí'n, M., et al. (2003). A prospective, randomized study in critically ill patients using the Oligon Vantex® catheter. *J. Hosp. Infect.* 55 (3), 212–219. doi:10.1016/j.jhin.2003.07.001
- da Silva, B. L., Paiva Abuçafy, M., Berbel Manaia, E., Augusto Oshiro Junior, J., Chiari-Andréo, B. G., Cl R Pietro, R., et al. (2019). Relationship between structure and antimicrobial activity of zinc oxide nanoparticles: An overview. *Int. J. Nanomed.* 14 (14), 9395–9410. doi:10.2147/IJN.S216204
- David, L., Jean-Marc, G., and Christophe, B. (2014). Biofilm-related infections: Bridging the gap between clinical management and fundamental aspects of recalcitrance toward antibiotics. *Microbiol. Mol. Biol. Rev.* 78 (3), 510–543. doi:10.1128/MMBR.00013-14
- Debanath, M. K., and Karmakar, S. (2013). Study of blueshift of optical band gap in zinc oxide (ZnO) nanoparticles prepared by low-temperature wet chemical method. *Mater. Lett.* 111, 116–119. doi:10.1016/j.matlet.2013.08.069
- Debbarma, M., Pala, N. A., Kumar, M., and Bussmann, R. W. (2017). Traditional knowledge of medicinal plants in tribes of Tripura in northeast India. *Afr. J. Tradit. Complement. Altern. Med.* 14 (4), 156–168. doi:10.21010/ajtcam.v14i4.19

Conflict of interest

AM is Co-Founder, Invisiobiome Pvt. Ltd., India.
The remaining authors declare that the research was conducted in the absence of any commercial or financial relationships that could be construed as a potential conflict of interest.

Publisher's note

All claims expressed in this article are solely those of the authors and do not necessarily represent those of their affiliated organizations, or those of the publisher, the editors and the reviewers. Any product that may be evaluated in this article, or claim that may be made by its manufacturer, is not guaranteed or endorsed by the publisher.

Supplementary material

The Supplementary Material for this article can be found online at: <https://www.frontiersin.org/articles/10.3389/fchem.2023.1138333/full#supplementary-material>

SUPPLEMENTARY FIGURE S1

Comparison of antibacterial efficacy of ZnO NPs synthesized using *E. odoratum* ethanolic extract with ZnO NPs synthesized by chemical method. Inhibition of: (A) *S. aureus*, (B) *E. coli*, and (C) *Proteus aeruginosa* growth in the presence of different concentrations of ZnO NPs.

- Doan Thi, T. U., Nguyen, T. T., Thi, Y. D., Ta Thi, K. H., Phan, B. T., and Pham, K. N. (2020). Green synthesis of ZnO nanoparticles using orange fruit peel extract for antibacterial activities. *RSC Adv.* 10 (40), 23899–23907. doi:10.1039/D0RA04926C
- El-Masry, R. M., Talat, D., Hassoubah, S. A., Zabermaui, N. M., Eleiwa, N. Z., Sherif, R. M., et al. (2022). Evaluation of the antimicrobial activity of ZnO nanoparticles against enterotoxigenic *Staphylococcus aureus*. *Life* 12 (10), 1662. doi:10.3390/12101662
- Faisal, S., Jan, H., Shah, S. A., Shah, S., Khan, A., Akbar, M. T., et al. (2021). Green synthesis of zinc oxide (ZnO) nanoparticles using aqueous fruit extracts of myristica fragrans: Their characterizations and biological and environmental applications. *ACS Omega* 6 (14), 9709–9722. doi:10.1021/acsomega.1c00310
- Ferreira Chacon, J. M., Hato de Almeida, E., de Lourdes Simões, R., Lazzarin, C., Ozório, V., Alves, B. C., et al. (2011). Randomized study of minocycline and edetic acid as a locking solution for central line (Port-A-Cath) in children with cancer. *Chemotherapy* 57 (4), 285–291. doi:10.1159/000328976
- Gudkov, S. v., Burmistrov, D. E., Serov, D. A., Rebezov, M. B., Semenova, A. A., and Lisitsyn, A. B. (2021). A mini review of antibacterial properties of ZnO nanoparticles. *Front. Phys.* 9. doi:10.3389/fphy.2021.641481
- Guleri, A., Kumar, A., Morgan, R. J. M., Hartley, M., and Roberts, D. H. (2012). Anaphylaxis to chlorhexidine-coated central venous catheters: A case series and review of the literature. *Surg. Infect.* 13 (3), 171–174. doi:10.1089/sur.2011.011
- Hanna, H., Benjamin, R., Chatzinikolaou, I., Alakech, B., Richardson, D., Mansfield, P., et al. (2004). Long-term silicone central venous catheters impregnated with minocycline and rifampin decrease rates of catheter-related bloodstream infection in cancer patients: A prospective randomized clinical trial. *J. Clin. Oncol.* 22 (15), 3163–3171. doi:10.1200/JCO.2004.04.124
- Husain, F. M., Zia, Q., Khan, M. F., Ahmad, E., Jamal, A., Alaidarous, M., et al. (2020). Anti-quorum sensing and anti-biofilm activity of zinc oxide nanospikes. *ACS Omega* 5 (50), 32203–32215. doi:10.1021/acsomega.0c03634
- Huygh, J., Peeters, Y., Bernards, J., and Malbrain, M. (2016). Hemodynamic monitoring in the critically ill: An overview of current cardiac output monitoring methods [version 1; peer review: 3 approved]. *F1000Research* 5, 2855. doi:10.12688/f1000research.8991.1
- Inya-agma, S. I., Oguntimein, B. O., Sofowora, A., and Benjamin, T. v. (1987). Phytochemical and antibacterial studies on the essential oil of eupatorium odoratum. *Int. J. Crude Drug Res.* 25 (1), 49–52. doi:10.3109/13880208709060911
- Iqbal, J., Abbasi, B. A., Yaseen, T., Zahra, S. A., Shahbaz, A., Shah, S. A., et al. (2021). Green synthesis of zinc oxide nanoparticles using *Elaeagnus angustifolia* L. leaf extracts and their multiple *in vitro* biological applications. *Sci. Rep.* 11 (1), 20988. doi:10.1038/s41598-021-99839-z
- Ivanova, A., Ivanova, K., Perelshtein, I., Gedanken, A., Todorova, K., Milcheva, R., et al. (2021). Sonochemically engineered nano-enabled zinc oxide/amylase coatings prevent the occurrence of catheter-associated urinary tract infections. *Mater. Sci. Eng. C* 131, 112518. doi:10.1016/j.msec.2021.112518
- Jeffery, G. A. (1957). “Elements of x-ray diffraction,” in *Journal of Chemical Education*. Editors B. D. Cullity 34 (4), A178. doi:10.1021/ed034pA178
- Kamarulzaman, N., Kasim, M. F., and Rusdi, R. (2015). Band gap narrowing and widening of ZnO nanostructures and doped materials. *Nanoscale Res. Lett.* 10 (1), 346. doi:10.1186/s11671-015-1034-9
- Kayani, Z. N., Abbas, E., Saddique, Z., Riaz, S., and Naseem, S. (2018). Photocatalytic, antibacterial, optical and magnetic properties of Fe-doped ZnO nano-particles prepared by sol-gel. *Mater. Sci. Semicond. Process.* 88, 109–119. doi:10.1016/j.mssp.2018.08.003
- Kim, H. J., Yun, J., Kim, H. J., Kim, K. H., Kim, S. H., Lee, S.-C., et al. (2010). Safety and effectiveness of central venous catheterization in patients with cancer: Prospective observational study. *J. Korean Med. Sci.* 25 (12), 1748–1753. doi:10.3346/jkms.2010.25.12.1748
- Kourmouli, A., Valenti, M., van Rijn, E., Beaumont, H. J. E., Kalantzi, O.-I., Schmidt-Ott, A., et al. (2018). Can disc diffusion susceptibility tests assess the antimicrobial activity of engineered nanoparticles? *J. Nanopart. Res.* 20 (3), 62. doi:10.1007/s11051-018-4152-3
- Krikava, I., Kolar, M., Garajova, B., Balik, T., Sevcikova, A., Pachel, J., et al. (2011). Polyhexanide anti-infective coating of central venous catheters in prevention of catheter colonization and bloodstream infection: Study HC-G-H-0507. *Crit. Care* 15 (1), P229. doi:10.1186/cc9649
- Kumar Jangir, L., Kumari, Y., Kumar, A., Kumar, M., and Awasthi, K. (2017). Investigation of luminescence and structural properties of ZnO nanoparticles, synthesized with different precursors. *Mater. Chem. Front.* 1 (7), 1413–1421. doi:10.1039/C7QM00058H
- Kusworo, T. D., Dalanta, F., Aryanti, N., and Othman, N. H. (2021). Intensifying separation and antifouling performance of PSf membrane incorporated by GO and ZnO nanoparticles for petroleum refinery wastewater treatment. *J. Water Process Eng.* 41, 102030. doi:10.1016/j.jwpe.2021.102030
- LaBella, G. D., and Tang, J. (2012). “Removal of totally implantable venous access device,” in *Totally implantable venous access devices: Management in mid- and long-term clinical setting*. Editors J. E. Niederhuber, I. di Carlo, and R. Biffi (Springer Milan), 247–255. doi:10.1007/978-88-470-2373-4_35
- Lebeaux, D., Chauhan, A., Létoffé, S., Fischer, F., de Reuse, H., Beloin, C., et al. (2014a). pH-mediated potentiation of aminoglycosides kills bacterial persisters and eradicates *in vivo* biofilms. *J. Infect. Dis.* 210 (9), 1357–1366. doi:10.1093/infdis/jiu286
- Lebeaux, D., Fernández-Hidalgo, N., Chauhan, A., Lee, S., Ghigo, J.-M., Almirante, B., et al. (2014b). Management of infections related to totally implantable venous-access ports: Challenges and perspectives. *Lancet. Infect. Dis.* 14 (2), 146–159. doi:10.1016/S1473-3099(13)70266-4
- Liu, Y., He, L., Mustapha, A., Li, H., Hu, Z. Q., and Lin, M. (2009). Antibacterial activities of zinc oxide nanoparticles against *Escherichia coli* O157:H7. *J. Appl. Microbiol.* 107 (4), 1193–1201. doi:10.1111/j.1365-2672.2009.04303.x
- Lorenzetti, M., Dogša, I., Stošić, T., Stopar, D., Kalin, M., Kobe, S., et al. (2015). The influence of surface modification on bacterial adhesion to titanium-based substrates. *ACS Appl. Mater. Interfaces* 7 (3), 1644–1651. doi:10.1021/am507148n
- Luković Golić, D., Branković, G., Počuča Nešić, M., Vojisavljević, K., Rečnik, A., Daneu, N., et al. (2011). Structural characterization of self-assembled ZnO nanoparticles obtained by the sol–gel method from Zn(CH₃COO)₂·2H₂O. *Nanotechnology* 22 (39), 395603. doi:10.1088/0957-4484/22/39/395603
- Lynch, I., Salvati, A., and Dawson, K. A. (2009). What does the cell see? *Nat. Nanotechnol.* 4 (9), 546–547. doi:10.1038/nnano.2009.248
- Mahamuni-Badiger, P. P., Patil, P. M., Badiger, M. v., Patel, P. R., Thorat-Gadgil, B. S., Pandit, A., et al. (2020). “Biofilm formation to inhibition: Role of zinc oxide-based nanoparticles,” in *Materials science and engineering C* (Elsevier), 108. doi:10.1016/j.msec.2019.110319
- Marco, R., Laura, M., Olga, R.-N., Celia, C., Pedro, P.-A., Marta, H.-M., et al. (2018). Short-term peripheral venous catheter-related bloodstream infections: Evidence for increasing prevalence of gram-negative microorganisms from a 25-year prospective observational study. *Antimicrob. Agents Chemother.* 62 (11), 008922–e918. doi:10.1128/AAC.00892-18
- Marotti, R. E., Giorgi, P., Machado, G., and Dalchiale, E. A. (2006). Crystallite size dependence of zinc oxide nanoparticles for electrodeposited ZnO grown at different temperatures. *Sol. Energy Mater. Sol. Cells* 90 (15), 2356–2361. doi:10.1016/j.solmat.2006.03.008
- Masri, A., Brown, D. M., Smith, D. G. E., Stone, V., and Johnston, H. J. (2022). Comparison of *in vitro* approaches to assess the antibacterial effects of nanomaterials. *J. Funct. Biomater.* 13 (4), 255. doi:10.3390/jfb13040255
- Mathur, P., Malpiedi, P., Walia, K., Srikantiah, P., Gupta, S., Lohiya, A., et al. (2022). Health-care-associated bloodstream and urinary tract infections in a network of hospitals in India: A multicentre, hospital-based, prospective surveillance study. *Lancet Glob. Health* 10 (9), e1317–e1325. doi:10.1016/S2214-109X(22)00274-1
- Memarzadeh, K., Sharili, A. S., Huang, J., Rawlinson, S. C. F., and Allaker, R. P. (2015). Nanoparticulate zinc oxide as a coating material for orthopedic and dental implants. *J. Biomed. Mater. Res. Part A* 103 (3), 981–989. doi:10.1002/jbm.a.35241
- Mermel, L. A., Allon, M., Bouza, E., Craven, D. E., Flynn, P., O’Grady, N. P., et al. (2009). Clinical practice guidelines for the diagnosis and management of intravascular catheter-related infection: 2009 update by the infectious diseases society of America. *Clin. Infect. Dis.* 49 (1), 1–45. doi:10.1086/599376
- Modena, M. M., Rühle, B., Burg, T. P., and Wuttke, S. (2019). Nanoparticle characterization: What to measure? *Adv. Mater.* 31 (32), 1901556. doi:10.1002/adma.201901556
- Moradpoor, H., Safaei, M., Mozaffari, H. R., Sharifi, R., Imani, M. M., Golshah, A., et al. (2021). An overview of recent progress in dental applications of zinc oxide nanoparticles. *RSC Adv.* 11 (34), 21189–21206. doi:10.1039/D0RA10789A
- Morais, J. P. S., Rosa, M. D. F., de Souza Filho, M., de Sá, M., Nascimento, L. D., do Nascimento, D. M., et al. (2013). Extraction and characterization of nanocellulose structures from raw cotton linter. *Carbohydr. Polym.* 91 (1), 229–235. doi:10.1016/j.carbpol.2012.08.010
- Naseer, M., Aslam, U., Khalid, B., and Chen, B. (2020). Green route to synthesize Zinc Oxide Nanoparticles using leaf extracts of *Cassia fistula* and *Melia azadirach* and their antibacterial potential. *Sci. Rep.* 10 (1), 9055. doi:10.1038/s41598-020-65949-3
- Niyyar, V. D. (2012). Catheter dysfunction: The role of lock solutions. *Semin. Dial.* 25 (6), 693–699. doi:10.1111/j.1525-139X.2011.00991.x
- O’Grady, N. P., Alexander, M., Burns, L. A., Dellinger, E. P., Garland, J., Heard, S. O., et al. (2011). Guidelines for the prevention of intravascular catheter-related infections. *Clin. Infect. Dis.* 52 (9), e162–e193. doi:10.1093/cid/cir257
- Ogunyemi, S. O., Abdallah, Y., Zhang, M., Fouad, H., Hong, X., Ibrahim, E., et al. (2019). Green synthesis of zinc oxide nanoparticles using different plant extracts and their antibacterial activity against *Xanthomonas oryzae* pv. *oryzae*. *Artif. Cells, Nanomed. Biotechnol.* 47 (1), 341–352. doi:10.1080/21691401.2018.1557671
- Padmavathy, N., and Vijayaraghavan, R. (2008). Enhanced bioactivity of ZnO nanoparticles—An antimicrobial study. *Sci. Technol. Adv. Mater.* 9 (3), 035004. doi:10.1088/1468-6996/9/3/035004
- Pitpisutkul, V., and Prachayawarakorn, J. (2022). Hydroxypropyl methylcellulose/carboxymethyl starch/zinc oxide porous nanocomposite films for wound dressing application. *Carbohydr. Polym.* 298, 120082. doi:10.1016/j.carbpol.2022.120082

- Pittiruti, M., Hamilton, H., Biffi, R., MacFie, J., and Pertkiewicz, M. (2009). ESPEN guidelines on parenteral nutrition: Central venous catheters (access, care, diagnosis and therapy of complications). *Clin. Nutr.* 28(4), 365–377. doi:10.1016/j.clnu.2009.03.015
- Prasad, K. S., Prasad, S. K., Veerapur, R., Lamraoui, G., Prasad, A., Prasad, M. N. N., et al. (2021). Antitumor potential of green synthesized ZnONPs using root extract of *Withania somnifera* against human breast cancer cell line. *Separations* 8 (1), 8. doi:10.3390/separations8010008
- Priyadarshini, S. S., Shubha, J. P., Shivalingappa, J., Adil, S. F., Kuniyil, M., Hatshan, M. R., et al. (2022). Photocatalytic degradation of methylene blue and metanil yellow dyes using green synthesized zinc oxide (ZnO) nanocrystals. *Crystals* 12 (1), 22. doi:10.3390/cryst12010022
- Puspasari, V., Ridhova, A., Hermawan, A., Amal, M. I., and Khan, M. M. (2022). ZnO-based antimicrobial coatings for biomedical applications. *Bioprocess Biosyst. Eng.* 45 (9), 1421–1445. doi:10.1007/s00449-022-02733-9
- Qing, Y., Yang, C., Hu, C., Zheng, Y., and Liu, C. (2015). A facile method to prepare superhydrophobic fluorinated polysiloxane/ZnO nanocomposite coatings with corrosion resistance. *Appl. Surf. Sci.* 326, 48–54. doi:10.1016/j.apsusc.2014.11.100
- Raad, I., Darouiche, R., Hachem, R., Mansouri, M., and Bodey, G. P. (1996). The broad-spectrum activity and efficacy of catheters coated with minocycline and rifampin. *J. Infect. Dis.* 173 (2), 418–424. doi:10.1093/infdis/173.2.418
- Ramesh, P., and Subramani, A. (2018). Effect of antimicrobial activity of Eupatorium odoratum against clinical microbes. *Int. J. Sci. Res. Biol. Sci.* 5 (5), 30–35. doi:10.26438/ijrsr/v5i5.3035
- Ranpariya, B., Salunke, G., Karmakar, S., Babiya, K., Sutar, S., Kadoo, N., et al. (2021). Antimicrobial synergy of silver-platinum nanohybrids with antibiotics. *Front. Microbiol.* 11, 610968. doi:10.3389/fmicb.2020.610968
- Rao, B. L., Asha, S., Madhukumar, R., Latha, S., Gowda, M., Shetty, G. R., et al. (2014). Structural, surface wettability and antibacterial properties of HPMC-ZnO nanocomposite. *AIP Conf. Proc.* 1591 (1), 807–809. doi:10.1063/1.4872763
- Ricardo, S. I. C., Anjos, I. I. L., Monge, N., Faustino, C. M. C., and Ribeiro, I. A. C. (2020). A glance at antimicrobial strategies to prevent catheter-associated medical infections. *ACS Infect. Dis.* 6 (12), 3109–3130. doi:10.1021/acsinfectdis.0c00526
- Safdar, N., and Maki, D. G. (2006). Use of vancomycin-containing lock or flush solutions for prevention of bloodstream infection associated with central venous access devices: A meta-analysis of prospective, randomized trials. *Clin. Infect. Dis.* 43 (4), 474–484. doi:10.1086/505976
- Sampath, L. A., Tambe, S. M., and Modak, S. M. (2001). *In vitro* and *in vivo* efficacy of catheters impregnated with antiseptics or antibiotics: Evaluation of the risk of bacterial resistance to the antimicrobials in the catheters. *Infect. Control Hosp. Epidemiol.* 22 (10), 640–646. doi:10.1086/501836
- Saravanan, M., Gopinath, V., Chaurasia, M. K., Syed, A., Ameen, F., and Purushothaman, N. (2018). Green synthesis of anisotropic zinc oxide nanoparticles with antibacterial and cytofriendly properties. *Microb. Pathog.* 115, 57–63. doi:10.1016/j.micpath.2017.12.039
- Shah, H., Bosch, W., Thompson, K. M., and Hellinger, W. C. (2013). Intravascular catheter-related bloodstream infection. *Neurohospitalist* 3 (3), 144–151. doi:10.1177/1941874413476043
- Singh, B. P., Ghosh, S., and Chauhan, A. (2021). Development, dynamics and control of antimicrobial-resistant bacterial biofilms: A review. *Environ. Chem. Lett.* 19 (3), 1983–1993. doi:10.1007/s10311-020-01169-5
- Smith, R. N., and Nolan, J. P. (2013). Central venous catheters. *Br. Med. J.* 347, f6570. doi:10.1136/bmj.f6570
- Stabryla, L. M., Johnston, K. A., Diemler, N. A., Cooper, V. S., Millstone, J. E., Haig, S.-J., et al. (2021). Role of bacterial motility in differential resistance mechanisms of silver nanoparticles and silver ions. *Nat. Nanotechnol.* 16 (9), 996–1003. doi:10.1038/s41565-021-00929-w
- Stressmann Franziska, A., Elodie, C.-D., Delphine, C., Ashwini, C., Aimee, W., Sylvaine, D.-F., et al. (2017). Comparative analysis of bacterial community composition and structure in clinically symptomatic and asymptomatic central venous catheters. *MSphere* 2 (5), 001466–e217. doi:10.1128/mSphere.00146-17
- Tan, S. T., Chen, B., Sun, X., Fan, W., Kwok, H., Zhang, X., et al. (2005). Blueshift of optical band gap in ZnO thin films grown by metal-organic chemical-vapor deposition. *J. Appl. Phys.* 98, 013505. doi:10.1063/1.1940137
- Tokumoto, M. S., Pulcinelli, S. H., Santilli, C., and Briois, V. (2002). Catalysis and temperature dependence on the formation of ZnO nanoparticles and of zinc acetate derivatives prepared by the Sol–Gel route. *J. Phys. Chem. B* 107, 568–574. doi:10.1021/jp0217381
- Vempati, S., Mitra, J., and Dawson, P. (2012). One-step synthesis of ZnO nanosheets: A blue-white fluorophore. *Nanoscale Res. Lett.* 7 (1), 470. doi:10.1186/1556-276X-7-470
- Venkata raman, B., La, S., Pardha Saradhi, M., Narashimha Rao, B., Naga Vamsi Krishna, A., and Radhakrishnan, T. M. (2012). Antibacterial, antioxidant activity and GC-MS analysis of Eupatorium odoratum. *Asian J. Pharm. Clin. Res.* 5.
- Verbič, A., Gorjanc, M., and Simončič, B. (2019). Zinc oxide for functional textile coatings: Recent advances. *Coatings* 9 (9), 550. doi:10.3390/coatings9090550
- Verhorstert, K. W. J., Guler, Z., de Boer, L., Riool, M., Roovers, J.-P. W. R., and Zaai, S. A. J. (2020). *In vitro* bacterial adhesion and Biofilm Formation on fully absorbable poly-4-hydroxybutyrate and nonabsorbable polypropylene pelvic floor implants. *ACS Appl. Mater. Interfaces* 12 (48), 53646–53653. doi:10.1021/acsami.0c14668
- Vimala, K., Sundarraj, S., Paulpandi, M., Vengatesan, S., and Kannan, S. (2014). Green synthesized doxorubicin loaded zinc oxide nanoparticles regulates the Bax and Bcl-2 expression in breast and colon carcinoma. *Process Biochem.*, 49 (1), 160–172. doi:10.1016/j.procbio.2013.10.007
- Waldner, B., Pittet, D., and Tramèr, M. R. (2002). Prevention of bloodstream infections with central venous catheters treated with anti-infective agents depends on catheter type and insertion time: Evidence from a meta-analysis. *Infect. Control Hosp. Epidemiol.* 23 (12), 748–756. doi:10.1086/502005
- Wang, R., Liu, C.-P., Huang, J., and Chen, S.-J. (2005). ZnO symmetric nanosheets integrated with nanowalls. *Appl. Phys. Lett.* 87, 053103. doi:10.1063/1.2005386
- Wang, H., Tong, H., Liu, H., Wang, Y., Wang, R., Gao, H., et al. (2018). Effectiveness of antimicrobial-coated central venous catheters for preventing catheter-related bloodstream infections with the implementation of bundles: A systematic review and network meta-analysis. *Ann. Intensive Care* 8 (1), 71. doi:10.1186/s13613-018-0416-4
- Wang, Y., Hua, H., Li, W., Wang, R., Jiang, X., and Zhu, M. (2019). Strong antibacterial dental resin composites containing cellulose nanocrystal/zinc oxide nanohybrids. *J. Dent.* 80, 23–29. doi:10.1016/j.jdent.2018.11.002
- Wang, Z., Wang, X., Wang, Y., Zhu, Y., Liu, X., and Zhou, Q. (2021). NanoZnO-modified titanium implants for enhanced anti-bacterial activity, osteogenesis and corrosion resistance. *J. Nanobiotechnol.* 19 (1), 353. doi:10.1186/s12951-021-01099-6
- Wetchakun, N., Chaiwichain, S., Inceesungvorn, B., Pingmuang, K., Phanichphant, S., Minett, A. I., et al. (2012). BiVO₄/CeO₂ nanocomposites with high visible-light-induced photocatalytic activity. *ACS Appl. Mater. Interfaces* 4 (7), 3718–3723. doi:10.1021/am300812n
- Wolf, J., Shenep, J. L., Clifford, V., Curtis, N., and Flynn, P. M. (2013). Ethanol lock therapy in pediatric hematology and oncology. *Pediatr. Blood Cancer* 60 (1), 18–25. doi:10.1002/pbc.24249
- Wu, E. (1989). POWD, an interactive program for powder diffraction data interpretation and indexing. *J. Appl. Crystallogr.* 22 (5), 506–510. doi:10.1107/S0021889889005066
- Yan, X., Xiao, X., Au, C., Mathur, S., Huang, L., Wang, Y., et al. (2021). Electrospinning nanofibers and nanomembranes for oil/water separation. *J. Mater. Chem. A* 9 (38), 21659–21684. doi:10.1039/D1TA05873H
- Ye, J. D., Gu, S. L., Qin, F., Zhu, S. M., Liu, S. M., Zhou, X., et al. (2005). Correlation between green luminescence and morphology evolution of ZnO films. *Appl. Phys. A* 81 (4), 759–762. doi:10.1007/s00339-004-2996-0
- Ye, J., Li, B., Li, M., Zheng, Y., Wu, S., and Han, Y. (2022). Formation of a ZnO nanorods-patterned coating with strong bactericidal capability and quantitative evaluation of the contribution of nanorods-derived puncture and ROS-derived killing. *Bioact. Mater.* 11, 181–191. doi:10.1016/j.bioactmat.2021.09.019
- Yong, H. E., Krishnamoorthy, K., Hyun, K. T., and Kim, S. J. (2015). Preparation of ZnO nanopaint for marine antifouling applications. *J. Indust. Eng. Chem.* 29, 39–42. doi:10.1016/j.jiec.2015.04.020
- Zhao, J.-H., Liu, C.-J., and Lv, Z.-H. (2016). Photoluminescence of ZnO nanoparticles and nanorods. *Optik* 127 (3), 1421–1423. doi:10.1016/j.jleo.2015.11.018
- Zhou, Y., Fu, S. Y., Zheng, L. M., and Zhan, H. Y. (2012). Effect of nanocellulose isolation techniques on the formation of reinforced poly(vinyl alcohol) nanocomposite films. *Express Polym. Lett.* 6, 794–804. doi:10.3144/expresspolymlett.2012.85



OPEN ACCESS

EDITED BY

Sirikanjana Thongmee,
Kasetsart University, Thailand

REVIEWED BY

Ramzan Ahmed,
University of Science and Technology,
Meghalaya, India
Mithun Kumar Ghosh,
Govt College Hattat, India

*CORRESPONDENCE

Devendra Jain,
✉ devroshan@gmail.com,
✉ devendrajain@mpuat.ac.in

SPECIALTY SECTION

This article was submitted to
Nanoscience,
a section of the journal
Frontiers in Chemistry

RECEIVED 30 January 2023

ACCEPTED 23 March 2023

PUBLISHED 07 April 2023

CITATION

Singh D, Jain D, Rajpurohit D, Jat G,
Kushwaha HS, Singh A, Mohanty SR,
Al-Sadoon MK, Zaman W and
Upadhyay SK (2023), Bacteria assisted
green synthesis of copper oxide
nanoparticles and their potential
applications as antimicrobial agents and
plant growth stimulants.
Front. Chem. 11:1154128.
doi: 10.3389/fchem.2023.1154128

COPYRIGHT

© 2023 Singh, Jain, Rajpurohit, Jat,
Kushwaha, Singh, Mohanty, Al-Sadoon,
Zaman and Upadhyay. This is an open-
access article distributed under the terms
of the [Creative Commons Attribution
License \(CC BY\)](#). The use, distribution or
reproduction in other forums is
permitted, provided the original author(s)
and the copyright owner(s) are credited
and that the original publication in this
journal is cited, in accordance with
accepted academic practice. No use,
distribution or reproduction is permitted
which does not comply with these terms.

Bacteria assisted green synthesis of copper oxide nanoparticles and their potential applications as antimicrobial agents and plant growth stimulants

Deepak Singh¹, Devendra Jain^{1*}, Deepak Rajpurohit¹,
Gajanand Jat², Himmat Singh Kushwaha³, Abhijeet Singh⁴,
Santosh Ranjan Mohanty⁵, Mohammad Khalid Al-Sadoon⁶,
Wajid Zaman⁷ and Sudhir K. Upadhyay⁸

¹Department of Molecular Biology and Biotechnology, Maharana Pratap University of Agriculture and Technology, Udaipur, India, ²Department of Soil Science and Agricultural Chemistry, Maharana Pratap University of Agriculture and Technology, Udaipur, India, ³Material Research Centre, Malviya National Institute of Technology, Jaipur, India, ⁴Department of Biosciences, Manipal University Jaipur, Jaipur, India, ⁵All India Network Project on Soil Biodiversity-Biofertilizers, ICAR-Indian Institute of Soil Science, Bhopal, India, ⁶Department of Zoology, College of Science, King Saud University, Riyadh, Saudi Arabia, ⁷Department of Life Sciences, Yeungnam University, Gyeongsan, Republic of Korea, ⁸Department of Environmental Science, V. B. S. Purvanchal University, Jaunpur, India

Copper oxide nanoparticles (CuO-NPs) have piqued the interest of agricultural researchers due to their potential application as fungicides, insecticides, and fertilizers. The *Serratia* sp. ZTB29 strain, which has the NCBI accession number MK773873, was a novel isolate used in this investigation that produced CuO-NPs. This strain can survive concentrations of copper as high as 22.5 mM and can also remove copper by synthesizing pure CuO-NPs. UV-VIS spectroscopy, DLS, Zeta potential, FTIR, TEM, and XRD techniques were used to investigate the pure form of CuO-NPs. The synthesized CuO-NPs were crystalline in nature (average size of 22 nm) with a monoclinic phase according to the XRD pattern. CuO-NPs were found to be polydisperse, spherical, and agglomeration-free. According to TEM and DLS inspection, they ranged in size from 20 to 40 nm, with a typical particle size of 28 nm. CuO-NPs were extremely stable, as demonstrated by their zeta potential of -15.4 mV. The ester (C=O), carboxyl (C=O), amine (NH), thiol (S-H), hydroxyl (OH), alkyne (C-H), and aromatic amine (C-N) groups from bacterial secretion were primarily responsible for reduction and stabilization of CuO-NPs revealed in an FTIR analysis. CuO-NPs at concentrations of $50 \mu\text{g mL}^{-1}$ and $200 \mu\text{g mL}^{-1}$ displayed antibacterial and antifungal activity against the plant pathogenic bacteria *Xanthomonas* sp. and pathogenic fungus *Alternaria* sp., respectively. The results of this investigation support the claims that CuO-NPs can be used as an efficient antimicrobial agent and nano-fertilizer, since, compared to the control and higher concentrations of CuO-NPs (100 mg L^{-1}) considerably improved the growth characteristics of maize plants.

KEYWORDS

novel bacterial isolate, 16s-rDNA sequencing, CuO-NPs-green synthesis, confirmatory tests, antimicrobial and plant growth-promoting activity

1 Introduction

Nanotechnology research is the most active research region in contemporary materials science (Singh et al., 2018; Rajput et al., 2021a; Bhavyasree and Xavier, 2022). Nanomaterials synthesis through conventional physical and chemical methods has several adverse features viz., critically high pressure and temperature conditions, utilization of expensive and hazardous chemicals, a longer reaction time and absorbance of toxic by-products on nanomaterial surface (Buazar et al., 2019; Sukumar et al., 2020). Properties of NPs determined by their size, shape, composition, crystalline, and structure (Sharma et al., 2020; Hidangmayum et al., 2022; Rajput et al., 2022). Recent years have seen a significant increase in the significance of green synthesis techniques for nanomaterials, making it one of the very popular methods in modern material sciences (Sukhwil et al., 2017; Mahboub et al., 2022).

Green synthesis has become one of the most preferred methods to overcome the adverse effects physical and chemical synthesis such as critical conditions of temperature and pressure, expensive and toxic chemicals, long reflux time of reaction, toxic by-products etc. (Sukhwil et al., 2017; Jain et al., 2020). Metal-tolerant bacteria are important nano-factories that not only accumulates and also detoxify heavy metals due to the various mechanism, i.e., reductase enzymes, EPS, etc., to reduce metal salts to nanomaterials (Jain et al., 2012; Jain et al., 2020; Garg et al., 2022). The nanomaterial synthesis using plant extracts may be easier than microbial synthesis however the microbial synthesis is more cost-effective and freer from any seasonal and plant growth stage variation.

Inorganic metal oxide NPs, viz., CuO, ZnO, MgO, TiO₂, SiO₂, etc., with significant antimicrobial features as well as their selective toxicity, point to potential applications of these materials in medical devices and diagnostics, therapeutics, and nanomedicine against human pathogens (Mohsen and Zahra, 2008; Sobha et al., 2010; Jain D. et al., 2022). These inorganic oxide NPs are beneficial as antibacterial agents because they are more effective against resistant pathogens. According to Makhluaf et al. (2005), crystalline structure and particle shape of nanomaterials have relatively little effect on antibacterial behavior, but a high concentration of smaller-size nanoparticles with a higher surface area does.

The simplest copper compound in the family is copper oxide, which has a variety of possibly practical physical characteristics (Buazar et al., 2019). Copper oxide (CuO) has drawn more interest than other nanomaterials because of its distinctive qualities, which include stability, conductivity, catalytic activity, and anticancer and antibacterial activities. Copper oxide nanoparticles (CuO-NPs) are receiving more attention owing to their availability and lower cost when compared to more costly and noble metals like gold and silver, as well as their effective potential for application as microbial agents (Sankar et al., 2014). Among them, CuO-NPs has drawn a lot of attention in research areas including solar cells, biodiesel, photocatalysis, water pollutant removal, supercapacitors, and electrocatalysis owing to their desired qualities, such as cheap cost, non-toxicity, and ease of manufacturing (Grigore et al., 2016).

By preventing the growth of bacteria, fungi, viruses, and algae, CuO-NPs have important antimicrobial qualities (Amin et al., 2021; Bukhari et al., 2021). Furthermore, compared to other organic antimicrobials like silver and gold, nanoscale copper oxide has a

longer shelf life. According to Keabadile et al. (2020) green synthesis of CuO-NPs with acceptable physio-chemical characteristics has previously been performed with several microbial precursors as reductants. However, very little study has been done on the synthesis of CuO-NPs employing bacteria that are copper-resistant. Hence, the current investigation was conducted to tackle this issue and build a bacteria-assisted synthesis of CuO-NPs and assessment of their antimicrobial and plant growth stimulating activities.

2 Materials and methods

2.1 Source, minimum inhibitory concentration, and molecular identification of copper-tolerant bacteria

The maximum copper tolerance concentration (MTC) was determined on LB agar medium (in triplicate) having an increased concentration of CuSO₄ (2.5–25 mM), and the MTCs were noted from the concentration of CuSO₄ at which the isolate failed to demonstrate growth. The different bacterial isolates were utilized in this study taken from our lab, which were isolated from Zn-Pb ore mine tailings areas of Zawar mines in Udaipur, Rajasthan, India (Jain et al., 2020). According to a previously illustrated method, the 16S rDNA region was amplified and sequenced to perform molecular characterization of copper-tolerant bacteria (Janda and Abbott, 2007).

2.2 Bacterial-assisted synthesis of copper oxide nanoparticles

The synthesis of CuO-NPs was borne out by using copper (Cu) tolerant bacterial isolate (ZTB29) with little modification technique of earlier published (John et al., 2021). The bacterial strain that showed the highest tolerance against copper ion, was inoculated in LB medium (100 mL) and incubated at 28°C with 150 rpm. After 24 h, 5 mM CuSO₄.5H₂O was dropped into the bacterial culture and incubated for 48 h at 28°C until the solution color changed from blue to green. This combination was then centrifuged at 4,000 rpm for 20 min at 4°C to separate the bacterial cell pellet, and the CuO-NPs were produced by centrifuging the residual supernatant at 14,000 rpm for 15 min at 4°C. The obtained CuO-NP pellet was washed twice with deionized water, dried at 80°C in an oven and used for further characterization. A control experiment without copper-tolerant bacteria was also done and upon inclusion of 5 mM CuSO₄.5H₂O, the color change was not seen which states no nanoparticles formation.

2.3 Characterization of CuO-NPs

CuO-NPs were primarily characterized using UV-Vis absorption scanning at 200–1,000 nm using a nanophotometer (Make: Implen, Germany) as the method outlined by Davaeifar et al. (2019). Dynamic Light Scattering (DLS) and Zeta potential were performed by the earlier described method (Rajput et al., 2021b) by using Malvern zeta-sizer nanoseries (United Kingdom). The FTIR spectroscopy (Perkin Elmer)

was performed for CuO-NPs (in KBr pellets) in the 4,100–400 cm^{-1} range (Garg et al., 2022). Around 10 μL of CuO-NPs dispersed in milli Q water were placed onto carbon-coated copper TEM grid for transmission electron microscopy (Tecnai G220 (FEI) S-Twin 200kv) (Sukhwil et al., 2017). The dried powder of CuO-NPs was further characterized by XRD (X'Pert Pro X-ray diffractometer, PAN analytical BV) with Cu K α radiation set with 40 kV and 30 mA (Sukhwil et al., 2017).

2.4 Antimicrobial activities of CuO nanoparticles

Antibacterial activities of bacterial-assisted CuO-NPs were studied by both disc diffusion method and well diffusion using LB agar medium against plant pathogenic bacteria *Xanthomonas* sp. Briefly, 1 mL bacterial suspension ($>10^7$ CFU mL^{-1}) was spread by spreader on LB agar Petri-plates, and in disc diffusion method, the sterile filter paper disk, dipped in a known concentration of CuO-NPs was placed on LB agar plates whereas, in well diffusion method, 5 mm wells (prepared by sterile cork-borer on LB agar Petri-plates) were loaded with CuO-NPs and incubated for inhibition zone development (Jain et al., 2020). The antifungal activities of CuO-NPs were investigated by using the poisoned food technique and spore germination test. The radial mycelia growth of test fungi *Alternaria* sp. was recorded on PDA containing different concentrations of CuO-NPs (50, 75, 100, 150, and 200 $\mu\text{g mL}^{-1}$). PDA plates without CuO-NPs were used as a control. These plates were kept for incubation at 25°C until full radical growth was observed in the control. The different concentration of CuO-NPs was used as per the CRD design in triplicate and the significant difference among treatment were determined by Turkey–Kramer HSD test at $p = 0.05$.

2.5 In vitro studies of CuO-NPs on the growth of maize

The experimental pot was filled with agricultural soil supplemented with sterile planting mixture, seeded with maize seed (PRATAP-3), and placed inside the plant growth chamber (humidity: 60%, light intensity: 750 $\mu\text{mol/m}^2\text{s}$ with 15 h light and 9 h dark conditions at 25°C–20°C). Seven days old maize seedlings were treated with CuO-NPs concentrations viz. 0, 25, 50, 75, 100, 200, and 300 mg L^{-1} (in Hoagland solution) as foliar spray. The shoot length (cm), root length (cm), chlorophyll content (SPAD-502 + Chlorophyll Meter, Spectrum Technologies, India), Copper content [atomic absorption spectroscopy (AAS), Make: Electronics co. India Ltd. Modal no. AAS4141] was studied in 21 days old seedlings (Garg et al., 2022).

3 Result

3.1 Source, screening of MTC against copper and molecular identification of potent copper-tolerant bacteria

The bacterial isolates ZTB15, ZTB24, ZTB28, and ZTB29 were tested for their maximum copper (CuSO_4) tolerance levels in

nutritional broth and observed Minimum inhibitory concentration (MIC). The bacterial isolate ZTB29 had a very maximum MIC of 22.5 mM copper in the medium and was able to withstand high doses of copper in the current experiment (Supplementary Table S1). A further selection of the ZTB29 strain was made for the bacterially aided synthesis of copper oxide CuO-NPs. The ZTB-29 isolate's 16S rRNA gene was sequenced in its entirety and put into nucleotide-nucleotide BLAST analysis. The strains' similarity and matches to previously published bacterial rDNA sequences allowed scientists to identify them as *Serratia* sp. (Figure 1). The ZTB29 nucleotide sequence was deposited to NCBI with the accession MK773873. The detailed biochemical, plant growth promoting and other physiological attributes of the ZTB29 strain were summarized in (Supplementary Table S2) which enables the ZTB29 strain to not only bioremediate excess copper but also to promote plant growth.

3.2 ZTB29 assisted copper oxide nanoparticles synthesis and its confirmatory examination

The easily observed synthetic bacterial growth in the bottom of the flask demonstrated the reaction between the bacterium and copper sulfate, the precursor salt. The starting solution's color changed from light blue to green when 5 mM copper sulfate was added drop by drop to the bacterial suspension, indicating the production of CuO-NPs. The greatest absorbance of 285 nm by using UV-visible spectroscopy was observed, indicating that copper sulfate (which does not produce any absorbance at 285 nm: Supplementary Figure S1), the starting material, was converted to CuO-NPs, as shown in (Figure 2).

The surface charge, size distribution, and potential stability of the nanoparticles contained in a liquid were characterized using dynamic light scattering (DLS) and zeta potential, respectively. Particles in the solution ranged in size from 15 nm to 30 nm and were homogeneous in size. The average CuO-NPs particle size was 21 ± 5.4 nm which was created with a homogenous dispersion (Figure 3A). The TEM investigations provided strong support for the DLS findings. The presence of bacterial cell artifacts or the agglomeration of nanoparticles may be responsible for the second large-size distribution peak at about 1,000 nm. The zeta potential's magnitude (–30 mV to +30 mV) determines the stability and primarily depends upon the surface charge of the generated nanomaterials. The produced nanoparticles have a Zeta potential of –15.4 mV, which demonstrates that they were quite stable at ambient temperature (Figure 3B). The similar zeta potential value was observed even after 1 year of synthesis with CuO-NPs suggesting CuO-NPs were stable for 1 year or more. Zeta potential with a negative value indicates a strong repelling force between the particles, which inhibits agglomeration.

Fourier transform infrared spectroscopy (FTIR) technique was utilized to recognize the occurrence of different functional groups found in a sample. Depending on the infrared absorption range 600–4,000 cm^{-1} in FTIR analysis, the absorbance range 3,200–3,550 cm^{-1} is indicated for O–H stretching, 2,371 cm^{-1} observance for O=C=O stretching, 1,624 cm^{-1} observance for C=C stretching, 1,058 cm^{-1} observance for C–OH stretching,

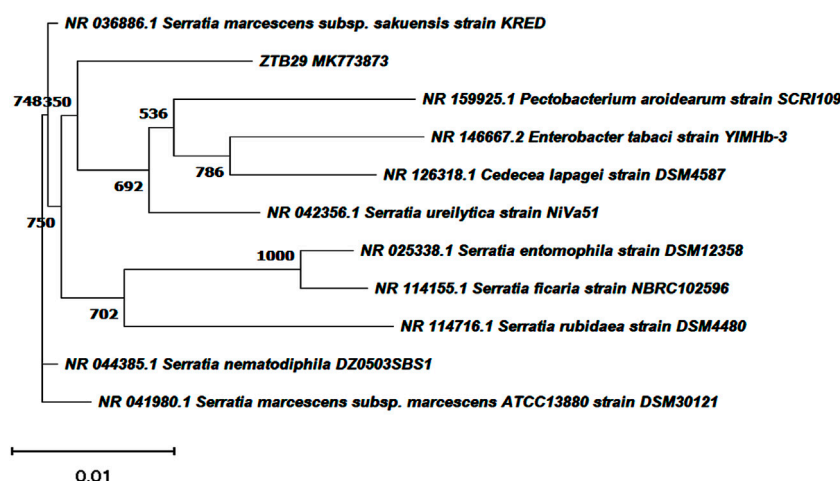


FIGURE 1

Neighbourhood joining tree showing the polygenetic relationship of copper tolerant bacterial strain ZTB29 *Serratia* sp. (NCBI Accession: MK773873).

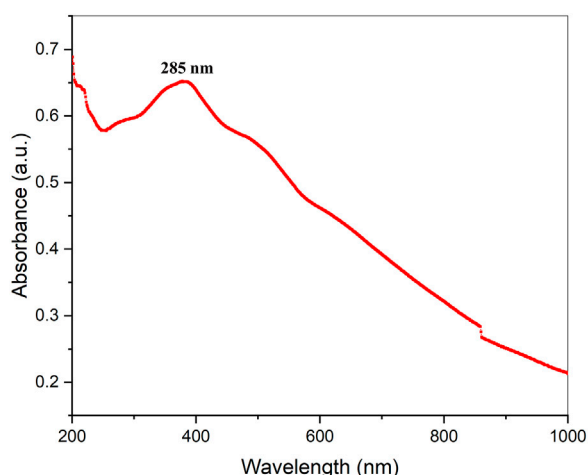


FIGURE 2

UV-Vis absorption spectrum of biogenic CuO nanoparticles.

1,377 cm^{-1} observance for the existence of CO_2 when compared with the standard database. The 608 cm^{-1} vibration attributed to CuO formation confirms the synthesis of pure CuO nanostructures. FTIR study revealed that the carboxyl (C=O), hydroxyl (OH), amine (NH), alkyne (C-H), thiol (S-H), ester (C=O) and aromatic amine (C-N) groups from the bacterial secretion are responsible for the copper reduction and CuO-NPs stabilization (Figure 4). The details of the different FTIR peaks observed in bacteria assisted CuO-NPs and the bacterial extract used for CuO-NPs synthesis were described in the Supplementary Table S3 and Supplementary Figure S2. The CuO-NP's size and shape were studied using TEM. TEM analysis revealed the formation of different shapes of copper oxide nanostructures (Figure 5). It was evident from TEM studies that CuO-NPs were polydisperse and spherical which were free from agglomeration. The particles were in the size range of 20–40 nm with 28 nm average particles size.

X-ray diffraction (XRD) was performed to study the phase (structure) and purity (composition) of the biosynthesized CuO-NPs using copper-tolerant bacteria. The XRD pattern (Figure 6) depicted the creation of pure and crystalline CuO-NPs. The peaks at $2\theta = 32.548$, 35.466 , and 38.769 were assigned to the (110) (002) and (111) reflection lines of monoclinic CuO-NPs compared to JCPDS file No. 01-080-1268. The average crystallite size calculated based on the Scherrer technique for synthesized CuO-NP was 22 nm.

3.3 Antimicrobial activities of CuO-NPs

The CuO-NPs ($50 \mu\text{g mL}^{-1}$) showed significant antibacterial activity by generating an inhibition zone in well diffusion assay (Figure 7A). The disc contacting $50 \mu\text{g mL}^{-1}$ CuO-NPs demonstrated antibacterial activity against *Xanthomonas* sp. as it showed a clear inhibition zone (Figure 7B), which was higher compare to Neomycin ($30 \mu\text{g mL}^{-1}$) and lower compare to Rifampicin ($5 \mu\text{g mL}^{-1}$). The highest inhibition of 91% in fungal mycelia and 88% spore germination was detected at the $200 \mu\text{g mL}^{-1}$ CuO-NPs concentration (Table 1). The rate of mycelia inhibition and spore germination was proportional to CuO-NPs concentration (Figure 8). The results observed in the present study revealed CuO-NP scan be used as an efficient nano fungicide against soil-born fungus.

3.4 Influence of CuO-NPs on maize seedling

The shoot and root length, plant biomass, total chlorophyll and copper content were considerably high in the maize plantlet (21 days old) compared to the untreated control plantlet (Table 2). The maximum shoot and root length, biomass and chlorophyll content were observed in 100 mg L^{-1} CuO-NPs application and contributed to plant growth significantly as efficient nano-fertilizers. The CuO-NPs ($<100 \text{ mg L}^{-1}$) caused significant toxicity to maize seedlings and resulted in decreased growth parameters.

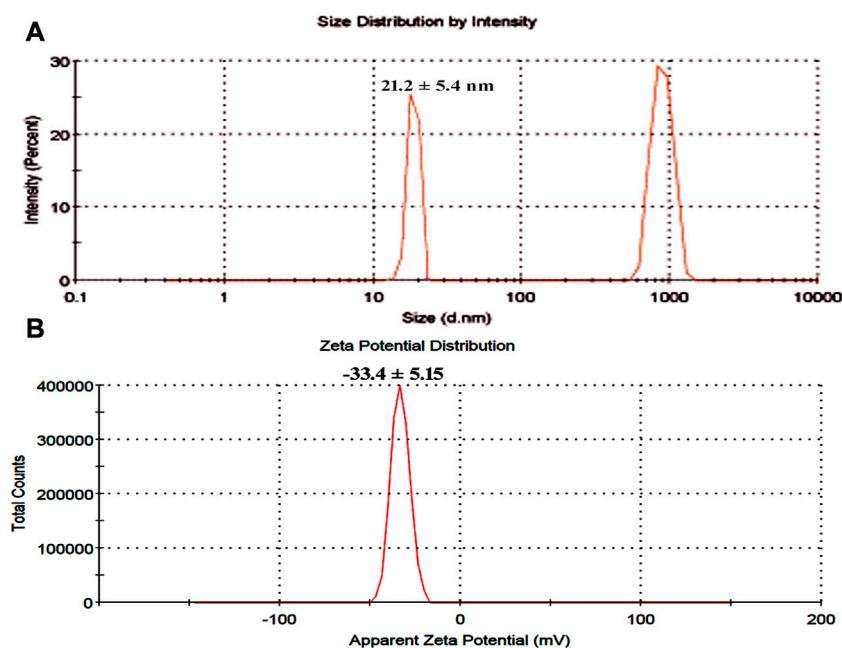


FIGURE 3

(A) Particle size determination using dynamic light scattering (B) Zeta potential analysis of bacterial assisted CuO nanoparticles.

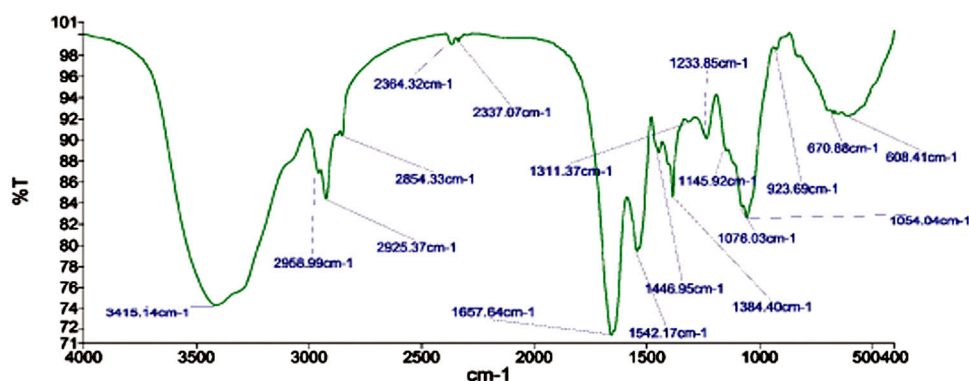


FIGURE 4

FTIR analysis of biogenic CuO nanoparticles.

4 Discussions

The new study could pave the way for bioprospecting for metal-tolerant microorganisms for the quick and easy synthesis of nanoparticles with a variety of applications (Jain et al., 2012; Jain et al., 2020). John et al. (2021) investigated bacterial strain copper tolerance at various CuSO₄ concentrations, and the bacterial strain *Marinomonas*, which tolerated 5 mM CuSO₄, was employed to produce copper and CuO-NPs. Similar findings were found in the current investigation. Tiwari et al. (2016) synthesized CuO-NPs from a copper-resistant *Bacillus cereus* isolate that tolerated >10 mM of copper. The *B. cereus* isolate was able to and was identified as *B. cereus* using 16S rDNA amplification and sequencing. The change of color depends on the surface plasmon vibration of the

nanoparticles (Abdulhameed et al., 2019). Shantkriti and Rani (2014) observed that the color of the reaction changed from blue to dark green when CuSO₄ was added to the *Pseudomonas fluorescens* solution, which corroborated the findings. The bacteria-assisted green synthesis of metal and metal oxide nanoparticles is dependent on the bacteria's ability to remediate harmful metal concentrations by reducing metal ions to nanoparticles (Jain et al., 2020). As a result, copper-tolerant bacteria produce copper and copper oxide nanomaterials by mimicking the natural biomineralization processes that these microbes have adapted to under dangerous copper concentrations (John et al., 2021).

UV-visible absorption spectroscopy can be used to characterize metallic nanoparticles based on surface plasmon resonance (SPR) (Upadhyay et al., 2023). UV-visible spectroscopy (wavelength scan

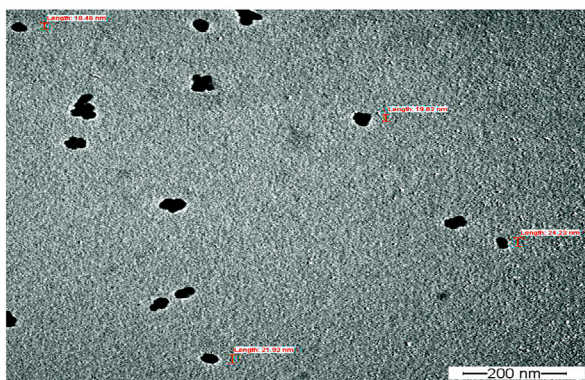


FIGURE 5
TEM analysis of biogenic CuO nanoparticles.

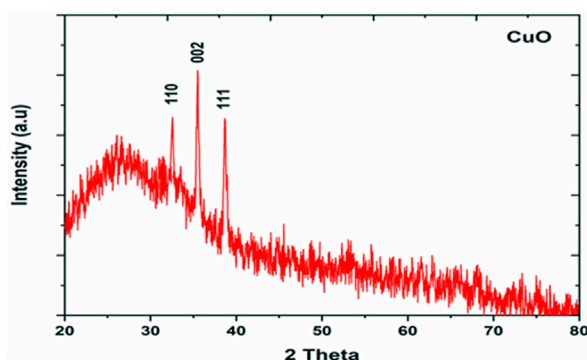


FIGURE 6
XRD analysis of bacterial assisted CuO nanoparticles.

between 200 and 1,000 nm) was used to observe the solution resulting from the bluish-to-greenish color alterations of copper-tolerant bacteria (Zhao et al., 2022). The spectra of CuO-NPs generated employing copper-tolerant bacteria showed pronounced absorption at 285 nm wavelength, confirming the conversion of the starting material (copper sulfate) to the final product (CuO nanoparticles) as shown in Figure 3. Tshireletso et al. (2021) revealed that the UV-VIS absorption spectra of green-produced CuO-NPs from citrus peel extracts resulted in a notable absorbance at 290 nm. Due to surface plasmon resonance, Sankar et al. (2014) found that the UV-Vis spectra of papaya leaf extract mediated CuO-NPs spanned between 250–300 nm. In contrast, the different experiments revealed distinct absorption peaks and spectrums, which could be attributable to different forms of copper and copper oxide nanomaterials and the technology employed for nanomaterial fabrication.

DLS confirmed that the produced CuO-NPs had a homogeneous particle size distribution (15 nm–30 nm) and an average particle size of 21 ± 5.4 nm (Figure 4A), which TEM investigations also validated. The CuO-NPs' -15.4 mV zeta value clearly demonstrated their fairly stable character, as illustrated in Figure 4B. Nardella et al. (2022) conducted DLS investigations of biosynthesized CuO-NPs and reported a 24.4 nm Z-average diameter, while the zeta potential value, which frequently analyses the stability of nanoparticles, was found to be -16.1 mV, confirming the nanoparticles' stability. Nagaraj et al. (2019) reported

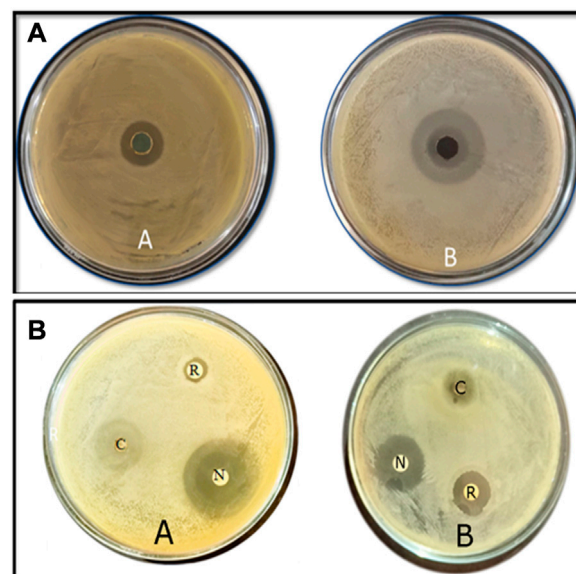


FIGURE 7
Antibacterial activities of biogenic CuO nanoparticles at $50 \mu\text{g mL}^{-1}$ the concentration against (A) *Xanthomonas* Sp. (B) *E. coli* using (a) well diffusion method (b) disc diffusion method along with Rifampicin $5 \mu\text{g mL}^{-1}$ and Neomycin $30 \mu\text{g mL}^{-1}$.

the *Pterolobium hexapetalum* leaf extract-mediated synthesized CuO-NPs and the synthesized nanoparticles were extensively distributed and highly dispersed in the 10–76 nm size range, however, the associated zeta potential was -27.6 mV attributed to moderate stability of nanoparticles.

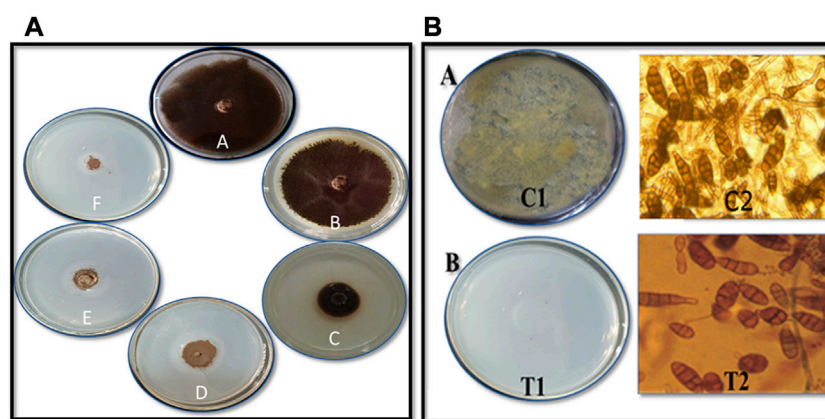
FTIR study indicated the presence of different compounds from the bacterial secretion involved in the reduction and stabilization of CuO-NPs. Amin et al. (2021) observed the FTIR peaks at 518.4 and 600.1 cm^{-1} (formation of CuO nanostructure and Cu–O stretching), $1,021.14$ and 800.58 cm^{-1} (assigned to C–O and C–H bending) and $1,412.3$ and $1,636.4 \text{ cm}^{-1}$ (O–H bending and C=C stretching). John et al. (2021) studied FTIR spectroscopy of CuO-NPs synthesized from marine bacteria indicating the presence of $-\text{C}=\text{O}$, $-\text{OH}$, $-\text{NH}$, $-\text{CH}_2$ scissor vibrations of aliphatic compounds and C=C bonds inside the biomolecules suggesting the interaction of these biomolecules with CuO-NPs also observed in the present study.

TEM analysis revealed the formation of polydisperse and roughly spherical CuO-NPs which were free from agglomeration with the 20–40 nm size range (average particle size is 28 nm). The CuO-NPs as water suspension are slightly agglomerated due to their interaction with water and due to such inter-particle interactions viz. van der Waals, electrostatic and magnetic forces, etc. Previously, similar results of biogenic CuO-NPs were reported by several studies (Ida et al., 2010; Cheng and Walker, 2010; Chandra et al., 2014; Sagadevan and Koteswari, 2015; Kimber et al., 2020; Singh et al., 2019) as observed in TEM. John et al. (2021) reported the TEM micrographs of CuO-NPs from marine bacteria and reported the synthesis of monodispersed, spherical/ovoidal NPs of 10 nm–70 nm size with ~ 40 nm average size. The irregular shape can be attributed to bacterial metabolites on the surface of nanoparticles as stabilizing and reducing agents. Bukhari et al. (2021) reported the *Streptomyces* sp. mediated Cu-NPs synthesis of uniform and spherical nanoparticles (1.72–13.49 nm) in the TEM

TABLE 1 Effect of varying concentrations of CuO nanoparticles on *in vitro* mycelial growth and spore germination of phytopathogenic fungi *Alternaria* sp.

Treatment (CuO nanoparticles)	Percent inhibition mycelia growth	Percent inhibition spore germination
Control	0.0 ± 0.0 _A	5.33 ± 1.52 _A
50 µg mL ⁻¹	15.0 ± 1.53 _B	15.0 ± 2.0 _B
75 µg mL ⁻¹	70.0 ± 1.53 _C	55.0 ± 2.0 _C
100 µg mL ⁻¹	77.0 ± 5.7 _{CD}	64.3 ± 2.51 _D
150 µg mL ⁻¹	81.0 ± 2.0 _D	74.0 ± 1.0 _E
200 µg mL ⁻¹	91.0 ± 1.52 _E	88.0 ± 2.0 _F

*Each value is mean of 3 replicates from 2 experiments. Mean ± SE, followed by same letter in column of each treatment is not significant difference at $p = 0.05$ by Tukey–Kramer HSD, test, % inhibition rate was calculated compared to the germination of the control (0%).

**FIGURE 8**

Antifungal activity of CuO nanoparticles against *Alternaria* sp. on (A) mycelial growth inhibition by poisoned food technique (A) Control (B) 50 µg mL⁻¹ (C) 75 µg mL⁻¹ (D) 100 µg mL⁻¹ (E) 150 µg mL⁻¹ and (F) 200 µg mL⁻¹ CuO nanoparticles (B) Spore germination inhibition by (A) Pour plate technique C1 - Crude spore suspension and T1 - 200 µg mL⁻¹ CuO nanoparticles (B) Microscopic studies C2: Control, T2: 200 µg mL⁻¹ CuO nanoparticles.

TABLE 2 *In vitro* studies on the effect of CuO-NPs on growth of maize seedling (Data are means of three replicates ±SD. Data are recorded after 21 days of germination).

Treatment	Average shoot length (cm)	Shoot dry weight (g)	Average root length (cm)	Chlorophyll index (SPAD)	Copper content in maize seedling (ppm)
Control	18.4 ± 1.7	4.4 ± 1.1	12.8 ± 2.1	10.03 ± 2.11	0.041 ± 0.02
T 1	24.5 ± 2.4	7.8 ± 2.3	14.8 ± 3.2	12.33 ± 2.65	0.055 ± 0.08
T 2	28.8 ± 2.8	8.3 ± 1.6	21.6 ± 2.4	13.63 ± 2.49	0.088 ± 0.06
T 3	32.4 ± 2.2	8.4 ± 2.1	24.1 ± 1.9	14.14 ± 2.43	0.092 ± 0.08
T 4	34.2 ± 3.1	10.6 ± 1.8	24.8 ± 2.3	16.86 ± 4.5	0.098 ± 0.09
T 5	29.4 ± 2.3	9.1 ± 1.5	22.7 ± 2.1	13.93 ± 2.8	0.012 ± 0.05
T 6	21.1 ± 1.9	7.5 ± 1.2	15.1 ± 1.7	11.26 ± 2.3	0.015 ± 0.05

images. Krishna et al. (2020) synthesized CuO nanoparticles from *Cinnamomum malabattrum* aqueous leaf extract and the TEM revealed spherically shaped CuO-NPs with 11 nm–24 nm size range which was also in close agreement with the present study.

The XRD pattern revealed the pure CuO-NPs were crystalline in nature. Ali et al. (2021) performed XRD of CuO-NPs and the detected peaks in their study confirmed the monoclinic phase of CuO compared to JCPDS card 000021040 which was also seen in the present study. Further, the characteristic crystallite size measured

using the Scherrer equation was found to be 24.7 nm also supports the finding of the present study. Buazaret al. (2019) reported that clear and sharp peaks in XRD can be ascribed to the highly crystalline structure of nanomaterials. Similar results of the crystallite size of CuO-NPs in the range of 9–23 nm were solely dependent on the precursor conditions (Tavakoli et al., 2019).

The CuO-NPs exhibited superior antimicrobial activities and have a significant potential to control phytopathogens. Krishna et al. (2020) reported significant antibacterial activities of CuO-NPs against human pathogenic bacteria viz., *Escherichia coli*, *Staphylococcus aureus*, *Pseudomonas aeruginosa* and *Proteus mirabilis* using well diffusion method and similar results were also observed against plant pathogenic bacteria in the present study. Abboud et al. (2014) reported significant antimicrobial activities of CuO-NPs synthesized from the alga extract against *Enterobacter aerogenes* and *S. aureus* and the observed radial diameter of the inhibition zone was 14 and 16 mm, respectively. Bhavyasree and Xavier (2022) extensively reviewed the copper and CuO nanomaterial and their antimicrobial properties and demonstrated the mechanism of antibacterial action which includes mechanical damage, gene toxicity, and oxidative stress injury. The bio-molecules absorbed on the surface may also help in the antimicrobial activities of CuO-NPs.

The CuO-NPs (200 g mL⁻¹ concentration) exhibited superior antifungal activities. Qamar et al. (2020) showed reasonable results for the antifungal activity of CuO-NPs against *Trichophyton rubrum*. Rabiee et al. (2020) synthesized *Achillea millefolium* extract-mediated CuO-NPs and reported significant *in vitro* antifungal activities against four different fungi. The biosynthesized CuO-NPs showed effective antifungal activities owing to the entering of CuO-NPs on fungal membranes and negatively effect the cell divisions *via* strong interaction on the respiratory chains.

The use of CuO-NPs (100 mg L⁻¹) resulted in the improvement of plant growth attributes as copper-based nano-fertilizer. The specific doses of CuO-NPs can play a remarkable role in plant growth promotion are advocated by several researchers (Singh et al., 2018; Rajput et al., 2022) due to the increase bio-availability of Cu²⁺ which led to accelerating the mobilization of food reserves during germination, greater activation of copper enzymes such as cytochrome C oxidase, etc. CuO-NPs in the optimum dose can significantly influence the plant growth and act as efficient nano-fertilizers.

5 Conclusion

In conclusion, we present a straightforward, quick, and environmentally friendly method for producing CuO-NPs with exceptional antibacterial properties. Different approaches have been applied to clarify the size, shape, composition, and stability, and the findings demonstrate that the synthesized nanoparticles are very stable and monoclinic, with the largest particles falling within the size range of 28 nm in diameter. The CuO-NPs may function as a potent bactericide and fungicide that may be employed to combat plant infections as a result of the positive results. With the right toxicological information, the greenly produced CuO-NPs have a large potential and may be used for a variety of tasks, including food processing and control, biomedical forms, product packaging, and more. According to the observations of this study, CuO-NPs are a novel class of antimicrobial agents that may be developed and applied in sustainable agriculture.

Data availability statement

The datasets presented in this study can be found in online repositories. The names of the repository/repositories and accession number(s) can be found below: <https://www.ncbi.nlm.nih.gov/->, MK773873.

Author contributions

DJ designed the research. DS, DR, GJ performed the experiments. SM, SU interpreted the data. HK and AS performed TEM, DLS, Zeta, FTIR and XRD. DJ and SU wrote manuscript. MS and WZ revised and proofread manuscript. All authors reviewed the manuscript.

Funding

Gratefully acknowledge the support by Researchers Supporting Project Number (RSP2023R410), King Saud University, Riyadh, Saudi Arabia. The financial assistance from All India Network Project on soil biodiversity and Bio-fertilizer project and MPUAT, India.

Acknowledgments

The authors would like to extend their sincere appreciation to the Researchers Supporting Project Number (RSP2023R410), King Saud University, Riyadh, Saudi Arabia. The financial assistance from All India Network Project on soil biodiversity & Bio-fertilizer project and the equipment support from IDP, NAHEP project are gratefully acknowledged.

Conflict of interest

The authors declare that the research was conducted in the absence of any commercial or financial relationships that could be construed as a potential conflict of interest.

Publisher's note

All claims expressed in this article are solely those of the authors and do not necessarily represent those of their affiliated organizations, or those of the publisher, the editors and the reviewers. Any product that may be evaluated in this article, or claim that may be made by its manufacturer, is not guaranteed or endorsed by the publisher.

Supplementary material

The Supplementary Material for this article can be found online at: <https://www.frontiersin.org/articles/10.3389/fchem.2023.1154128/full#supplementary-material>

References

- Abboud, Y., Saffaj, T., Chagraoui, A., Bouari, A. El., Brouzi, K., and Tanane, O. (2014). Biosynthesis, characterization and antimicrobial activity of copper oxide nanoparticles (CONPs) produced using Brown alga extract (*Bifurcariabifurcata*). *Appl. Nanosci.* 4, 571–576. doi:10.1007/s13204-013-0233-x
- Abdulhameed, A. S., Jawad, A. H., and Mohammad, A. K. T. (2019). Synthesis of chitosan-ethylene glycol diglycidyl ether/TiO₂ nanoparticles for adsorption of reactive orange 16 dye using a response surface methodology approach. *Bioresour. Technol.* 293, 122071. doi:10.1016/j.biortech.2019.122071
- Ali, M., Ijaz, M., Ikram, M., Ul-Hamid, A., Avais, M., and Anjum, A. A. (2021). Biogenic synthesis, characterization and antibacterial potential evaluation of copper oxide nanoparticles against *Escherichia coli*. *Nanoscale Res. Lett.* 16, 148. doi:10.1186/s11671-021-03605-z
- Amin, F., Khattak, B., Alotaibi, A., Qasim, M., Ahmad, I., Ullah, R., et al. (2021). Green synthesis of copper oxide nanoparticles using *Aerjavanica* leaf extract and their characterization and investigation of *in vitro* antimicrobial potential and cytotoxic activities. *Evidence-Based Complement. Altern. Med.* 5589703, 1–12. doi:10.1155/2021/5589703
- Bhavyasree, P. G., and Xavier, T. S. (2022). Green synthesised copper and copper oxide-based nanomaterials using plant extracts and their application in antimicrobial activity: Review. *Curr. Res. Green Sustain. Chem.* 5, 100249. doi:10.1016/j.crgsc.2021.100249
- Buazar, F., Sweidi, S., Badri, M., and Kroushaw, F. (2019). Biofabrication of highly pure copper oxide nanoparticles using wheat seed extract and their catalytic activity: A mechanistic approach. *Green Process. Synthesis* 8, 691–702. doi:10.1515/gps-2019-0040
- Bukhari, S. I., Hamed, M. M., Al-Agamy, M. H., Gazwi, H. S. S., Radwan, H. H., and Youssif, A. M. (2021). Biosynthesis of copper oxide nanoparticles using *Streptomyces* MHM38 and its biological applications. *Hindawi J. Nanomater.* 6693302, 1–16. doi:10.1155/2021/6693302
- Chandra, S., Kumar, A., and Kumar, T. (2014). Synthesis and characterization of copper nanoparticles by reducing agent. *J. Saudi Chem. Soc.* 18 (2), 149–153. doi:10.1016/j.jscs.2011.06.009
- Cheng, G., and Walker, A. R. H. (2010). Transmission electron microscopy characterization of colloidal copper nanoparticles and their chemical reactivity. *Anal. Bioanal. Chem.* 396, 1057–1069. doi:10.1007/s00216-009-3203-0
- Davaeifar, S., Modarresi, M. H., Mohammadi, M., Hashemi, E., Shafiei, M., Maleki, H., et al. (2019). Synthesizing, characterizing, and toxicity evaluating of phycocyanin-ZnO nanorod composites: A back to nature approaches. *Colloids Surfaces B Biointerfaces* 175, 221–230. doi:10.1016/j.colsurfb.2018.12.002
- Garg, K. K., Jain, D., Rajpurohit, D., Kushwaha, H. S., Daima, H. K., Stephen, B. J., et al. (2022). Agricultural significance of silica nanoparticles synthesized from a silica Solubilizing Bacteria. *Comments Inorg. Chem.* 42 (4), 209–225. doi:10.1080/02603594.2021.1999234
- Grigore, M. E., Biscu, E. R., Holban, A. M., Gestal, M. C., and Grumezescu, A. M. (2016). Methods of synthesis, properties and biomedical applications of CuO nanoparticles. *Pharm. (Basel)* 9 (4), 75. doi:10.3390/ph9040075
- Hidangmayum, A., Debnath, A., Guru, A., Singh, B. N., Upadhyay, S. K., and Dwivedi, P. (2022). Mechanistic and recent updates in nano-bioremediation for developing green technology to alleviate agricultural contaminants. *Int. J. Environ. Sci. Technol.*, 1–26. doi:10.1007/s13762-022-04560-7
- Ida, K., Sugiyama, Y., YukiChujyo, Y., Tomonari, M., Tomoharu Tokunaga, T., Sasaki, K., et al. (2010). *In-situ* TEM studies of the sintering behavior of copper nanoparticles covered by biopolymer nanoskin. *J. Electron Microsc.* 59, 75–80. doi:10.1093/jmicro/dfq055
- Jain, N., Bhargava, A., Tarafdar, J. C., Singh, S. K., and Panwar, J. (2012). A biomimetic approach towards synthesis of zinc oxide nanoparticles. *Appl. Microbiol. Biotechnol.* 97 (2), 859–869. doi:10.1007/s00253-012-3934-2
- Jain, D., Kour, R., Bhojiya, A. A., Meena, R. H., Singh, A., Mohanty, S. R., et al. (2020). Zinc tolerant plant growth promoting bacteria alleviates phytotoxic effects of zinc on maize through zinc immobilization. *Sci. Rep.* 10, 13865. doi:10.1038/s41598-020-70846-w
- Jain, D., Kushwaha, H. S., Rathore, K. S., Stephen, B. J., Daima, H. K., Jain, R., et al. (2022). Fabrication of iron oxide nanoparticles from ammonia vapor and their importance in plant growth and dye degradation. *Part. Sci. Technol.* 40, 97–103. doi:10.1080/02726351.2021.1929601
- Jain, R., Bohra, N., Singh, R. K., Upadhyay, S. K., Srivastava, A. K., and Rajput, V. D. (2022). “Nanomaterials for plants: From ecophysiology to signaling mechanisms and nutrient uptake,” in *The role of nanoparticles in plant nutrition under soil pollution. Sustainable plant nutrition in a changing world*. Editors V. D. Rajput, K. K. Verma, N. Sharma, and T. Minkina (Cham: Springer). doi:10.1007/978-3-030-97389-6-8
- Janda, J. M., and Abbott, S. L. (2007). 16S rRNA gene sequencing for bacterial identification in the diagnostic laboratory: Pluses, perils, and pitfalls. *J. Clin. Microbiol.* 45 (9), 2761–2764. doi:10.1128/JCM.01228-07
- John, M. S., Nagothi, J. A., Zannotti, M., Giovannetti, R., Mancini, A., Ramasamy, K., P., et al. (2021). Biogenic synthesis of copper nanoparticles using bacterial strains isolated from an antarctic consortium associated to a psychrophilic marine ciliate: Characterization and potential application as antimicrobial agents. *Mar. Drugs* 19 (5), 263. doi:10.3390/md19050263
- Keabadile, O. P., Aremu, A. O., Elugoke, S. E., and Fayemi, O. E. (2020). Green and traditional synthesis of copper oxide nanoparticles-comparative study. *Nanomater. (Basel)* 10 (12), 2502. doi:10.3390/nano10122502
- Kimber, R. L., Bagshaw, H., Smith, K., Buchanan, D. M., Coker, V. S., Cavet, J. S., et al. (2020). Biomineralization of Cu 2S nanoparticles by geobactersulfurreducens. *Appl. Environ. Microbiol.* 86, 009677–e1020. doi:10.1128/AEM.00967-20
- Krishna, B. A., Kumar, P. N., and Prema, P. (2020). Green synthesis of copper oxide nanoparticles using *Cinnamomum malabattrum* leaf extract and its antibacterial activity. *Indian J. Chem. Technol.* 27, 525–530.
- Mahboub, H. H., Rashidian, G., Hoseinifar, S. H., Kamel, S., Zare, M., Ghafarifarani, H., et al. (2022). Protective effects of Allium hirtifolium extract against foodborne toxicity of Zinc oxide nanoparticles in Common carp (*Cyprinus carpio*). *Comp. Biochem. Physiol. Part C Toxicol. Pharmacol.* 257, 109345. doi:10.1016/j.cbpc.2022.109345
- Makhlu, S., Dror, R., Nitzan, Y., Abramovich, R. J., and Gedanken, A. (2005). Microwave-assisted synthesis of nanocrystalline MgO and its use as a bactericide. *Adv. Funct. Mater.* 15, 1708–1715. doi:10.1002/adfm.200500029
- Mohsen, J., and Zahra, B. (2008). Protein nanoparticle: A unique system as drug delivery vehicles. *Afr. J. Biotechnol.* 7, 4926.
- Nagaraj, E., Karuppannan, K., Shanmugam, P., and Venugopal, S. (2019). Exploration of biosynthesized copper oxide nanoparticles using pterolobiumhexapetalum leaf extract by photocatalytic activity and biological evaluations. *J. Clust. Sci.* 30, 1157–1168. doi:10.1007/s10876-019-01579-8
- Nardella, M. I., Fortino, M., Barbanente, A., Natile, G., Pietropaolo, A., and Arnesano, F. (2022). Multinuclear metal-binding ability of the N-terminal region of human copper transporter Ctr1: Dependence upon pH and metal oxidation state. *Front. Mol. Biosci.* 9, 897621. doi:10.3389/fmolb.2022.897621
- Qamar, H., Rehman, S., Chauhan, D. K., Tiwari, A. K., and Upmanyu, V. (2020). Green synthesis, characterization and antimicrobial activity of copper oxide nanomaterial derived from momordica charantia. *Int. J. Nanomed.* 15, 2541–2553. doi:10.2147/IJN.S240232
- Rabiee, N., Bagherzadeh, M., Kiani, M., Ghadiri, A. M., Etesamifar, F., Jaberzadeh, A. H., et al. (2020). Biosynthesis of copper oxide nanoparticles with potential biomedical applications. *Int. J. Nanomed.* 15, 3983–3999. doi:10.2147/IJN.S255398
- Rajput, V. D., Minkina, T., Fedorenko, A., Chernikova, N., Hassan, T., Mandzhieva, S., et al. (2021a). Effects of zinc oxide nanoparticles on physiological and anatomical indices in spring barley tissues. *Nanomaterials* 11, 1722. doi:10.3390/nano11071722
- Rajput, V. D., Singh, A., Minkina, T., Rawat, S., Mandzhieva, S., Sushkova, S., et al. (2021b). Nano-enabled products: challenges and opportunities for sustainable agriculture. *Plants* 10, 2727. doi:10.3390/plants10122727
- Rajput, V. D., Minkina, T., Upadhyay, S. K., Kumari, A., Ranjan, A., Mandzhieva, S., et al. (2022). Nanotechnology in the restoration of polluted soil. *Nanomaterials* 12, 769. doi:10.3390/nano12050769
- Sagadevan, S., and Koteeswari, P. (2015). Analysis of structure, surface morphology, optical and electrical properties of copper nanoparticles. *J. Nanomed. Res.* 2 (5), 133–136. doi:10.15406/jnmr.2015.02.00040
- Sankar, R., Manikandan, P., Malavizhi, V., Fathima, T., and ShivashangariRavikumar, K. S. V. (2014). Green synthesis of colloidal copper oxide nanoparticles using Carica papaya and its application in photocatalytic dye degradation. *Spectrochim. Acta Part A Mol. Biomol. Spectrosc.* 121, 746–750. doi:10.1016/j.saa.2013.12.020
- Shantkriti, S., and Rani, P. (2014). Biological synthesis of Copper nanoparticles using *Pseudomonas fluorescens*. *Int. J. Curr. Microbiol. Appl. Sci.* 3 (9), 374–383.
- Sharma, M., Sharma, A., and Majumder, S. (2020). Synthesis, microbial susceptibility and anti-cancerous properties of copper oxide nanoparticles-review. *Nano Express* 1 (1), 012003. doi:10.1088/2632-959x/ab9241
- Singh, J., Dutta, T., Kim, K. H., Rawat, M., Samddar, P., and Kumar, P. (2018). ‘Green’ synthesis of metals and their oxide nanoparticles: Applications for environmental remediation. *J. Nanobiotechnol.* 16 (1), 84. doi:10.1186/s12951-018-0408-4
- Singh, J., Kumar, V., Kim, K. H., and Rawat, M. (2019). Biogenic synthesis of copper oxide nanoparticles using plant extract and its prodigious potential for photocatalytic degradation of dyes. *Environ. Res.* 177, 108569. doi:10.1016/j.envres.2019.108569
- Sobha, K., Surendranath, K., Meena, V. K., Jwala, T., Swetha, N., and Latha, K. S. M. (2010). Emerging trends in nanobiotechnology. *J. Biotechnol. Mol. Rev.* 5, 01–12.
- Sukhwai, A., Jain, D., Joshi, A., Rawal, P., and Kushwaha, H. S. (2017). Biosynthesized silver nanoparticles using aqueous leaf extract of *Tagetuspatala* L. and evaluation of their antifungal activity against phytopathogenic fungi. *IET Nanobiotechnol.* 11, 531–537. doi:10.1049/iet-nbt.2016.0175
- Sukumar, S., Rudrasenan, A., and PadmanabhanNambiar, D. (2020). Green-Synthesized rice-shaped copper oxide nanoparticles using *Caesalpinia bonducella*

seed extract and their applications. *ACS-Omega* 5 (2), 1040–1051. doi:10.1021/acsomega.9b02857

Tavakoli, S., Kharaziha, M., and Ahmadi, S. (2019). Green synthesis and morphology dependent antibacterial activity of copper oxide nanoparticles. *J. Nanostruct.* 9 (1), 163–171. doi:10.22052/JNS.2019.01.018

Tiwari, M., Jain, P., Hariharapura, R., Kashinathan, N., Bhat, B., Nayanabhirama, U., et al. (2016). Biosynthesis of copper nanoparticles using copper-resistant *Bacillus cereus*, a soil isolate. *Process Biochem.* 51, 1348–1356. doi:10.1016/j.procbio.2016.08.008

Tshireletso, P., Ateba, C. N., and Fayemi, O. E. (2021). Spectroscopic and antibacterial properties of CuONPs from orange, lemon and tangerine peel

extracts: Potential for combating bacterial resistance. *Molecules* 26, 586. doi:10.3390/molecules26030586

Upadhyay, S. K., Devi, P., Kumar, V., Pathak, H. K., Kumar, P., Rajput, V. D., et al. (2023). Efficient removal of total arsenic ($\text{As}^{3+}/5+$) from contaminated water by novel strategies mediated iron and plant extract activated waste flowers of marigold. *Chemosphere* 313, 137551. doi:10.1016/j.chemosphere.2022.137551

Zhao, H., Maruthupandy, M., Al-mekhlafi, F. A., Chackaravathi, G., Ramachandran, G., and Chelliah, C. K. (2022). Biological synthesis of copper oxide nanoparticles using marine endophytic actinomycetes and evaluation of biofilm producing bacteria and A549 lung cancer cells. *J. King Saud Univ. - Sci.* 34 (3), 101866. doi:10.1016/j.jksus.2022.101866



OPEN ACCESS

EDITED BY

Sirikanjana Thongmee,
Kasetsart University, Thailand

REVIEWED BY

Lakshmi Narayanan Mosur Saravana
Murthy,
Intel, United States
Devendra Jain,
Maharana Pratap University of Agriculture
and Technology, India

*CORRESPONDENCE

Joanna Trzcińska-Wencel,
✉ trzcinska@doktorant.umk.pl
Patrycja Golińska,
✉ golinska@umk.pl

RECEIVED 06 June 2023

ACCEPTED 20 July 2023

PUBLISHED 04 August 2023

CITATION

Trzcińska-Wencel J, Wypij M, Terzyk AP,
Rai M and Golińska P (2023),
Biofabrication of novel silver and zinc
oxide nanoparticles from *Fusarium solani*
IOR 825 and their potential application in
agriculture as biocontrol agents of
phytopathogens, and seed germination
and seedling growth promoters.
Front. Chem. 11:1235437.
doi: 10.3389/fchem.2023.1235437

COPYRIGHT

© 2023 Trzcińska-Wencel, Wypij, Terzyk,
Rai and Golińska. This is an open-access
article distributed under the terms of the
[Creative Commons Attribution License](#)
(CC BY). The use, distribution or
reproduction in other forums is
permitted, provided the original author(s)
and the copyright owner(s) are credited
and that the original publication in this
journal is cited, in accordance with
accepted academic practice. No use,
distribution or reproduction is permitted
which does not comply with these terms.

Biofabrication of novel silver and zinc oxide nanoparticles from *Fusarium solani* IOR 825 and their potential application in agriculture as biocontrol agents of phytopathogens, and seed germination and seedling growth promoters

Joanna Trzcińska-Wencel^{1*}, Magdalena Wypij¹, Artur P. Terzyk²,
Mahendra Rai^{1,3} and Patrycja Golińska^{1*}

¹Department of Microbiology, Faculty of Biological and Veterinary Sciences, Nicolaus Copernicus University in Toruń, Toruń, Poland, ²Physicochemistry of Carbon Materials Research Group, Department of Chemistry of Materials, Adsorption and Catalysis, Faculty of Chemistry, Nicolaus Copernicus University in Toruń, Toruń, Poland, ³Nanobiotechnology Laboratory, Department of Biotechnology, SGB Amravati University, Amravati, India

Introduction: Plant pathogenic microorganisms adversely affect the growth and yield of crops, which consequently leads to losses in food production. Metal-based nanoparticles (MNPs) can be a remedy to solve this problem.

Methods: Novel silver nanoparticles (AgNPs) and zinc oxide nanoparticles (ZnONPs) were biosynthesized from *Fusarium solani* IOR 825 and characterized using Dynamic Light Scattering (DLS), Fourier Transform Infrared (FTIR) spectroscopy, Transmission Electron Microscopy (TEM), X-ray diffraction (XRD) and measurement of Zeta potential. Antibacterial activity of NPs was evaluated against four plant pathogenic strains by determination of the minimum inhibitory (MIC) and biocidal concentrations (MBC). Micro-broth dilution method and poisoned food technique were used to assess antifungal activity of NPs against a set of plant pathogens. Effect of nanopriming with both types of MNPs on maize seed germination and seedlings growth was evaluated at a concentration range of 1–256 $\mu\text{g mL}^{-1}$.

Results: Mycosynthesis of MNPs provided small (8.27 nm), spherical and stable (zeta potential of -17.08 mV) AgNPs with good crystallinity. Similarly, ZnONPs synthesized by using two different methods (ZnONPs(1) and ZnONPs(2)) were larger in size (117.79 and 175.12 nm, respectively) with Zeta potential at -9.39 and -21.81 mV , respectively. The FTIR spectra showed the functional groups (hydroxyl, amino, and carboxyl) of the capping molecules on the surface of MNPs. The values of MIC and MBC of AgNPs against bacteria ranged from 8 to 256 $\mu\text{g mL}^{-1}$ and from 512 to 1024 $\mu\text{g mL}^{-1}$, respectively. Both types of ZnONPs displayed antibacterial activity at 256–1024 $\mu\text{g mL}^{-1}$ (MIC) and 512–2048 $\mu\text{g mL}^{-1}$ (MBC), but in the concentration range tested, they revealed no activity against *Pectobacterium carotovorum*. Moreover, AgNPs and ZnONPs inhibited the

mycelial growth of *Alternaria alternata*, *Fusarium culmorum*, *Fusarium oxysporum*, *Phoma lingam*, and *Sclerotinia sclerotiorum*. MIC and MFC values of AgNPs ranged from 16–128 and 16–2048 $\mu\text{g mL}^{-1}$, respectively. ZnONPs showed antifungal activity with MIC and MFC values of 128–2048 $\mu\text{g mL}^{-1}$ and 256–2048 $\mu\text{g mL}^{-1}$, respectively. The AgNPs at a concentration of $\geq 32 \mu\text{g mL}^{-1}$ revealed sterilization effect on maize seeds while ZnONPs demonstrated stimulatory effect on seedlings growth at concentrations of $\geq 16 \mu\text{g mL}^{-1}$ by improving the fresh and dry biomass production by 24% and 18%–19%, respectively.

Discussion: AgNPs and ZnONPs mycosynthesized from *F. solani* IOR 825 could be applied in agriculture to prevent the spread of pathogens. However, further toxicity assays should be performed before field evaluation. In view of the potential of ZnONPs to stimulate plant growth, they could be crucial in increasing crop production from the perspective of current food assurance problems.

KEYWORDS

applied microbiology, biocontrol, biofabrication, biogenic nanoparticles, bionanotechnology, crop protection, mycosynthesis, plant pathogens

1 Introduction

Plant diseases caused by pathogenic microorganisms adversely affect the growth and yield of crops, which consequently leads to losses in food production (Peng et al., 2021). Recently, Van Dijk et al. (2021) presented a set of projections on the growth of food demand between 2010 and 2050 and the risks of food shortage and hunger. The majority of food safety research focuses on common denominators such as climate change, resistant pathogens, and the need for sustainable agriculture while addressing human health and environmental concerns (Zakirov et al., 2021). The use of technological advances, including mechanization, pesticides or fertilizers, allowed to achieve higher productivity of crop plants (Jacquet et al., 2022). It is estimated that 70%–80% of plant diseases are caused by fungal pathogens particularly by secretion of toxins that cause various physiological disorders, growth inhibition, chlorosis, wilting, etc. (Peng et al., 2021). Maize belongs to the most frequent crop plants worldwide, including Poland (Król et al., 2018), and is particularly vulnerable to pathogenic fungi, e.g., *Fusarium* spp. (Czembor et al., 2015). In addition, microbial diseases lead to yield losses, while mycotoxins produced by fungi contaminate and reduce the quality of maize grains (Czembor et al., 2015). A number of synthetic chemical pesticides are required to prevent crop diseases. However, some negative aspects of pesticides on the environment and human health have been unequivocally documented, therefore limiting their use is of high priority (Jacquet et al., 2022). A number of studies have been conducted to design the remedy for addressing this excessive and seemingly irreplaceable application of traditional chemicals which showed that a prospective solution may be the use of products at the nanoscale (Pestovsky and Martinez-Antonio, 2017). Metal-based nanoparticles (MNPs) show promising potential for use in agriculture field as they demonstrate broad range of antibacterial and antifungal activities (Singh et al., 2021). The use of bio-nanoparticles (bio-NPs) as antimicrobial agents might empower a significant reduction in the dose used while maintaining antimicrobial efficacy compared to conventional materials. From an agro-ecological point of view, the application of nanoparticles (NPs) obtained from biological sources may mitigate the negative consequences of agriculture procedures imposed on the environment (Hazarika et al., 2022).

To date, various studies on the potential use of MNPs as fungicides have been reported (Malandrakis et al., 2022). Silver and zinc oxide nanoparticles (AgNPs and ZnONPs, respectively) display antimicrobial activity depending, in particular, on their physicochemical properties and the targeted pathogen (Gudkov et al., 2021). Some reports showed antimicrobial activity of biosynthesized AgNPs and ZnONPs against, e.g., *Escherichia coli*, *Pseudomonas aeruginosa*, *Staphylococcus aureus*, *Xanthomonas oryzae* pv. *oryzae*, *Alternaria alternata*, *Pyricularia oryzae*, *Sclerotinia sclerotiorum*, and many more (Consolo et al., 2020; El Sayed and El-Sayed, 2020; Ogunyemi et al., 2020; Pillai et al., 2020). It is suggested that the high ability of biosynthesized NPs to control microbial pathogens is due to their large surface area, small size, and high concentration of released ions or capping agents on the surface of the metallic core (Gudkov et al., 2021). In addition, zinc plays an important role in cell function and proliferation (membrane stability, metabolic processes, enzymatic activity, photosynthesis) and consequently in plant physiology (Cakmak et al., 2010; Faizan et al., 2020). It has been reported that the foliar and soil use of ZnONPs for maize biofortification resulted in higher Zn availability and uptake and affected Zn content in edible crop organs than the commonly used zinc sulfate (ZnSO_4). The higher bioavailability of zinc in nano form is attributed to its lower solubility than that of ZnSO_4 salts (Umar et al., 2021). In another study, maize and wheat supplementation with ZnONPs in lower doses (100 mg L^{-1}) improved seedling length and biomass production, and enzyme activity (α -amylase, antioxidative system enzymes), which suggests potential application of ZnONPs as stimulators of crop plant growth (Srivastav et al., 2021). However, some phytotoxic effects of MNPs to plant development has been summarized by Abedi et al. (2022). This aspect is important before the evaluation of plant growth protection and/or promotion with the use of nanoparticles in the field. The diverse properties (small sizes, variable shapes, chemical nature) of MNPs determine their high reactivity and subsequently their uptake, translocation, and interactions in plants (de la Rosa et al., 2021). Some studies reported, that MNPs affect basic cellular processes by inducing oxidative stress, disrupting cell membrane transport or altering gene expression (Lee et al., 2013; Akhtar et al., 2022). Recently, Wan and coworkers (2019) found that ZnONPs (at

concentration $>100 \text{ mg L}^{-1}$) caused endocytosis and led to the rearrangement of microfilament in the epidermal cells of elongation zones of *Arabidopsis* seedlings. However, above changes were temporary, and plants after NPs-related stress recovered faster than those treated with Zn^{2+} ions. In addition, MNPs introduced into the soil environment may cause changes in soil fertility, as well as affect microorganisms and invertebrates. Wei and coworkers (2021) reported diversified effects of ZnO , Cu , and $\gamma\text{-Fe}_2\text{O}_3$ NPs on plant (*Salvia miltiorrhiza*) growth and soil environment. For instance, the effect of NPs on seedling aboveground biomass depended on the type of NPs and dose applied (100 and 700 mg kg^{-1}). CuNPs showed no effect on plant biomass production at tested concentrations. In the case of ZnONPs, their lower concentrations (100 mg kg^{-1}) promoted growth, while higher concentrations (700 mg kg^{-1}) reduced it. In turn, $\gamma\text{-Fe}_2\text{O}_3$ NPs at both tested concentrations promoted plant growth. Moreover, the increase in the relative abundance of *S. miltiorrhiza* rhizosphere microorganisms, namely, the plant growth-promoting bacteria (*Sphingomonas*), superoxide dismutase producers (*Aminobacter*), and the metal-tolerant bacteria (*Thiobacillus* and *Metarhizium*) after MNPs-treatment was observed (Wei et al., 2021). The above findings indicate that various nanomaterials introduced into the environment might have undesirable effects, thus there is an urgent need to properly identify and study the effects of plant exposure to nanoparticles.

The synthesis of nanoparticles covers a variety of approaches, which include physical, chemical, biological, and their combination (Rai et al., 2021). The formation and structural parameters of nanoparticles depend on the reaction conditions and type of the stabilizing agent used in the synthesis (Lallo da Silva et al., 2019). Numerous studies have shown that the ability to form nanoparticles is demonstrated by plants (Balachandar et al., 2019; Verma and Bharadvaja, 2022), bacteria (Quinteros et al., 2019; Saeed et al., 2020), actinomycetes (Wypij et al., 2021, 2022), fungi (Feroze et al., 2020), and viruses (Le et al., 2017) by using their live cultures, biomass, extracts, and metabolites. Mycosynthesis of various nanoparticles is intensively studied by many researchers (Ingle et al., 2009; Abd El-Aziz et al., 2015; Clarence et al., 2020). The benefits of fungal-mediated synthesis of nanoparticles include the simplicity of preparation and the relatively undemanding stages of the synthesis process (Ganachari et al., 2012; Zare et al., 2017). Moreover, these microorganisms seem to possess an outstanding ability to tolerate metals, and fungal metabolites are involved in the reduction of metal salts as well as the further formation of metallic nanoparticles (Kobashigawa et al., 2019; Rai et al., 2021). Further research needs to focus on optimizing the synthesis process to obtain efficient scale production and nanoproductions with the sought-after bioactivity important for their potential application (Sasani et al., 2023). The adaptation of environmental conditions to the growth of microorganisms as well as synthesis conditions assists in the efficient production of nanoparticles with well-defined morphology and biological activity (Paul and Roychoudhury, 2021; Murillo-Rábago et al., 2022).

The aim of the study was to evaluate the ability of fungal extract from *F. solani* IOR 825 to synthesize AgNPs and ZnONPs and to optimize the reaction parameters for high production yields and biological activity of generated nanoproductions. It is the first report on the synthesis of silver and zinc oxide

nanoparticles from *Fusarium solani* IOR 825 strain. The novel nanoparticles were assessed for antimicrobial activities against a wide set of phytopathogenic bacteria, fungi, and oomycetes. Moreover, the potential of these AgNPs and ZnONPs for sterilization of maize (*Zea mays*) seeds and the effect of seeds nanoprimering on their germination and seedling growth (shoot and root elongation, fresh and dry mass production) was also evaluated. This is also the first report on the potential use of nanoparticles from *F. solani* species in agriculture for the protection and promotion of maize growth.

2 Material and methods

2.1 Biosynthesis and determination of physical and chemical properties of metal-based nanoparticles

2.1.1 Optimization of fungal growth

For the synthesis of AgNPs and ZnONPs fungal extracts obtained from *F. solani* IOR 825 isolated from parsley was used. The fungal strain was purchased from the bank of plant pathogens of the Institute of Plant Protection (IOR), the National Research Institute of Poland. In order to optimize efficient production of fungal biomass, each strain was cultured in three kinds of media, namely, potato dextrose broth (PDB, A&A Biotechnology), Sabouraud dextrose broth (SDB, Becton Dickinson) and Czapek dox (CDB, Oxoid). Broths (200 mL) were inoculated with the disc ($\varnothing 5 \text{ mm}$) of fungal strain grown for 7 days at 26°C on potato dextrose agar (PDA, Becton Dickinson) cut with a sterile cork borer. Inoculated broth was incubated for 10 days at 26°C in shaking conditions at 150 rpm. Next, fungal biomass was harvested at 6000 rpm for 10 min and washed three times with sterile distilled water to remove medium components. Obtained biomass was weighed and the fungal culture medium that promoted the most efficient biomass production was selected for further studies on mycosynthesis of nanoparticles.

2.1.2 Preparation of fungal extract and mycosynthesis of nanoparticles

The fungal extract used for the synthesis of silver and zinc oxide nanoparticles was prepared from the fungal biomass, as described previously by Wypij et al. (2022) and Trzcińska-Wencel et al. (2023).

Synthesis of AgNPs was carried out as described previously by Trzcińska-Wencel et al. (2023).

Zinc oxide nanoparticles were synthesized after challenging the fungal extract with the aqueous solution of ZnSO_4 (100 mM), as a precursor. Two methods were developed for sufficient synthesis of nanoparticles. The first synthesis method (1) involved the combination of the fungal extract, ZnSO_4 , and NaOH in a ratio of 1:1:1 (v/v/v) with a final volume of 150 mL and heating for 15 min at 40°C . In the second method (2), the pH of the mixture of fungal extract and ZnSO_4 (1:1, v/v) was adjusted at pH 11 with NaOH (0.4 M). Finally, biosynthesized ZnONPs were centrifuged at $6000 \times g$ for 10 min (Thermo Scientific, United States), washed three times with sterile distilled water to remove unwanted components, and obtained pellet was dried at 37°C .

2.1.3 Detection and characterization of NPs

Confirmation of the NPs synthesis and evaluation of the physico-chemical properties of the nanoparticles were carried out as previously described by Wypij et al. (2021). The formation of NPs was verified using UV-Vis spectrometry (NanoDrop One, Thermo Fisher Scientific, United States) in the wavelength range from 200 to 700 nm at the resolution of 1 nm.

Transmission Electron Microscopy (TEM) and Energy Dispersive X-ray Spectroscopy (EDX) The morphology, size, and elemental composition of the NPs were specified by TEM and EDX analysis using a transmission electron microscope coupled with energy dispersive X-ray spectrometer (FEI Tecnai F20 X-Twintool, Fei, Hillsboro, OR, United States). Sample preparation involved the suspension of NPs in deionized water and deposition of the solution (2 µL) on a carbon-coated copper grid (mesh size 400 µm). Samples were dried at room temperature for 24 h prior to measurements.

X-ray diffraction (XRD) The powder of NPs was deposited on the sample holder acquiring a smooth surface and used for XRD studies. Analysis was performed with X' Pert PRO Analytical X6 diffractometer (PANalytical, Netherlands) with Ni filter and CuKα ($\lambda = 1.54056 \text{ \AA}$) radiation source. The diffraction was recorded over a 2θ range of 5° – 120° and compared with the standard database.

Fourier Transform Infrared Spectroscopy (FT-IR) For FTIR analysis, the potassium bromide (KBr) method was used, briefly dried NPs were ground with KBr (1:1, w/w) and used for measurements. The spectrum was recorded in the range of $4,000$ – 400 cm^{-1} using a spectrometer (Spectrum 2000; Perkin-Elmer, Waltham, Massachusetts, United States) running at the resolution of 4 cm^{-1} .

Dynamic light scattering (DLS) Dynamic light scattering and zeta potential measurement were used for the determination of size distribution (hydrodynamic diameter) and stability (zeta potential value) of biosynthesized NPs. Dried NPs were suspended in ultrapure Milli-Q water and sonicated for 15 min at 30 kHz prior to measurements. The analysis was performed using Particulate Systems, NanoPlus HD (Micromeritics, Particulate Systems, Norcross, GA, United States).

2.2 Antimicrobial activity studies

2.2.1 Antibacterial activity

The antibacterial activity of synthesized MNPs was assessed against plant pathogenic bacterial strains, namely, *Agrobacterium tumefaciens* IOR 911, *Pectobacterium carotovorum* PCM 2056, *Pseudomonas syringae* IOR 2188 and *Xanthomonas campestris* IOR 512 according to Clinical Laboratory Standard Institute (CLSI, 2012). Strains were grown in 20 mL of trypticase soy broth (TSB, Becton Dickinson) for 24 h at 26°C under shaking conditions (120 rpm) and used for the preparation of inocula in distilled water at an optical density of 0.5 McFarland scale ($1.5 \times 10^8 \text{ CFU mL}^{-1}$). Minimal inhibitory concentrations (MICs) of nanoparticles were determined, in triplicate, by the 2-fold microdilution method in 96-well plates at the concentration range 1 – 2048 µg mL^{-1} . The final concentration of bacteria in each well was $1.5 \times 10^6 \text{ CFU mL}^{-1}$ while the final volume of sample in the wells was 150 µL. Both a negative control (sterile medium) and a

positive control (inoculated medium) were performed. The MICs of NPs were defined as the concentrations for which no visible growth was noted after 24 h of incubation at 26°C .

After the determination of MICs of NPs, an aliquot (100 µL) of samples from wells with no visible bacterial growth was spread on tryptic soy agar (TSA, Becton Dickinson) in Petri plates and incubated for 24 h at 26°C . The lowest concentration of NPs which resulted in the elimination of 99.9% of bacteria was identified as minimal biocidal concentration (MBC).

2.3 Antifungal activity

2.3.1 Tested microorganisms

Antifungal activity of MNPs was evaluated against: *Alternaria alternata*, *Alternaria alternata* IOR 1783, *Aspergillus niger*, *Botrytis cinerea* IOR 1873, *Colletotrichum acutatum* IOR 2153, *Fusarium culmorum*, *Fusarium culmorum* IOR 2333, *Fusarium culmorum* DSM 114849, *Fusarium graminearum* A, *Fusarium graminearum* D, *Fusarium oxysporum*, *Fusarium oxysporum* IOR 342, *Fusarium oxysporum* D, *Fusarium poae* A, *Fusarium tricinctum*, *Penicillium* sp., *Penicillium spinulosum*, *Phoma lingam* IOR 2284, *Sclerotinia sclerotiorum* IOR 2242 and oomycetes *Phytophthora megasperma* IOR 404, *Phytophthora cryptogea* IOR 2080 and *Phytophthora plurivora* IOR 2303.

2.3.2 Inhibition of fungal mycelia growth

Antifungal activity of nanoparticles was evaluated, in triplicate, using poisoned food technique. The final NPs concentrations in the PDA medium were 100 and 200 µg mL^{-1} for AgNPs, and 100 and 1000 µg mL^{-1} for ZnONPs. The aqueous stock solution of nanoparticles was used to prepare the final concentration of NPs in the agar medium. The required stock solution of nanoparticles was added into cooled molten PDA (45°C) followed by manual rotation in a sterile Erlenmeyer flask to disperse the NPs in the medium. The medium (20 mL) was dispensed into sterile Petri dishes (9 cm in diameter) with a sterile serological pipette to avoid bubbles. The medium was allowed to solidify at room temperature ($23^\circ\text{C} \pm 2^\circ\text{C}$) for 1 hour. Agar discs with fungal mycelia (6 mm in diameter), grown on PDA medium for 7 days, were cut using a sterile cork borer and aseptically inoculated at the center of the Petri plates. Control plates were PDA media without the nanoparticles inoculated following the same procedure. The plates were incubated at 28°C . The fungal colony diameter was recorded after 7 days of incubation. The percentage inhibition of the mycelial growth of the test fungi by the nanoparticles was calculated using the formula by Philippe et al. (2012).

$$\text{Inhibition of mycelial growth (MGI) (\%)} = \frac{dc - dct}{dc} \times 100$$

where dc is the mean diameter of the colony in the control sample, and dct is the mean diameter of the colony in the treated sample.

2.3.3 Inhibition of spore germination

To assess the ability of NPs to inhibit spore germination, minimum inhibitory and minimum fungicidal concentrations (MICs and MFCs) were determined according to the Clinical Laboratory Standard Institute (CLSI, 2012) protocol with slight

modifications. Spore suspensions were prepared by washing fungal colonies grown on PDA medium for 14 days at 26°C with 5 mL sterile distilled water. The spore suspensions were then filtered through a sterile cotton wool filter to remove any residual mycelia. The density of spores in the suspension was set at approx. 1×10^6 spores per mL by using a cell counting chamber (Brand, Germany), 10-fold diluted and used for assays. Assay was performed as earlier described for bacteria, albeit in potato dextrose broth (PDB). The final concentration of spores in each well was 1×10^3 spores per mL. Sterile broth provided negative control while inoculated with spores was positive control. Inoculated plates were incubated for 2 days at 26°C and recorded for MIC. Finally, aliquots (100 µL) from wells without visible microbial growth were spread on the PDA surface and incubated under the same conditions for 7 days for MFC determination. MFC was defined as the lowest concentration at which no fungal growth was observed.

2.4 Influence of NPs on maize (*Zea mays*) seed germination and seedling growth

2.4.1 Seeds sterilization and priming with NPs

For germination assays, seeds of maize were purchased from Torseed S.A (Toruń, Poland). Seeds were surface sterilized for 30 min with 30% H₂O₂ and 70% ethanol (1:1, v:v), followed by 5 times washing with sterile distilled water and placed on ½ Murashige and Skoog (MS) agar medium in sterile culture boxes for 10 days at 22°C ± 2°C for germination. In order to analyze sterilization efficiency, 100 µL of post-wash water from each variant was spread on sterile PDA and Reasoner's 2A agar (R2A) media and incubated for 7 days for the detection of microbial contaminations.

Two varieties of experiments were performed. In the first one, the sterilization potential of both types of NPs to seed surface was evaluated. The 15 non-sterile seeds were soaked for 30 min with 25 mL of AgNPs or ZnONPs solution in water at concentrations of 1, 8, 32, 64, 128, and 256 µg mL⁻¹, washed 5 times with sterile distilled water. Seed sterilized by the standard method and soaked with sterile distilled water served as the control. All seeds were placed on ½ Murashige and Skoog (MS) agar medium in sterile Petri plates for 3 days at 22°C ± 2°C for germination. The germinated seeds were transferred into culture boxes with ½ MS and grown for another 7 days for seedling growth.

As treatment with ZnONPs did not result in seed sterilization, in the second variant of the experiment, seeds treatment with ZnONPs at a concentration range of 1–256 µg mL⁻¹ was preceded by standard sterilization method to determine effect of nanoparticles on seed germination and seedling growth. In both experiments seeds treated with sterile distilled water were implemented as a control, and all experiments were performed in triplicate.

2.4.2 Estimation of germination and growth parameters

The root and shoot length were measured with the ruler in centimeters [cm]. Fresh and dry weight mass were also determined in milligrams [mg]. Various parameters of germination and seedlings growth were calculated using the following formulas:

$$\text{Germination percentage (\%)} = \left(\sum n / N \right) \times 100$$

where $\sum n$ —the total number of seeds germinated after 10 days; N is the total number of seeds used for analysis. Scott et al. (1984)

$$\text{Mean germination time (MGT)} = \sum f \cdot x / \sum n$$

where f —number of germinated seeds at day x ; x —number of day from sowing; $\sum n$ —total number of germinated seeds. Orchard (1997)

$$\text{Germination Rate Index (GRI)} = G_1/1 + G_2/2 + \dots + G_x/x$$

where $G_1, G_2 \dots G_x$ —germination percentage in the subsequent days after sowing. Esechie (1994)

$$\text{Vigour index I} = \text{Germination \%} \times \text{SL}$$

where SL - Seedling length (Root + Shoot). Abdul-Baki and Anderson (1973)

$$\text{Vigour index II} = \text{Germination \%} \times \text{SDW}$$

where SDW - Seedling dry weight (Root + Shoot)

2.5 Statistical analyses

Statistica software (StatSoft Inc., Tulsa, OK, United States States) was used for data analysis. Results were shown as mean ± standard error (SE). The means were then compared to determine statistical significance (if $p < 0.05$) by One-way ANOVA followed by Tukey's test.

3 Results

3.1 Biosynthesis and determination of physical and chemical properties of metal-based nanoparticles

3.1.1 Optimization of fungal growth

The most efficient growth of *Fusarium solani* IOR 825 was observed in SDB medium (42.75 ± 1.58 g L⁻¹), followed by CDB (34.22 ± 1.21 g L⁻¹) and PDB (20.44 ± 1.03 g L⁻¹). For further studies, SDB was selected for *F. solani* IOR 825 biomass production.

3.1.2 Mycosynthesis, visual detection, and characterization of NPs

The UV-visible spectrometry of fungal extract from *F. solani* IOR 825 combined with AgNO₃ showed a maximum absorbance peak at 420 nm and indicated the formation of AgNPs (Supplementary Figure S1). Synthesis efficiency was estimated at 26.35 mg of AgNPs per 100 mL of fungal extract as presented in Supplementary Table S1. Fungal-mediated synthesis resulted in the formation of spherical and oval-shaped small AgNPs with an average size of 8.27 ± 3.07 and sizes ranging from 2.99 to 21.53 nm (Figures 1A, B). The EDX studies of AgNPs displayed silver and carbon contents at 55.43% and 44.56%, respectively (Supplementary Table S2). X-ray pattern of AgNPs demonstrated peaks at 38.20, 46.31, 64.59, and 77.58 corresponding to reflections of the crystallographic planes (111), (200), (220), and (311), respectively, and revealed the formation of AgNPs (Figure 1C). AgNPs showed Zeta potential of −17.08 mV, while hydrodynamic

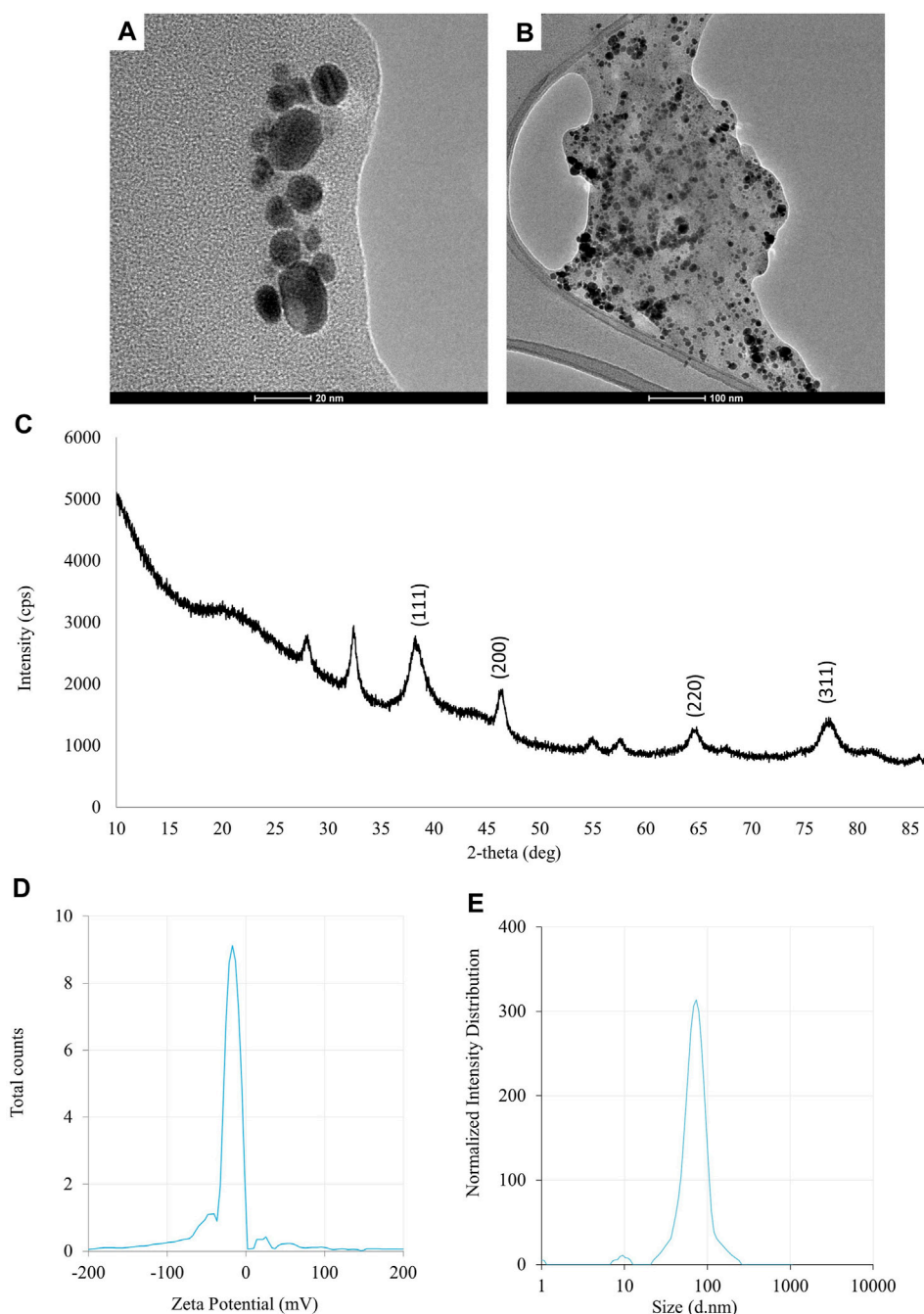


FIGURE 1

The results of the evaluation of physico-chemical properties of AgNPs synthesized from *Fusarium solani* IOR 825: TEM micrographs (A, B), X-ray diffractogram (C), Zeta potential (D) and particle diameter from DLS analysis (E).

diameter ranged from 20.6 to 260.5 nm with the highest frequency in the size of 68.3 ± 1.23 nm (Figures 1D, E). FTIR spectra of synthesized AgNPs showed adsorption bands at 3429.39, 2923.83, 2852.66, 1743.48, 1631.79, 1384.43, 1353.79, 1082.81 and 607.31 cm^{-1} (Figure 2).

The synthesis of ZnONPs (1) was observed as a white precipitate in the reaction mixture and confirmed by the presence of maximum absorbance peak at wavelength 375 nm (Supplementary Figure S1). The synthesis yield of ZnONPs (1) was found to be 435.56 mg per 100 mL of fungal extract (Supplementary Table S1). TEM micrographs of

ZnONPs (1) showed irregularly shaped structures with an average size of 117.79 ± 4.71 and a size ranging from 54.44 to 209.69 nm (Figures 3A, B). ZnONPs (1) consisted of 70.94% of zinc, 18.76% of oxygen and 10.03% of other minor elements (Mo, Al, Si) (Supplementary Table S2). The diffractogram of ZnONPs (1) showed peaks at 32.10, 34.80, 36.60, 48.10, 57.00, 63.00, 68.40 corresponding to (100), (002), (101), (102), (110), (103), (200), (112), (201) lattice plane values, respectively, and was recognized as hexagonal wurtzite phase of ZnO (Figure 3C). ZnONPs (1) were found

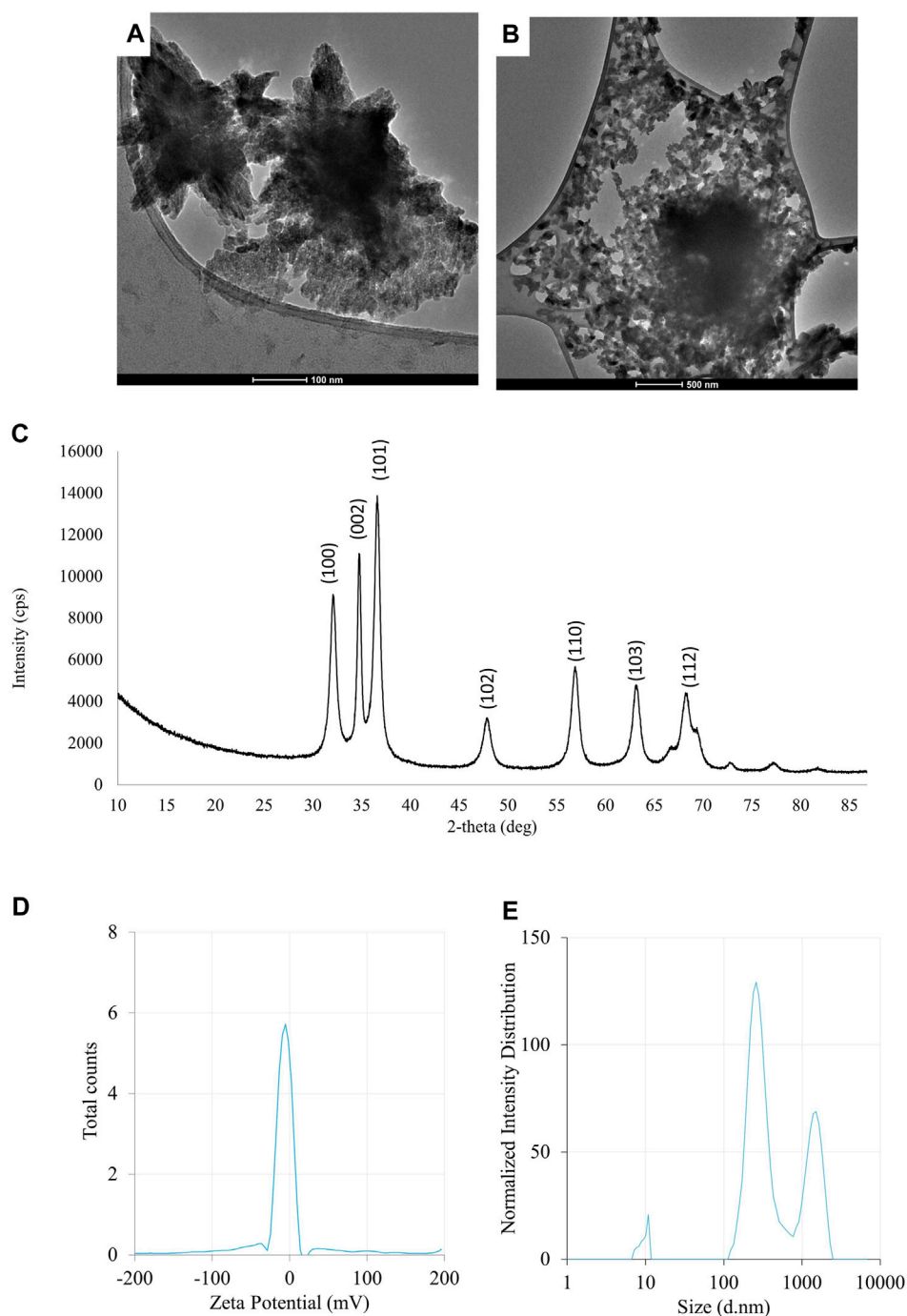


FIGURE 2

The results of the evaluation of physico-chemical properties of ZnONPs (1) synthesized from *Fusarium solani* IOR 825: TEM micrographs (A,B), X-ray diffractogram (C), Zeta potential (D) and particle diameter from DLS analysis (E). (1); first method of ZnONP synthesis.

to be negatively charged (-9.39 mV), with hydrodynamic diameters from 112.9 to 2495.9 nm and the largest fraction of size of 261.23 ± 53.5 (Figures 3D, E). The FTIR spectrum showed peaks at 3393.27 , 2961.51 , 2926.43 , 1589.56 , 1553.60 , 1512.21 , 1388.66 , 1352.63 , 1329.21 , 1119.10 , 1045.11 , 940.98 , 830.97 , 738.83 , 694.20 , 608.67 and 480.24 cm^{-1} (Figure 2).

The UV-vis spectrum of ZnONPs (2) demonstrated an adsorption peak at the wavelength of 375 nm (Supplementary

Figure S1). The synthesis efficiency reached 525.8 mg of NPs per 100 mL of fungal extract (Supplementary Table S1). TEM analysis displayed nanorods-like NPs with an average length 175.12 ± 7.96 and size ranging from 64.84 to 443.02 nm (Figures 4A, B). The elemental composition from the EDX analysis demonstrated 78.67% of zinc, 19.35% of oxygen and 1.98% of carbon and aluminum (Supplementary Table S2). The XRD peaks at 32.10 , 34.80 , 36.60 , 48.10 , 57.00 , 63.00 , 66.00 , 68.40 , 69.55 were assigned to

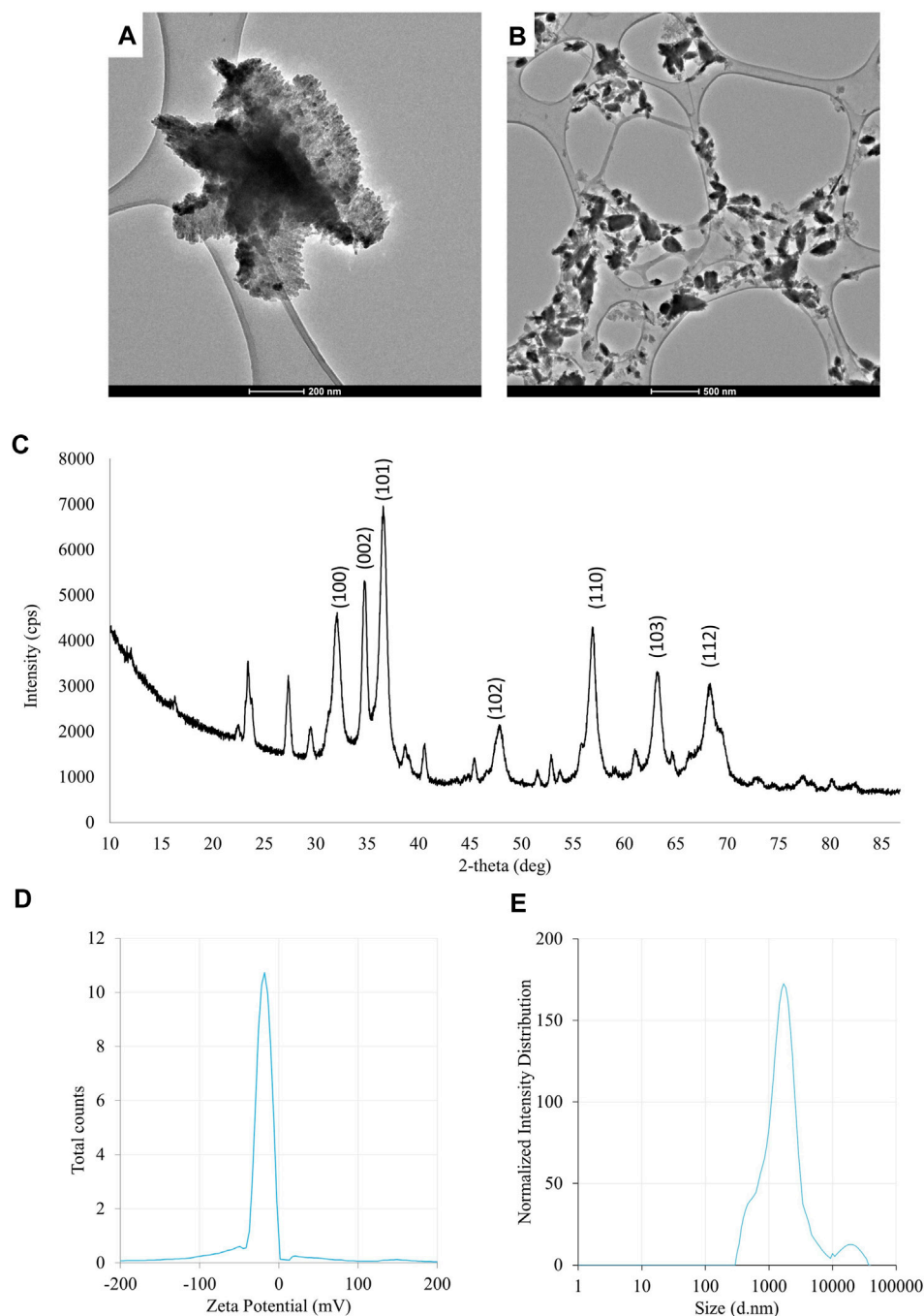


FIGURE 3

The results of the evaluation of physico-chemical properties of ZnONPs (2) synthesized from *Fusarium solani* IOR 825: TEM micrographs (A,B), X-ray diffractogram (C), Zeta potential (D) and particle diameter from DLS analysis (E). (2); second method of ZnONP synthesis.

(100), (002), (101), (102), (110), (103), (200), (112), (201) lattice plane of hexagonal wurtzite phase of ZnO (Figure 4C). DLS analyses revealed NPs size between 292.9–9264.2 nm, with the maximum amount of NPs in the size of 1711.82 ± 123.59 nm while Zeta potential measurements showed negatively charged (-21.81 mV) ZnONPs (2) (Figures 4D, E). As shown in Figure 2, FTIR analysis revealed peaks at 3398.02, 2925.85, 2855.49, 1631.63, 1503.82, 1400.67, 1385.79, 1042.27, 912.62, 705.43, 640.79 and 536.84 cm^{-1} . Results from FTIR

spectroscopy, summarized in Table 1, indicate the presence of various functional groups on the surface of NPs.

3.2 Antimicrobial activity

Antibacterial activity of NPs from *F. solani* IOR 825 against plant pathogens was determined based on minimal inhibitory (MIC) and biocidal (MBC) concentrations, as presented in Table 2.

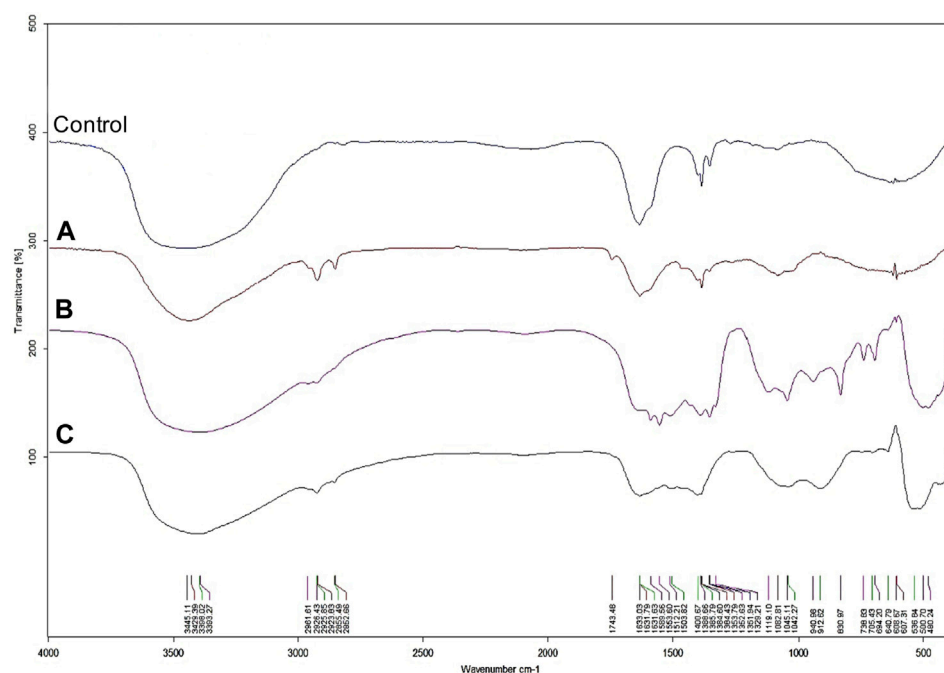


FIGURE 4

FTIR spectra of AgNPs (A), ZnONPs (1) (B), ZnONPs (2) (C) synthesized from *Fusarium solani* IOR 825. (1); first method of ZnONP synthesis, (2); second method of ZnONP synthesis.

TABLE 1 An overview of functional groups identified on the surface of AgNPs and ZnONPs from *Fusarium solani* IOR 825 based on FTIR analysis.

Band position [cm ⁻¹], assigned functional groups	AgNPs	ZnONPs (1)	ZnONPs (2)
3393–3445 cm ⁻¹ (N–H stretching, primary amine)	+	+	+
2960–2925 (C–H stretching, aromatic compound)	+	+	+
2855 (O–H stretching, intramolecular bonded)	+	+	+
1740 (C–H bending, aromatic compound)	+	–	–
1632 (C=C stretching, alkene)	+	+	+
1590–1510 (C=O carbonyl group)	–	+	+
1450 (C–H bending, alkane, methyl group)	+	–	–
1400–1350 (C–H bending, aldehyde, alkane)	+	+	+
1120–1040 (C–N stretching, aromatic and aliphatic amine)	+	+	+
940–700 (C=C bending, alkene)	–	+	+
610–480 (metal)	+	+	+

+: – peak determined in an analyzed sample, –: peak not recorded in the analyzed sample.

ZnONP (1); first method of nanoparticle synthesis, ZnONP (2); second method of nanoparticle synthesis.

The highest antibacterial activity of AgNPs was observed against *Pseudomonas syringae*, followed by *Xanthomonas campestris*, *Agrobacterium tumefaciens* and *Pectobacterium carotovorum*; the MIC and MBC values ranged from 8 to 256 µg mL⁻¹ and from 512 to 1024 µg mL⁻¹, respectively.

The MIC values for ZnONPs (1) were determined at a concentration of 256 µg mL⁻¹ against *A. tumefaciens* and *X. campestris*, and 1024 µg mL⁻¹ against *P. syringae*. In turn, the corresponding MBC values of these nanoparticles were found to be 512, 2048 and 2048 µg mL⁻¹, respectively.

The ZnONPs (2) showed inhibitory effect against *P. syringae* and *X. campestris* at a concentration of 512 µg mL⁻¹ while the corresponding biocidal activity of NPs was not determined at the tested concentration range. The inhibitory and biocidal activities against *A. tumefaciens* were recorded at a concentration of 1024 µg mL⁻¹.

None of the ZnONPs were found to be active against *P. carotovorum* at the tested concentration range.

The results of antifungal activity of AgNPs and ZnONPs are shown in Table 3. The food poisoned method revealed that *S. sclerotiorum* was most susceptible to AgNPs, followed by *Phoma lingam*, *Botrytis*

TABLE 2 Antibacterial activity against phytopathogens of NPs synthesized from *Fusarium solani* IOR 825 presented as minimal inhibitory and biocidal concentrations (MICs and MBCs) [$\mu\text{g mL}^{-1}$].

Bacterial phytopathogens	AgNPs		ZnONPs (1)		ZnONPs (2)	
	MIC	MBC	MIC	MBC	MIC	MBC
<i>Agrobacterium tumefaciens</i> IOR 911	128	1024	256	512	1024	1024
<i>Pectobacterium carotovorum</i> PCM 2056	256	1024	>2048	>2048	>2048	>2048
<i>Pseudomonas syringae</i> IOR 2188	8	512	1024	2048	512	>2048
<i>Xanthomonas campestris</i> IOR 512	256	512	256	2048	512	>2048

ZnONP (1); first method of nanoparticle synthesis, ZnONP (2); second method of nanoparticle synthesis.

TABLE 3 Antifungal activity of NPs synthesized from *Fusarium solani* IOR 825 against phytopathogens presented as minimal inhibitory and minimal fungicidal concentrations (MICs and MFCs) [$\mu\text{g mL}^{-1}$] and mycelial growth inhibition (MGI) [%].

NPs concentrations [$\mu\text{g mL}^{-1}$]	AgNPs				ZnONPs (1)				ZnONPs (2)			
	% MGI		MIC	MBC	% MGI		MIC	MBC	% MGI		MIC	MBC
	100	200			100	1000			100	1000		
<i>Alternaria alternata</i>	-	57	32	32	-	52	1024	>2048	-	57	1024	>2048
<i>Alternaria alternata</i> IOR 1783	-	48	32	32	-	52	512	512	-	57	256	512
<i>Aspergillus niger</i>	-	-	32	64	-	19	512	2048	-	35	512	2048
<i>Botrytis cinerea</i> IOR 1873	45	58	32	32	-	-	1024	2048	-	-	1024	1024
<i>Colletotrichum acutatum</i> IOR 2153	-	-	64	64	-	-	1024	2048	-	-	1024	2048
<i>Fusarium culmorum</i>	-	-	64	2048	-	-	2048	2048	-	-	2048	2048
<i>Fusarium culmorum</i> IOR 2333	-	-	64	256	-	-	2048	2048	-	-	1024	1024
<i>Fusarium culmorum</i> DMS 114849	-	19	64	2048	-	25	2048	2048	-	23	2048	2048
<i>Fusarium graminearum</i> A	-	-	64	256	-	47	2048	2048	-	53	1024	1024
<i>Fusarium graminearum</i> D	-	-	32	32	-	-	2048	2048	-	-	1024	>2048
<i>Fusarium oxysporum</i>	-	-	64	64	-	-	2048	2048	-	-	1024	2048
<i>Fusarium oxysporum</i> IOR 342	-	-	128	>2048	40	100	128	512	62	100	256	256
<i>Fusarium oxysporum</i> D	14	20	32	32	-	31	2048	2048	22	34	2048	2048
<i>Fusarium poae</i> A	-	-	32	32	-	38	1024	2048	-	37	2048	2048
<i>Fusarium tricinctum</i>	-	-	64	64	-	-	2048	2048	-	-	>2048	>2048
<i>Penicillium</i> sp.	-	-	64	1024	-	-	2048	>2048	-	-	2048	>2048
<i>Penicillium spinulosum</i>	-	-	64	1024	-	-	2048	>2048	-	-	512	>2048
<i>Phoma lingam</i> IOR 2284	49	61	64	64	39	63	2048	1024	29	60	1024	1024
<i>Sclerotinia sclerotiorum</i> IOR 2242	52	100	16	16	-	72	512	512	-	72	1024	1024
<i>Phytophthora megasperma</i> IOR 404	-	-	32	32	-	-	>2048	>2048	-	-	>2048	>2048
<i>Phytophthora cryptogea</i> IOR 2080	-	-	32	32	-	-	>2048	>2048	-	-	>2048	>2048
<i>Phytophthora plurivora</i> IOR 2303	-	-	32	32	-	-	>2048	>2048	-	-	>2048	>2048

ZnONP (1); first method of nanoparticle synthesis, ZnONP (2); second method of nanoparticle synthesis.

(-); no antifungal activity.

cinerea, and both *Alternaria alternata* strains. The remaining strains were found to be less or not susceptible to AgNPs at the tested concentration range. Determination of MIC and MFC of AgNPs against fungal spores

showed their highest activity against *S. sclerotiorum* (MIC and MBC values at $16 \mu\text{g mL}^{-1}$). The slightly lower antifungal activity (MIC and MBC = $32 \mu\text{g mL}^{-1}$) of AgNPs was noted for both *A. alternata* strains, *B.*

TABLE 4 Germination parameters of maize seeds after sterilization with various concentrations of AgNPs and pretreatment with ZnONPs (1) and ZnONPs (2).

	Treatment [$\mu\text{g mL}^{-1}$]	% germination	MGT [day]	GRI [%/day]	Vigour index I	Vigour index II
AgNPs	0	90.00	3.78	28.01	2206.16	3957.62
	32	82.50	3.61	29.14	2304.39	4326.20
	64	82.50	3.64	28.89	2436.06	4363.58
	128	87.50	3.66	29.00	2427.12	4347.94
	256	87.50	3.57	29.52	2335.58	3884.63
ZnONPs (1)	0	90	3.78	28.01	2209.35	3957.62
	1	92.5	3.78	27.93	2240.51	3806.82
	8	97.5	3.64	29.19	2324.32	4168.38
	16	90	3.86	27.18	2584.22	4711.75
	32	92.5	3.81	27.48	2854.74	5316.10
	64	90	3.69	28.52	2754.78	4910.63
	128	90	3.75	28.15	2803.71	4932.74
	256	95	3.72	28.38	3036.71	5247.18
ZnONPs (2)	0	90	3.78	28.01	2209.35	3957.62
	1	90	3.76	28.07	2416.50	4234.28
	8	90	3.53	29.95	2498.03	3994.16
	16	100	3.83	27.38	2996.54	5199.35
	32	90	3.83	27.31	2653.71	4602.11
	64	90	3.69	28.52	2792.48	4710.99
	128	92.5	3.73	28.29	3038.07	5111.09
	256	95	3.74	28.20	3093.61	5150.36

ZnONP (1); first method of nanoparticle synthesis, ZnONP (2); second method of nanoparticle synthesis.
MGT; mean germination time, GRI; germination rate index.

cinerea, *Fusarium graminearum* D, *Fusarium oxysporum* D, *Fusarium poae* A and three *Phytophthora* strains. The AgNPs inhibited spore germination of *Aspergillus niger* at a concentration of $32 \mu\text{g mL}^{-1}$ while their biocidal effect was achieved at a concentration of $64 \mu\text{g mL}^{-1}$. Similarly, MIC and MFC of AgNPs against *P. lingam* spores were noted at $64 \mu\text{g mL}^{-1}$. The higher MIC and MBC values of AgNPs, from 64 to $2048 \mu\text{g mL}^{-1}$, were determined against the other tested microorganisms, with the exception of *F. oxysporum* IOR 342 for which the MBC values were not determined in the tested concentration range.

The highest mycelial growth inhibition, determined by food poisoned technique, was found for *F. oxysporum* IOR 342, followed by *S. sclerotiorum*, *P. lingam* and both *A. alternata* strains, when treated with ZnONPs (1). MIC and MFC of ZnONPs (1) against fungal spores were found in the range of 128 – $2048 \mu\text{g mL}^{-1}$. The most sensitive to ZnONPs (1) were spores of *F. oxysporum* IOR 342; the inhibitory and biocidal effects were observed at a concentration of 128 and $512 \mu\text{g mL}^{-1}$, respectively. The high susceptibility to ZnONPs (1) was also observed for *A. alternata* IOR 1783 and *S. sclerotiorum* IOR 2242 (MIC and MBC of $512 \mu\text{g mL}^{-1}$).

In the case of ZnONPs (2) similar pattern was observed, as described for ZnONPs (1), with exception for MIC and MBC values against *S. sclerotiorum* which were found to be two times higher (Table 3).

None of ZnONPs showed spore inhibition activity, within the concentration ranges tested, against oomycete strains from the genus *Phytophthora* (Table 3).

3.3 Effect of NPs on germination and growth of maize (*Zea mays*) seedlings

The pretreatment of maize seeds with AgNPs at concentrations equal to or higher than $32 \mu\text{g mL}^{-1}$ was found to be an effective method of seed surface sterilization. However, priming of seeds with ZnONPs within tested concentration range (1 – $256 \mu\text{g mL}^{-1}$) showed no sterilization effect. The sterilization of seeds with AgNPs and seeds priming with ZnONPs had no significant effect on maize seed germination, when compared to the control (Table 4).

Values of both vigor indexes (I and II) (Table 4) showed an acceleration of seedling growth after treatment with AgNPs at concentrations of 32, 64 and $128 \mu\text{g mL}^{-1}$, as indicated by significantly longer shoots and higher seedling dry weight (Figures 5A, C). However, application of the maximum tested concentration of AgNPs ($256 \mu\text{g mL}^{-1}$) resulted in significantly lower fresh biomass of seedlings (507.11 mg) when compared to

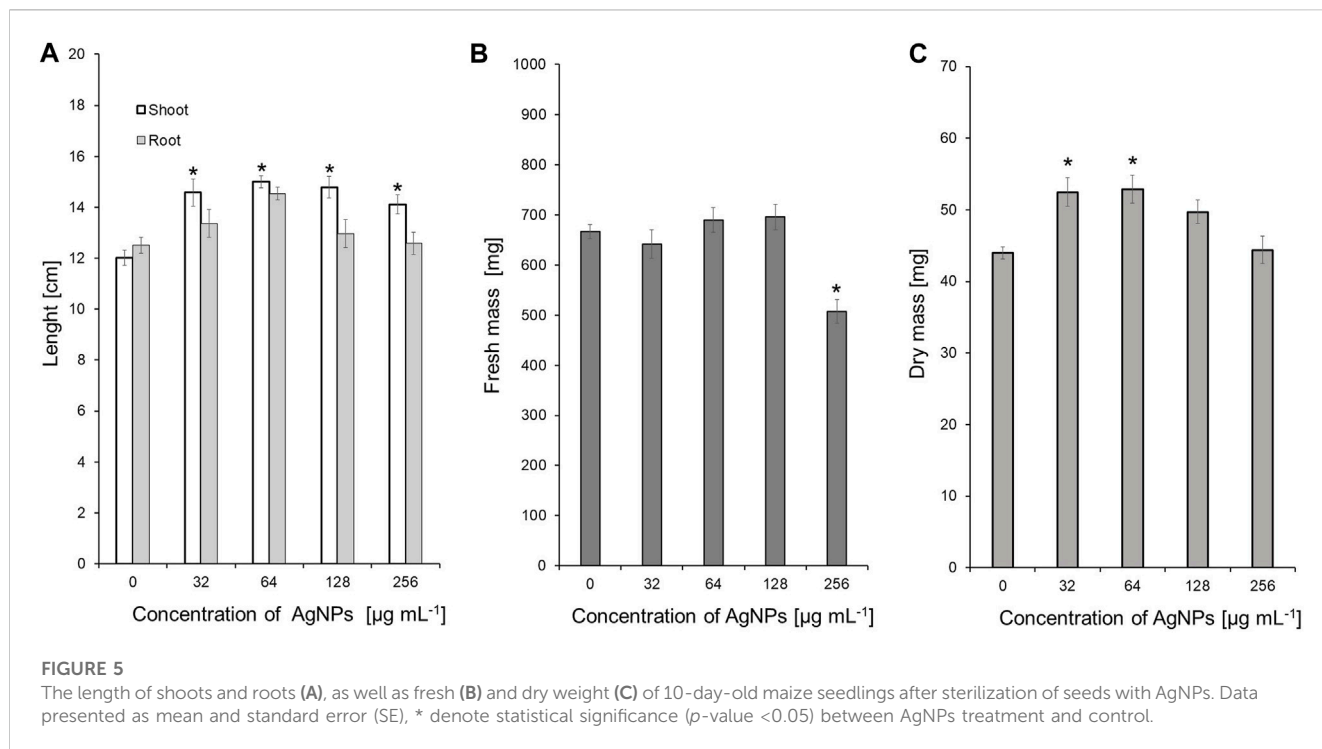


TABLE 5 Variation in the growth parameters of maize seedlings after treatment of seeds with various concentrations of NPs compared to the control expressed as %.

Treatment [$\mu\text{g mL}^{-1}$]	Seedling length			Fresh mass			Dry mass		
	AgNPs	ZnONPs (1)	ZnONPs (2)	AgNPs	ZnONPs (1)	ZnONPs (2)	AgNPs	ZnONPs (1)	ZnONPs (2)
1		-1.3	9.4		-6.1	-1.4		-6.4	7.0
8		-2.9	13.1*		-4.9	-5.2		-2.8	0.9
16		17.0	22.1*		24.2*	23.8*		19.1*	18.2*
32	13.9*	25.7*	20.1*	-3.7	32.1*	24.9*	19.3*	30.7*	16.3*
64	20.5*	24.7*	26.4*	3.5	25.7*	27.6*	20.3*	24.1*	19.0*
128	13.2*	26.9*	33.8*	4.3	29.5*	40.5*	13.0	24.6*	25.7*
256	8.9	30.2*	32.7*	-24.0*	30.0*	34.0*	1.0	25.6*	23.3*

*Denote statistical significance (p -value < 0.05) between NPs, treatment and control.

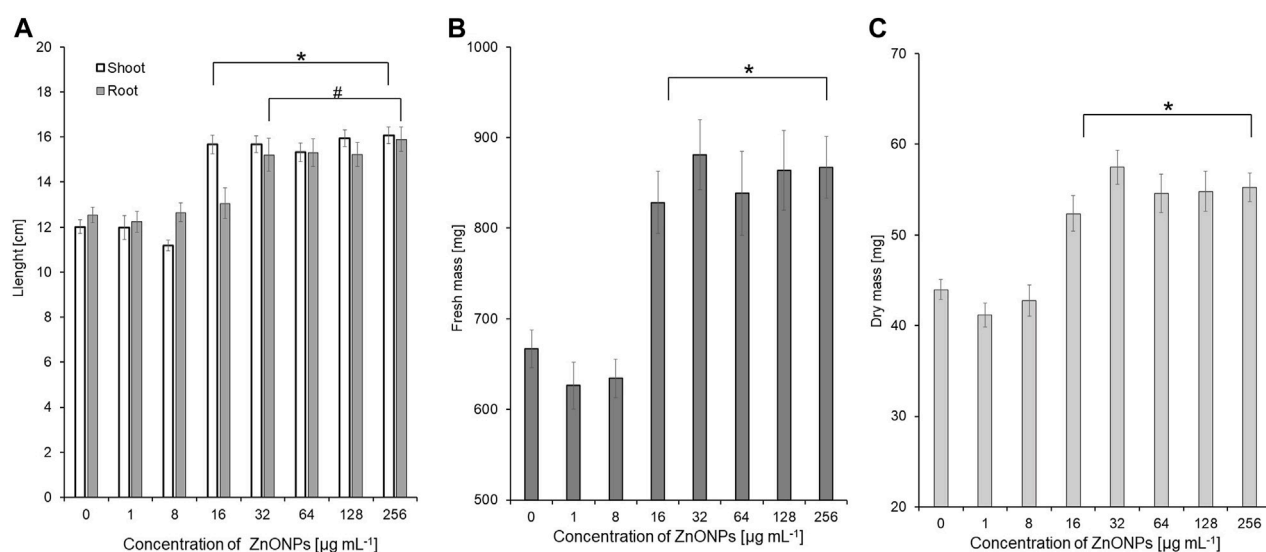
ZnONP (1); first method of nanoparticle synthesis, ZnONP (2); second method of nanoparticle synthesis.

control (666.85 mg) (Figure 5B). Although AgNPs were used for sterilization purpose, their lowest effective concentrations (32 and 64 $\mu\text{g mL}^{-1}$) significantly improved parameters of seedlings, especially seedling length (13.9%–20.5%) and dry mass (19.3%–20.3%), as summarized in Table 5.

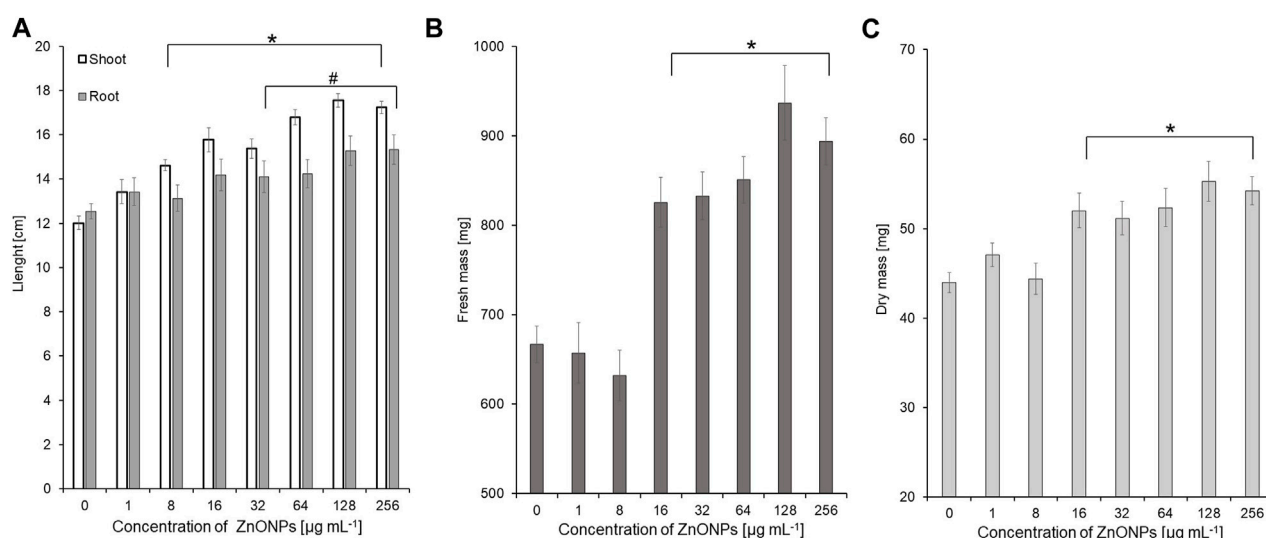
The vigour indexes of seedlings were found to be higher after treatment with ZnONPs (1) at concentrations above 16 $\mu\text{g mL}^{-1}$. Seedling vigour index I increased after treatment with ZnONPs (1) at concentrations of 16–256 $\mu\text{g mL}^{-1}$ from 2209 in control to 2584–3037 in tested samples. The highest vigour index II (5316) was found at concentrations of 32 $\mu\text{g mL}^{-1}$ (Table 4). Growth of seedlings roots and shoots was improved by ZnONPs (1) at concentrations of ≥ 16 and ≥ 32 $\mu\text{g mL}^{-1}$, respectively (Figures 6A, B). ZnONPs (1)

stimulated the growth of maize seedlings as indicated by higher plant fresh and dry weight. A statistically significant increase in maize biomass production was noted for ZnONPs (1) at concentrations of ≥ 16 $\mu\text{g mL}^{-1}$, when compared to the control (Figures 6C, D). Overall, the growth parameters of maize seedlings were increased after seeds pretreatment with ZnONPs (1) at concentration ranges between 32 and 256 $\mu\text{g mL}^{-1}$, namely, length (by 26%–30%), fresh weight (by 24%–30%), dry weight (by 19%–30%) (Table 5).

Seedling vigour index I after treatment with ZnONPs (2) at concentrations of 8–256 $\mu\text{g mL}^{-1}$ increased to 2498–3094 in tested seedlings when compared to control (2209). The strongest effect on improving seedling condition was observed after treatment of maize seeds with ZnONPs (2) at a concentration of 16 $\mu\text{g mL}^{-1}$, as proved

**FIGURE 6**

The length of shoots and roots (A), as well as fresh (B) and dry weight (C) of 10-day-old maize seedlings after seed pretreatment with ZnONPs (1) at different concentrations. Data presented as mean and standard error (SE), * and # denote statistical significance (p -value <0.05) between ZnONPs treatment and control. (1); first method of ZnONP synthesis

**FIGURE 7**

The length of shoots and roots (A), as well as fresh (B) and dry weight (C) of 10-day-old maize seedlings after seed pretreatment with ZnONPs (2) at different concentrations. Data presented as mean and standard error (SE), * and # denote statistical significance (p -value <0.05) between ZnONPs treatment and control. (2); second method of ZnONP synthesis.

by seedling vigour indexes (5199) when compared to untreated control (3958) (Table 4). ZnONPs (2) concentrations ≥ 8 and $128 \mu\text{g mL}^{-1}$ stimulated elongation of shoots and roots, respectively (Figure 7A). The fresh and dry weight of seedlings increased after seeds priming with ZnONPs (2); a statistically significant difference was noted for concentrations of $\geq 16 \mu\text{g mL}^{-1}$, when compared to the control (Figures 7B, C). To sum up, parameters of maize seedlings were increased after seed pretreatment with ZnONPs (2) at concentration ranges between

32 and $256 \mu\text{g mL}^{-1}$. The length of seedlings was improved by 13%–34%, their fresh weight by 24%–40% and dry weight by 16%–26%, as presented in Table 5.

4 Discussion

Fungi play a pivotal role in synthesis of different kinds of nanoparticles. Among these, various *Fusarium* species have

garnered attention by the researchers (Rai et al., 2021). Several researchers successfully synthesized variety of nanoparticles including silver, gold, copper, and zinc oxide NPs synthesis from different strains of *F. solani* (Ingle et al., 2009; Abd El-Aziz et al., 2015; Vijayan et al., 2016; Clarence et al., 2020; El Sayed and El-Sayed, 2020; Sasani et al., 2023). Nevertheless, there is no standard synthesis protocol, as there are many factors that affect the synthesis yields of final product sizes, shapes, and other physicochemical characteristics (Sonawane et al., 2022). Therefore, the present work focuses on optimization of *F. solani* IOR 825 growth, high-throughput synthesis process, and fabrication of biologically active nanoparticles. The main requirements for the biosynthesis of NPs are solutions of metal ions as well as reducing and coating agents (fungal origin), the initial aim was to optimize the growth of the fungus in order to acquire a large portion of biomass, with a view to its subsequent use in preparing a cell-free extract after autolysis. The SDB medium was selected and used for further culture of *F. solani* IOR 825, as the highest fungal growth rate was recorded when compared with PDB or CDB, which may be due to the medium content consisting of dextrose, digested animal tissues (amino acids source) and casein, which provide carbon and nitrogen sources for growth. Similarly, Merlin et al. (2013) pointed out dextrose as the preferred carbon source, and the supplementation of amino acids to the growth medium that resulted in increased growth of *F. solani* strain LCPANF01.

The fungal extract obtained after cell autolysis, which contains variable biomolecules, is preferably used for the synthesis of NPs along with metal precursors. This extracellular process allows for more efficient synthesis of NPs and reduction of post-production steps, such as purification (Michael et al., 2022). Similarly, El Sayed and El-Sayed (2020) used cell-free extracts from *F. solani* KJ 623702 and silver nitrate (AgNO_3 ; final concentration of 0.5 mM) or zinc sulfate (ZnSO_4 ; 0.005 mM), as precursors, for green synthesis of corresponding nanoparticles. A basic visual observation of changes in the color of the mixture to dark brown (AgNPs) or white (ZnONPs) indicated that the synthesis reaction had been initiated. The reduction of metal ions and nanoparticles formation were confirmed by UV-visible spectroscopy and the detection of maximum absorbance peaks at wavelengths 422 nm and 375 nm for AgNPs and ZnONPs, respectively (El Sayed and El-Sayed, 2020), which is in line with our observations. It is well known, that the maximum absorption for AgNPs and ZnONPs ranges from 420 to 450 nm and 330–380 nm, respectively (Musa et al., 2017; Anjum et al., 2023). However, the slight shifts in the UV-vis spectra are due to differences in particle size or the presence of molecules from the biological extracts used for the synthesis (Saion et al., 2013; Ballotin et al., 2016; Musa et al., 2017; Guilger-Casagrande et al., 2019; Urnukhsaikhani et al., 2021). A number of studies on the synthesis of ZnONPs by precipitation method using fungal extracts have been reported (Ghorbani et al., 2015). In our study, two factors, namely, temperature, and pH, were considered for ZnONPs synthesis, as these factors are of great importance for the morphology and size of formed NPs (Moezzi et al., 2011). The heating of the reaction mixture (fungal extract and salt precursor) improves the kinetics of the reaction and affect NPs properties (Moezzi et al., 2011). Authors reported that an increase in the temperature of the reaction from 25°C to 90°C between addition of ZnSO_4 and NaOH led to the lower solubility of the final product, which is important for further

applications. In another study, Abdullah et al. (2020) indicated that strong alkaline (pH > 10) reaction environment favors the formation of ZnONPs. It is consistent with observation from this study, the ZnONPs were formed after a temperature rise to 40°C or at room temperature after adjusting the pH to 11.

TEM analysis showed the formation of small and spherical AgNPs from extract of *F. solani* IOR 835 which is in line with recently published reports on the fungal synthesis of such nanoparticles (Lofty et al., 2021; Sasani et al., 2023). These authors synthesized spherical and small (7–23 and 27.5–58.3 nm) AgNPs from *Aspergillus terreus* and *F. solani*, respectively. In contrast, ZnONPs synthesized from *F. solani* IOR 825 were irregularly shaped and bigger (54.44–209.69 nm and 64.84–443.02 nm) than those synthesized from *Trichoderma asperellum* (44–78 nm), it may be related to the use of another salt precursor ($\text{Zn}(\text{NO}_3)_2$ (Shobha et al., 2023). Whereas, Elrefaey et al., 2022 synthesized rectangular ZnONPs with size between 23 and 140 nm using extract of marine alga *Cystoseira crinite*, ZnSO_4 (0.05 M aqueous solution), as a precursor, and 1 M NaOH and heating the reaction mixture up to 45°C for 30 min. Apart from the reaction parameters (precursor, temperature, pH), the physicochemical properties of the bio-NPs are determined by the composition of the fungal extract (Lofty et al., 2021). Similar results, confirming the fungal-mediated formation of AgNPs and ZnONPs with crystalline structures were reported by other researchers (Talam et al., 2012; Nallal et al., 2021; Shobha et al., 2023). Furthermore, Singh D. et al. (2014) revealed that low concentration of precursor (1 mM AgNO_3) as well as room temperature (below 25°C) allowed for efficient mycosynthesis of small AgNPs (average size 18 nm) with good stability (Zeta potential–33.4 mV) which prevented their agglomeration. Jain et al. (2020) used zinc sulfate for microbial-mediated synthesis of ZnONPs and suggested that a larger hydrodynamic diameter of biologically synthesized ZnONPs might result from aggregation of particles. The zeta potential is an indicator of surface charge potential which is an important parameter for understanding the stability of nanoparticles in aqueous suspensions. In our studies, a low value of Zeta potential (–9.39 mV) indicated lower stability of ZnONPs (2) and the tendency to aggregate therefore larger particles diameter were observed in DLS analysis. It has been stated in the literature that nanoparticles with a Zeta potential higher than +30 mV or lower than –30 mV are considered to be very stable in the dispersion medium by pushing the same charges (Rai et al., 2018). In another study, Singh K. et al. (2014) pointed out that the DLS results encompass the layer of solvent at the interface and capping biomolecules on the nanoparticles' surface. This was also indicated by the results of FTIR analysis, where bands identified suggest the presence of functional groups from biomolecules such as proteins (N–C and C–C), aromatic compounds (C–H), amines (C–N), hydrocarbons (C–H, C=C) from the fungal extract which are employed in the synthesis and take part in the reduction of metal ions and subsequent stabilization of the nanoparticles (Abdullah et al., 2020; Wypij et al., 2022). The bands detected between 400 cm^{-1} –600 cm^{-1} imply the formation of bonding between metal and biomolecules present in fungal extract. Our results agree with the findings reported by Salem (2022) and Shobha et al. (2023) where bands for biosynthesized nanoparticles were found at 609.3 and 414.6 cm^{-1} for AgNPs and 534 cm^{-1} for ZnONPs, respectively.

Mycosynthesized NPs from *F. solani* IOR 825 showed antimicrobial activity against a wide range of bacterial and fungal pathogens of plants in a dose-dependent manner, highly depending on the targeted strain. In a similar study by Namburi and coworkers (2021), antibacterial activity of biosynthesized AgNPs was found against *Xanthomonas oryzae* pv. *oryzae* at concentration of $2.5 \mu\text{g mL}^{-1}$ while another report indicated effectiveness of AgNPs synthesized from *Ulva fasciata* extract against *X. campestris* pv. *malvacearum* at higher concentration of $40 \mu\text{g mL}^{-1}$ (Rajesh et al., 2012). In a study conducted by Manosalva et al. (2019) AgNPs showed activity against *E. coli*, *P. syringae*, and *Staphylococcus aureus*. The activity of AgNPs was affected by both the bacterial strain and the size of the NPs (23, 92, and 220 nm); the highest sensitivity to AgNPs was detected for *Escherichia coli* (MIC $5\text{--}30 \mu\text{g mL}^{-1}$ and MBC $10\text{--}50 \mu\text{g mL}^{-1}$), followed by *P. syringae* (MIC $10\text{--}40 \mu\text{g mL}^{-1}$ and MBC $30\text{--}60 \mu\text{g mL}^{-1}$) and *S. aureus* (MIC $50\text{--}80 \mu\text{g mL}^{-1}$ and MBC $60\text{--}80 \mu\text{g mL}^{-1}$). In addition, the growth of bacterial strains, namely, *Ralstonia solanacearum*, *P. syringae*, *X. campestris*, and *X. oryzae* was inhibited by ZnONPs synthesized from *C. tomentosa* leaf extract at various concentrations of 125, 500, 250 and $250 \mu\text{g mL}^{-1}$, respectively. A similar trend was found in our study, where *P. syringae* showed lower sensitivity to ZnONPs than *X. campestris*. The growth of *P. syringae* was inhibited by ZnONPs (1) and ZnONPs (2) at concentrations of 1024 and $512 \mu\text{g mL}^{-1}$, respectively, while *X. campestris* at concentrations of 256 and $512 \mu\text{g mL}^{-1}$, respectively. Several studies indicated that antibacterial mechanisms of metal nanoparticles include the destruction of membrane integrity, cell morphology changes, the release of metal ions, and the generation of reactive oxygen species generation (Reddy et al., 2007; Jiang et al., 2016; Gallón et al., 2019). To date, the antifungal activity of biosynthesized AgNPs and ZnONPs were tested against plant pathogens, e.g., *Alternaria brassicae* (Dhiman et al., 2021), *F. oxysporum* (González-Merino et al., 2021; Macías Sánchez et al., 2023) and *F. graminearum* (Ibrahim et al., 2020). For example, Talie et al. (2020) showed lower antifungal activity of AgNPs biosynthesized from *Helvella leucopus* which at a concentration of 20 mg mL^{-1} inhibited spore germination of *Penicillium chrysogenum*, *A. niger*, and *A. alternata* by 83.21, 77.32% and 69.10%, respectively. The dose-dependent antifungal activity of AgNPs biosynthesized from *Trichoderma viride* against *F. oxysporum* and *Alternaria brassicicola* was reported by Kumari et al. (2019). These results corroborate our studies. Inhibition of mycelial growth was observed at AgNPs concentration of 5%, while complete suppression was determined at a nanoparticle concentration of 25%. In addition, they suggested that the action of AgNPs against *A. brassicicola* led to the generation of superoxide radicals, as well as the disruption of the mycelial structure (Kumari et al., 2019). Jain et al. (2020) evaluated antimicrobial activity of bio-ZnONPs against *X. oryzae* and *Alternaria* sp. with the maximum effect at concentration of 100 and $250 \mu\text{g mL}^{-1}$, respectively. Similarly to the results of the present work, Jamdagni et al. (2018) found that ZnONPs synthesized from *Nyctanthes arbor-tristis* flower extract showed MIC values of $16 \mu\text{g mL}^{-1}$ against *A. niger*, $64 \mu\text{g mL}^{-1}$ against *A. alternata* and *F. oxysporum*, and $128 \mu\text{g mL}^{-1}$ against *B. cinerea* and *Penicillium expansum*. Whereas, Zhu et al. (2021) reported inhibitory effect of ZnONPs synthesized from *Cinnamomum camphora* (L.) leaf extract on mycelial growth and spore germination of *A. alternata* at concentrations of 20–160 mg mL^{-1} . The proposed mechanisms of antifungal activity of ZnONPs included

excessive synthesis and accumulation of malondialdehyde in *A. alternata* cells and damage to the cell membrane, leading to leakage of proteins and nucleic acids (Zhu et al., 2021). In turn, Nandhini et al. (2019) observed the plasmolysis of spores of *Sclerospora graminicola* after treatment with ZnONPs at a concentration of 50 ppm. The differences in antimicrobial activity of both types of ZnONPs biosynthesized from *F. solani* IOR 825 may result from different protocols used for their biofabrication. There are several important factors that affect the synthesis of nanoparticles, including pH of the reaction solution, temperature, pressure and time of the reaction, the concentration of the extracts and precursors, and above all the protocols that are followed for the synthesis process (Patra and Baek, 2014; Wypij et al., 2019). Consequently, nanoparticles of different sizes, shapes, structures and properties are formed which affect their biological activity, including antimicrobial activity (Patra and Baek, 2014; Wypij et al., 2019), as discussed above.

A notable antimicrobial activity of mycosynthesized AgNPs was further confirmed in seeds sterilization tests. The minimum concentration of AgNPs that effectively sterilized maize seeds ($32 \mu\text{g mL}^{-1}$) was equal to or twice lower than the majority of MICs determined against the tested bacterial and fungal plant pathogens. It is noteworthy that at this concentration no negative effects of AgNPs on seed germination or seedling growth were observed, as mentioned previously. Previously, Morsy et al. (2014) used bioAgNPs from cyanobacteria for sterilization of maize, sorghum, soybean and sesame seeds. Although the authors used 2.5 higher AgNPs dose than in the present study, they noted incomplete sterilization of seeds indicated by the presence of fungi from genera *Fusarium* and *Alternaria* sp. *Aspergillus* spp. or *Penicillium* spp. The results of the present study showed that overall AgNPs at tested concentration range did not negatively affected seedling parameters, except of fresh biomass production at concentration of $256 \mu\text{g mL}^{-1}$. It may suggest phytotoxicity of AgNPs at higher doses. Similarly, dose-dependent plant responses to AgNPs priming of seeds were reported by other authors. In the study by Labeed et al. (2020), AgNPs at concentrations of 20 and 40 mg L^{-1} increased germination of seeds and root length of green pea (*Pisum sativum* L.), while higher concentrations (80 and 160 mg L^{-1}) decreased seed germination and reduced seedling growth. It has been suggested that the phytotoxicity of AgNPs, especially at higher doses, may be related to their small size which facilitates their transport. Once penetrating into plant tissues and cells, they display cytotoxic and genotoxic effects (Scherer et al., 2019).

Although ZnONPs from *F. solani* IOR 825 were found to display non-sterilizing properties, they significantly improved seedling growth by stimulating shoot and root elongation, and fresh and dry matter production. A number of reports have proven the importance of Zn for plant growth and development as well as their resistance to biotic or abiotic stresses, that result from its involvement in physiological processes (Camp, 1945; Rudani et al., 2018). Zn content is essential for plants as a component of the cytochrome complex, for membrane integrity or as a cofactor or complexing ion for enzyme activity (Hacisalihoglu, 2020). Some other reports highlight a significant role of Zn in cell elongation and synthesis of tryptophan, a precursor of indole-3-acetic acid (Mašev and Kutáček, 1966; Sharifi et al., 2016; Sharma et al., 2021). The beneficial effects of ZnONPs on seeds germination and early seedling growth were reported by other authors who showed enhanced wheat grains germination and seedlings growth after priming the seeds with ZnONPs at a

concentration of 10 mg L⁻¹ (Rai-Kalal and Jajoo, 2021). Recently, the mechanisms of ZnONPs action as a nanobiofertilizer for plant growth promotion were studied by Sun et al. (2020), Khan et al. (2021) and El-Badri et al. (2021). They found that these NPs increased zinc uptake by plants, maximized plant production and improved plant resistance to biotic and abiotic stresses. In turn, Itroutwar and coworkers (2020a) identified the accumulation of ZnONPs in maize seeds endosperm leading to improved germination. It has been suggested that ZnONPs facilitate water uptake and increase α -amylase activity during germination (Itroutwar et al., 2020b; Rai-Kalal and Jajoo, 2021; Sharma et al., 2021). Moreover, study conducted by El-Badri and coworkers (2021) showed that ZnONPs activity as plant growth promoter was associated with increasing metabolic activity and modulating the expression of hormone genes (abscisic acid (ABA) and gibberellic acid (GA)) during seed germination. In another study, Rawashdeh et al. (2020) showed improved germination and enhanced biomass production under salt stress after nanoprimer seeds with ZnONPs. The mechanism of action of ZnONPs was attributed to stimulation of enzyme biosynthesis, induction of carbohydrate decomposition and increased activity of the antioxidant system.

Both positive and negative effects of ZnONPs on seed germination and plant growth have been reported, but many studies have shown that bio-synthesized ZnONPs are more stable and biocompatible (due to capping and stabilizing agents of natural origin on their surface) compared to chemical ones (Singh et al., 2018). The use of bio-ZnONPs in the preparation of seeds of agronomically important crops can contribute to increased crop productivity and quality. Although there is still limited information on the interaction of nanoparticles with plants, further efforts should be made to clarify them (Tondy et al., 2021).

5 Conclusion

In this study, AgNPs and ZnONPs were effectively synthesized from *F. solani* IOR 825. They were comprehensively characterized using UV-vis, TEM, XRD, DLS, Zeta potential measurements, and FTIR which revealed the small size and spherical shape of AgNPs, the larger size of ZnONPs, and for both stability, crystalline nature, and that mycosynthesized nanoparticles were capped with biomolecules. The AgNPs were found to have strong antimicrobial potential against bacterial pathogens of plants. The lower sensitivity of pathogenic bacteria was demonstrated to ZnONPs. In addition, both types of NPs showed the potential to inhibit fungal spore germination, which is crucial in the fungal spread in the environment, and growth of fungal mycelia. The AgNPs revealed sterilization effect on maize seeds while ZnONPs demonstrated stimulatory effect on seedlings growth by improving fresh and dry biomass production. The present work highlights that mycosynthesized silver and zinc oxide nanoparticles in view of their unique properties, have a high potential as a promising agent to control or prevent the growth of pathogens in agriculture and enhance crop productivity. Nevertheless, continued investigations into their effects on plant development, growth and long-term toxicity are required.

Data availability statement

The original contributions presented in the study are included in the article/Supplementary Material, further inquiries can be directed to the corresponding authors.

Author contributions

PG, MR, and MW conceived research, PG and JT-W designed research, JT-W carried out experiments, APT performed Zeta-potential and DLS analyses, JT-W analyzed data and wrote the manuscript, PG and MR edited and reviewed it. JT-W acquired the funds. All authors contributed to the article and approved the submitted version.

Funding

This research was funded by grant No. 2022/45/N/NZ9/01483 from National Science Centre, Poland. The ACP was funded from IDUB of Nicolaus Copernicus University in Toruń, Poland.

Acknowledgments

MR and PG would like to thank Polish National Agency for Academic Exchange Programme, for financial support under the grant PPN/ULM/2019/1/00117/U/00001.

Conflict of interest

The authors declare that the research was conducted in the absence of any commercial or financial relationships that could be construed as a potential conflict of interest.

Publisher's note

All claims expressed in this article are solely those of the authors and do not necessarily represent those of their affiliated organizations, or those of the publisher, the editors and the reviewers. Any product that may be evaluated in this article, or claim that may be made by its manufacturer, is not guaranteed or endorsed by the publisher.

Supplementary material

The Supplementary Material for this article can be found online at: <https://www.frontiersin.org/articles/10.3389/fchem.2023.1235437/full#supplementary-material>

References

- Abd El-Aziz, A. R. M., Al-Othman, M. R., Mahmoud, M. A., and Metwaly, H. A. (2015). Biosynthesis of silver nanoparticles using *Fusarium solani* and its impact on grain borne fungi. *Dig. J. Nanomater. Biostructures* 10, 655–662.
- Abdullah, F. H., Bakar, N. A., and Bakar, M. A. (2020). Low temperature biosynthesis of crystalline zinc oxide nanoparticles from *Musa acuminata* peel extract for visible-light degradation of methylene blue. *Optik* 206, 164279. doi:10.1016/j.jleo.2020.164279
- Abdul-Baki, A. A., and Anderson, J. D. (1973). Vigor determination in soybean seed by multiple criteria 1. *Crop Sci.* 13, 630–633. doi:10.2135/cropsci1973.0011183X001300060013x
- Abedi, T., Gavanji, S., and Mojiri, A. (2022). Lead and zinc uptake and toxicity in maize and their management. *Plants* 11, 1922. doi:10.3390/plants11151922
- Akhtar, N., Khan, S., Jamil, M., Rehman, S. U., Rehman, Z. U., and Rha, E. S. (2022). Combine effect of ZnO NPs and bacteria on protein and gene's expression profile of rice (*Oryza sativa* L.) plant. *Toxics* 10, 305. doi:10.3390/toxics10060305
- Anjum, S., Vyas, A., and Sofi, T. A. (2023). Fungi-mediated synthesis of nanoparticles: Characterization process and agricultural applications. *J. Sci. Food Agric.* 103, 4727–4741. doi:10.1002/jsfa.12496
- Balachandrar, R., Gurumoorthy, P., Karmegam, N., Barabadi, H., Subbaiya, R., Anand, K., et al. (2019). Plant-mediated synthesis, characterization and bactericidal potential of emerging silver nanoparticles using stem extract of *Phyllanthus pinnatus*: A recent advance in phytonanotechnology. *J. Clust. Sci.* 30, 1481–1488. doi:10.1007/s10876-019-01591-y
- Ballottin, D., Fulaz, S., Souza, M. L., Corio, P., Rodrigues, A. G., Souza, A. O., et al. (2016). Elucidating protein involvement in the stabilization of the biogenic silver nanoparticles. *Nanoscale Res. Lett.* 11, 313–319. doi:10.1186/s11671-016-1538-y
- Cakmak, I., Kalayci, M., Kaya, Y., Torun, A. A., Aydin, N., Wang, Y., et al. (2010). Biofortification and localization of zinc in wheat grain. *J. Agri. Food Chem.* 58, 9092–9102. doi:10.1021/jf101197h
- Camp, A. F. (1945). Zinc as a nutrient in plant growth. *Soil Sci.* 60, 157–164. doi:10.1097/00010694-194508000-00009
- Clarance, P., Luvankar, B., Sales, J., Khushro, A., Agastian, P., Tack, J. C., et al. (2020). Green synthesis and characterization of gold nanoparticles using endophytic fungi *Fusarium solani* and its *in-vitro* anticancer and biomedical applications. *Saudi. J. Biol. Sci.* 27, 706–712. doi:10.1016/j.sjbs.2019.12.026
- Clinical and Laboratory Standards Institute (CLSI) (2004). Method for antifungal disk diffusion susceptibility Testing of Yeasts, approved guideline. *Document M44-A*. USA: CLSI Wayne.
- Clinical and Laboratory Standards Institute (CLSI) (2012). Methods for dilution antimicrobial susceptibility Tests for Bacteria that grow aerobically; approved standard 9th. *Document M07-A9*. USA: CLSI Wayne.
- Consolo, V. F., Torres-Nicolini, A., and Alvarez, V. A. (2020). Mycosynthetized Ag, CuO and ZnO nanoparticles from a promising *Trichoderma harzianum* strain and their antifungal potential against important phytopathogens. *Sci. Rep.* 10, 20499–9. doi:10.1038/s41598-020-77294-6
- Czembor, E., Stępień, L., and Waśkiewicz, A. (2015). Effect of environmental factors on *Fusarium* species and associated mycotoxins in maize grain grown in Poland. *PloS one* 10, e0133644. doi:10.1371/journal.pone.0133644
- de la Rosa, G., Vázquez-Núñez, E., Molina-Guerrero, C., Serafin-Muñoz, A. H., and Vera-Reyes, I. (2021). Interactions of nanomaterials and plants at the cellular level: Current knowledge and relevant gaps. *Nanotechnol. Environ. Eng.* 6, 7–19. doi:10.1007/s41204-020-00100-1
- Dhiman, S., Singh, S., Varma, A., and Goel, A. (2021). Phytofabricated zinc oxide nanoparticles as a nanofungicide for management of *Alternaria* blight of Brassica. *Biometals* 34, 1275–1293. doi:10.1007/s10534-021-00342-9
- El Sayed, M. T., and El-Sayed, A. S. (2020). Biocidal activity of metal nanoparticles synthesized by *Fusarium solani* against multidrug-resistant bacteria and mycotoxigenic fungi. *J. Microbiol. Biotechnol.* 30, 226–236. doi:10.4014/jmb.1906.06070
- El-Badri, A. M., Batool, M., Wang, C., Hashem, A. M., Tabl, K. M., Nishawy, E., et al. (2021). Selenium and zinc oxide nanoparticles modulate the molecular and morpho-physiological processes during seed germination of *Brassica napus* under salt stress. *Ecotoxicol. Environ. Saf.* 225, 112695. doi:10.1016/j.ecoenv.2021.112695
- Elrefaey, A. A. K., El-Gamal, A. D., Hamed, S. M., and El-Belely, E. F. (2022). Algae-mediated biosynthesis of zinc oxide nanoparticles from *Cystoseira crinita* (Fuciales; Sargassaceae) and its antimicrobial and antioxidant activities. *Egypt. J. Chem.* 65, 0–240. doi:10.21608/EJCHEM.2021.87722.4231
- Esechie, H. (1994). Interaction of salinity and temperature on the germination of sorghum. *J. Agron. Crop Sci.* 172, 194–199. doi:10.1111/j.1439-037X.1994.tb00166.x
- Faizan, M., Hayat, S., and Pichtel, J. (2020). “Effects of zinc oxide nanoparticles on crop plants: A perspective analysis,” in *Sustainable agriculture Reviews 41. Sustainable agriculture Reviews*. Editors S. Hayat, J. Pichtel, M. Faizan, and Q. Fariduddin (Cham: Springer), 83–99. doi:10.1007/978-3-030-33996-8_4
- Feroze, N., Arshad, B., Younas, M., Afridi, M. I., Saqib, S., and Ayaz, A. (2020). Fungal mediated synthesis of silver nanoparticles and evaluation of antibacterial activity. *Microsc. Res. Tech.* 83, 72–80. doi:10.1002/jemt.23390
- Gallón, S. M. N., Alpaslan, E., Wang, M., Larese-Casanova, P., Londoño, M. E., Atehortúa, L., et al. (2019). Characterization and study of the antibacterial mechanisms of silver nanoparticles prepared with microalgal exopolysaccharides. *Mater. Sci. Eng. C* 99, 685–695. doi:10.1016/j.msec.2019.01.134
- Ganachari, S. V., Bhat, R., Deshpande, R., and Venkataraman, A. (2012). Extracellular biosynthesis of silver nanoparticles using fungi *Penicillium diversum* and their antimicrobial activity studies. *BioNanoScience* 2, 316–321. doi:10.1007/s12668-012-0046-5
- Ghorbani, H. R., Mehr, F. P., Pazoki, H., and Rahmani, B. M. (2015). Synthesis of ZnO nanoparticles by precipitation method. *Orient. J. Chem.* 31, 1219–1221. doi:10.13005/ojc/310281
- González-Merino, A. M., Hernández-Juárez, A., Betancourt-Galindo, R., Ochoa-Fuentes, Y. M., Valdez-Aguilar, L. A., and Limón-Corona, M. L. (2021). Antifungal activity of zinc oxide nanoparticles in *Fusarium oxysporum* - *Solanum lycopersicum* pathosystem under controlled conditions. *J. Phytopathol.* 169, 533–544. doi:10.1111/jph.13023
- Gudkov, S. V., Burmistrov, D. E., Serov, D. A., Rebezov, M. B., Semenova, A. A., and Lisitsyn, A. B. (2021). A mini review of antibacterial properties of ZnO nanoparticles. *Front. Phys.* 9, 641481. doi:10.3389/fphys.2021.641481
- Guilger-Casagrande, M., Germano-Costa, T., Pasquato-Stigliani, T., Fraceto, L. F., and Lima, R. D. (2019). Biosynthesis of silver nanoparticles employing *Trichoderma harzianum* with enzymatic stimulation for the control of *Sclerotinia sclerotiorum*. *Sci. Rep.* 9, 14351. doi:10.1038/s41598-019-50871-0
- Hacisalihoglu, G. (2020). Zinc (Zn): The last nutrient in the alphabet and shedding light on Zn efficiency for the future of crop production under suboptimal Zn. *Plants* 9, 1471. doi:10.3390/plants9111471
- Hazarika, A., Yadav, M., Yadav, D. K., and Yadav, H. S. (2022). An overview of the role of nanoparticles in sustainable agriculture. *Biocatal. Agric. Biotechnol.* 43, 102399. doi:10.1016/j.bcab.2022.102399
- Ibrahim, E., Zhang, M., Zhang, Y., Hossain, A., Qiu, W., Chen, Y., et al. (2020). Green-synthesis of silver nanoparticles using endophytic bacteria isolated from garlic and its antifungal activity against wheat *Fusarium* head blight pathogen *Fusarium graminearum*. *Nanomaterials* 10, 219. doi:10.3390/nano10020219
- Ingle, A., Rai, M., Gade, A., and Bawaskar, M. (2009). *Fusarium solani*: A novel biological agent for the extracellular synthesis of silver nanoparticles. *J. Nanopart. Res.* 11, 2079–2085. doi:10.1007/s11051-008-9573-y
- Itrotwar, P. D., Govindaraju, K., Tamilselvan, S., Kannan, M., Raja, K., and Subramanian, K. S. (2020b). Seaweed-based biogenic ZnO nanoparticles for improving agro-morphological characteristics of rice (*Oryza sativa* L.). *J. Plant. Growth Regul.* 39, 717–728. doi:10.1007/s00344-019-10012-3
- Itrotwar, P. D., Kasivelu, G., Raguraman, V., Malaichamy, K., and Sevathapandian, S. K. (2020a). Effects of biogenic zinc oxide nanoparticles on seed germination and seedling vigor of maize (*Zea mays*). *Biocatal. Agric. Biotechnol.* 29, 101778. doi:10.1016/j.bcab.2020.101778
- Jacquet, F., Jeuffroy, M. H., Jouan, J., Le Cadre, E., Litrico, I., Malausa, T., et al. (2022). Pesticide-free agriculture as a new paradigm for research. *Agron. Sustain. Dev.* 42, 8–24. doi:10.1007/s13593-021-00742-8
- Jain, D., Bhojiya, A. A., Singh, H., Daima, H. K., Singh, M., Mohanty, S. R., et al. (2020). Microbial fabrication of zinc oxide nanoparticles and evaluation of their antimicrobial and photocatalytic properties. *Front. Chem.* 8, 778. doi:10.3389/fchem.2020.00778
- Jamdnagi, P., Khatri, P., and Rana, J. S. (2018). Green synthesis of zinc oxide nanoparticles using flower extract of *Nyctanthes arbor-tristis* and their antifungal activity. *J. King. Saud. Univ. Sci.* 30, 168–175. doi:10.1016/j.jksus.2016.10.002
- Jiang, Y., Zhang, L., Wen, D., and Ding, Y. (2016). Role of physical and chemical interactions in the antibacterial behavior of ZnO nanoparticles against *E. coli*. *Mater. Sci. Eng. C* 69, 1361–1366. doi:10.1016/j.msec.2016.08.044
- Khan, M. I., Fatima, N., Shakil, M., Tahir, M. B., Riaz, K. N., Rafique, M., et al. (2021). Investigation of *in-vitro* antibacterial and seed germination properties of green synthesized pure and nickel doped ZnO nanoparticles. *Phys. B Condens. Matter* 601, 412563. doi:10.1016/j.physb.2020.412563
- Kobashigawa, J. M., Robles, C. A., Ricci, M. L. M., and Carmarán, C. C. (2019). Influence of strong bases on the synthesis of silver nanoparticles (AgNPs) using the ligninolytic fungi *Trametes troglia*. *Saudi J. Biol. Sci.* 26, 1331–1337. doi:10.1016/j.sjbs.2018.09.006
- Król, A., Książek, J., Kubińska, E., and Rozakis, S. (2018). Evaluation of sustainability of maize cultivation in Poland. A Prospect theory—PROMETHEE approach. *Sustainability* 10, 4263. doi:10.3390/su10114263
- Kumari, M., Giri, V. P., Pandey, S., Kumar, M., Katiyar, R., Nautiyal, C. S., et al. (2019). An insight into the mechanism of antifungal activity of biogenic nanoparticles than their chemical counterparts. *Pestic. Biochem. Physiol.* 157, 45–52. doi:10.1016/j.pestbp.2019.03.005
- Labeeb, M., Badr, A., Haroun, S. A., Mattar, M. Z., El-Kholy, A. S., and El-Mehasseb, I. M. (2020). Ecofriendly synthesis of silver nanoparticles and their effects on early growth and cell division in roots of green pea (*Pisum sativum* L.). *Gesunde Pflanz.* 72, 113–127. doi:10.1007/s10343-019-00491-5

- Lallo da Silva, B., Abuçafy, M. P., Berbel Manaia, E., Oshiro Junior, J. A., Chiari-Andréo, B. G., Pietro, R. C. R., et al. (2019). Relationship between structure and antimicrobial activity of zinc oxide nanoparticles: An Overview. *Int. J. Nanomedicine* 14, 9395–9410. doi:10.2147/IJN.S216204
- Lee, D. H., Lee, K. L., Shukla, S., Commandeur, U., and Steinmetz, N. F. (2017). Potato virus X, a filamentous plant viral nanoparticle for doxorubicin delivery in cancer therapy. *Nanoscale* 9, 2348–2357. doi:10.1039/C6NR09099K
- Lee, S., Kim, S., Kim, S., and Lee, I. (2013). Assessment of phytotoxicity of ZnO NPs on a medicinal plant, *Fagopyrum esculentum*. *Environ. Sci. Pollut. Res.* 20, 848–854. doi:10.1007/s11356-012-1069-8
- Lotfy, W. A., Alkersh, B. M., Sabry, S. A., and Ghoslan, H. A. (2021). Biosynthesis of silver nanoparticles by *Aspergillus terreus*: Characterization, optimization, and biological activities. *Front. Bioeng. Biotechnol.* 9, 633468. doi:10.3389/fbioe.2021.633468
- Macías Sánchez, K. L., González Martínez, H. D. R., Carrera Cerritos, R., and Martínez Espinosa, J. C. (2023). *In vitro* evaluation of the antifungal effect of AgNPs on *Fusarium oxysporum* f. sp. *lycopersici*. *Nanomater. (Basel)* 13, 1274. doi:10.3390/nano13071274
- Malandrakis, A. A., Kavroulakis, N., and Chrysikopoulos, C. V. (2022). Metal nanoparticles against fungicide resistance: Alternatives or partners? *Pest Manag. Sci.* 78, 3953–3956. doi:10.1002/ps.7014
- Manosalva, N., Tortella, G., Cristina Diez, M., Schalchli, H., Seabra, A. B., Durán, N., et al. (2019). Green synthesis of silver nanoparticles: Effect of synthesis reaction parameters on antimicrobial activity. *World J. Microbiol. Biotechnol.* 35, 88–89. doi:10.1007/s11274-019-2664-3
- Mašev, N., and Kutáček, M. (1966). The effect of zinc on the biosynthesis of tryptophan, andol auxins and gibberellins in barley. *Biol. Plant.* 8, 142–151. doi:10.1007/BF02930623
- Merlin, J. N., Christudas, I. V. S. N., Kumar, P. P., and Agastian, P. (2013). Optimization of growth and bioactive metabolite production. *Fusarium solani* Asian J. Pharm. Clin. Res. 6, 98–103.
- Michael, A., Singh, A., Roy, A., and Islam, M. (2022). Fungal and algal-derived synthesis of various nanoparticles and their applications. *Bioinorg. Chem. Appl.* 2022, 1–14. doi:10.1155/2022/3142674
- Moezzi, A., Cortie, M., and McDonagh, A. (2011). Aqueous pathways for the formation of zinc oxide nanoparticles. *Dalton Trans.* 40, 4871–4878. doi:10.1039/C0DT01748E
- Morsy, F. M., Nafady, N. A., Abd-Alla, M. H., and Elhady, D. A. (2014). Green synthesis of silver nanoparticles by water soluble fraction of the extracellular polysaccharides/matrix of the cyanobacterium *Nostoc commune* and its application as a potent fungal surface sterilizing agent of seed crops. *Univ. J. Microbiol. Res.* 2, 36–43. doi:10.13189/ujmr.2014.020303
- Murillo-Rábago, E. I., Vilchis-Nestor, A. R., Juárez-Moreno, K., García-Marín, L. E., Quester, K., and Castro-Longoria, E. (2022). Optimized synthesis of small and stable silver nanoparticles using intracellular and extracellular components of fungi: An alternative for bacterial inhibition. *Antibiotics* 11, 800. doi:10.3390/antibiotics11060800
- Musa, I., Qamhi, N., and Mahmoud, S. T. (2017). Synthesis and length dependent photoluminescence property of zinc oxide nanorods. *Results Phys.* 7, 3552–3556. doi:10.1016/j.rinp.2017.09.035
- Nallal, V. U. M., Prabha, K., VethaPotheher, I., Ravindran, B., Baazeem, A., Chang, S. W., et al. (2021). Sunlight-driven rapid and facile synthesis of Silver nanoparticles using *Allium ampeloprasum* extract with enhanced antioxidant and antifungal activity. *Saudi J. Biol. Sci.* 28, 3660–3668. doi:10.1016/j.sjbs.2021.05.001
- Namburi, K. R., Kora, A. J., Chetukuri, A., and Kota, V. S. M. K. (2021). Biogenic silver nanoparticles as an antibacterial agent against bacterial leaf blight causing rice phytopathogen *Xanthomonas oryzae* pv. *Oryzae*. *Bioprocess Biosyst. Eng.* 44, 1975–1988. doi:10.1007/s00449-021-02579-7
- Nandhini, M., Rajini, S. B., Udayashankar, A. C., Niranjana, S. R., Lund, O. S., Shetty, H. S., et al. (2019). Biofabricated zinc oxide nanoparticles as an eco-friendly alternative for growth promotion and management of downy mildew of pearl millet. *Crop Prot.* 121, 103–112. doi:10.1016/j.cropro.2019.03.015
- Ogunyemi, S. O., Zhang, M., Abdallah, Y., Ahmed, T., Qiu, W., Ali, M. A., et al. (2020). The bio-synthesis of three metal oxide nanoparticles (ZnO, MnO₂, and MgO) and their antibacterial activity against the bacterial leaf blight pathogen. *Front. Microbiol.* 11, 588326. doi:10.3389/fmicb.2020.588326
- Orchard, T. (1977). Estimating the parameters of plant seedling emergence. *Seed Sci. Technol.* 5, 61–69.
- Patra, J. K., and Baek, K. H. (2014). Green nanobiotechnology: Factors affecting synthesis and characterization techniques. *J. Nanomat.* 2014, 1–12. doi:10.1155/2014/417305
- Paul, A., and Roychoudhury, A. (2021). Go green to protect plants: Repurposing the antimicrobial activity of biosynthesized silver nanoparticles to combat phytopathogens. *Nanotechnol. Environ. Eng.* 6, 10. doi:10.1007/s41204-021-00103-6
- Peng, Y., Li, S. J., Yan, J., Tang, Y., Cheng, J. P., Gao, A. J., et al. (2021). Research progress on phytopathogenic fungi and their role as biocontrol agents. *Front. Microbiol.* 12, 670135. doi:10.3389/fmicb.2021.670135
- Pestovsky, Y. S., and Martínez-Antonio, A. (2017). The use of nanoparticles and nanoformulations in agriculture. *J. Nanosci. Nanotechnol.* 17, 8699–8730. doi:10.1166/jnn.2017.15041
- Philippe, S., Souaibou, F., Guy, A., Sébastien, D. T., Boniface, Y., Paulin, A., et al. (2012). Chemical Composition and Antifungal activity of Essential oil of Fresh leaves of *Ocimum gratissimum* from Benin against six Mycotoxigenic Fungi isolated from traditional cheese wagashi. *Int. Res. J. Biol. Sci.* 1, 22–27.
- Pillai, A. M., Sivasankarapillai, V. S., Rahdar, A., Joseph, J., Sadeghfar, F., Rajesh, K., et al. (2020). Green synthesis and characterization of zinc oxide nanoparticles with antibacterial and antifungal activity. *J. Mol. Struct.* 1211, 128107. doi:10.1016/j.molstruc.2020.128107
- Quinteros, M. A., Bonilla, J. O., Alborés, S. V., Villegas, L. B., and Páez, P. L. (2019). Biogenic nanoparticles: Synthesis, stability and biocompatibility mediated by proteins of *Pseudomonas aeruginosa*. *Colloids Surf. B* 184, 110517. doi:10.1016/j.colsurfb.2019.110517
- Rai, M., Gupta, I., Ingle, A. P., Biswas, J. K., and Sinitsyna, O. V. (2018). “Nanomaterials, what are they, why they cause ecotoxicity, and how this can be dealt with?,” in *Nanomaterials, Ecotoxicity, safety, and public Perception* Editors M. Rai and J. K. Biswas 1st ed. (Switzerland: Springer Cham), 3–18. doi:10.1007/978-3-030-05144-0_1
- Rai, M., Ingle, A. P., Trzcińska-Wencel, J., Wypij, M., Bonde, S., Yadav, A., et al. (2021). Biogenic silver nanoparticles: What we know and what do we need to know? *Nanomaterials* 11, 2901. doi:10.3390/nano11112901
- Rai-Kalal, P., and Jajoo, A. (2021). Priming with zinc oxide nanoparticles improve germination and photosynthetic performance in wheat. *Plant Physiol. biochem.* 160, 341–351. doi:10.1016/j.plaphy.2021.01.032
- Rajesh, S., Raja, D. P., Rath, J. M., and Sahayraj, K. (2012). Biosynthesis of silver nanoparticles using *Ulva fasciata* (Delile) ethyl acetate extract and its activity against *Xanthomonas campestris* pv. *Malvacearum*. *J. Biopestic.* 5, 119.
- Rawashdeh, R. Y., Harb, A. M., and AlHasan, A. M. (2020). Biological interaction levels of zinc oxide nanoparticles; lettuce seeds as case study. *Heliyon* 6, e03983. doi:10.1016/j.heliyon.2020.e03983
- Reddy, K. M., Feris, K., Bell, J., Wingett, D. G., Hanley, C., and Punnoose, A. (2007). Selective toxicity of zinc oxide nanoparticles to prokaryotic and eukaryotic systems. *Appl. Phys. Lett.* 90, 2139021–2139023. doi:10.1063/1.2742324
- Rudani, L., Vishal, P., and Kalavati, P. (2018). The importance of zinc in plant growth-A review. *Int. Res. J. Nat. Appl.* 5, 38–48.
- Saeed, S., Iqbal, A., and Ashraf, M. A. (2020). Bacterial-mediated synthesis of silver nanoparticles and their significant effect against pathogens. *Environ. Sci. Pollut. Res.* 27, 37347–37356. doi:10.1007/s11356-020-07610-0
- Saion, E., Gharibshahi, E., and Naghavi, K. (2013). Size-controlled and optical properties of monodispersed silver nanoparticles synthesized by the radiolytic reduction method. *Int. J. Mol. Sci.* 14, 7880–7896. doi:10.3390/ijms14047880
- Salem, S. S. (2022). Baker's yeast-mediated silver nanoparticles: Characterisation and antimicrobial biogenic tool for suppressing pathogenic microbes. *BioNanoScience* 12, 1220–1229. doi:10.1007/s12668-022-01026-5
- Sasani, M., Fatehi, E., Safari, R., Nasehi, F., and Mosayyebi, M. (2023). Antimicrobial potentials of Iron oxide and silver nanoparticles green-synthesized in *Fusarium solani*. *J. Chem. Health Risks* 13, 95–104. doi:10.22034/JCHR.2021.1928198.1293
- Scherer, M. D., Sposito, J. C., Falco, W. F., Grisolia, A. B., Andrade, L. H., Lima, S. M., et al. (2019). Cytotoxic and genotoxic effects of silver nanoparticles on meristematic cells of *Allium cepa* roots: A close analysis of particle size dependence. *Sci. Total Environ.* 660, 459–467. doi:10.1016/j.scitotenv.2018.12.444
- Scott, S. J., Jones, R. A., and Williams, W. (1984). Review of data analysis methods for seed germination 1. *Crop Sci.* 24, 1192–1199. doi:10.2135/cropsci1984.0011183X002400060043x
- Sharifi, R., Mohammadi, K., and Rokhzadi, A. (2016). Effect of seed priming and foliar application with micronutrients on quality of forage corn (*Zea mays*). *Environ. Exp. Bot.* 14, 151–156. doi:10.22364/eeb.14.21
- Sharma, D., Afzal, S., and Singh, N. K. (2021). Nanoprimering with phytosynthesized zinc oxide nanoparticles for promoting germination and starch metabolism in rice seeds. *J. Biotechnol.* 336, 64–75. doi:10.1016/j.jbiotec.2021.06.014
- Shobha, B., Ashwini, B. S., Ghazwani, M., Hani, U., Atwah, B., Alhumaidi, M. S., et al. (2023). Trichoderma-mediated ZnO nanoparticles and their antibiofilm and antibacterial activities. *J. Fungi* 9, 133. doi:10.3390/jof9020133
- Singh, A., Singh, N. Á., Afzal, S., Singh, T., and Hussain, I. (2018). Zinc oxide nanoparticles: A review of their biological synthesis, antimicrobial activity, uptake, translocation and biotransformation in plants. *J. Mat. Sci.* 53, 185–201. doi:10.1007/s10853-017-1544-1
- Singh, D., Rathod, V., Ningnanagouda, S., Hiremath, J., Singh, A. K., and Mathew, J. (2014). Optimization and characterization of silver nanoparticle by endophytic fungi *Penicillium* sp. isolated from *Curcuma longa* (turmeric) and application studies against MDR *E. coli* and *S. aureus*. *Bioinorg. Chem. Appl.* 2014, 1–8. doi:10.1155/2014/408021
- Singh, K., Panghal, M., Kadyan, S., Chaudhary, U., and Yadav, J. P. (2014). Green silver nanoparticles of *Phyllanthus amarus*: As an antibacterial agent against multi drug resistant clinical isolates of *Pseudomonas aeruginosa*. *J. Nanobiotechnol.* 12, 40–49. doi:10.1186/s12951-014-0040-x
- Singh, R. P., Handa, R., and Manchanda, G. (2021). Nanoparticles in sustainable agriculture: An emerging opportunity. *J. Control. Release* 329, 1234–1248. doi:10.1016/j.jconrel.2020.10.051
- Sonawane, H., Shelke, D., Chambhare, M., Dixit, N., Math, S., Sen, S., et al. (2022). Fungi-derived agriculturally important nanoparticles and their application in crop

- stress management—Prospects and environmental risks. *Environ. Res.* 212, 113543. doi:10.1016/j.envres.2022.113543
- Srivastav, A., Ganjewala, D., Singhal, R. K., Rajput, V. D., Minkina, T., Voloshina, M., et al. (2021). Effect of ZnO nanoparticles on growth and biochemical responses of wheat and maize. *Plants* 10, 2556. doi:10.3390/plants10122556
- Sun, H., Du, W., Peng, Q., Lv, Z., Mao, H., and Kopittke, P. M. (2020). Development of ZnO nanoparticles as an efficient Zn fertilizer: Using synchrotron-based techniques and laser ablation to examine elemental distribution in wheat grain. *J. Agric. Food Chem.* 68, 5068–5075. doi:10.1021/acs.jafc.0c00084
- Talam, S., Karumuri, S. R., and Gunnam, N. (2012). Synthesis, characterization, and spectroscopic properties of ZnO nanoparticles. *Int. Sch. Res. Not.* 2012, 1–6. doi:10.5402/2012/372505
- Talie, M. D., Wani, A. H., Ahmad, N. U. S. R. A. T., Bhat, M. Y., and War, J. M. (2020). Green synthesis of silver nanoparticles (AgNPs) using *Helvella leucopus* Pers. and their antimycotic activity against fungi causing fungal rot of Apple. *Asian J. Pharm. Clin. Res.* 13, 161–165. doi:10.22159/ajpcr.2020.v13i4.37024
- Tonday, M., Kalia, A., Singh, A., Dheri, G. S., Taggar, M. S., Nepovimova, E., et al. (2021). Seed priming and coating by nano-scale zinc oxide particles improved vegetative growth, yield and quality of fodder maize (*Zea mays*). *Agronomy* 11, 729. doi:10.3390/agronomy11040729
- Trzcińska-Wencel, J., Wypij, M., Rai, M., and Golińska, P. (2023). Biogenic nanosilver bearing antimicrobial and antibiofilm activities and its potential for application in agriculture and industry. *Front. Microbiol.* 14, 1125685. doi:10.3389/fmicb.2023.1125685
- Umar, W., Hameed, M. K., Aziz, T., Maqsood, M. A., Bilal, H. M., and Rasheed, N. (2021). Synthesis, characterization and application of ZnO nanoparticles for improved growth and Zn biofortification in maize. *Arch. Agron. Soil Sci.* 67, 1164–1176. doi:10.1080/03650340.2020.1782893
- Urnukhsaikhan, E., Bold, B. E., Gunbileg, A., Sukhbaatar, N., and Mishig-Ochir, T. (2021). Antibacterial activity and characteristics of silver nanoparticles biosynthesized from *Carduus crispus*. *Sci. Rep.* 11, 21047. doi:10.1038/s41598-021-00520-2
- van Dijk, M., Morley, T., Rau, M. L., and Saghai, Y. (2021). A meta-analysis of projected global food demand and population at risk of hunger for the period 2010–2050. *Nat. Food* 2, 494–501. doi:10.1038/s43016-021-00322-9
- Verma, A., and Bharadvaja, N. (2022). Plant-mediated synthesis and characterization of silver and copper oxide nanoparticles: Antibacterial and heavy metal removal activity. *J. Clust. Sci.* 33, 1697–1712. doi:10.1007/s10876-021-02091-8
- Vijayan, S., Koilaparambil, D., George, T. K., and Manakulam Shaikmoideen, J. (2016). Antibacterial and cytotoxicity studies of silver nanoparticles synthesized by endophytic *Fusarium solani* isolated from *Withania somnifera* (L.). *J. Water Environ. Nanotechnol.* 1, 91–103. doi:10.7508/JWENT.2016.02.003
- Wan, J., Wang, R., Wang, R., Ju, Q., Wang, Y., and Xu, J. (2019). Comparative physiological and transcriptomic analyses reveal the toxic effects of ZnO nanoparticles on plant growth. *Environ. Sci. Technol. Lett.* 53, 4235–4244. doi:10.1021/acs.est.8b06641
- Wei, X., Cao, P., Wang, G., Liu, Y., Song, J., and Han, J. (2021). CuO, ZnO, and γ -Fe₂O₃ nanoparticles modified the underground biomass and rhizosphere microbial community of *Salvia miltiorrhiza* (Bge) after 165-day exposure. *Ecotoxicol. Environ. Saf.* 217, 112232. doi:10.1016/j.ecoenv.2021.112232
- Wypij, M., Jędrzejewski, T., Trzcińska-Wencel, J., Ostrowski, M., Rai, M., and Golińska, P. (2021). Green synthesized silver nanoparticles: Antibacterial and anticancer activities, biocompatibility, and analyses of surface-attached proteins. *Front. Microbiol.* 12, 632505. doi:10.3389/fmicb.2021.632505
- Wypij, M., Ostrowski, M., Piska, K., Wójcik-Pszczola, K., Pękala, E., Rai, M., et al. (2022). Novel antibacterial, cytotoxic and catalytic activities of silver nanoparticles synthesized from acidophilic actinobacterial SL19 with Evidence for protein as coating biomolecule. *J. Microbiol. Biotechnol.* 32, 1195–1208. doi:10.4014/jmb.2205.05006
- Wypij, M., Świecimska, M., Dahm, H., Rai, M., and Golinska, P. (2019). Controllable biosynthesis of silver nanoparticles using actinobacterial strains. *Green process. Synth.* 8, 207–214. doi:10.1515/gps-2018-0070
- Zakirov, I. V., Khamadeeva, Z. A., and Aleshkina, O. V. (2021). Problems and prospects of ensuring food security in conditions of economic instability: Regional aspect. *IOP Conf. Ser. Earth Environ. Sci.* 666, 042053. doi:10.1088/1755-1315/666/4/042053
- Zare, E., Pourseyedi, S., Khatami, M., and Darezereshki, E. (2017). Simple biosynthesis of zinc oxide nanoparticles using nature's source, and it's *in vitro* bio-activity. *J. Mol. Struct.* 1146, 96–103. doi:10.1016/j.molstruc.2017.05.118
- Zhu, W., Hu, C., Ren, Y., Lu, Y., Song, Y., Ji, Y., et al. (2021). Green synthesis of zinc oxide nanoparticles using *Cinnamomum camphora* (L) Presl leaf extracts and its antifungal activity. *J. Environ. Chem. Eng.* 9, 106659. doi:10.1016/j.jece.2021.106659

Frontiers in Chemistry

Explores all fields of chemical science across the periodic table

Advances our understanding of how atoms, ions, and molecules come together and come apart. It explores the role of chemistry in our everyday lives - from electronic devices to health and wellbeing.

Discover the latest Research Topics

[See more →](#)

Frontiers

Avenue du Tribunal-Fédéral 34
1005 Lausanne, Switzerland
frontiersin.org

Contact us

+41 (0)21 510 17 00
frontiersin.org/about/contact

